INFORMATION TO USERS

This manuscript has been reproduced from the microfilm master. UMI films the text directly from the original or copy submitted. Thus, some thesis and dissertation copies are in typewriter face, while others may be from any type of computer printer.

The quality of this reproduction is dependent upon the quality of the copy submitted. Broken or indistinct print, colored or poor quality illustrations and photographs, print bleedthrough, substandard margins, and improper alignment can adversely affect reproduction.

In the unlikely event that the author did not send UMI a complete manuscript and there are missing pages, these will be noted. Also, if unauthorized copyright material had to be removed, a note will indicate the deletion.

Oversize materials (e.g., maps, drawings, charts) are reproduced by sectioning the original, beginning at the upper left-hand corner and continuing from left to right in equal sections with small overlaps. Each original is also photographed in one exposure and is included in reduced form at the back of the book.

Photographs included in the original manuscript have been reproduced xerographically in this copy. Higher quality 6" x 9" black and white photographic prints are available for any photographs or illustrations appearing in this copy for an additional charge. Contact UMI directly to order.

UMI

A Bell & Howell Information Company
300 North Zeeb Road, Ann Arbor MI 48106-1346 USA
313/761-4700 800/521-0600

IMPROVEMENTS IN THE DETECTION OF GUNSHOT RESIDUE AND CONSIDERATIONS AFFECTING ITS INTERPRETATION

by

Peter A. Pizzola, M.S., M.Phil.

A dissertation submitted to the Graduate Faculty in Criminal Justice in partial fulfillment of the requirements for the degree of Doctor of Philosophy, The City University of New York.

1998

This manuscript has been read and accepted for the Graduate Faculty in Criminal Justice in satisfaction of the dissertation requirement for the degree of Doctor of Philosophy.

January 16, 1998

Date

Chair of Examining Committee

January 16, 1998

Date

Executive Officer

Dr. Peter R. De Forest

Dr. David C. Locke

Dr. Robert Rothchild

Supervisory Committee

THE CITY UNIVERSITY OF NEW YORK

Abstract

This research focused on two major areas of criminalistics and crime scene reconstruction; the estimation of the distance to a target from which a firearm was discharged, called the muzzle-to-target distance, and gunshot residue dynamics. The estimate of the muzzle-to-target distance is critical to crime scene reconstruction since it can either help corroborate or refute suspects' or witnesses' statements. Methods currently used in criminalistics laboratories for the estimate of the muzzle-to-target distance have changed little over the past fifty years. These methods employ transfer techniques, rather than a direct pattern development and visualization approach, since color reactions do not provide an adequate contrast with dark fabrics. Unfortunately, a critical assessment of these transfer methods has not been made.

A detailed study of these transfer methods was conducted. This research demonstrated that these methods suffer from several problems which can influence their interpretation. Alternate approaches for direct pattern visualization involving photoluminescence were studied and developed. Several techniques for the detection of particles and the metal deposits have been identified. These include:

1. use of native fluorescence for the detection of partially burned propellant particles,

2. low temperature enhancement of photoluminescent methods for particles and the metal deposits,

3. a phosphorescent method for the detection of partially burned propellant particles,

4. chemical treatment to induce fluorescence of propellant particles and metal deposits,

5. a fluorescence method for vastly improving the detection of reaction sites on the transfer medium for partially burned propellant particles.

Several sequentially integrated approaches, incorporating the above improvements for the detection and enhancement of discharge patterns, have been developed and described. Most of these newly developed techniques are integrated with the long accepted classical methods, and build on them.

High speed photography of the formation and movement of gunshot residue, in the form of particles and a cloud, has helped explain some of the difficulties experienced by criminalists in their analyses of physical evidence. Additionally, it has provided valuable information for crime scene reconstruction purposes. These findings should also help non-scientists, such as attorneys and judges, comprehend some of the complexities and anomalies involved.

Acknowledgment

I would like to express my sincere gratitude to the following:

— National Institute of Justice for providing the funds (Grant No. 92-IJ-CX-K043) that made a large portion of this work possible. Dr. Richard Rau, NIJ Program Manager, of the Forensic Sciences and Criminal Justice Technology Program, was especially supportive of this project.

— Commissioner of Police, Donald Christopher, Yonkers Police Department for his encouragement to conduct research in this area.

— Police Officers Stephen Kwechin and Charles Cieslinski, Sgt. Michael Slattery, and other members of the Yonkers Police Department Criminal Identification Unit, for technical assistance in printing photographs.

— Kirby Martir, Mark Sargeant, Linda Rourke, Debra Nelson, Kevin Bynum, and Katherine Roberts, for technical assistance in the laboratory.

— Thomas Kubic for providing the microspectrofluorometer and assistance with reflected light microspectrofluorimetry.

— Mao-Xion Lin of the Central Police University, Taiwan, R.O.C., for translating several papers.

— my wife, Lori Pizzola, and my father, Peter Pizzola, as well as the remainder of my family for their moral support and encouragement.

— Doctors Robert Rothchild and David Locke, Professors of Chemistry at John Jay College of Criminal Justice, and Queens College respectively, for their critical reviews of the dissertation proposal, dissertation drafts, and for their helpful advice.

— Doctor Peter R. De Forest, Professor of Criminalistics at John Jay College of Criminal Justice, who served as mentor on my dissertation committee, and who was a consistent source of sage advice and encouragement.

Table of Contents

List of Tables

List of Figures

Chapter One

Gunshot Residue and Crime Scene Reconstruction

Firearms continue to be utilized in the commission of many crimes in the United States. For example, the yearly percentage of homicides committed with a firearm has held steady during the early portion of this decade. Annually, during the five year period from 1991 to 1995, 66% to 70% of the homicides that occurred nationwide were gun-related (Federal Bureau of Investigation [FBI], 1996, p. 18). It is unlikely that the nation will experience a significant reduction in the percentage of gun-related crimes in the near future.

Obviously, many victims in shooting cases are either seriously wounded or killed. It is especially important in these cases to utilize critical physical evidence to its fullest potential, both because of the seriousness of the crime and also since the victim, even if alive, is very often unable to give an accurate account of what has transpired. There are several aspects of the discharging of firearms, related to gunshot residue (GSR), that can be valuable to criminalists and investigators in assisting with the solution of crimes, particularly in the area of crime scene reconstruction. For example, the distance from which a shot was fired at a target, commonly referred to as the "muzzle-to-target" distance, can often be estimated from the distribution pattern of gunshot residue around the bullet entrance site, the determination of which can either help corroborate or refute suspects' or witnesses' statements (Ceccaldi, 1962, pp. 630-635).

Another extremely important type of physical evidence is the gunshot residue on the hands of the shooter. The identification of this residue and an understanding of its significance can help immensely in the investigative stages of the case and also at the adjudicative stage (Midkiff, 1975, p.77). For example, the detection of gunshot residue can be detected on objects that were in close proximity to the weapon when it was fired can be of considerable importance in the reconstruction of a crime scene (De Forest et al., 1983). Other related aspects of crime scene reconstruction include: a knowledge of the dynamics of gunshot residue formation and adhesion to objects; the detection and identification of bullet holes, ricochet marks; knowledge of the retention and persistence of GSR; the estimate of how recently a weapon was fired (Voskertchian et al., 1993); trajectory reconstruction; trace metal detection to learn if a person has handled a weapon (National Institute of Law Enforcement & Criminal Justice, 1970).

When a firearm is discharged, particles and clouds of vaporized materials are projected from the barrel in the direction of the path of the projectile as well as to the sides and rear of the weapon. The matter projected forward consists of incompletely burned propellant particles, unburned propellant particles, propellant additives and decomposition products, materials derived from the primer detonation, materials present from a previous discharge, as well as metallic components arising from the cartridge case, and the projectile itself. Additionally, GSR containing many of the same components

in differing amounts propagate toward the sides and rear of the weapon (Lichtenberg, 1990; Maehly & Stromberg, 1981). Whatever physical objects are in close proximity to the weapon at the time the weapon is fired can act as receiving surfaces for gunshot residue. The detection and analysis of gunshot residue on such surfaces can assume great significance in crime scene reconstruction. Gunshot residue consists of many different materials. Experimental studies are complicated because of variations in the composition of both the propellant charge (smokeless gunpowder) in the cartridge case and the primer charge. Maloney & Thornton (1982, p. 319) have reported the following possible components of smokeless gunpowder:

Table 1. Organic Compounds found in Propellant Charge

Cresol	Cyclonite (RDX)	2,4-Dinitrodiphenylamine
Resorcinol	Diethyl phthalate	Ethylcentralite
Carbazole	Nitroglycerin	Dibutylphthalate
Diphenylamine	Trinitrotoluene	Butylcentralite
Dimethyl phthalate	Dimethylsebacate	Dinitrocresol
N-Nitrosodiphenylamine	Methylcentralite	carbanilide
Nitrodiphenylamine	Triacetin	Nitrocellulose
Nitrotoluene	Pentaerythritol Tetranitrate	

Additionally, according to Wallace (1990, pp. 378-379) numerous inorganic compounds, as well as other organic compounds, and other components, may be present in the propellant charge: barium nitrate, potassium nitrate, starch, paraffin oil, tin, graphite, potassium sulphate, aurin, candelilla wax, methyl cellulose, sodium sulphate, calcium carbonate. It is also known that some manufacturers of bulk propellant include polyester. Attempts to obtain

composition information of propellant from a variety of manufacturing sources proved futile.

Traditional primer components were tetracene, lead styphnate, antimony sulfide, and barium nitrate. However, there are different compositions containing the above in addition to calcium silicide, lead dioxide, aluminum powder, ground glass, lead hypophosphite, lead peroxide, zirconium, pentaerythritol tetranitrate, gum type binder, and so forth. (Wallace, 1990, pp. 367-375). Recently, there has been a move from toxic materials in the primer composition to safer ones. These are: zinc peroxide, diazole, and titanium in conjunction with the traditionally used tetracene (Hagel & Redecker, 1986, p. 187). Even more recently, a new composition has been reported in CCI lead-free primers: tetracene, diazodinitrophenol, finely divided smokeless powder, and strontium nitrate (Harris, 1995, p. 28). The introduction of smokeless powder in the lead-free formulation can be a source of many different compounds as indicated above in Table 1.

Interpretation of GSR on Shooter's Hands

The analysis of gunshot residue on a person's hands for the purpose of determining whether or not he or she has recently fired a weapon is an important aspect of criminalistics and crime scene reconstruction. In homicides and other shooting cases, if it can be shown that a person has indeed fired a weapon, this is often critical evidence and is very helpful in establishing guilt or

innocence. The state of the art in this area of criminalistics is poor. Current methods, primarily bulk techniques, are only useful if the alleged shooter denies shooting, handling or being near a weapon during the time of the incident. The definitive presence of specific GSR particles can be demonstrated but distinguishing between the foregoing means of deposition is not possible. These methods do not utilize a pattern visualization feature, despite the general belief among criminalists that the back of the hand, thumb, web, index finger, and middle finger, should be analyzed for gunshot residue (Wessel et al., 1974, pp. 27-28).

An older technique for the detection of gunshot residue on the hands of the shooter, which was abandoned because of a lack of specificity, was the so-called "Paraffin Test" or the "Dermal Nitrate Test." Some authors realized that despite shortcomings, one aspect of the test had considerable merit. This desirable aspect was the production of a characteristic pattern that could be recognized by the experienced criminalist (O'Hara, 1976, pp. 772-779). Despite this opposing viewpoint, the test was, for the most part, completely abandoned by the law enforcement and forensic science communities.

The paraffin test for propellant residues containing nitrates was replaced with microchemical and instrumental techniques which were used to identify and determine the levels of particular elements, generally antimony (Sb) and barium (Ba), which are found in bullet primers. Harrison and Gilroy (1959) first proposed microchemical methods for this purpose. Because of problems with

sensitivity in actual casework samples, the microchemical methods were replaced by instrumental methods for accomplishing the same type of bulk analyses. These methods, such as Neutron Activation Analysis (NAA) or Atomic Absorption Spectroscopy (AAS), were specific for the elements and were excellent tests for both chemical identification and quantitation purposes. However, the material for examination was sampled from the hand by washing with water or swabbing with dilute acidic solutions. The process of removing the gunshot residue, which was effective for the purpose for which it was designed (high recoveries) actually obliterated, if present, the characteristic gunshot residue pattern. Thus, an important interpretative feature may have been destroyed. With this arrangement there is no pattern evaluation capability available to the criminalist, no matter how sophisticated or complex the instrumental technique used to identify and quantitate the GSR-related elements. Ba and Sb are not unique to GSR. Studies of the hands of non-shooters, known as "hand blank studies", have found significant levels of these elements (Cornelius & Timperman, 1974). This has made it necessary to set somewhat arbitrary threshold levels below which a case is called inconclusive. Unfortunately, in many experiments, the levels of Ba and Sb from known shooters are below some hand blank levels and the threshold level. Instrumental methods of bulk analysis for detecting propellant residues in forensic science casework have also been proposed but have not been perfected for practical use.

Recently, some researchers have proposed the use of micellar electrokinetic capillary electrophoresis (MECE) to address the problem of identifying the presence of the organic propellant residues (Northrop et al., 1991,1992). This technique, too, suffers from a lack of pattern distribution information, that is the distribution of the residues on the hand surfaces are destroyed by sample collection and preparation. Since MECE does not provide a molecular identification, it suffers from a lack of specificity. Additionally, some of the components of propellants and residue are used commercially for other purposes, such as plasticizers and antioxidants.

Another technique for the analysis of gunshot residue particles is Scanning Electron Microscopy (SEM) which is typically coupled with Energy Dispersive X-ray Spectrometers (Nesbitt et al., 1974). This system allows the examiner to identify the characteristic morphological features of GSR particles and to confirm their identity by elemental analysis. In contrast to the earlier methods, this SEM method allows a definitive identification of GSR particles. Unfortunately, analytical expediency dictates a sampling technique in which the particles are concentrated in a small area as they are removed from the hand surface. Of course, this process destroys the potentially characteristic distribution pattern. One modification of the SEM approach which records the distribution of the particles was proposed by Gansau & Becker (1982). Their proposal consists of tape-lifting portions of the hand. These areas were the thumb, forefinger and outer edge. For some reason the web area of the hand

was omitted from their work. They utilized ten 1mm wide "tracks" across the width of the tape for analysis. Up to two hours might be used for examining one of the sampling tapes. In practice, even longer times may be necessary in casework. The drawback here is obviously the length of time involved for analysis. It is not the validity of the chemistry of the aforementioned instrumental techniques which is being questioned, but, rather, the forensic applications. Thus, sophisticated, expensive techniques may not even be worth pursuing. Large amounts of resources have been consumed for research attempting to find the ideal approach to detect and interpret GSR on the hands of suspected shooters. Even larger sums of money have been expended for equipment and personnel costs in connection with actual casework with little or no return of value. Other researchers have found, under laboratory conditions, that GSR is often not found on the hands of known shooters when it was expected to be present. These seemingly inexplicable results could stem, in part, from movements of the shooter's hand during or immediately after the discharge of the weapon. This explanation is valid if the GSR cloud moves back toward the shooter at a relatively low speed. Concepts of this nature have not been carefully considered in the past. High speed photographic experiments have shed light on this question and have the potential for saving the criminal justice system enormous resources. At the very least, such studies enable prosecutors to explain why gunshot residue was not detected on a suspect's hands. The lack of gunshot residue is often utilized by defense attorneys to

indicate their client's innocence. These experiments can help explain seemingly inexplicable laboratory results which can often inappropriately influence a jury.

Empirical studies that would explain the formation of the gunshot residue "cloud" as it leaves the weapon and interacts with targets would be helpful to an understanding of the dynamics involved. Clearly, many nagging questions still exist, such as the one discussed above. There have been some attempts to describe the formation of gunshot residue but the mechanism is still the subject of debate in the forensic scientific community. Relatively little research has been done to describe GSR dynamics, especially in North America. Basu et al. (1997) claimed that if the firearm is thoroughly cleaned prior to discharging, the residues of the muzzle blast "seldom settle from the air onto the shooter's hands." They used scanning electron microscopy and energy dispersive X-ray analysis to examine glue lifts of the hands of shooters after alternately blocking muzzle blasts and trigger blasts (claimed or assumed to exist) to separately study their influence on hand deposits. The existence of a trigger blast has never been proven. It is difficult to see in theory how it exists. Additionally, they apparently did not consider the possibility that an interrelationship exists between the muzzle blast and the claimed trigger blast. An artificial separation of the two mechanisms, assuming the existence of a trigger blast, as reported in their paper, may likewise produce an unrealistic hand deposit of gunshot residue. Further they claimed that "...if the gun hasn't been cleaned the residues of previous discharges are blown off through the breeches and the

muzzle. These residues occasionally overlap with the fresh breech deposits of the shooter's hands." It would be a rare instance indeed for a criminalist to know if a weapon had been thoroughly cleaned before discharge.

Some high speed photographic studies have been done in Europe. Lichtenberg, a German researcher and forensic scientist, in a detailed, twenty-five page review of methods for determining the muzzle-to-target distance, discussed GSR dynamics in brief fashion, although he himself had conducted high speed photographic studies (1990). He reported that he did not find "..any indications that gunshot particles move along in the turbulent region at the base of a high velocity particle." Lichtenberg's comment was made in response to findings by other authors which presumed that a vacuum zone exists around high speed projectiles that is able to transport gunshot residue relatively long distances. Another German researcher and practitioner, Ruprecht Nennstiel, has utilized high speed photography to illustrate a bullet's passage through a piece of soap. Nennstiel's intent was to demonstrate how high speed photography was useful in studying the movement of gases emerging from the discharged weapon and the effect they have on objects in close proximity. He found soap particles in the barrel of the weapon and likened this to the situation where tissue is found in the barrel when a weapon is fired at skin. He also illustrated how high speed photography could be used to study the production of marks on cartridge cases by semi-automatic pistols. He further indicated that he had studied shotgun ammunition (slugs & pellets) via high speed

photography. Nennstiel advocated the use of Schlieren photography or shadowgraphy to study muzzle blast phenomena. The illustrations published in this report were of photographs taken within several inches of the muzzle (1983). A considerably less impressive sequence of high speed photographs of a muzzle blast and bullet was recently published by Beijer (1994), a forensic scientist from The Netherlands.

The entire dynamic process of gunshot residue formation and the mechanics of deposition were studied in detailed experiments and reported in this work. Additional research in the future should be conducted under different experimental conditions. There are several related issues concerning the dynamics of propellant particles in general. Prior to the research reported here there were no studies concerning the magnitude or distribution of velocities obtained by propellant particles. Most of the published photography has been taken in close proximity to the muzzle. While this is certainly of great importance, studies downrange appear to be lacking. There does not appear to have been any serious discussion of how fast the propellant particles decelerate. Additional questions that needed to be considered were the influence of wind, movements of the suspect or victim, and other factors, on particle behavior. Similarly, there has been essentially no discussion in the forensic science literature considering how quickly the fine lead cloud moves away from the shooter, or how rapidly it moves backward toward the shooter. There remain many questions to be posed and answered through such

research. Using detailed, high speed, single and multiple-flash (stroboscopic) photographic and videographic methods, this study aimed to address these questions and help provide a stronger scientific basis for shooting reconstructions.

Muzzle-to-Target Distance

As indicated earlier, another important aspect of the scientific investigation of shooting incidents is the determination of the "muzzle-to-target" distance. This examination has important implications in criminal investigations since the determination of this distance can help refute or corroborate an alibi of a suspect, or help confirm whether a death, by gunshot, is the result of a suicide or homicide. Little fundamental research has been done in this area.

It is reported that Goroncy conducted the first systematic studies for estimating the muzzle-to-target distance (Walker, 1940). In 1928, he incorporated the already well-known diazotization-coupling "Griess Reaction" to detect nitrites which are produced from incomplete combustion of ignited gunpowder particles. The method suffered from one serious drawback, that is, no pattern distribution information was provided.

Walker, in 1937, recognized the weakness of the Goroncy approach and devised a method for providing the spatial information that is essential to an adequate interpretation of the gunshot residue pattern (Walker, 1940). This kind of method is regarded as a "mapping" technique of the distribution of the

particles. The "Walker Test" involved a transfer of the reaction product or propellant particles to desensitized photographic paper previously treated with the diazocoupling reagents. Thus, the color reaction of the particles and the overall pattern of particles could be observed unhindered by the color of the fabric.

Modern day methods for the estimation of the muzzle-to-target distance have not changed in any significant way over the past fifty-eight years. A number of minor modifications of the "Walker Test" concerning the reagents have been proposed, but the basic transfer or "print" method itself became the mainstay of most laboratories involved in gunshot residue examinations in the United States (O'Hara & Osterburg, 1949; Dillon, 1990a; Steinberg, 1984). There has been some movement toward reliance on instrumental methods, especially in Europe (Lichtenberg, 1990), but this trend has done little to significantly improve the overall process (Maehly & Stromberg, 1981). Recently, Brazeau & Wong (1997) proposed using X-Ray Microfluorescence to map the elemental distribution of metals in gunshot residue around bullet holes in clothing and skin. However, it is not clear that large patterns on fabric could be analyzed in such a manner since the scans they presented were only 6 x 6cm in area on a piece of paper. Furthermore, it is not likely that many laboratories would be in a position to purchase the requisite equipment. Unfortunately, too, the organic portion of propellant, which is the major constituent of such particles, is not detected by the proposed method. The less sophisticated

Walker Test is a more accurate method than most instrumental ones because an entire, generally characteristic pattern is being interpreted. However, early researchers did not adequately prove whether or not transfer visualization methods are efficient. In addition to the "Griess Test" for nitrites a commonly used method for the detection and interpretation of lead is the "Rhodizonate Test" (Dillon, 1990c, pp. 257-268). It is carried out in a manner similar to that for the nitrites, and generally in sequence after the Griess Test has been carried out. The transfer and visualization methodology utilized for both these tests is not always efficient, and may prevent subsequent examinations. The reasons for this with respect to propellant residues and lead are different. With respect to lead it is rarely quantitative, even with the sheerest of fabrics. Bashinski et al. (1974, p.5) have found that a preferred approach is to directly apply the reagent, since only a "fair portion" of the lead is transferred. However, a direct approach is only feasible on light colored fabrics when the lead rhodizonate complex is visible. Until now, despite these drawbacks, a transfer method was required for dark fabric. Various grey fabrics are particularly problematic for the direct detection of lead associated with bullet wipe or vaporous lead. The rhodizonate reaction complex is quite difficult to detect on dark fabrics in general. In the case of testing for nitrites using the Griess reaction, an intermediate in the reaction is gaseous. This gas diffuses to the reaction sites on the test paper. Transfer efficiency, per se, is not a problem. However, in the case of visible particles some may make contact but yield no

reaction with reagents. Reactions with certain particles may provide a color whose intensity falls below the limit detectible by the human eye. Not all the particles necessarily make contact with the chemically treated paper. Some particles may actually be driven further into the fabric matrix when pressure is applied for testing. This latter situation is not a function of the Griess reaction itself, but the way in which the mechanism of the transfer takes place.

Research Questions Studied

A high-speed photographic and videographic study of the formation and motion of gunshot residue was conducted. The following questions were studied: What velocities are attained by projected propellant particles? What is the distribution of these velocities with respect to the muzzle? What is their rate of deceleration? Can the propellant particles penetrate or perforate clothing? Do these particles sometimes have unpredictable or surprising trajectories? How quickly does the fine lead-containing cloud move away from the shooter? Is there a retrograde cloud and how rapidly does it move backward toward the shooter? The overall dynamics of both cloud and particle behavior was studied. What implications does the information generated from this study have for crime scene reconstruction?

Are currently used transfer methods efficient or is a sequential integrated approach in conjunction with a direct method better? Can existing transfer methods be improved by utilizing a photoluminescence method for the

examination of the transfer paper to lower the limit of detection?

Would a direct photoluminescence method for estimate of the muzzle-to-target distance be more valuable than a transfer technique, or should it be used in an integrated fashion with a conventional technique?

High Speed Studies

A commercial, multiple arc microflash unit was purchased for the high speed photography of gunshot discharges. The most important components of this equipment are atmospheric pressure argon discharge arcs that deliver carefully timed sequences of an extremely short burst of intense visible light. A flash possessing an extremely short flash duration, approximately a half a millionth of a second, is very important for obtaining crisp photographs for study of the rapidly moving projectiles and gunshot residue particles that are traveling at relatively high velocities. A vibration sensitive detector mounted on the weapon was used to trigger the flash sequence. A sequencing accessory was utilized to select and control the lengths of each of the intervals between successive light pulses. Repeatable delays from microseconds to seconds are possible with this device. The use of three or four sequential flashes at precise time intervals is valuable for observing GSR formation. Multiple images of residue cloud fronts were photographed. The interpretation and examination of these photographs permitted the calculation of velocities and rates of deceleration at different distances from the weapon. Further, as a result of the

high speed photography, the effect of turbulence was observed and the behavior of self-propelled powder particles on residue deposition was described.

Velocity data was acquired from three common caliber bullets; 9mm, .38 special and .357 Magnum calibers (nine different sources; three of each type were studied). Six of these (three 9mm sources, and three .38 caliber sources) were plotted on an X/Y rectangular coordinate system relative to the muzzle. The x-axis represents the distance from the muzzle up to a distance of beyond forty-eight inches, and the y-axis represents the distance above and below the muzzle. Although the 357 Magnum-type ammunition was also studied in detail, the number of propellant particles was often so great that it was not possible to accurately measure distances between images on photographs. However, some data was obtained from these sources and is presented in the form of a table.

In addition to studying the distribution of particles via high speed photography, particles were also studied from their patterns of deposition. Ammunition was discharged at cloth placed at twelve inch intervals from the muzzle of the weapon up to a maximum distance of about four to five feet. The resulting GSR patterns were studied and compared to the results obtained from the high speed photography.

The movement of both the muzzle and retrograde cloud were also studied via single and multiple flash photography. Additionally, the movement of the retrograde cloud was observed by videography.

Muzzle-to-Target Distance

Critical Assessment of Transfer Methods

There are general questions that need to be considered regarding the commonly used transfer methods. How efficient are the most commonly used transfer methods, that is, the Modified Griess Test and the Rhodizonate Test? In the case of the Modified Griess test, what percentage of particles present on the substrate bearing the GSR pattern produce a color reaction with the diazo/coupling reagents on the test paper? Does a color reaction have sufficient sensitivity, and do a large percentage of reaction sites remain undetected? These questions were studied. A variety of ammunition was discharged at a shooting distance of about twelve inches onto white fabric to facilitate the counting of particles. The same patterns were subjected to the Modified Griess Test procedure, and the results compared with a visual stereoscopic examination. The Rhodizonate transfer procedure was also critically assessed.

Direct Photoluminescent Method

To improve the state-of-the-art in the determination of the muzzle-to-target distances, a photoluminescence method to visualize the gunshot residue pattern directly around the bullet hole was developed. A number of possible sequential integrated methods were identified. One of these methods involves an examination for native fluorescence followed by one for photoluminescence

after chemical treatment. From a chemical treatment perspective, the ideal reagent for the visualization process would not be fluorescent but would produce a fluorescent product after reaction with specific components of gunshot residue which could then be easily distinguished from the cloth substrate. The possibility of using a series of sequentially applied reagents or wavelengths was explored. In actual casework, the developed pattern would then be photographed and its components subsequently identified by microscopical or instrumental techniques. The reacted particles can still be positively identified by traditional methods. In addition, some success was achieved with a method for causing propellant particles to fluoresce natively (without chemical treatment) by exciting them with radiation from a tunable high intensity light source (THILS). In an actual case, the fluorescing pattern would be photographed or videotaped. Particles comprising the pattern would be selected at random and identified by instrumental means if considered necessary. This is discussed in more detail subsequently. While image intensification methods were not explored in any detail during the course of this research, it should be recognized that this technology can be readily applied to any of the methods developed here, to increase the ability of the examiner to detect photoluminescing species that comprise a gunshot residue pattern.

The choice of excitation source for photoluminescence is critical. At the outset of this research, a light source (Omniprint 1000) was utilized that is commonly used by crime scene examiners for detecting latent fingerprints,

fibers and other trace evidence. While this unit was of value for particle fluorescence its use was limited since the range of tunability was narrow and the excitation source was weak. This light source was compared to another more recently available commercial unit and the difference in results was found to be dramatic. If the source of excitation is weak, the subject will not provide visible fluorescence. Subsequently, the much more powerful unit, manufactured by Spex Industries, which is capable of fine tuning over a wavelength range from about 400nm to 670nm, was purchased. This unit, marketed as the Crimescope (CS-16), has a 300W Xenon Arc energy source, and 25 excitation filters. Sixteen of these are bandpass filters. Fine tuning is achieved by rotating the filters about an axis normal to the light path. This arrangement, using interference filters, results in greater energy output than is achieved with grating monochromators used by some manufacturers. A relatively large diameter (10mm) liquid light guide is used with the CS-16 instead of the fiber optic cord (8mm) commonly supplied with such equipment. The larger diameter guide permits considerably more energy to reach the subject. Selected excitation wavelengths are read out on a digital display. Two relatively powerful sources of ultra-violet radiation were also purchased from Spex Industries and Spectroline Co. Interference barrier filters were purchased for observing the emissions.

Native Fluorescence - Propellant Particles & Nitrites

The approach here was to use a tunable high intensity light source to

produce fluorescence in discharged propellant particles at relatively short excitation wavelengths and photograph or videotape the emission at longer wavelengths. The intensity of the radiation from the light source as well as the excitation wavelength bandwidth is very important. Excitation wavelengths used with success were 254nm, 365nm, and in the range of 400 to 535nm. The partially burned propellant particles are known to contain a relatively high concentration of nitrites (Dillon, 1990a & b) which are known to form nitrous acid under acidic conditions. These particles can be identified with the Griess Test (Feigl, 1937/1975, p.683).

To assess the general utility of the native fluorescence method, it was compared directly to the method conventionally used in criminalistics laboratories now, that is, the Modified Griess Test. For this study, about forty different GSR patterns were produced, from different ammunition, calibers, and so forth. One quadrant was selected from each pattern for examination, or an entire pattern. Discharges were made at a muzzle-to-target distance of twelve inches to eliminate interference from the fine lead deposit. Each pattern contained several hundred to approximately three thousand particles. To compare the results of the examination directly, each pattern was examined for native fluorescence. Wherever a fluorescent GSR particle was detected, a corresponding mark was placed on a transparent overlay. After this step was completed, the Modified Griess Test was conducted in the usual manner and the results compared with the fluorescence results. Counts of the fluorescent

particles v. color reactions associated with particles on the paper were the main criterion for comparison of the effectiveness of the two techniques. The Griess test paper, after transfer, was saved for subsequent examination for fluorescence.

Additionally, reference standards of the compounds that are commonly present as additives in smokeless gunpowder were purchased and examined, in the solid state, to determine if they exhibit native fluorescence. This study helped assess the general utility of a native fluorescence method. Also, additional smokeless gunpowders that are sold in bulk were purchased and were examined for native fluorescence. Some of the powders that were examined were taken from commercially loaded cartridges.

Low Temperature Enhancement - Photoluminescence of Particles

A series of experiments was conducted at liquid nitrogen temperature to determine if there is an increase in differential fluorescence of particles at low temperatures. These observations were found to be consistent with the theoretical concept that fluorescence efficiency decreases with increased temperatures (Hercules, 1966, pp. 28,29,52). At very low temperatures, phosphorescence was also observed. The fluorescence of propellant particles, excited in the range of 455-500nm, was found to increase considerably after being cooled from room temperature to liquid nitrogen temperatures.

Gunshot residue patterns on fabric were produced from the discharge of

ammunition from the major ammunition manufacturers comprising about twenty five different sources. Two quadrants from each were compared visually at room and liquid nitrogen temperatures. The difference in results were obvious. Several patterns were also photographed under the same conditions at room and liquid nitrogen temperatures. The number of particles detected in each quadrant was counted and compared via photography. Additionally, the fluorescence intensity of particles from the selected quadrants was measured and compared. This was accomplished by photographing the fluorescence of particles at room and liquid nitrogen temperatures. The photographic images were digitized and then placed on a floppy disk using a high resolution scanner. Utilization of imaging software permitted the measurement of pixel intensity of the individual particles on a PC. Another method used to compare particle fluorescence intensities was to compare the photographic images with a densitometer. Unfortunately, the latter approach was found to be considerably more tedious and difficult than the software method which was also quite tedious. Thus, after preliminary examination the densitometer approach was abandoned.

Photoluminescence - Post Reaction

The following reagents were studied to determine if they would be of value in producing fluorescence with nitrite in gunshot residue:

1. Griess
2. 2-aminophenol & resorcinol

3. p-chloroaniline & 2,6-diaminopyridine
4. Coumarin 120

In order to properly assess the utility of each chemical treatment, a model series of experiments was used as described below. This phase helped determine whether it was worthwhile to continue on to the next phase of the experimentation. Prior to experimenting with partially burned propellant particles in Phase I, the above reactions were subjected to preliminary examination using inorganic nitrite. Some chemical methods were excluded from such detailed experimentation because of specific problems, for example, their negative controls exhibited significant fluorescence that could not be reduced without chemical extraction or separation.

Phase I: Initial Evaluation

The protocol utilized was:

1. Using ammunition from the major manufacturers, from a variety of sources (five different powders), discharge patterns were produced at the same distance (12") and on the same type and color fabric.
2. Representative particles were removed from one quadrant from each pattern.
3. The particles were subdivided from this quadrant into groups that gave differing gross appearances. For example, all the pale yellow particles were placed together in one group, the black ones into another, and a mixture of light and dark into a third group.

4. Each group was placed into separate wells of a ceramic or glass spot plate.

5. One well of spot plate had all the reagents (solvent, and so forth) present minus the fluorescence reagent itself. This allowed the determination of any fluorescence that may be due to some unknown chemical or physical reaction. For example, it was found that the application of solvent and physical manipulation, heat, and so forth, can remove opaque material from the surface of the particle and expose fluorescent material. The mixture of the light and dark particles were placed into this well.

6. Photography:

   a. the particles were placed onto a non-reflective black cardboard surface and photographed using white light, and no filters, to demonstrate their appearance prior to chemical treatment.

   b. the particles were then photographed for native fluorescence without being moved from the cardboard.

   c. the particles were transferred to ceramic or glass plates and reagents applied.

   d. the excess reagent was removed and the particles washed with water.

   e. the particles were returned to their original position on the cardboard prior to chemical treatment.

   f. the particles were photographed under the same condition as before chemical treatment.

7. The fluorescence intensities of each particle were compared before and after chemical treatment. The comparison was conducted in essentially the same manner as was done for the room vs. cold temperature experiments, using the imaging software.

8. If deemed worthy of further study, subsequent phases of evaluation were conducted.

Phase II. Direct Application onto Pattern

The next step was to remove another quadrant of each discharge pattern and initiate the chemical reaction as previously conducted.

1. This was done to evaluate the differential contrast between the particles and the substrate.
2. Any deleterious effect on the substrate was noted. A variety of fabrics was likewise tested for such effects with chemical treatments considered of utility for observation of photoluminescence.
3. The number of particles detected with the direct application technique was counted, and compared against the Griess test results from another quadrant.

Phase III. Evaluation of Results & Other Considerations

In the final phase of the experimentation, the specificity of the reaction of the chemical treatment was considered: (a) within the context of pattern

recognition, and (b) relative to the Modified Griess test. These methods were considered in regard to the feasibility of conducting subsequent examinations for lead. Integrated sequential approaches were studied and are discussed in the final chapter.

Chemical Treatment for Photoluminescent Detection of Lead

HCl, low temperature

Hydrochloric acid was studied as a reagent for the direct application to the target to determine if it would be of value in producing fluorescence with lead and other metals in gunshot residue. The application of hydrochloric acid was originally intended for experiments concerning the fine lead deposit. However, it was found that it also produced photoluminescence with particles. Thus, the behavior of this reagent with particles was further evaluated.

Integrated Sequential Method for Muzzle-to-Target Estimate

A carefully selected sequence of the aforementioned methods could be utilized to maximize the amount of information collected from a GSR pattern with minimal sample destruction. Each step could easily be documented by photography or video recording. The criminalist would then be free to conduct classical chemical examinations such as the Griess or Rhodizonate Tests. Experiments involving sequential integrated methods were conducted and are discussed in the final chapter.

Chapter Two

Theoretical Considerations: Luminescence Theory

When light interacts with matter the energy of the incoming radiation may be partially or wholly transmitted, absorbed, or reflected. Energy that is absorbed is transferred to molecules placing them in the so-called excited state. This energy, acquired by the molecule, can be given up as a result of inter-molecular collisions in the form of heat as a radiationless deactivation (Hercules, 1966, pp. 28-29) and the molecule returns to ground state. Many molecules, however, release a portion this energy in the form of another photon before returning to ground state. The electron, after being promoted to a higher energy level by the radiation that was absorbed, first drops to an intermediate vibrational level. If the molecule should now liberate the remaining excess energy as a photon the energy released will be less than that absorbed. Thus, the emission will be at a longer wavelength than the exciting radiation. This is the most commonly observed situation with re-emission. The emission of photons, which possess a longer wavelength (less energy) than the photons that were absorbed, is referred to as "Stokes Fluorescence" (p. 6, Guilbault, 1973).

The process of releasing energy in the form of photons, after excitation from electromagnetic radiation, is commonly referred to as photoluminescence. If the excitation source is removed and the emission ends within 10^{-9}-10^{-7}

seconds, the process is called fluorescence. If the emission takes longer to cease the process is referred to as phosphorescence. Phosphorescence lifetimes range from microseconds to hours. For phosphorescence to occur, there must be a change from the excited singlet state (paired electrons) to the triplet state (involving a change in electron spin) by intersystem crossing. The electron spin must change again for an emission of a photon and a return to the ground state. As a result of collisions with other molecules, in solution, some of the excitation energy may be transferred to another molecule, or to a solvent molecule, and lost in the form of heat. In solutions, the number of collisions increases as the temperature is increased, which result in a radiationless loss of the energy of excitation. For many molecules to phosphoresce, it is necessary to form rigid glasses of solutions (at liquid nitrogen temperatures) to reduce the frequency of intermolecular collisions. The above concepts served as the impetus for attempting experiments with gunshot residue at low temperature, both natively and after chemical treatment.

In summary, the phenomenon of fluorescence takes place by the molecular absorption of a photon of light raising the electron to a higher energy level. The change of the electron, placing the molecule in the excited state, is comprised of electronic, vibrational, and rotational transitions. If the increased energy does not cause the decomposition of the molecule, and if all the energy is not given up by molecular collisions, a photon will be emitted when the electron returns to the lower energy level. The energy of the emitted radiation is

determined by the difference between the final state and the initial state. This emission, known as fluorescence, has lower energy (longer wavelength) than the absorbed light (Undenfriend, 1962, pp. 11-12).

The shift to the longer wavelength for emission, as a part of the process of fluorescence and phosphorescence, provides a convenient tool for the forensic scientist to use in attempting photoluminescence experiments. By careful selection of excitation source wavelength, as well as by use of barrier filters, the unwanted shorter wavelength radiation can be blocked, allowing the less energetic, longer wavelength radiation to be observed. Thus, this system allows for differential contrast to be observed between the substrate and the material under study, when the substrate does not fluoresce significantly in the same region of the electromagnetic spectrum.

Chapter Three

Apparatus

Thermocouple Thermometer

Cole Parmer Instrument Company, Vernon Hills, Illinois. Digi-Sense®, Model No. 8528-20, "T" type thermocouple for -250 to 400°C designed for precision measurements at low temperatures was used for low temperature experiments. It was calibrated according to manufacturer's directions with boiling water.

High Speed Flash System consisting of flash (Palflash 500), sequencer (Palseq), and trigger (Mazof VIS II)

Palflash 500:

Photonics Analysis, Ltd. Waterloo, Ontario, Canada. Purchased from The Cooke Corporation, Tonawanda, New York. The Palflash 500 is a short duration spark gap light source designed for photography of rapidly moving objects. It utilizes discharge arcs that deliver an extremely short burst of intense visible light (Figures 1-3). All experiments reported here were conducted in conjunction with a flow of argon gas through the gap of the electrodes. A flash duration of approximately 500 nanoseconds was selected to permit crisp photographs of projectiles and gunshot residue particles traveling at relatively high velocities. A vibration sensitive detector was mounted on the weapon being discharged to

trigger the flash sequence. See Figures 4 and 5 for diagrams of the entire system and darkroom setup. Optics: coated relay lens between each spark gap. The output condenser is adjustable. The light output is collimated with a 90mm focal length lens.

Palseq Sequencer:

Photonics Analysis, Ltd. Waterloo, Ontario, Canada. Purchased from The Cooke Corporation, Tonawanda, New York. This unit is a sequencing device used to select and control the duration of each interval between successive light pulses. Repeatable delays from microseconds to seconds are possible. Up to four sequential flashes at precise intervals were used.

Mazof Trigger:

Mazof Inc. England. Purchased from The Cooke Corporation, Tonawanda, New York. Model VIS II trigger. The trigger was used to initiate the circuit to trigger the Palflash. This is a multi-sensor unit designed for high speed photography. It has a built-in sound receiver, a wide spectrum optical sensor, and a vibration probe which is detachable. The vibration probe was used for all the results reported in Chapter Four, and the corresponding appendix. Early experiments were attempted with both the sound receiver and the optical sensor. Both these latter arrangements suffered from inconsistent behavior due, apparently, to ammunition variables. Additionally, it was difficult for the light beam, aligned normal to the bullet path and across the muzzle, to consistently trigger the circuit. Sometimes the interruption of the light beam by

the bullet was sufficient to initiate the circuit. However, in many instances, the early muzzle flame and cloud appeared to do this. Reasonably reproducible observations were not possible with either the optical or sound sensor (because of cloud interference and noise variation). The Mazof trigger possesses a built-in delay with three different ranges. The "F" range (2 microseconds to 0.5 milliseconds) was utilized, since it was designed to provide the fastest response for ultra fast events. It was always set on the minimum delay (2 microseconds).

The entire system was calibrated with the Tektronix oscilloscope on two occasions. The system was also calibrated by the manufacturer on two occasions (when a spark gap failed to discharge repeatedly). The behavior of the system was monitored regularly by the examination of the multiple bullet images in the photographs. If an image was missing, or appeared where it should not, the data from that photograph was not used. Also, as an additional check on the system, the muzzle velocity of the bullets was regularly calculated and compared to the nominal or published values.

Oscilloscope

Tektronix, Inc. Wilsonville, Oregon. Model TDS 340. It is a digital real-time unit used to calibrate the Palflash. It possesses a maximum sampling rate of 500 megasamples/second. 100 MHz analog bandwidth and fastest time base setting of 5ns/division. The calibration conditions were: rapid response photosensor attached to Channel One lead on oscilloscope. The Palflash was

manually triggered from the switch on the Palseq (sequencer). Timing on the sequencer was set at 200, 210, 220, 230 microseconds using 10X range (2000 to 2300 microseconds). This was the approximate setting selected for measuring particle velocities. Oscilloscope settings: Y-axis 100mv/box; x-axis 50 microseconds/box (see Figure 6). Channel One, slope = +, triggering level = 216mv. edge mode normal, holdoff = 500ns.

Tunable High Intensity Light Sources

Crimescope CS-16:

Instruments S.A. Inc. (Jobin Yvon-Spex) . Edison, New Jersey. Dual filter wheel system. 300W Xenon arc source. Automatic fifteen position bandpass filter wheel controlled with up/down push-buttons on front panel and on remote control located on hand grip of liquid light guide (Figure 7). Continuous fine tuning with knob on front panel between center wavelengths of excitation bandpass filters: 555, 535, 515, 495, 475, 455, 445, 430, 415 nanometers. Fine tuning is accomplished by tilting the filter. Manual contrast wheel with four edge filters, white light, shutters, and empty positions for additional filters. Liquid light guide for U.V. and visible light (six feet long, 10mm active diameter). U.V. system possesses 90 degree optics for broadband output from xenon arc (280-380nm). Emissions monitored with barrier filters (longpass) or longpass viewing goggles (see the appendix for transmission data for filters and goggles). This unit was used for most of the particle fluorescence results reported here.

The Omnichrome unit discussed below was used for preliminary experimentation involving particles, and for comparison of the two light sources as reported in Chapter Six (Native Fluorescence).

Omniprint 1000:

Omnichrome Inc., Chino, California. This light source was used for preliminary experiments prior to purchase of the Spex unit. Light source: 350 watt, metal vapor arc discharge lamp. Six foot fiber optic viewing cable. Its tuning is restricted to coarse adjustments at the following settings: 570nm, <530nm, 525nm, 485nm, 450nm, and white light.

Digital Flowmeter

Humonics Inc. Fairfield, California. Model Optiflow 520. This was used to measure argon gas flow rate for the Palflash 500 atmosphere.

Cameras & Related Accessories:

Various 35mm SLR cameras, lenses and tripods were used.

Digital Photometer

Eseco Inc., Cushing, Oklahoma. Model 2001 M-100A, Speedmaster. The photometer was used to measure the output of the light source (CS-16) for particle intensity experiments. These measurements were necessary, for calibration purposes, since the intensity of illumination, across the field, at

different particle positions was different. The data from such calibration was incorporated into the results reported in Chapter Ten (Chemical Treatments to Induce Photoluminescence).

Ultraviolet Light Sources (in addition to UV port on CS-16):

Spectronics Corp. Westbury, New York. Spectroline Model ENF-280C/12. Long Wave/Short Wave Combination. Long wave peak intensity: 470 microwatts/cm^2, short wave peak intensity: 650 microwatts/cm^2 at six inches. Housing dimensions: 8.3cm W x 33.7cm L x 6.4cm H).

Spectronics Corp. Westbury, New York. Spectroline Model R-51A. Short wave ultraviolet lamp. Purchased from Instruments S.A. Inc. (Jobin Yvon-Spex) Edison, New Jersey. Peak intensity: 1,000 microwatts/cm^2 at six inches. Housing dimensions: 8.3cm W x 19.5cm L x 6.4cm H.

Insulated Tray

An insulated tray was fabricated from styrofoam and a plastic housing (commercially available tray) to slow down the evaporation of liquid nitrogen. Dimensions of plastic housing: 46cm L x 33cm W x 13cm H. The styrofoam was placed between the stainless steel tray (used to hold the target and liquid nitrogen) and the plastic housing.

Video Lamp

A special lamp was constructed for video experiments reported in Section III (High Speed Photographic Studies). It consists of a sheet metal housing with halogen bulbs (300 watts each) recessed six inches (Figure 8). The lamp intensity is controlled with a dimmer switch. See Chapter Four for details regarding video camera.

Microspectrofluorometer

Farrand Optical Co., Valhalla, New York. Model MSA (Microscope Spectrum Analyzer). The microspectrofluorometer was fitted to an Olympus BH Microscope for reflected light experiments. The MSA was utilized to examine the native fluorescence of a variety of discharged propellant particles (see Chapter Six).

Spectrofluorometer

Perkin Elmer Norwalk, Connecticut. Model LS-S. The spectrofluorometer was used to examine the azo dye solution from the Griess reaction for fluorescence (Chapter Ten).

UV/VIS Spectrophotometer

Cecil Instruments Limited. Cambridge, England. Series 3000 Scanning Spectrophotometer. Wavelength Range:190-1000nm

Digital Caliper

Digimatic Model CD-6" BS. Mitutoyo Co. Tokyo, Japan. Purchased from Cole Parmer Instrument Company, Vernon Hills, Illinois. The caliper was used for measuring photographic images of particles, clouds, and so forth.

Handgun Machine Rest

Ransom Rest®. Ransom International Corporation. Prescott, Arizona. The handgun machine rest was used to safely and consistently hold whatever handgun was being discharged.

Steam Iron

General Electric Co. "Light n Easy" model. Unless otherwise indicated, the iron was used dry (no steam) on the cotton setting. The temperature at this setting was measured with the thermocouple thermometer. Based on 40 measurements, the mean temperature was found to be 301^0F (SD = 20^0).

Figure One: Diagram of a Single Spark Gap in the Palflash 500 (4-Flash System)

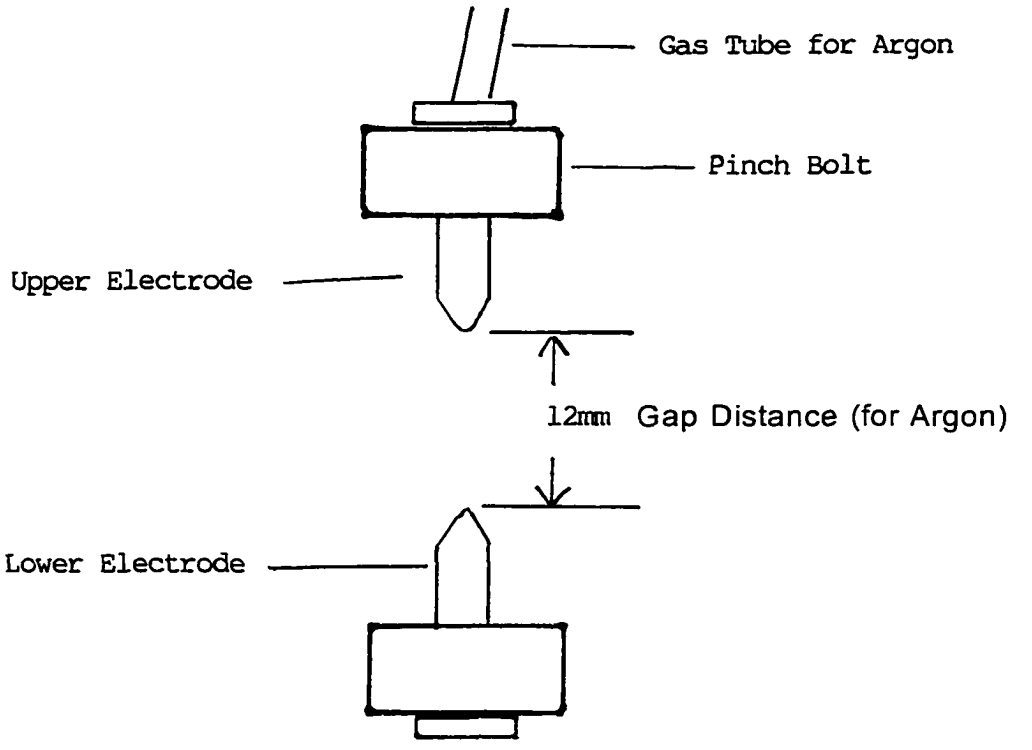

Figure Two: Optical Path of 4-Flash System

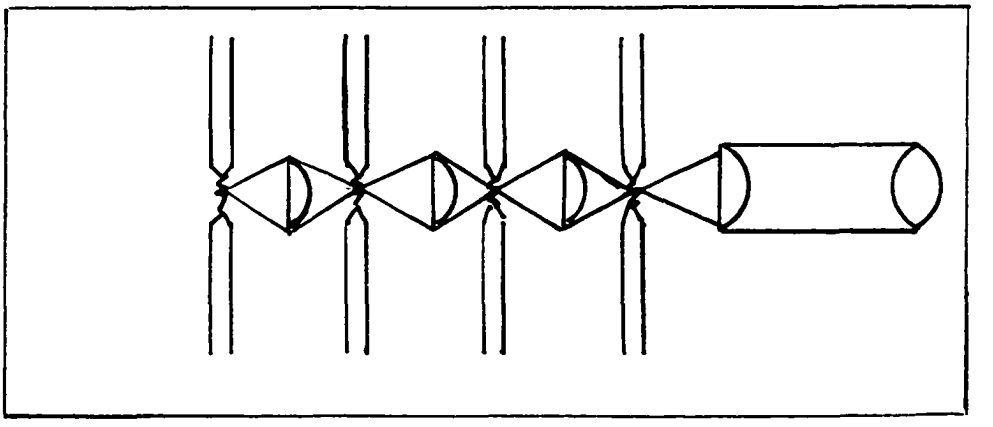

Figure 3. High Speed Flash Equipment

Palflash 500

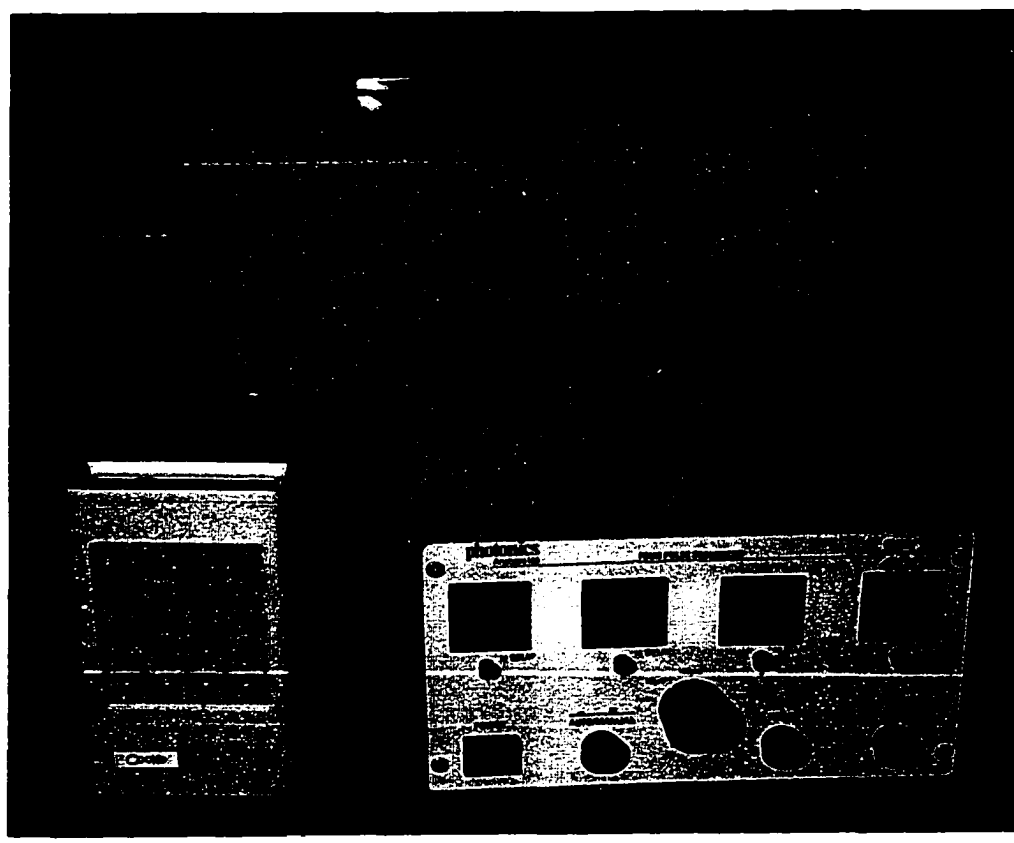

Mazof Trigger

Palseq Sequencer

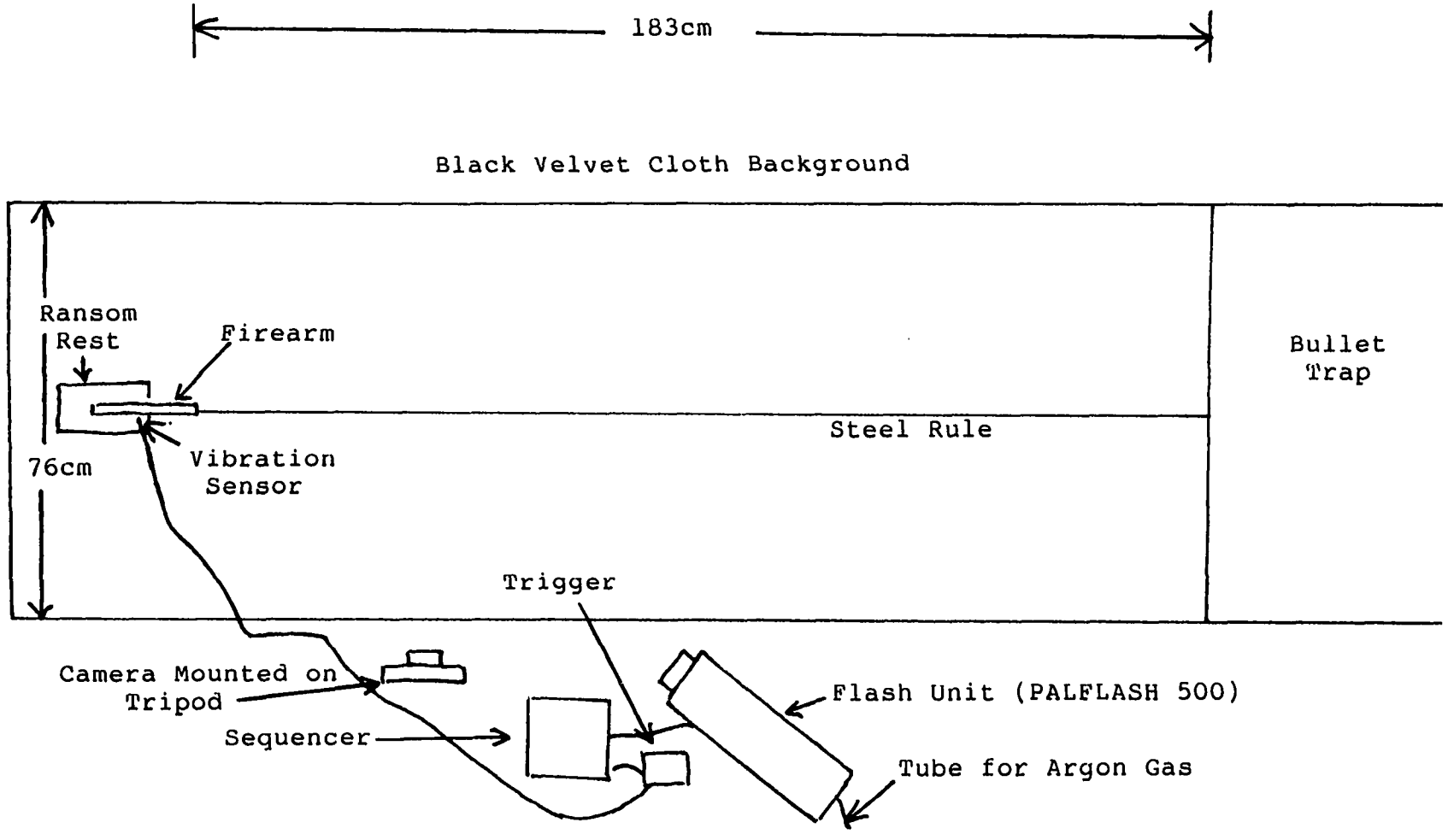

Figure 4. Diagram of Typical Photographic Darkroom Setup for High Speed Multiple Flash Photography

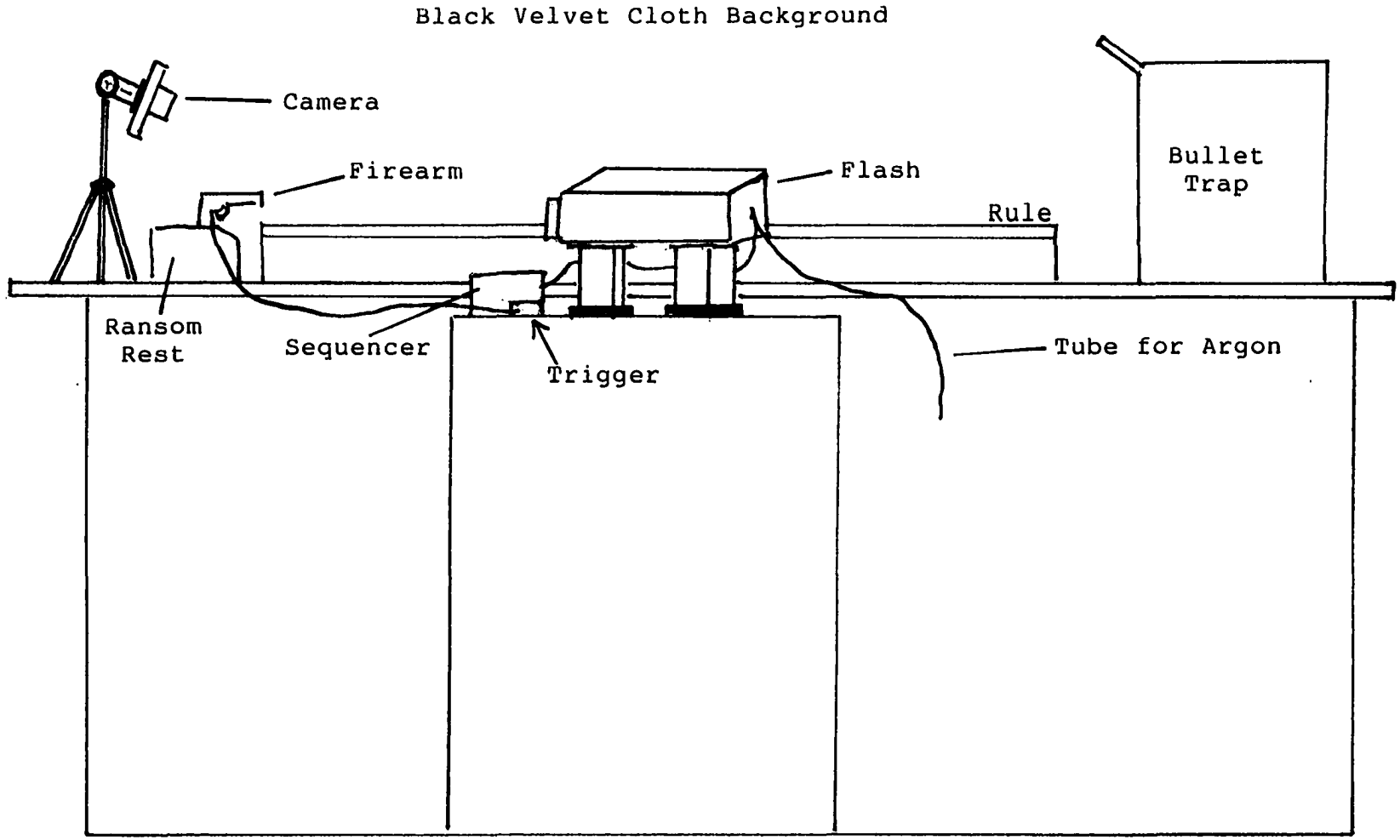

Figure 5. Diagram of Photographic Darkroom Setup for High Speed Multiple Flash Photography of Lateral Spread of Gunshot Residue

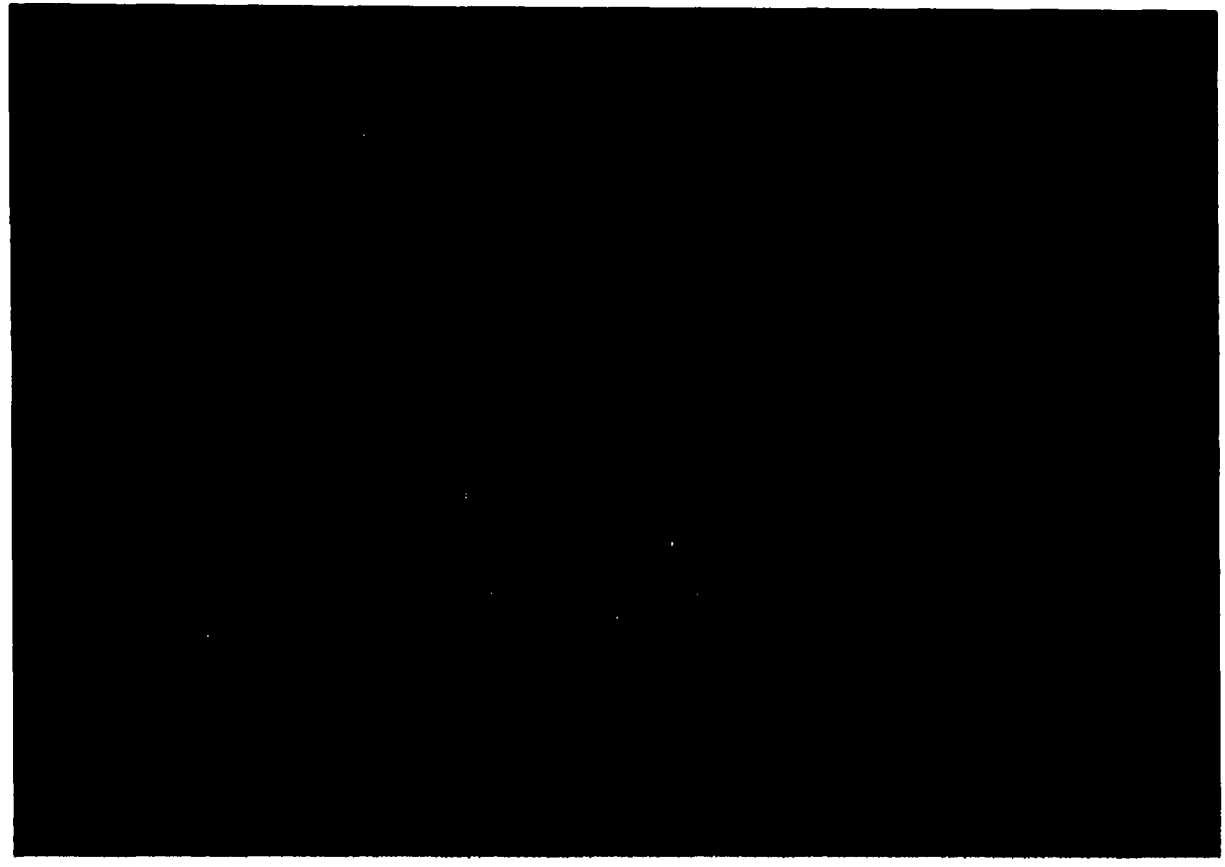

Figure 6. Photograph of Tektronix Oscilloscope Display During Calibration of Palflash 500/Palseq Sequencer (100 microseconds between gap discharges; 50 microseconds per division) Utilizing a Photosensor to Detect Spark Gap Discharge

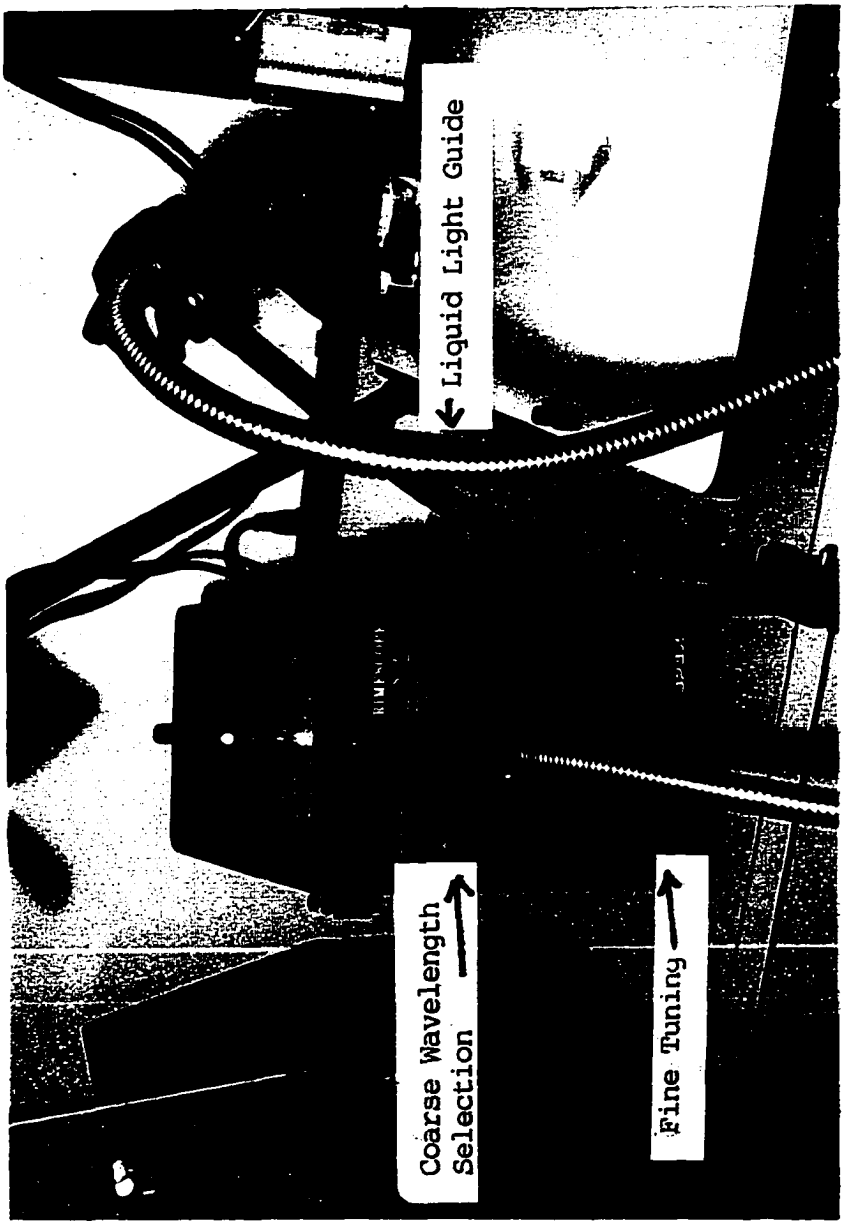

Figure 7. Crimescope CS-16 Tunable High Intensity Light Source

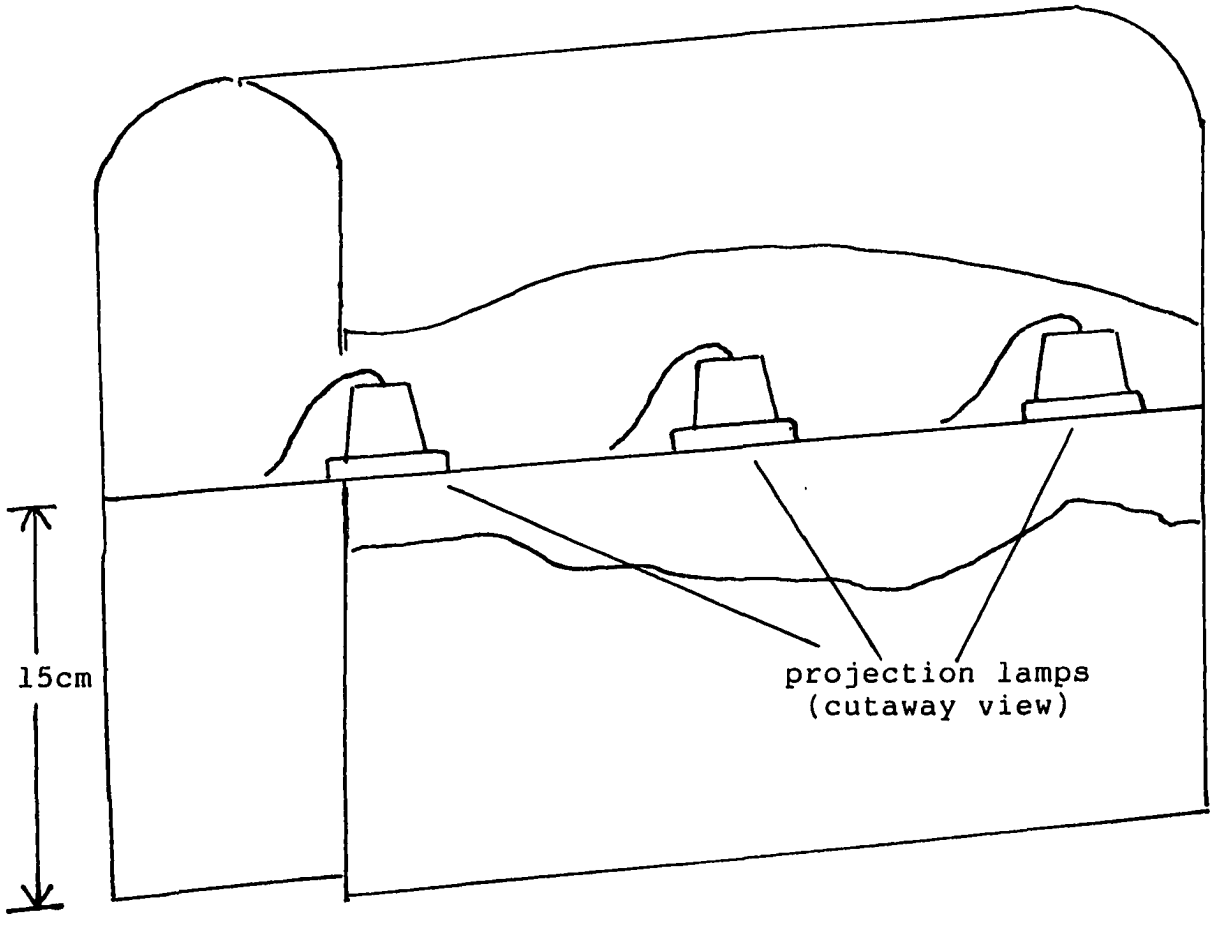

Figure 8. Fabricated Lamp for Videotaping Retrograde Cloud. Consists of Three Projection Lamps (300 watts per lamp) Recessed Six Inches in Sheet Metal Housing. Lamps Connected to a Dimmer Switch.

Chapter Four

GSR Cloud and Particle Dynamics

Both cloud and particle dynamics will be discussed in this chapter. A portion of this chapter is devoted solely to particles, whereas another section pertains to the movement and changes in the cloud of residue. Additionally, in another portion of this chapter, experiments involving the dynamics of both the cloud and particles will be presented and discussed.

Often, when taking the high-speed flash photographs, the bullet could be easily seen by the unaided eye within the range of several hundred particles. An excellent example of this is seen from the discharge of a 357 Magnum cartridge (Figure 9). This is true for both single and multiple flash photography. In the case of multiple flash photography, a corresponding number of bullet images could be recognized amongst a large number of particles, as in Figure 9. The ability to see the bullet in actual flight provided a valuable guide to setting up the equipment for flash delay, flash intervals, and the horizontal positioning of camera along the bullet trajectory. The observer also acquires a certain amount of knowledge or appreciation for the interrelationship of these objects, from seeing them in three dimensional space as they exist, a dynamic process that is difficult to demonstrate photographically.

Methods and Materials

Below is the basic equipment used for most of the experiments

presented and discussed in this chapter. The type of ammunition, and other specific items or exceptions are listed in each section that follows.

Palflash 500

Palseq Sequencer

Mazof Trigger

Camera: Pentax Spotmatic, 35mm SLR, f/1.8 lens

Argon

Tripod

Ransom Rest ® - gun rest used to safely hold and discharge the weapon

Video:RCA VHS Pro Edit camcorder (CCD solid state image sensor), manual shutter, manual focus, zoom lens 8-80mm 1:1.4

Lamp for videotaping cloud

Kodak Ektapress 400 (pushed 2X to ASA 1600)

Atmosphere: Argon gas, flow rate of 5-15ml/min.

Humonics Optiflow 520 digital flowmeter

Mitutoyo Digital caliper.

Tektronix Digital Real-Time oscilloscope, Model TDS 340

Basic Photographic Arrangement

The relatively simple arrangement used for the bulk of these experiments is illustrated in Figure 4. For the calculation of particle velocities the camera was positioned on a tripod with the optic axis of the lens perpendicular to the bullet trajectories. A non-reflective black velvet cloth, was used as the

background. The pistol or revolver to be used was affixed to a Ransom Rest®. The camera and flash were moved together horizontally to photograph particles at different distances from the muzzle. The distance from the muzzle was documented by means of a 48 inch steel rule placed on the bench with its zero position at the muzzle. The rule was oriented so that its longitudinal axis was aligned with the plane of the trajectory. For the preliminary set up the camera was focused on a wooden dowel protruding from the barrel of the firearm. A vibration sensor was placed between the frame of the weapon and the Ransom rest grip insert which holds the weapon. The wire lead from the sensor was placed into the corresponding terminal of the triggering device. The sensitivity of the trigger was adjusted so that the vibration from the hammer, when using revolvers, striking the weapon initiated the circuit. While the lights were on, the hammer was cocked. The room was partially ventilated between discharges and a complete change of room air was made with a fan after six discharges during the course of particle experiments. After the hammer was cocked, the lights were turned off. The camera shutter, which was set on the bulb ("B") position, was then opened with a cable release. The aperture was set at a stop of f/1.8. For this lens this setting provided the maximum amount of light to strike the film, and the minimum depth of field to reduce parallax error. The trigger was then gently squeezed. The hammer fell, the gun discharged, the flash fired, and the shutter was then closed.

Argon gas was used for all experiments to purge the atmosphere of the

Palflash and provide argon discharge illumination. The argon discharge allowed a significantly more brilliant flash output than a discharge in air. The flash also appeared to behave with more stability when using the argon gas, and provided a longer life to the gap electrodes. A flow valve was affixed to the gas line. The flow rate was set at 5-15 milliliters per minute using a digital flowmeter. This flow rate was maintained for all experiments, after some initial experimentation and optimization at different rates.

Several experiments were conducted to photograph the lateral spread of the particles. In this series of experiments, an additional camera was placed on a tripod directly behind the weapon. Figure 5 depicts the position and orientation of this second camera. The other aspects of the photography were conducted as previously mentioned.

After a number of experiments were conducted with a variety of different films, Kodak Ektapress 400 35mm film was selected and used for almost all experiments. A technical service representative from Kodak was also contacted to determine which film provided an adequate light sensitivity and possessed reasonably fine grain characteristics. Ektapress 400 can be "push processed" to ASA 1600 (two stops) using the traditional C-41 development process providing adequate sensitivity. Based on numerous experiments, grain characteristics of the film were considered excellent compared to other films of equal sensitivity, and the film was always push-processed two stops. If it was not pushed two stops, the particle images were much too faint to study and measure.

An entirely different set of conditions was used for the videography experiments to capture images of the retrograde cloud movement. Those conditions will be presented in the video section of this chapter.

Particle Experiments

The velocity of several hundred particles from eight different sources of ammunition was determined using multiple flash photography. The ammunition studied for this purpose was:

Winchester .38+P	CCI 9mm	CCI 357
CCI .38+P	Remington 9mm	PMC 357
Federal .38+P	MagTech 9mm	Federal 357

While the PMC 357 discharges were photographed as described, no calculations were made regarding this ammunition since the number of particles was too great to permit an accurate measurement (Figure 20).

The velocity distribution of the measured particles was plotted in a rectangular coordinate system as profiles for the six .38 & 9mm caliber bullets (Figures 10 -15). The x-axis represents the distance from the muzzle. The y-axis represents the distance of the particles above and below the firearm. Points were plotted from twelve inches to beyond forty-eight inches, corresponding to the distance from the muzzle, and a vertical range of about ten inches centered at the muzzle. It was generally too difficult, and inaccurate, to obtain measurements closer to the muzzle. At distances closer than twelve inches, particles were obscured by the cloud, flames and an over-abundance of

other particles. The data used to construct the velocity profiles are contained in the appendix. A selected number of particles from each ammunition were used to approximate the deceleration.

Velocity calculations were based on the distances traversed by particles, in most experiments, during the elapse of 100 microseconds. Only particles in good focus were used for measurement. A digital caliper was used to measure the distance between particle images to the nearest tenth of a millimeter. A fingerprint magnifier was used, in conjunction with a light box, to facilitate the measurements.

Results and Discussion

While these particles were found to decelerate rapidly, the velocities that many of them acquired was surprising. A large percentage of the particles photographed had velocities in the range of 750 to 1000 fps (Figures 10 - 15). Most of the particles that could be measured possessed velocities in the range of 400 to 800 fps (Table 2). Many of these particles can be seen surrounding the flight of the bullet as it moves forward (Figures 9,16-21, 23). It is also instructive to note the movement of the particles relative to the cloud propagation and the movement of the bullet (see Figures 23 & 24). The velocity of these particles can help explain the phenomenon of "stippling" found on the skin of individuals that have a gunshot wound from close range (within three feet). The rapid deceleration of the particles explains why they are not found far from the muzzle (Table 3).

Because of the high velocity many particles acquire from the discharge of the propellant, they can penetrate or even easily perforate relatively porous materials. Fabric is readily penetrated or perforated (Figure 22). Particles will exhibit varying degrees of size, and velocity. They can be found in large numbers below the upper surface of fabric. Particles will often be found well embedded within fabric between fibers. This behavior is greatly dependent upon the type of fabric involved. Although no particles may be apparent on the upper surface of a garment or upholstery fabric it should not be assumed that no GSR is present. While loosely adhering particles may have fallen or transferred to another surface, many others may be anchored quite effectively below the outer surface. The interior side of the fabric could possess an equal or greater number of particles than the surface facing the muzzle (Figure 22).

Propellant particles also travel laterally as well as forward. Several photographs were taken with an additional camera positioned above and behind the handgun as depicted in Figure 5. This camera was situated at an angle in order to obtain images of the weapon, cloud, and particles over a considerable range. Because of the resulting photographic distortion, no attempt was made to calculate exact particle velocities. However, with this arrangement it was possible to obtain useful data regarding the lateral movement of the particles, as well as the cloud, while also being able to view the leading edge of the particle group, cloud, and bullet. Shown in Figure 23 is a photograph of the discharge of a CCI 9mm, 115 grain TMJ bullet. This photograph has its

limitations in terms of symmetry because of the unavoidable uneven illumination (the particles closer to the flash are well illuminated, while those on the other side of the field are not). Despite this limitation, useful data are obtainable from the photograph. There is a significant lateral spread of the particles. Measurements from this series of photographs demonstrate that the particles have spread at least nine inches from the muzzle. If one assumes that the lateral spread (horizontal and perpendicular to the trajectory) is generally symmetrical, and there is no reason not to, its cross-sectional diameter, measured at its maximum distance from the trajectory, is approximately 18 inches at a distance of about twenty inches from the muzzle. The distance from the muzzle was approximated by the examination of another photograph taken from the usual camera position, normal to the trajectory for measuring particle velocities, and of the same discharge. These observations have been confirmed via experiments conducted by placing targets up to twelve inches from the bullet trajectory. The lateral and forward spread of the cloud will be discussed subsequently.

The photographic image of the angle and lateral spread of the particles demonstrate their possible impact upon crime scene reconstruction. The outermost particle trajectory, in this experiment, was (in Figure 23) approximately 55° from normal to the bullet trajectory (using the muzzle as the vertex). This finding indicates that an object in close proximity to the muzzle is less likely to be impacted by propellant particles than an object positioned

further downrange. Many of the particles at that distance from the muzzle travel at relatively high rates of speed. Thus, objects at least as close as nine inches to the bullet trajectory can have particles strike them and become embedded (fabric type substrates) significantly below their upper surface.

Particle and Muzzle Cloud Experiments

Weapon: 357 Magnum, S&W

Ammunition: Winchester, 38+P, 158 grain, SWC

Flash Parameters: Single Flash

The propagation of the muzzle cloud and propellant particles for this ammunition is discussed here. To illustrate the development of the muzzle cloud and movement of the particles a synthesized montage was prepared from a delay of one microsecond to 2300 microseconds (Figure 24) in 200 or 300 microsecond intervals. The cylinder gap cloud is barely visible in this series of photographs. Thus, it will only be described briefly. This montage is quite useful for recognizing the relative movement of muzzle cloud, particles, and projectile. The propellant particles are readily visible in this series of photographs.

Results and Discussion

Shortly after the firearm has been discharged a prominent flame has emerged from the muzzle and has extended about six inches downrange. A cloud has begun to form at the front cylinder gap. Approximately 500

microseconds later a cloud is present at the muzzle and has the same shape as the flame which is still apparent. It should be noted that the flame is self-luminous and is independent of the flash, along with the associated time delay. The bullet is visible seven inches from the muzzle after about 200 additional microseconds have elapsed. Additionally, propellant particles are clearly visible ahead of the bullet in the range of 5 to 12 inches from the muzzle.

In the succeeding photographs (900-1700 microseconds delay) it is apparent that the muzzle cloud is moving fairly rapidly downrange since it has not lagged far behind the bullet. During the elapse of this period of time the approximate velocity of the muzzle cloud is 625 feet/second, compared to a bullet velocity of about 937 feet/second. Throughout this time interval the cloud has undergone interesting shape changes. At a delay of approximately 1100 microseconds, there is a noticeable protrusion just behind the bullet. At 1300 microseconds, prominent eddy currents have formed at the rear section of the muzzle cloud above and below the bullet path. These eddies maintain their shape while moving forward throughout the entire sequence of photographs (beyond a delay of 2300 microseconds). The forward portion of the muzzle cloud is still quite dense after 2300 microseconds have elapsed, and has traveled about fifteen inches from the muzzle. Conversely, during this entire period of time, the flame has not moved significantly downrange and appears to be holding steady at about 5-6 inches. Additionally, it has not spread very much vertically. The presence of the eddy currents underscore the turbulence

experienced by the muzzle cloud. Thus, it is obvious that the flow of the cloud is not entirely laminar. As a result of turbulence, the entire cloud is not moving at the same rate, nor in exactly the same direction (in the case of the eddy currents the cloud is moving in circles), and thus is more prone to being influenced differentially by external forces. One could reasonably expect to find variability in resulting patterns due to turbulent conditions in the muzzle cloud. The average muzzle cloud velocity, based on seven discharges, was found to be in excess of 400 feet per second (Appendix: Table A1).

The particles continued, as a group, to stay abreast of the bullet. Even after the elapse of 2300 microseconds, many particles were further downrange than the bullet, although many more were now lagging behind. These observations indicate that the particles attained velocities near that of the bullet. This is not surprising in view of the particle velocities calculated during the course of additional experimentation discussed shortly.

This ammunition exhibits interesting characteristics. It is apparently consistent with regard to the propagation of the muzzle cloud, particles, and bullet. Yet, several anomalies cropped up during the course of discharging numerous rounds. Unusual plumes of flame, in unsymmetrical fashion, were observed during photography involving the short time delays (Figure 24: single photographs at 1, and 500 microseconds). Also, note the photograph corresponding to the 1900 microsecond delay (Figure 24). In the latter photograph an unusual flame appears at the upper portion of the muzzle cloud.

These observations help illustrate why relatively consistent discharge patterns are obtained from a series of test firings which may also be accompanied by one or more inexplicable patterns. Since these observations occurred during the early stages of development (prior to or immediately after the appearance of the projectile), and because a considerable amount of localized heat was generated in the vicinity of these phenomena, a significant impact on the resulting patterns can be expected. Thermal energy is probably a key factor in the retention of the fine lead deposits on materials in close proximity to the muzzle. A similar anomaly is shown in Figure 25, observed during the course of another set of single flash experiments with Winchester .38 special ammunition. These observations suggest that more than one discharge should be made at each predetermined distance when preparing exemplar patterns in casework. Similar variations were noted with other ammunition.

Similar variations were noted with other ammunition as well. One of the most notable sources of disparities between discharges was Federal .38+P, 125 grain, JHP (Figure 26). For example, in the left photograph the flame reached approximately twenty inches from the muzzle, whereas no flame is seen in the corresponding area in a consecutive discharge (right photograph). In fact, it was noted during the discharge that little muzzle flame was produced, and that it had not traveled more than about five or six inches downfield from the muzzle. Similar observations occurred several times from the same box of ammunition in consecutive order, that is, large versus a relatively small flame.

Self-luminous particles whose trajectories are often somewhat unpredictable were often observed during the course of the experiments described throughout this chapter. Noteworthy examples of these objects are apparent in Figures 21 & 23. The trajectory of the particle shown in Figure 21 at approximately 28 inches from the muzzle appears to have turned approximately 180 degrees and then changed direction dramatically a second time. The observation of these particles did not appear to be entirely predictable. No consistency of these observations was found even within discharges from a single box of ammunition. An apparent factor contributing to the unpredictable nature of the trajectories is that these particles are partially self-propelled by continuing to burn unilaterally (as in a jet effect), producing a volume of gas, at a considerable distance from the muzzle.

Cloud Experiments

Weapon: 357 Magnum, S&W

Ammunition: Federal, .38 158grain, LRN

Flash Parameters: Single Flash

Film: Kodak Ektapress 400 (pushed 2x)

The cloud dynamics of this ammunition is presented. Most cloud experiments involved single flash photography since multiple flash photography of cloud dynamics often provides a somewhat confusing picture, resulting from

partially superimposed images. Hence it is difficult to accurately determine where a cloud image begins and ends. To assist in the description of this group of experiments a synthesized montage of nine photographs has been prepared (Figure 27). The description of GSR dynamics regarding the rearward moving cloud in this specific discussion is limited since photographs were not taken in the range of 300 to 400 milliseconds. Despite this, much useful information can be gained about the behavior and interrelationships of the muzzle and cylinder gap clouds, as well as the projectile, during this relatively short interval.

Results and Discussion

At a time shortly after discharge a light grey cloud has emerged from the front cylinder gap. The cloud is about 1 7/8" wide x 3 7/8" in height. A small flame is present under the image of the cylinder gap cloud. A substantial flame is visible at the muzzle. However, no muzzle cloud has formed up to this point in time. The flame has traveled 4" downrange relative to the muzzle. The central portion of the flame is extremely bright, and exhibits a characteristic shape. A 1" gap exists between the cylinder gap cloud and the muzzle flame. The bullet is not yet visible. A self-luminous object has left evidence of an erratic trajectory leading from the front cylinder gap to the rear portion of the Ransom Rest. This object could have easily impacted a hand if the gun had been held. This particular event is not associated with any point in time since the trajectory could have been left as an image on the emulsion up until the time that the shutter was closed.

After a delay of about 300 microseconds, a light grey cloud is now visible and superimposed over the muzzle flame. It has an interesting shape which is easily recognized after observing photographs taken under similar conditions. The forward most position is relatively small, that is, about 1-1.5" in diameter and protrudes from the larger portion of the cloud. This protrusion is very similar in shape to the previously mentioned bright inner portion of the flame (Figure 28) In fact, the entire muzzle cloud appears strikingly similar in shape to that of the muzzle flame immediately after discharge. The muzzle flame is self-luminous and has no relation to the time delay. The muzzle cloud has grown to just over 5" in length. The cylinder gap cloud has grown in all directions. It is now about 3" across at its greatest width. The gap between the muzzle flame/cloud and the cylinder gap cloud has decreased significantly.

After 700 microseconds, the protrusion has extended further downrange and become thinner in appearance. The shape of the muzzle cloud has changed dramatically. The bullet can be seen on close inspection within the protruding portion of the muzzle cloud. The space between the cylinder gap cloud and the muzzle cloud is almost gone.

Three pairs of visible eddies have formed in the muzzle cloud after a time delay of approximately 1300 microseconds. These are depicted in Figure 29 as Set A, B, and C respectively. One pair of eddies (set A) is present at the leading portion of the muzzle cloud. The central portion of Set B is located at about 5 inches from the muzzle. The bullet is now clearly evident at the leading

edge of the muzzle cloud. The tip of the bullet has attained a distance of 11 1/4 inches from the muzzle. Additional eddies (set C) have formed between those in the central portion of the muzzle cloud and the muzzle. Set C appears to have a rotation opposite to that of Set B. The void between the cylinder gap cloud and the muzzle cloud only exists at its uppermost position. The approximate bullet velocity, during the interval from 700 to 1300 microseconds, was 745 feet per second.

A significant gap is beginning to form between the two groups of eddies after a delay of about 1700 microseconds. The latter forming eddies appear to be dissipating. The projectile has now moved ahead of the forward edge of the cloud.

At a delay of approximately 2900 microseconds, there is a fully developed gap between the leading portion of the muzzle cloud and the other large section in proximity to the muzzle. In this gap, a longitudinal zone is visible which appears to have been caused by the bullet passing through the cloud. Additionally, the creation of this zone may have been influenced by an unusual protrusion of flame into the path vacated by the bullet. This protrusion of flame extends to muzzle distance of 5 7/8 inches.

During the entire course of these experiments little or no flame appeared to travel beyond four to five inches. Occasionally, some minor portion located along the axis of the muzzle traveled as far as six inches.

As can be seen from the montage, the rear moving cloud, while moving

fairly rapidly immediately after discharge, slowed down quite quickly. From about 700 microseconds to 3500 microseconds, it appeared to be standing still. While the cylinder gap cloud was essentially motionless, the muzzle cloud had moved forward to a muzzle distance of 13 inches, at a rate of about 470 feet per second. The average velocity of the forward moving cloud, based on eleven discharges, was in excess of 400 feet per second (Appendix: Table A1).

Weapon: 357 Magnum, S&W

Ammunition: Winchester .38 special, 158 grain, SWC LR

Flash Parameters: Single Flash

Film: Kodak Ektapress 400 (pushed 2x)

The same methods used above for single flash photography were used for the study of the cloud movement toward the shooter for this particular type of ammunition. To illustrate the retrograde movement of the cylinder gap cloud, a synthesized montage was prepared (Figure 30) from a delay of one microsecond to 350 milliseconds. The approximate velocity of the retrograde cloud, measured from four discharges, illustrated by the montage, is about four feet per second (Appendix: Table A1). This relatively low velocity points to problems for the reproducible deposition of gunshot residue on the hands of the shooter. Its deposition can be unpredictable because of a number of variables that cannot be controlled or determined in casework. Air currents are just one

factor that can affect the outcome of the gunshot residue deposition. To illustrate this, vector analysis was conducted (Figure 31) which demonstrates the influence of a gentle breeze of five miles per hour (7.3 feet per second).

Weapon: 357 Magnum, S&W

Ammunition: Remington 357 Magnum 180 Grain, SJHP

Flash Parameters: Single Flash

Film: Kodak Ektapress 400 (pushed 2x)

The same methods used above for single flash photography were used for the study of the muzzle cloud movement downrange (away from the shooter) for this particular type of ammunition. The average muzzle cloud velocity, based on six discharges, was nearly 400 feet per second (Appendix: Table A1).

Weapon: Heckler & Koch, 9mm, Model VP70Z

Ammunition: Remington 9mm+P, 115 Grain, JHP and Federal 9mm, 115 Grain, JHP

Flash Parameters: Single Flash

Film: Kodak Ektapress 400 (pushed 2x)

The same methods used above for single flash photography were used

for the study of the muzzle cloud movement downrange (away from the shooter) for this particular type of ammunition. The average muzzle cloud velocity, based on eleven discharges, was in excess of 400 feet per second (Appendix: Table A1).

The average velocity calculated from all the muzzle cloud discharges was 429 feet per second (35 discharges; five ammunition sources; one revolver and one semi-automatic pistol).

Video Experiments

Studying the cloud propagation from synthesized montages is not the most accurate approach since it is a collection of single flash photographic images from many different firearm discharges (there is a degree of variation between each discharge). A more accurate way of calculating the velocity of the retrograde cloud would be to determine it from a single discharge. A number of discharges could then be made with the same type of ammunition, with the average velocity calculated from the single determinations to obtain a value that is representative of the ammunition (and weapon). Multiple flash photography was also attempted using the Palflash. Although this approach might (theoretically) be more accurate than a single flash approach, it produces a confusing picture of overlapping images of the cloud formation. Thus, videography was attempted to confirm the velocity of the retrograde cloud. A lamp device was constructed to project a roughly slab-shaped beam of light at

right angles to the camera lens axis to further study the cloud propagation with a video camera (Figure 8).

Results and Discussion

The specially fabricated lamp for use with video recording of cloud movements provides superior illumination for this purpose as compared to the Palflash. Its illumination intensity is much greater, covers a much larger area, and is orthogonal to the viewing direction providing a type of dark field illumination. It is clear from the video experiments that a substantial portion of the retrograde cloud moves relatively slowly, that is, on the order of 2 -10 fps (Appendix: Table A2), while another portion arrives near an area corresponding to the hand of the shooter somewhat more rapidly. This latter portion was visible during the first frame of each video sequence. With the currently available equipment, it is not possible to calculate the velocity of the retrograde cloud as it moves into the position recorded during the first frame. However, it appeared to be moving at nearly the same rate as that of the upper aspects of the cloud, and its velocity measured corresponding to the interval between the first and second frame of tape. Future experimentation to further explore this issue could involve new high speed video equipment with a faster frame rate. This question can also be addressed using video recording of a series of test firings where downrange air flows of known linear velocity are used. Additional experimentation that is less expensive would involve a comparison of elemental analyses (hand swabbings) obtained with and without an air flow near the

weapon when discharged.

Conclusion

Knowledge of the rate of movement of the gunshot residue cloud toward the shooter has shed light on some of the interpretative problems associated with the analysis of residue on the hands of suspected shooters. Single flash photography and videography were utilized to calculate the retrograde cloud velocity. It is clear from these studies that at least the major portion of the GSR cloud moves relatively slowly towards the shooter. These results are consistent with the findings of Nesbitt et al. (1977, p. 303) involving the photoluminescent detection of lead and antimony on the hands. They found that "indoor firings consistently produced more residue in samples than did outdoor firings." They did not investigate the reasons for this. Recordings made with flow velocities where the rearward motion of the cloud is just cancelled should provide useful information. A limited number of such experiments have been conducted. The results of these experiments are not complete enough to report here. Some factors that could have an influence on the acquiring of at least some GSR by the hands of the shooter are wind, rapid movement of the hands, and so forth Earlier, Wessel et al. suggested that "the direction and force of wind currents" are some of several factors that can affect the amount of GSR deposited on hands (1974, p. 2-29). The experimentation presented here supports these concepts, but points to the need for further experimentation beyond the scope

of this work.

Based on single flash experiments it is clear that the muzzle cloud moves forward (down range) at a relatively high rate of speed, that is, on average, on the order of 400-500 feet per second. Thus, it is far less influenced by external forces, such as air currents, movement of nearby objects, and so forth.

Particles acquire surprisingly high velocities from the propellant ignition (Table 2, Figures 10-15). Thus, they have sufficient energy to imbed themselves deeply within certain nearby targets. Because of their relatively high velocity, normal wind velocity will not significantly influence their motion near the muzzle. In the still photographic records, self-luminous particles are frequently encountered, some of which have unusual trajectories. The results of these observations are summarized in the Appendix (Table A3).

Ammunition	mean v.	# of particles measured	region measured
Federal 357 Magnum, 110 Grain, JHP	600 fps	50	19"-28"
CCI 357 Magnum, 158 Grain, JHP	600 fps	40	33"-41"
CCI .38+P, 125 Grain, JHP	500 fps	178	10"-48"
CCI 9mm, 115 Grain, TMJ	500 fps	107	18"-52"
Remington 9mm+P, 115 Grain, JHP	500 fps	69	18"-52"
Magtech 9mm, 124 Grain, FMC	400 fps	97	26"-46"
Winchester .38+P, 158 Grain, HP	500 fps	180	6"-44"
Federal .38+P, 125 Grain, JHP	500 fps	119	18"-42"

Table 2. Velocity (v) Data of Particles from Eight Different Sources (rounded to the nearest hundred feet per second.

Ammunition	Distance from Muzzle	Δ in Velocity (100 us interval)	# of particles measured
Federal 357 Magnum, 110 Grain, JHP	19"-28"	- 35 fps	17
CCI 357 Magnum, 158 Grain, JHP	33"-41"	- 24 fps	16
CCI .38+P, 125 Grain, JHP	10"-48"	- 21 fps	13
CCI 9mm, 115 Grain, TMJ	18"-52"	- 18 fps	11

Table 3. Deceleration Data from Four Different Sources

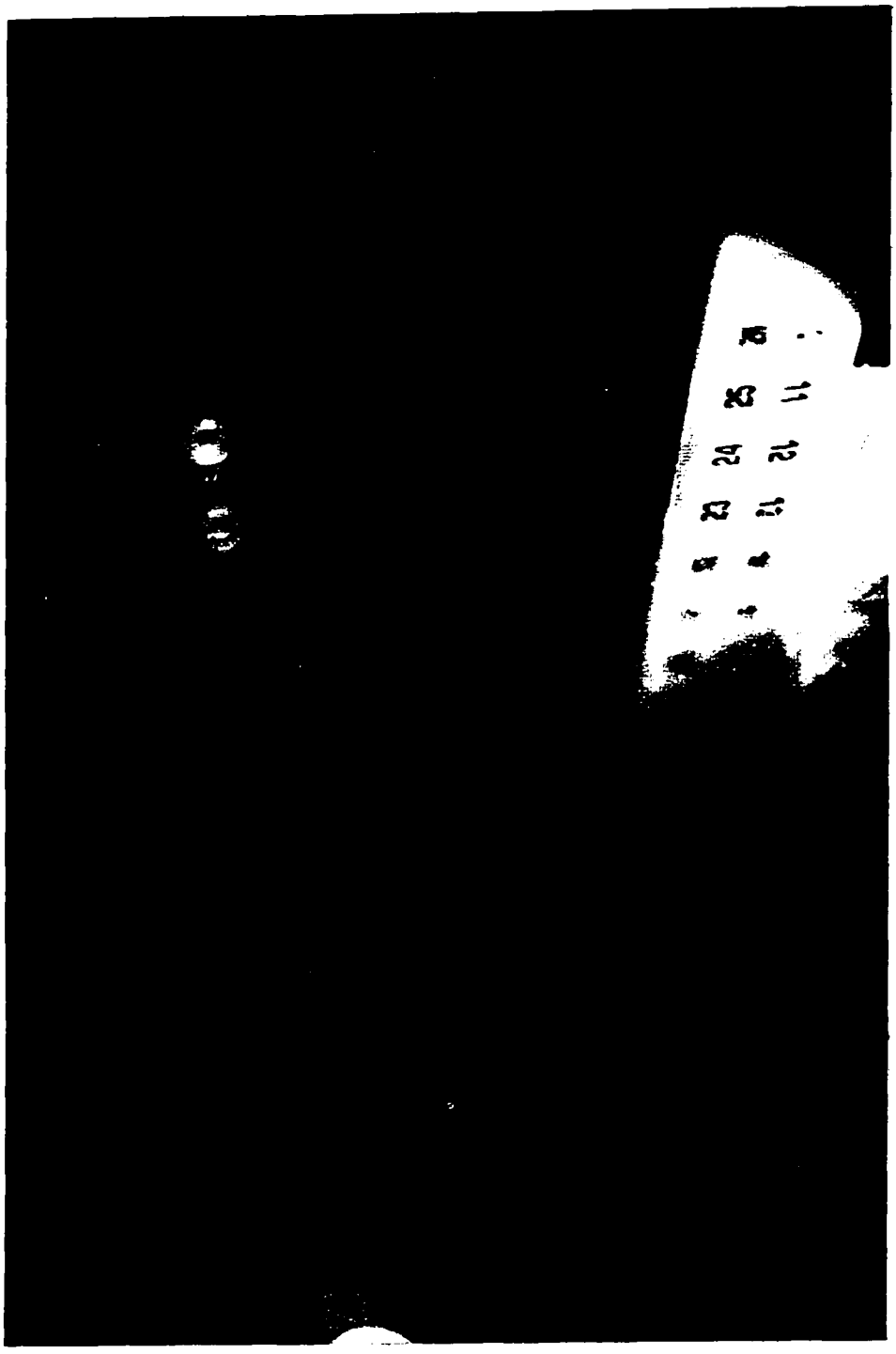

Figure 9. **High Speed Multiple Flash Photograph of Discharge from S&W 357 Magnum Revolver. Ammunition Discharged: Remington 357 Magnum, 180 Grain, SJHP.**

X-axis Represents the Horizontal Position (inches) of the Particles from the Muzzle.
Y-axis Represents the Vertical Distance Above and Below the Line of Fire (inches).
Remington 9mm+P 115 grain, JHP

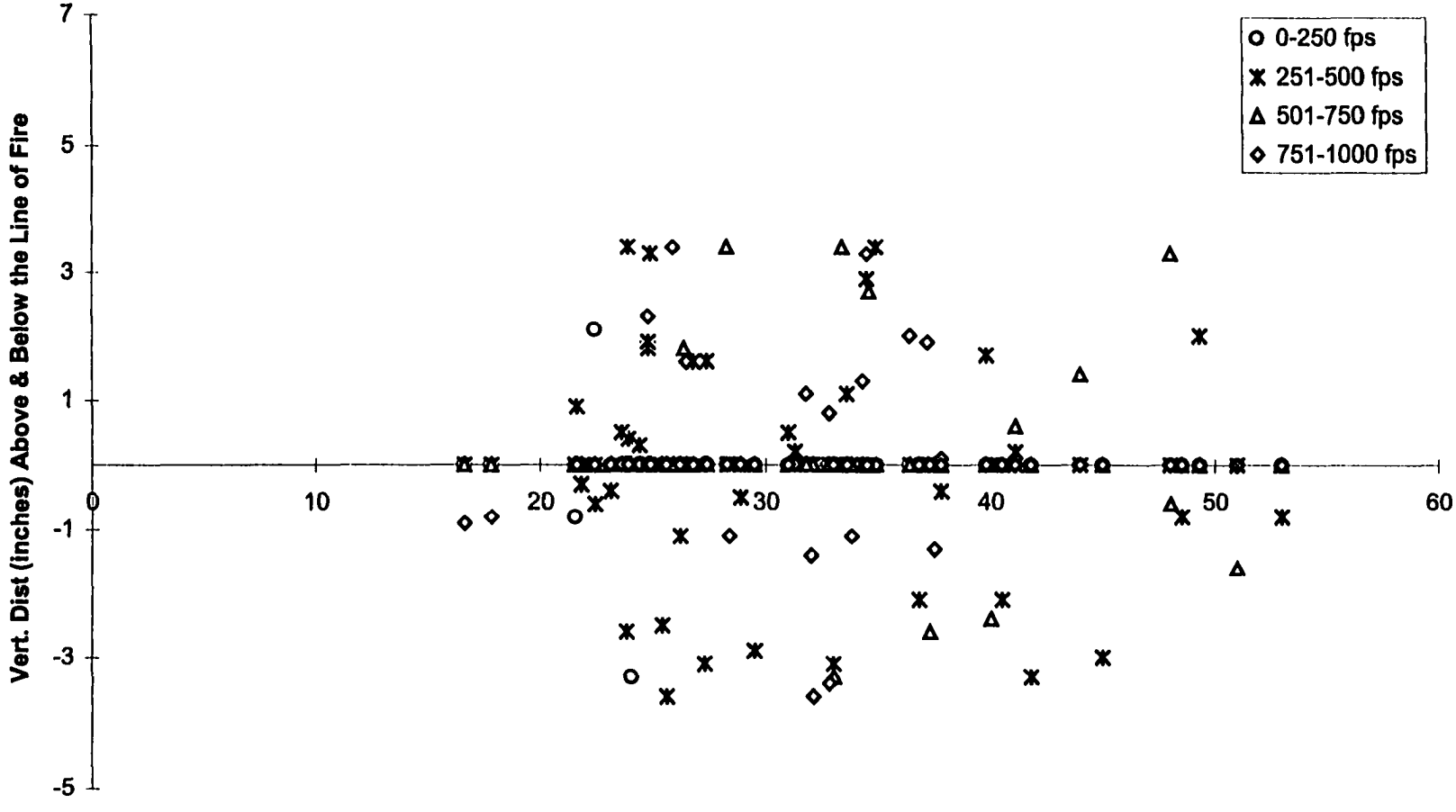

Figure 10. Velocity Ranges of Individual Propellant Particles as a Function of Position

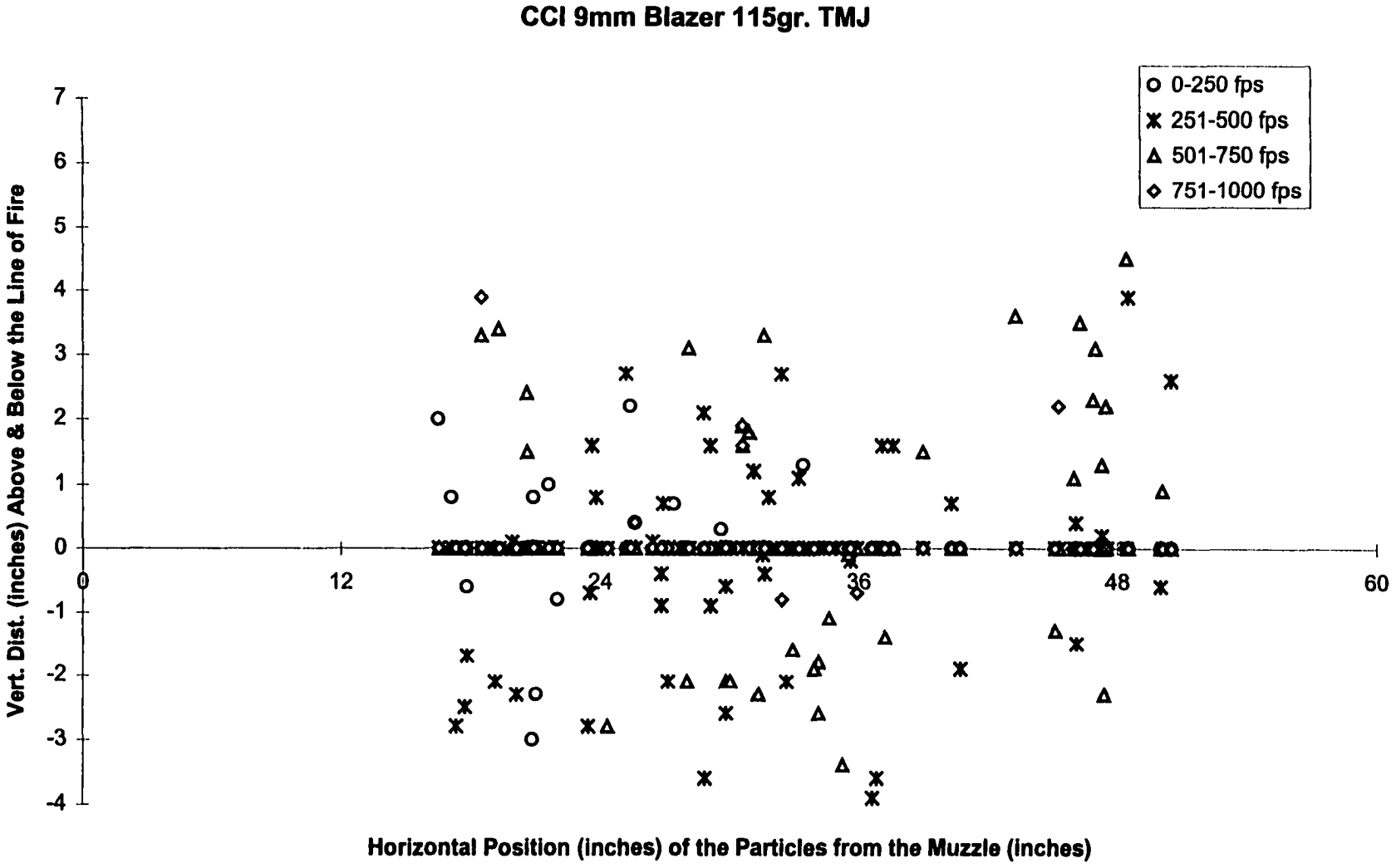

Figure 11. Velocity Ranges of Individual Propellant Particles as a Function of Position

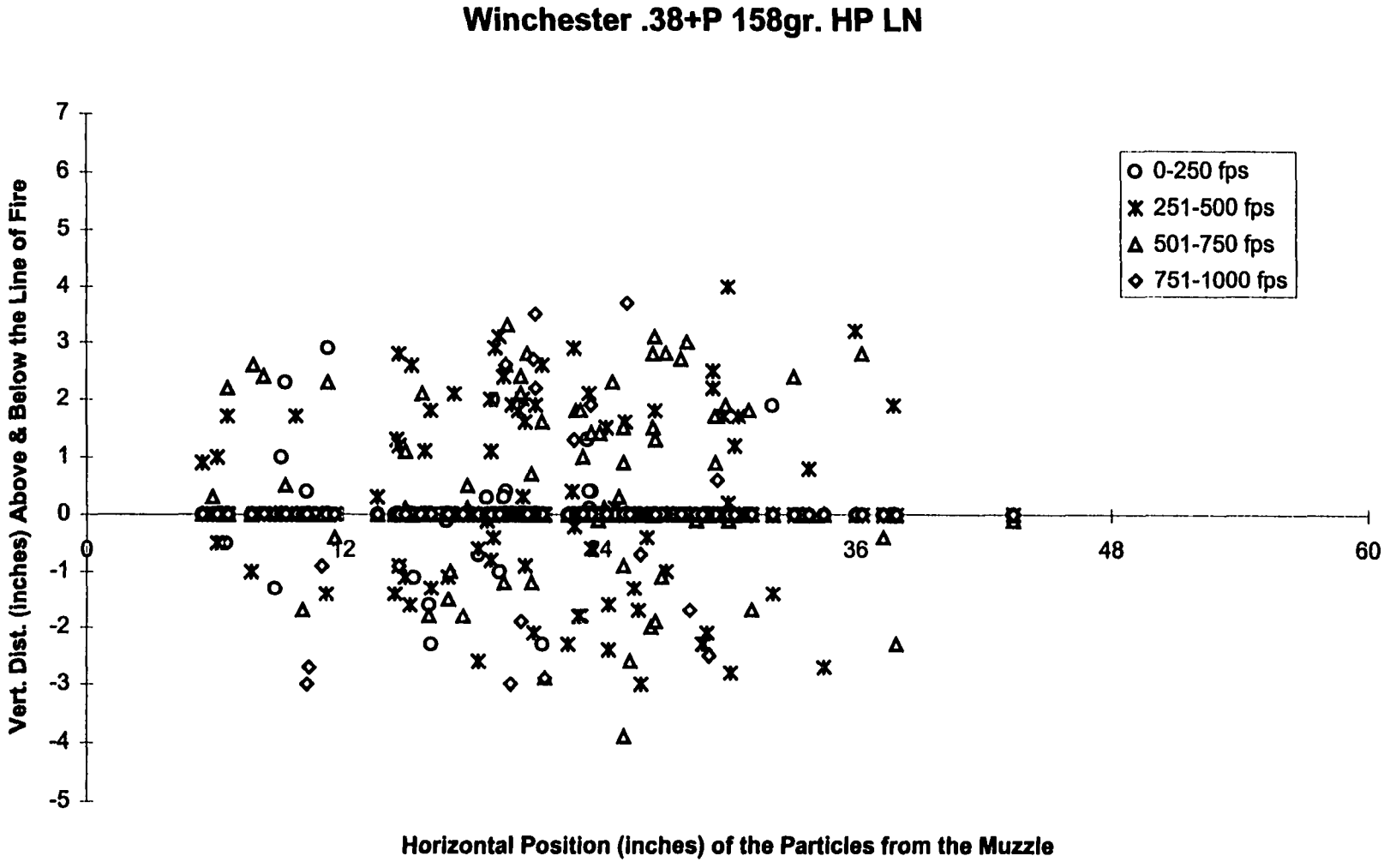

Figure 12. Velocity Ranges of Individual Propellant Particles as a Function of Position

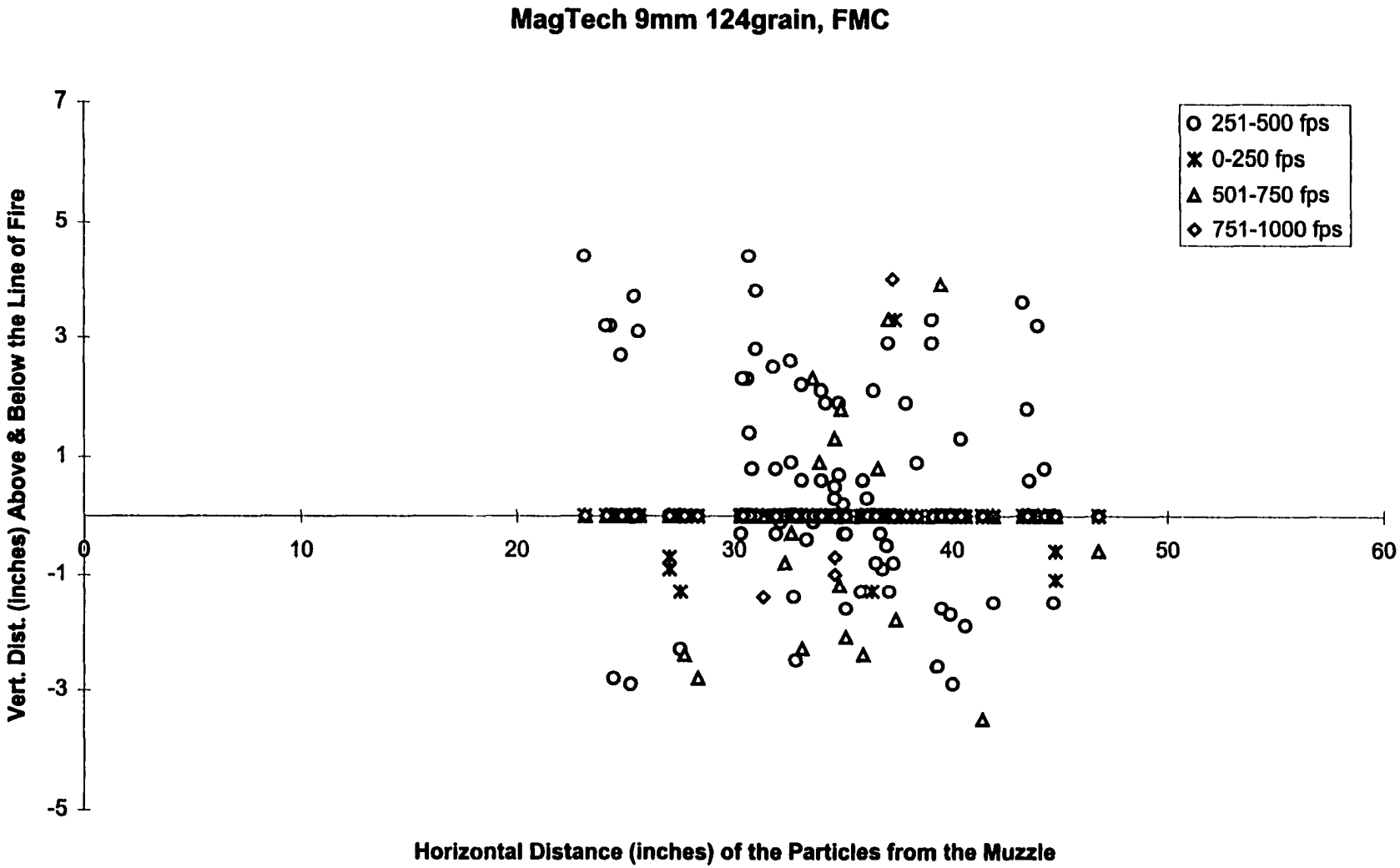

Figure 13. Velocity Ranges of Individual Propellant Particles as a Function of Position

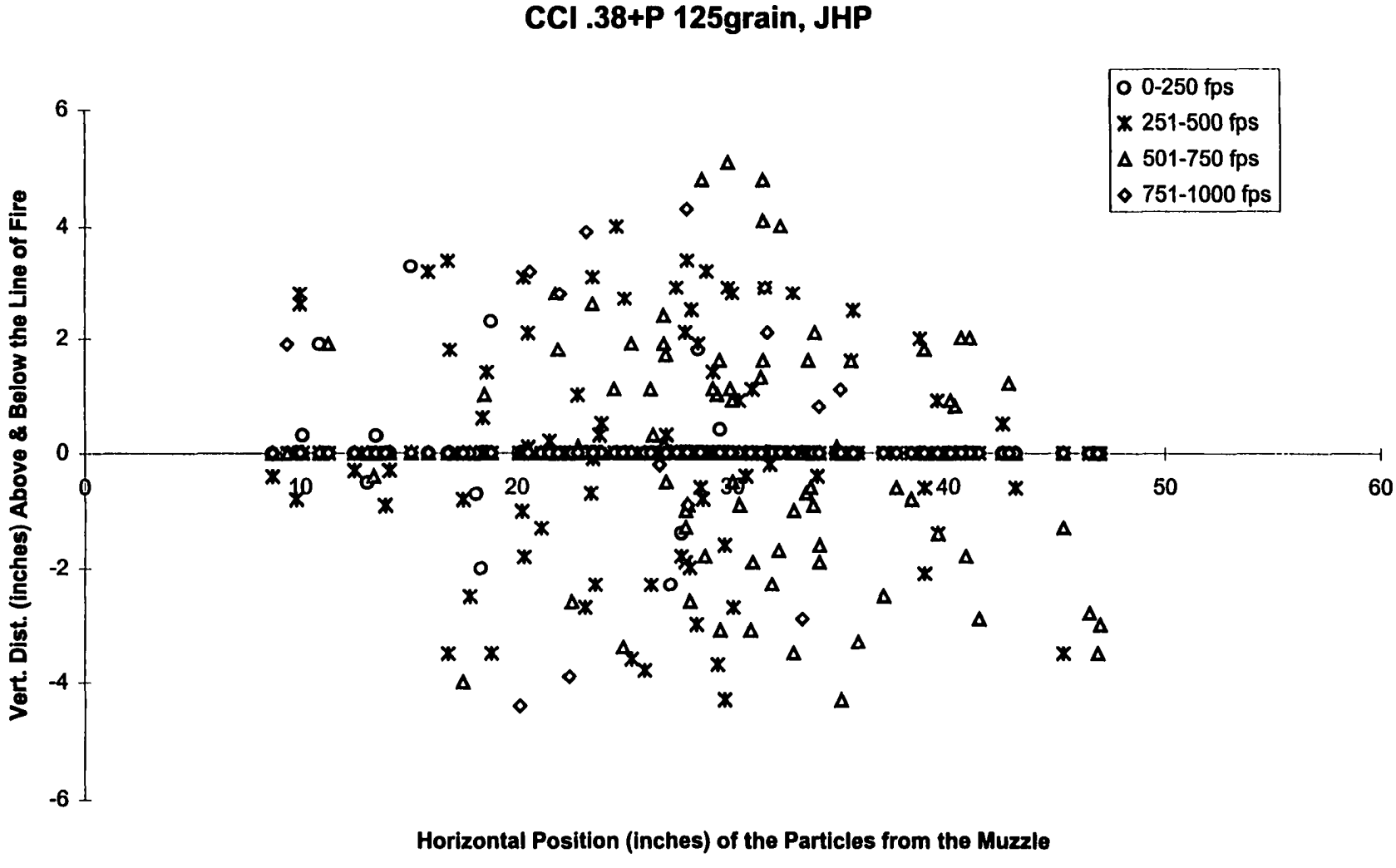

Figure 14. Velocity Ranges of Individual Propellant Particles as a Function of Position

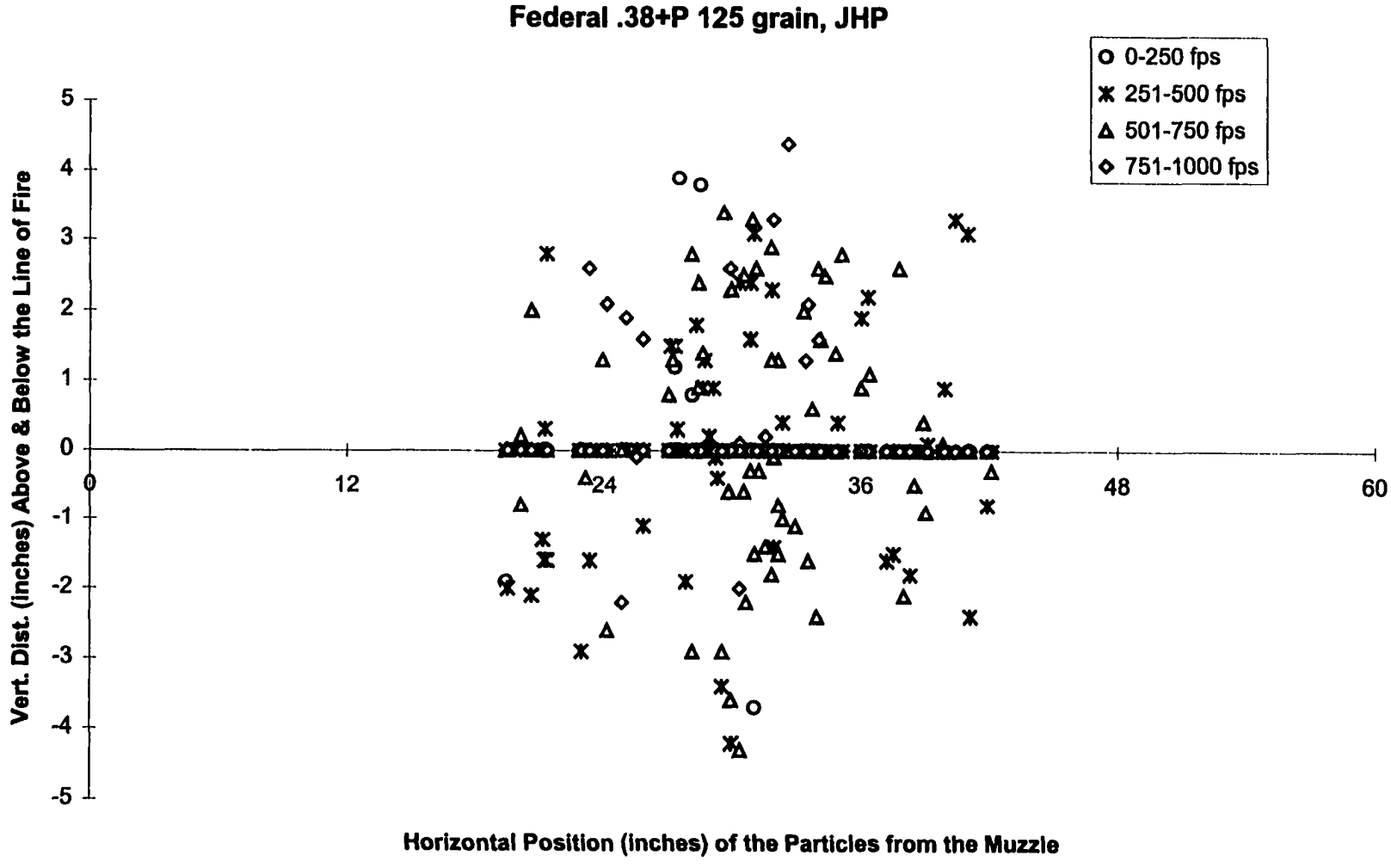

Figure 15. Velocity Ranges of Individual Propellant Particles as a Function of Position

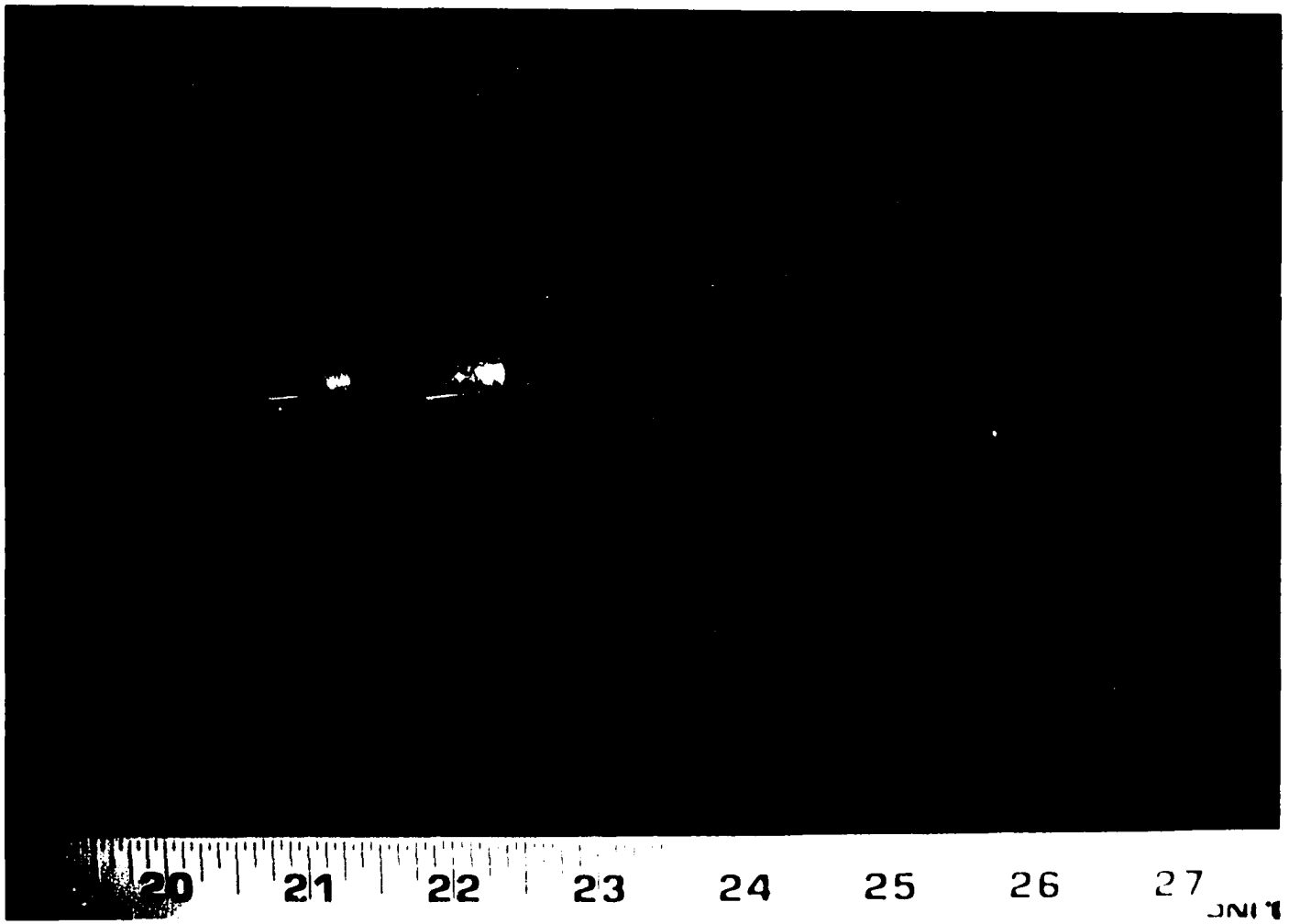

Figure 16. High Speed Multiple Flash Photograph of Bullet & Particles in Flight from Discharge of a Federal Cartridge .38+P, 125 Grain, JHP. Time Delay = 1900, 2000, & 2100 microseconds.

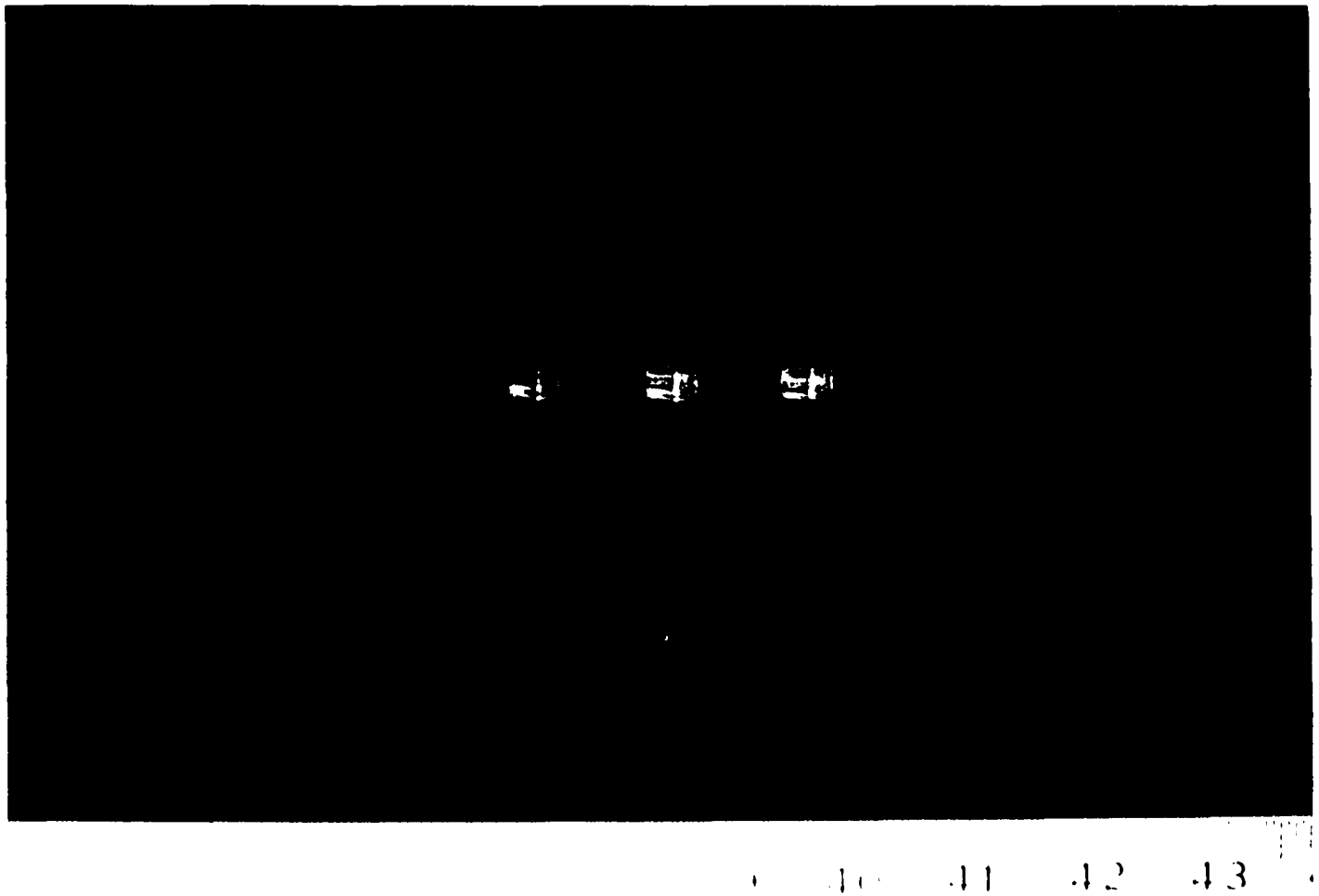

Figure 17. High Speed Multiple Flash Photograph of Bullet & Particles in Flight from Discharge of a CCI Cartridge .38+P, 125 Grain, JHP. Time Delay = 3500, 3600, & 3700 microseconds

Figure 18. High Speed Multiple Flash Photograph of Bullet & Particles in Flight from Discharge of a CCI Cartridge 357 Magnum, 158 Grain, JHP. Time Delay = 2900, 3000, & 3100 microseconds

Figure 19. High Speed Multiple Flash Photograph of Bullet & Particles in Flight from Discharge of a Magtech Cartridge 9mm, 124 Grain, FMC. Time Delay = 5200, 5300, 5400, & 5500 microseconds.

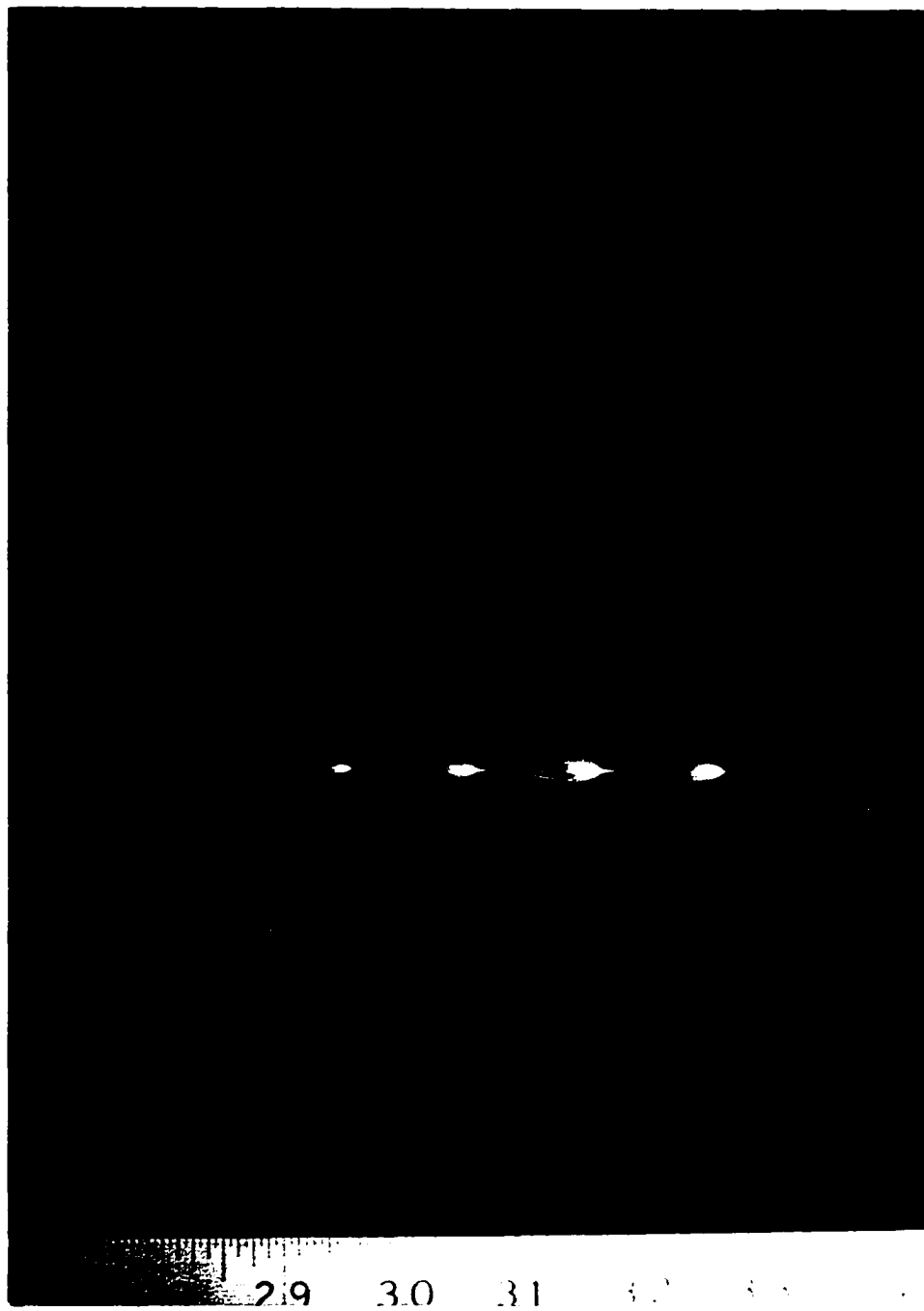

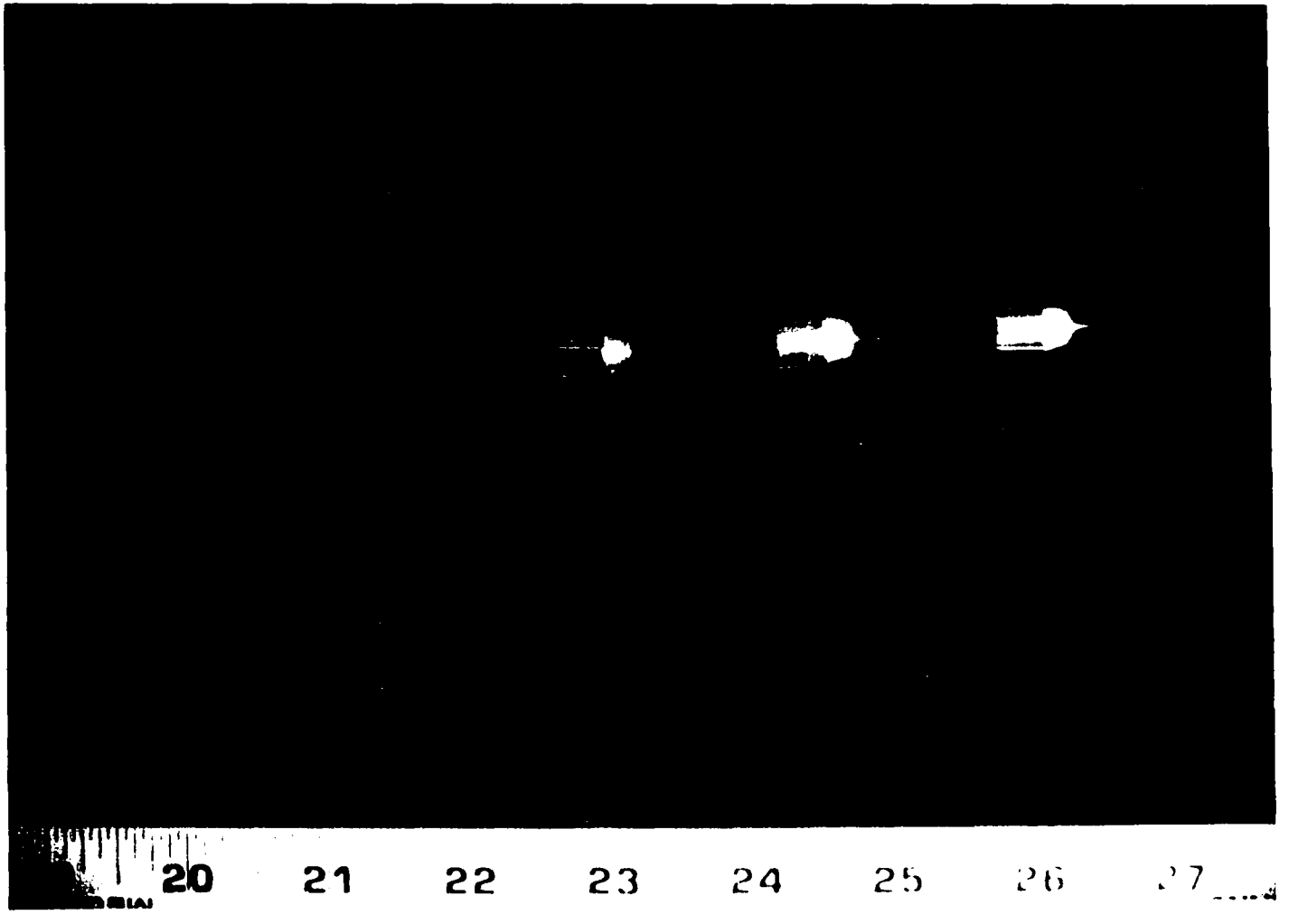

Figure 20. High Speed Multiple Flash Photograph of Bullet & Particles in Flight from Discharge of PMC Cartridge 357 Magnum, 125 Grain, JHP. Time Delay = 1400, 1500, & 1600 microseconds

Figure 21. Self-Luminous Particle with an Unusual Trajectory in Upper Portion of Photograph. High Speed Multiple Flash Photograph of Bullet & Particles in Flight from Discharge of a CCI Cartridge .38+P, 125 Grain, JHP. Time Delay = 2500, 2600, & 2700 microseconds.

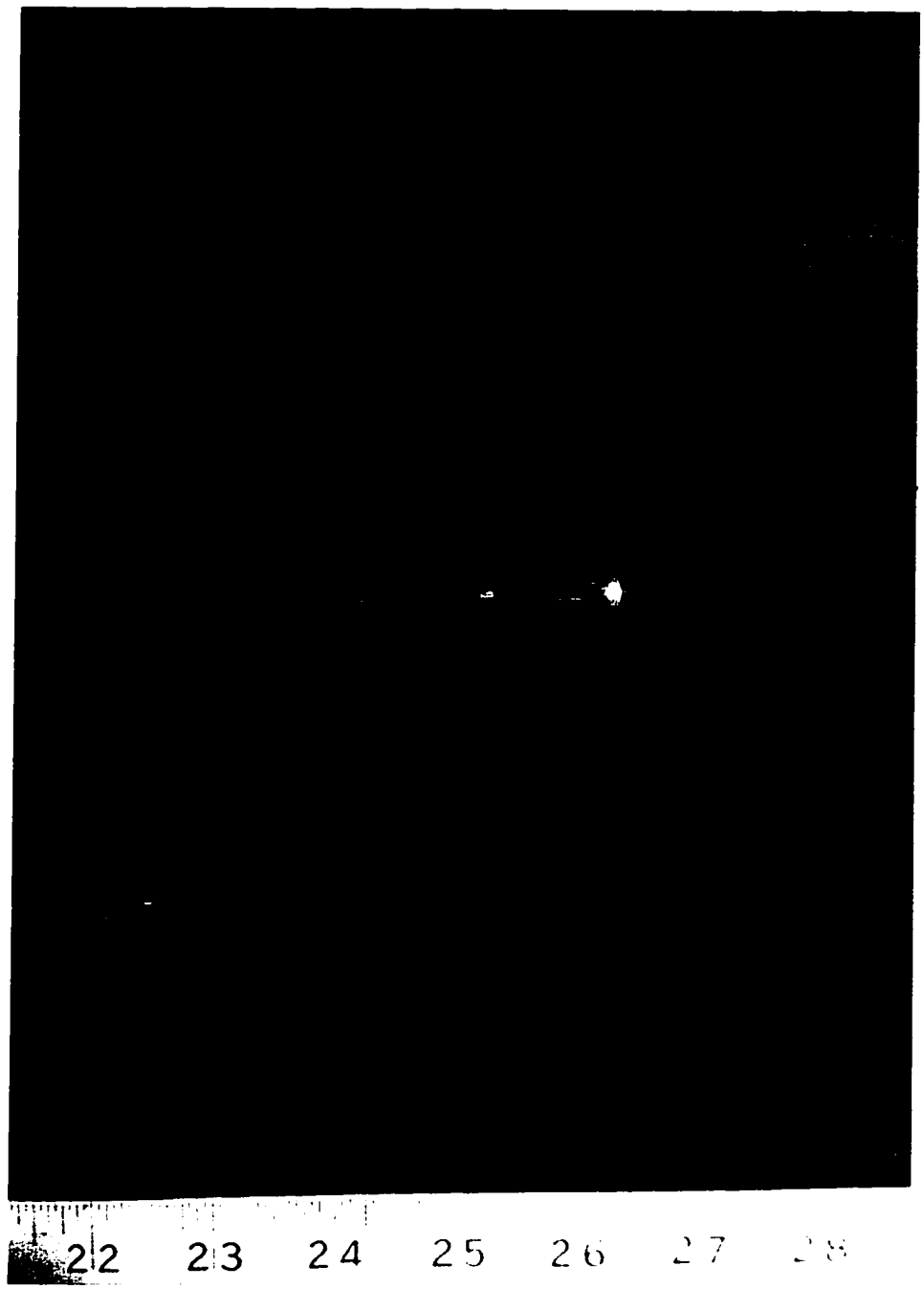

Figure 22. Perforation of Upper Layer of Double Layer of Fabric by Propellant Particles. Particles Visualized via Native Fluorescence. Excited at 455nm; orange barrier filter. Room Temperature. Magtech 357 Magnum, 158 Grain, SJSP. Muzzle Distance = 20cm (8 inches). Upper Photo: Outermost Layer of Fabric. Lower Photo: Interior Layer of Fabric.

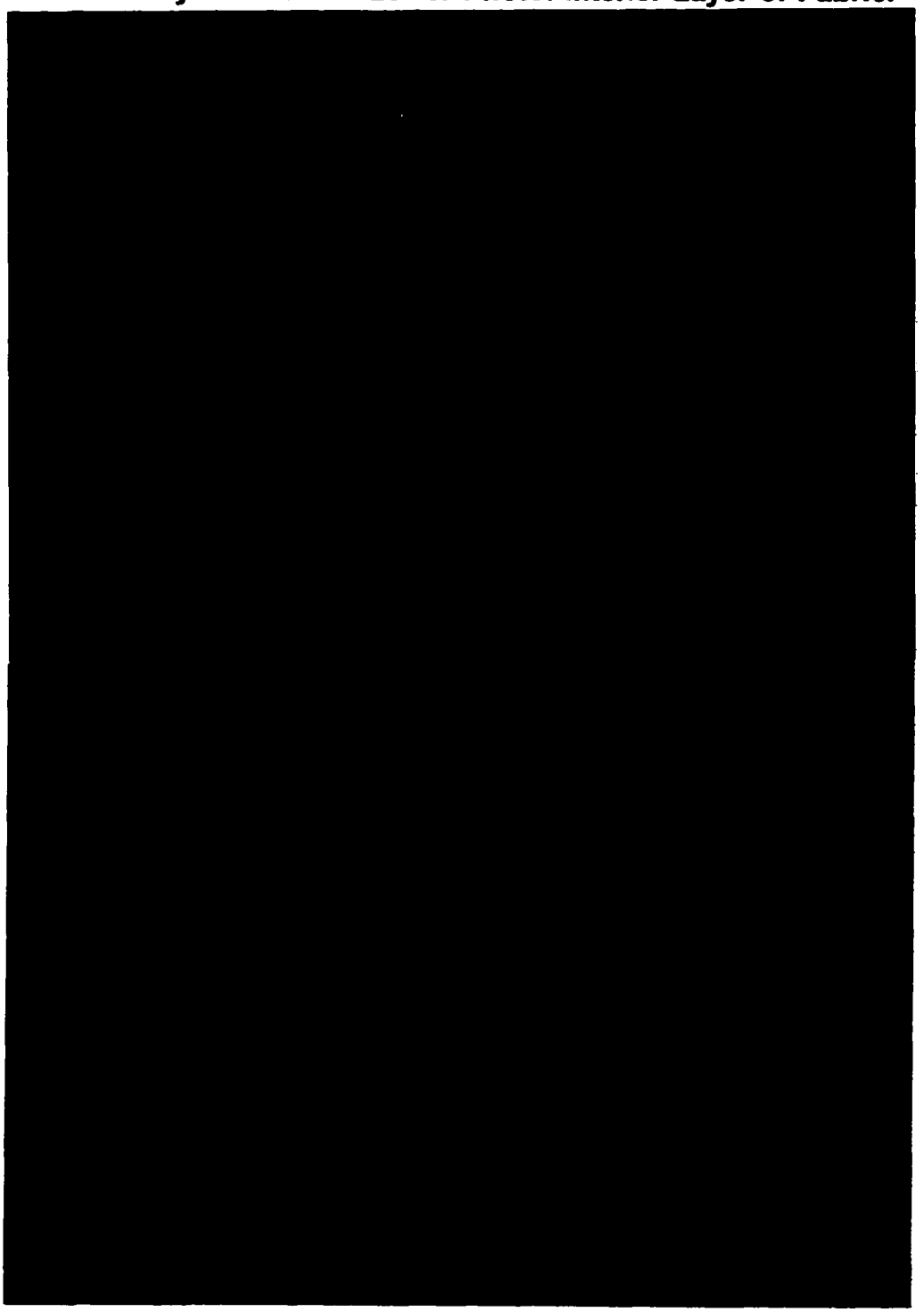

Figure 23.

Lateral Spread of Particles from Firearm Discharge. CCI 9mm, 115 grain, TMJ. Multiple Flash Photograph. Smith & Wesson 357 Magnum.

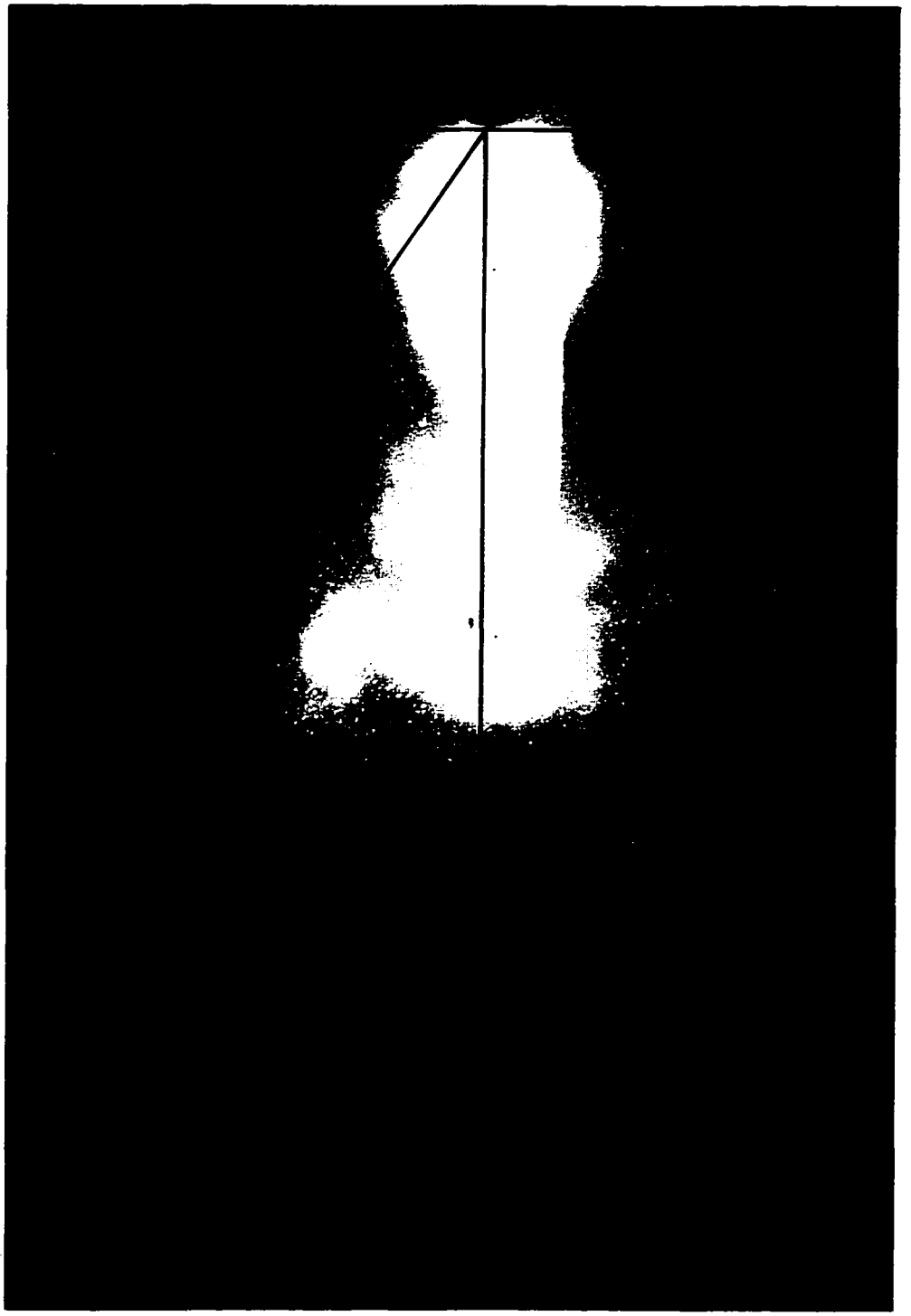

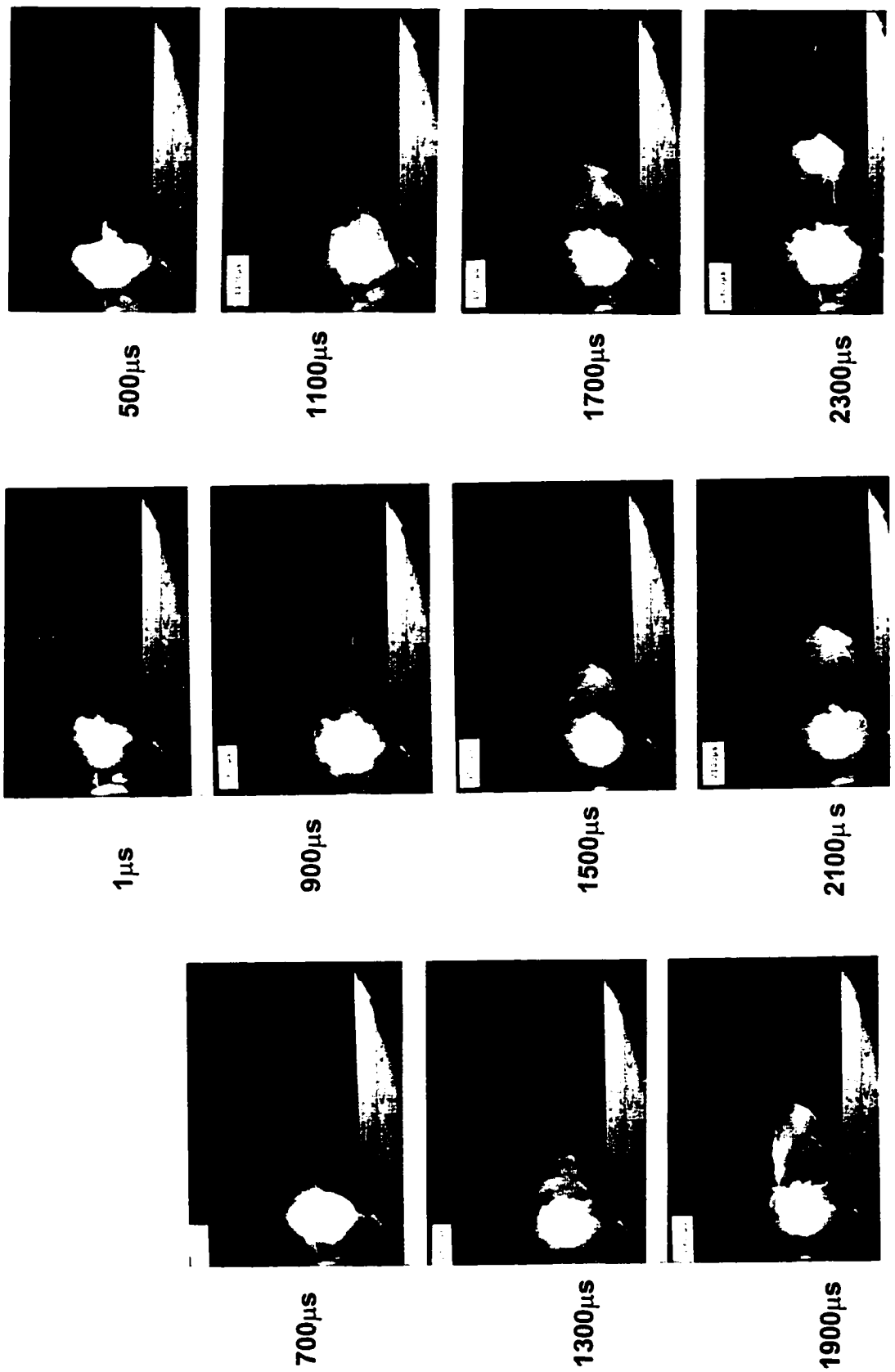

Figure 24. Synthesized Montage of Single Flash Photographs of Firearm Discharge. Winchester .38+P, 158 Grain, SWC. Smith & Wesson 357 Magnum.

Figure 25.

Unusual Flare from Muzzle Flame (example of anomalous occurrence). Multiple Flash Photography. Winchester .38spl, 158 grain, SWC. Smith & Wesson 357 Magnum.

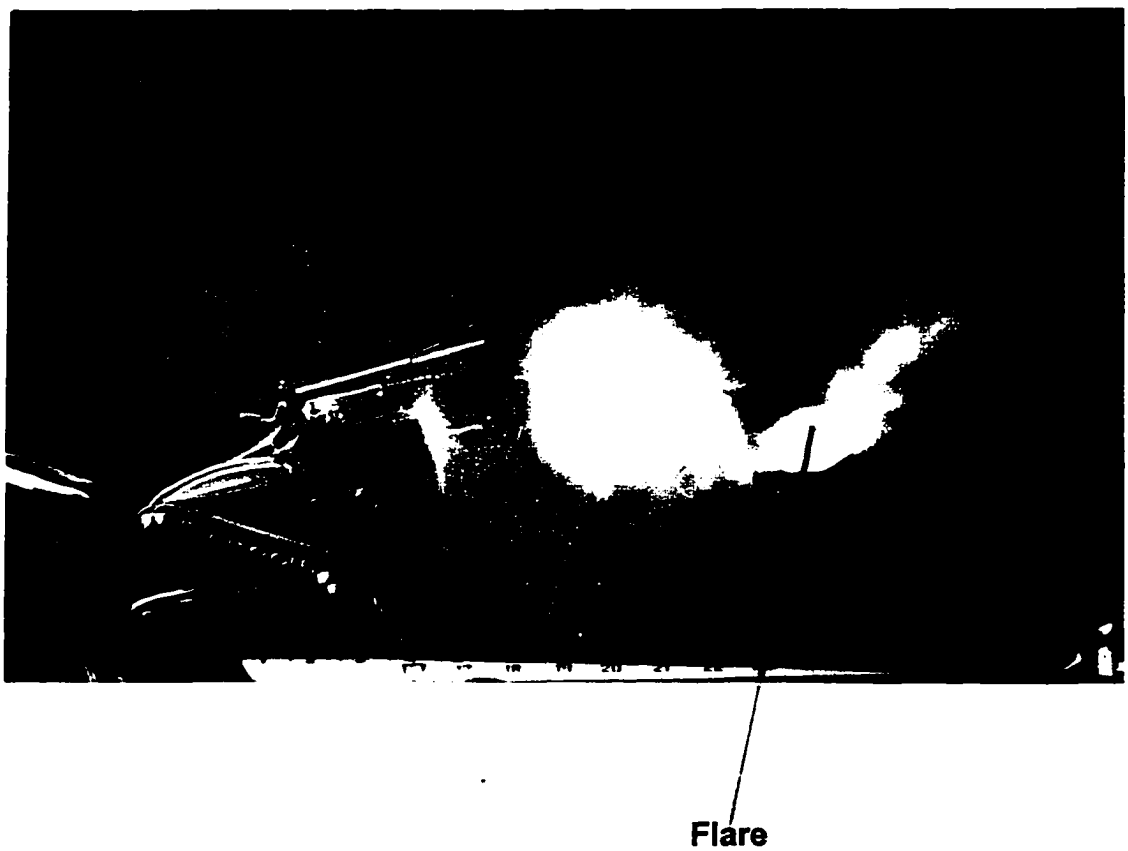

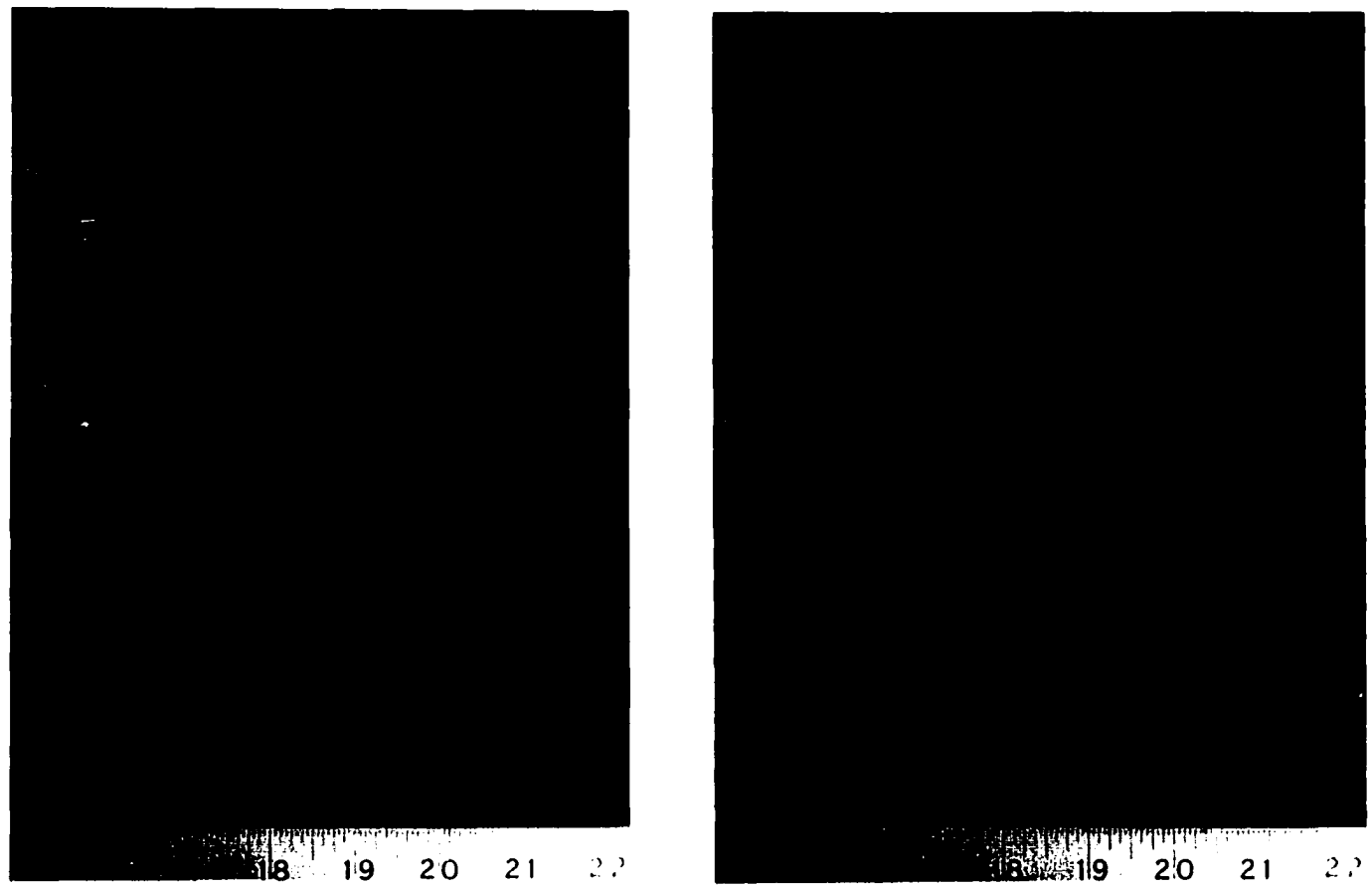

Figure 26. Disparity of Flame from Discharges of Cartridges from the Same Box. Ammunition: Federal .38+P, 125 grain, JHP. S&W 357 Magnum. Left Photograph: Flame Propagated Nearly Twenty Inches from Muzzle; Right Photograph: No Indication of Flame in Same Region from Muzzle (flame only traveled about five inches from muzzle).

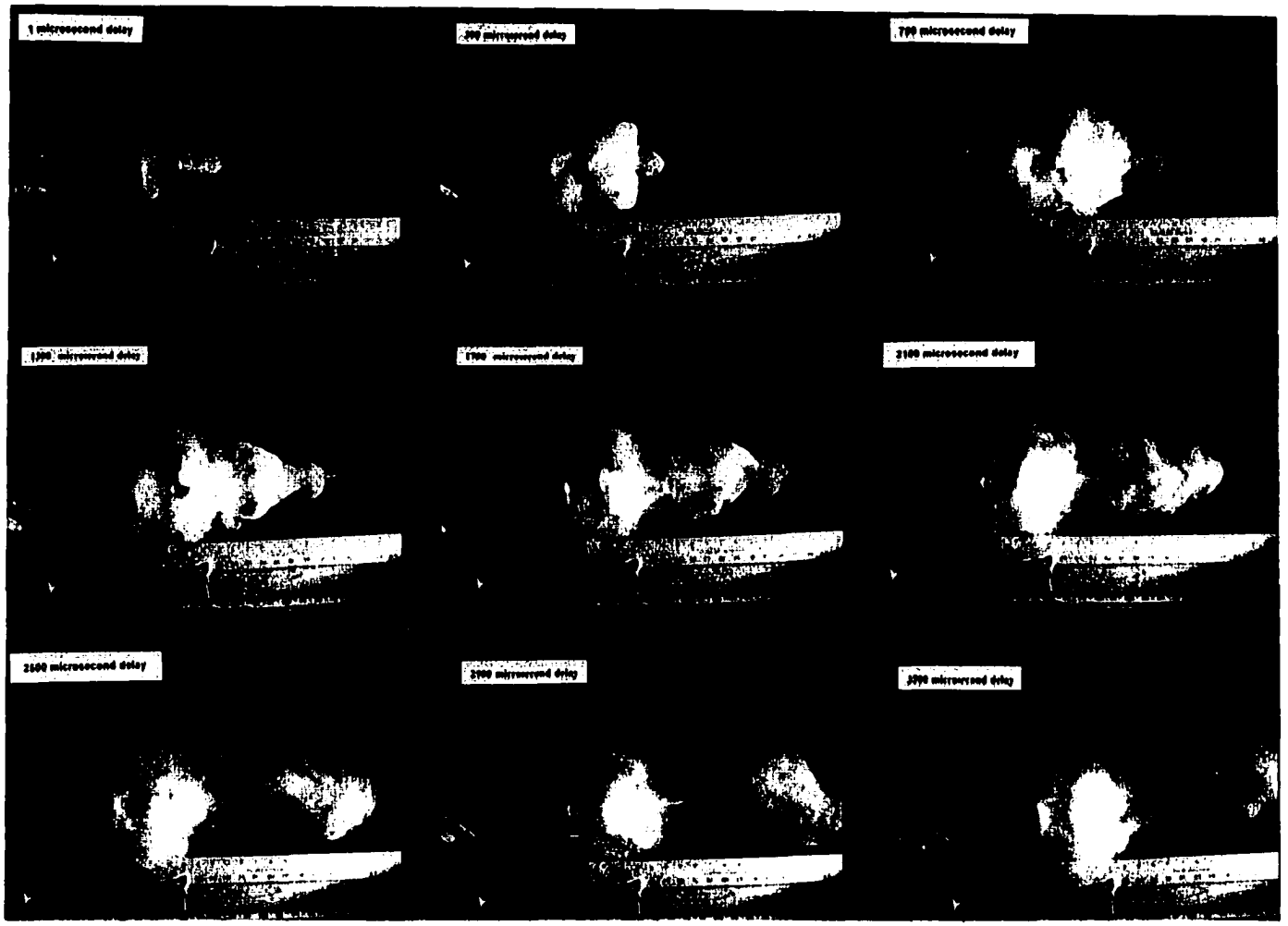

Figure 27. Synthesized Montage of Single Flash Photographs of Firearm Discharge. Federal .38spl, 158 grain, Lead, RN. Smith & Wesson 357 Magnum.

Figure 28.

Corresponding Shape of Flame and Muzzle Cloud. Federal .38spl., 158 grain, Lead, RN. Smith & Wesson 357 Magnum. Upper Photograph: 1 microsecond delay; Lower Photograph: 300 microsecond delay.

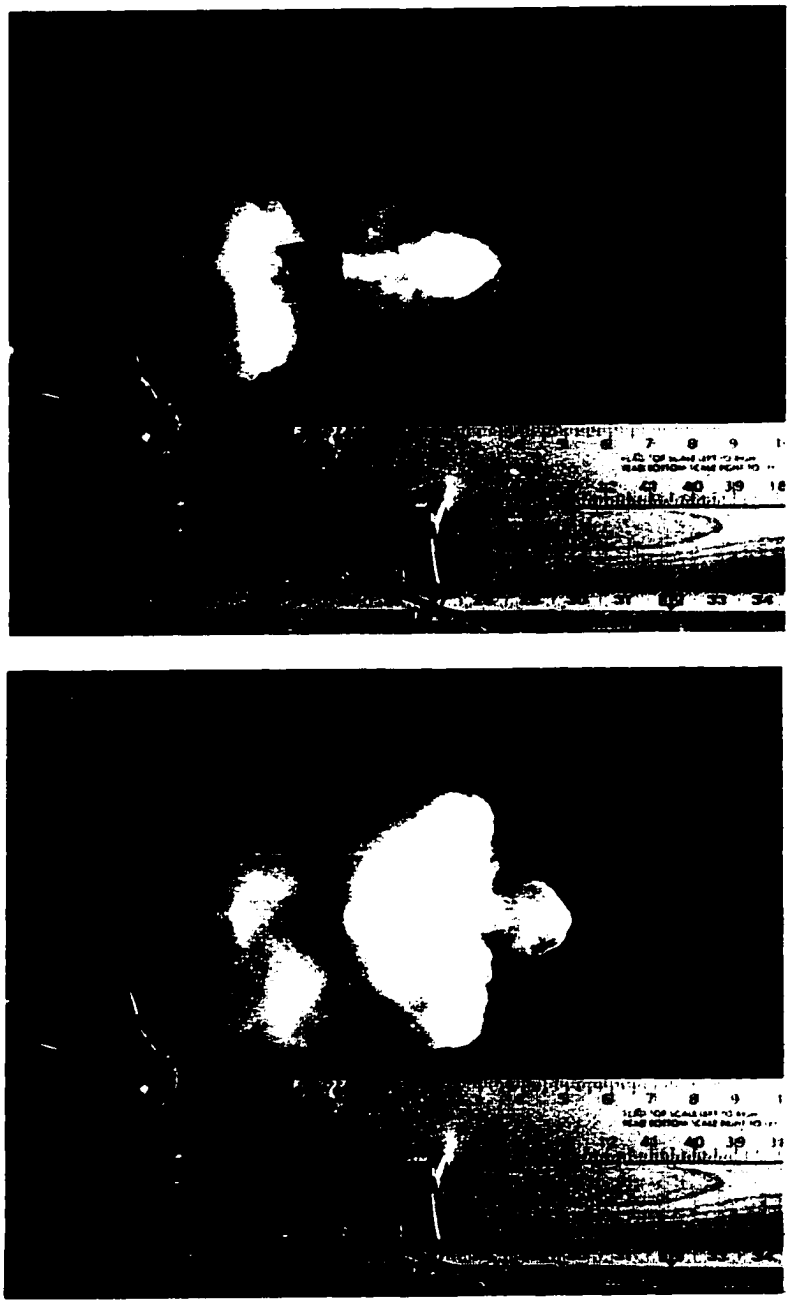

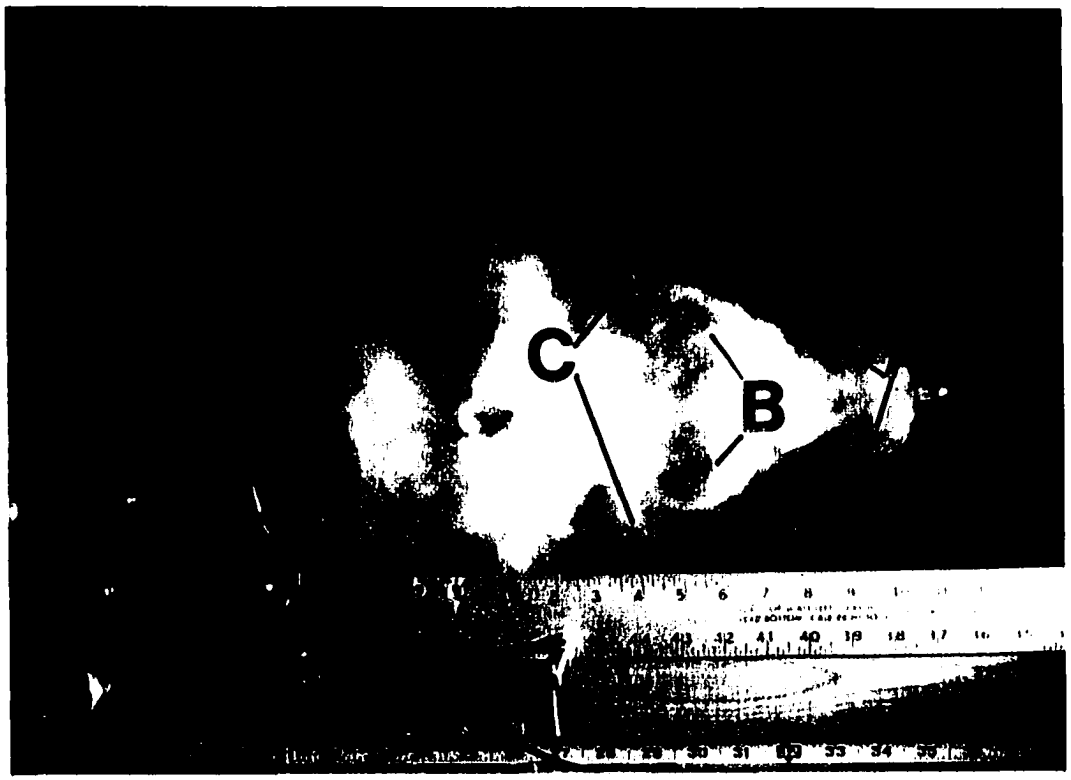

Figure 29. Single Flash Photograph of Turbulence in Muzzle Cloud. Three Pairs of Eddy Currents Indicated Respectively as A, B, & C. Federal .38spl., 158 grain, Lead, RN. Smith & Wesson 357 Magnum. Time Delay = 1300 microseconds.

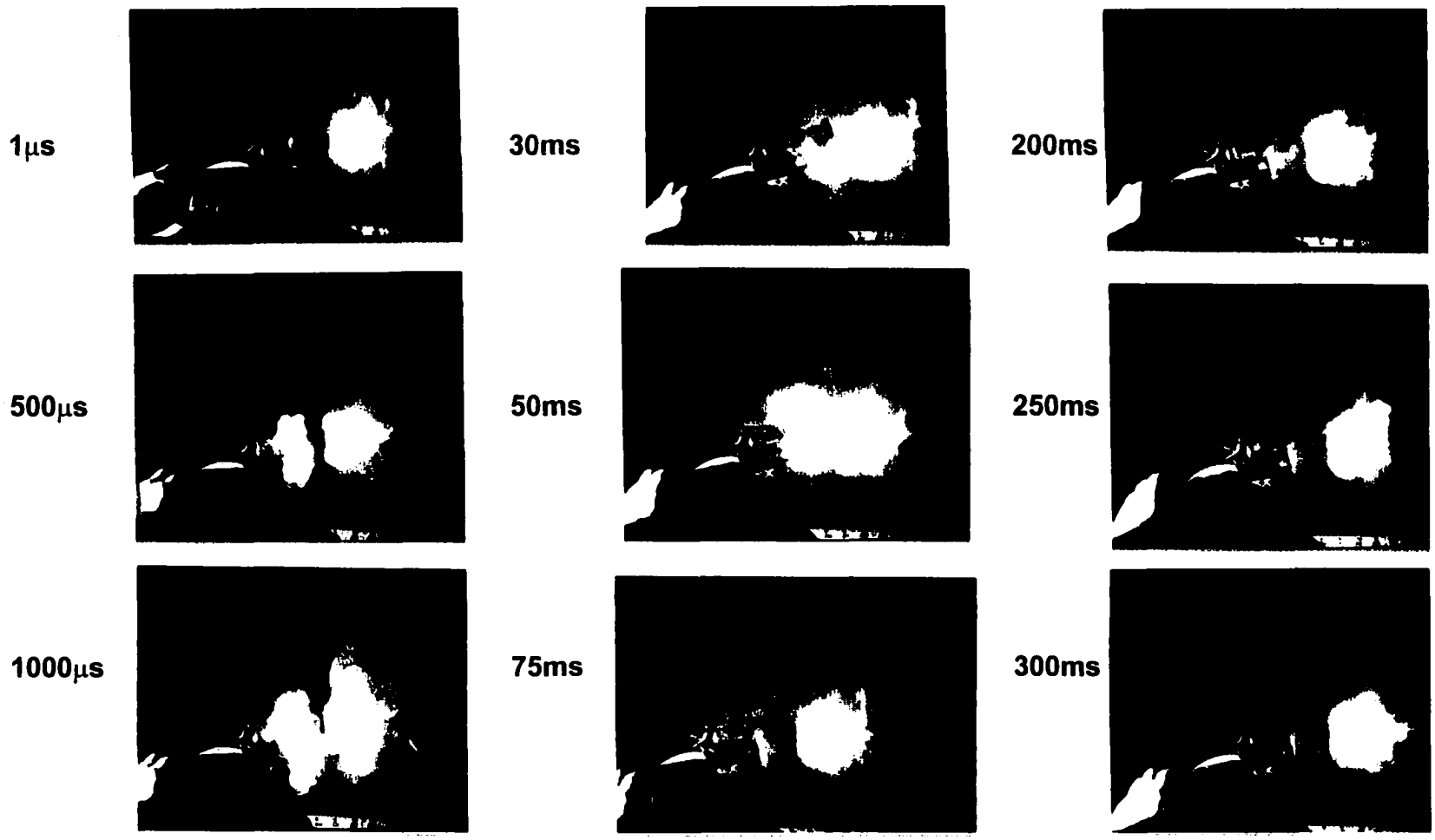

Figure 30. Synthesized Montage of Single Flash Photographs of Firearm Discharge. Winchester .38 Special, 158 Grain, SWC. Smith & Wesson 357 Magnum.

Figure 31. Vector Diagram of the Influence of Wind Velocity on Retrograde Cloud Movement

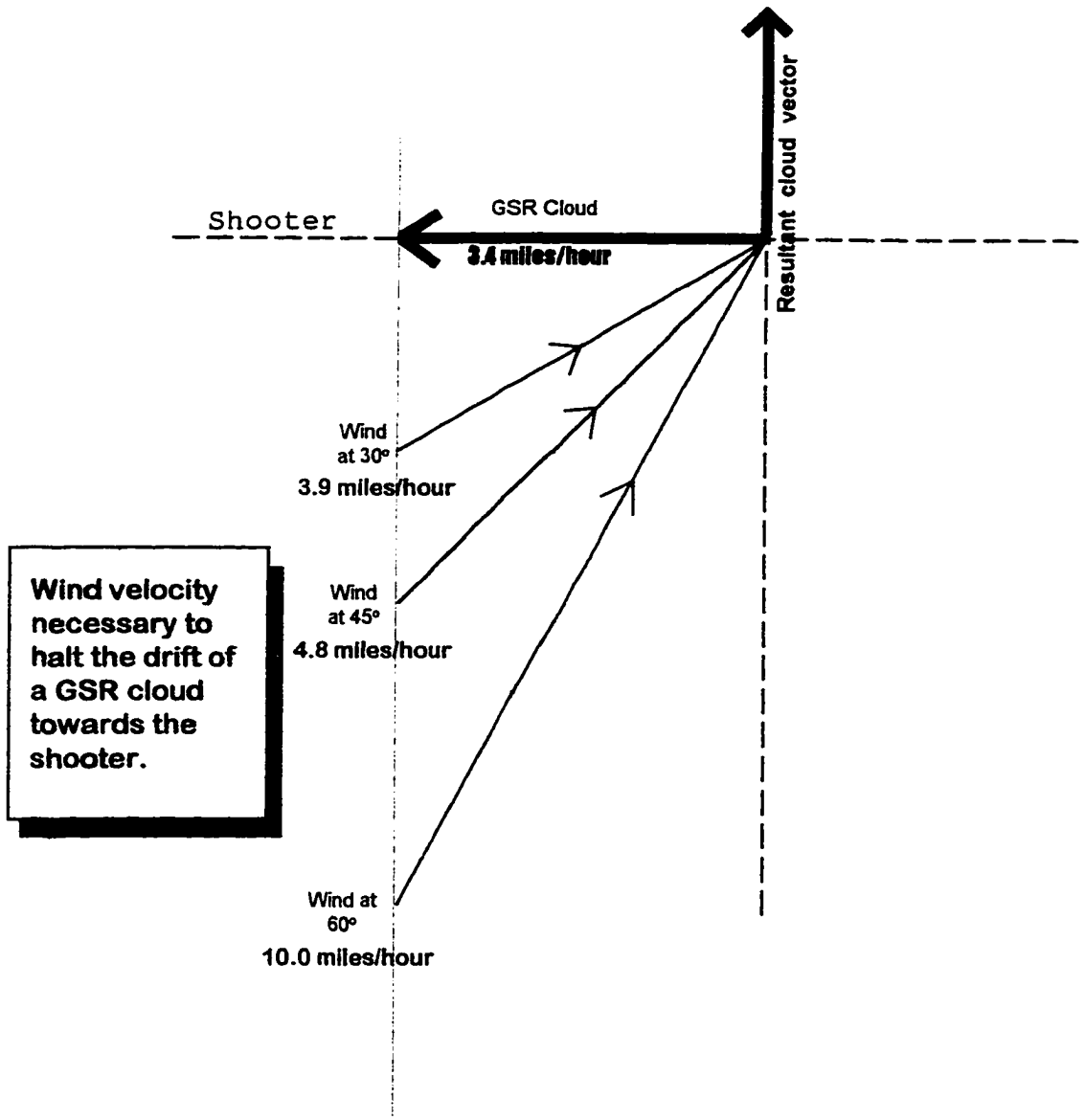

Chapter Five

Critical Assessment of "Walker" Transfer Methods: Modified Griess & Sodium Rhodizonate Tests

Modified Griess Test (MGT)

This study was conducted to assess the value and interpretability of the Modified Griess Test (MGT) as it is currently used in criminalistics today. There are several variations of this test but the most commonly used one appears to be that described by Dillon of the FBI laboratory (pp. 243-250, 1990). This variation utilizes sulfanilic acid and alpha-naphthol as the diazotization and coupling reagents respectively. The reaction is carried out in acetic acid (15% v/v). In acidic media, nitrous acid is produced from nitrite and reacts with primary aromatic amines (for example, aniline derivatives) to form a diazonium ion. This product reacts with a coupling reagent (most often a naphthalene derivative) to produce a colored azo dye. Not only have there been a number of variations of the process in criminalistics, but also in general analytical chemistry as well. The diazo-coupling reaction has been extensively studied since it was first described in detail by Johann Peter Griess in 1879. Actually Even earlier, in 1864, Griess had shown that pigments could be formed from a number of different nitrosatable compounds, nitrous acid, and a variety of coupling reagents (Fox, 1979, p. 1493). Since the research regarding the Griess reaction has provided significant information in general chemistry, some

relevant aspects are discussed here.

Originally, Griess used sulfanilic acid and 1-naphthylamine as the diazotization/coupling reagents in the presence of sulfuric acid. A short time later, Warington is reported to have modified the test by replacing the sulfuric acid with hydrochloric acid. In 1889, Ilosvay showed that superior results could be obtained with acetic acid instead of hydrochloric acid. This modification became known as the "Griess-Ilosvay" test. Similarly, in 1905, Weston reported that the reaction proceeded more rapidly and with less affect upon sensitivity (from excess acid) if acetic acid rather than hydrochloric acid was used. Weston recommended that the reagents be made more concentrated for convenience. This form of the test was widely used (Boltz, 1978, pp.216-217). These variations of the test were also, on occasion, referred to as "Modified Griess" methods in a non-criminalistics context. Sawicki et al., studied forty-two different reactions, for the detection of nitrite, spectrophotometrically (1963). Earlier, Rider and Mellon (1946) studied the diazotization and coupling reaction with respect to the effect of pH, reagent concentration, order of addition of reagents, temperature, light, nitrite concentration, and the presence of various ions. They found that strongly acidic and low temperature conditions are important for diazotization. Also, they reported that coupling should take place only after diazotization is complete and should be carried out in as low an acidity as is consistent with colorimetric stability. Except for a 1981 quantitative method for the determination of nitrites to estimate the muzzle-to-target distance on fabric

substrates by Petraco et al., low temperatures apparently have not been utilized for the diazotization reaction in a criminalistics setting. Different pH or buffer systems also, it would seem, have not been fully discussed in the criminalistics literature. Optimal reaction conditions may not be possible when the MGT is done either directly on the target or by the traditional transfer. An elevated temperature is required during the Griess reaction to obtain a visible nitrite reaction from propellant particles unless a saponification reagent has been introduced (Figure 32). It appears that much of what reacts at elevated temperatures is not inorganic nitrite. Saponification produces free inorganic nitrite from unburned propellant particles. This will be discussed in more detail subsequently. Another factor which could have a significant impact on the transfer is that it has been known for a long time that "a large excess of nitrite" produces only yellow colors (Fox, 1979, p. 1493).

The assessment of the Modified Griess Test (MGT) transfer method for the detection of gunshot residue was conducted considering a number of factors. The main criterion was efficiency (measured by the percentage of particles known to be present that provided a detectable reaction). Resolution, too, is a factor that has apparently been taken for granted. The Modified Griess Test cannot be properly assessed from one perspective, such as the number of times azo dye reaction product may be detected on the transfer medium from the same set of particles. A more important issue is whether the pattern on the transfer paper is representative of the pattern of partially burnt particles present

on the target, since the pattern transference has the most direct impact on the pattern interpretation phase of the technique. There is no evidence in the scientific literature that any researcher has ever conducted or even proposed an examination of this type. It is likely that this has not been attempted before because of the tedium involved in counting several hundred to three thousand particles on one pattern using a stereomicroscope. Additionally, these efforts must be repeated since a count of the reaction sites detected on the transfer paper must also be made. Interestingly, Dillon has stated (1990, Vol.22, p.248), in a casework context, that "..it is normally not productive and often not possible to attempt to relate a given positive point reaction on the test medium to a corresponding visible point source on evidence items." A number of variables such as differential reactivities of the particles, contrast, surface phenomena, and so forth, make the assessment more complex. The basis for the use of the Modified Griess Test in criminalistics has been that partially burnt particles are coated with or have nitrites embedded in their outer surface, formed during the combustion process from cellulose nitrate and glycerol trinitrate, which can be detected via a Griess type reaction (Walker, 1940). It has not been established how tightly bound the nitrite-containing molecules are to the surface of the particle or how they occur in the particle matrix. Why is heat required to obtain a positive Griess reaction with them? Is there a weak non-ionic or other chemical interaction between nitrites and other molecules at the surface of the particles? Do physical properties of the surface and nitrite molecules in their

organic environment play a role in conjunction with chemical factors?

I am not the first to assert that the Walker approach to the detection of partially burned particles with Griess may have some problems. According to Nesbitt and Jones (page 2-29, 1974), Krishnan (1973) reported that the "..method of Walker for detection of nitrites sometimes lacks the necessary sensitivity, and it fails to reveal many visible residue particles that can be easily observed with the optical microscope." Krishnan had also stated (1968, p. 314) that the Walker test, "..under certain circumstances are lacking in accuracy... Since 1937, not much work has been done to improve the accuracy of the methods, nor has any new method been developed." Krishnan advocated the use of an autoradiography technique for the detection of antimony around bullet holes (using a nuclear reactor). Recently, Bonfanti & Gallasser (1996, pp. 108-109) reported that "...results obtained by visual inspection do not always correspond with those obtained with the Modified Griess Test." They found that some sources of ammunition provide more visible residue than is detected by the Modified Griess Test. They reported that poor results were obtained with discharge patterns from NORMA .38 special in comparison to the heavy visible deposit. Additionally, colored wool substrates were found to cause serious background problems for the Griess transfer.

Evaluation of Modified Griess Test

Method and Materials

The Modified Griess Test results were compared with the results obtained from a stereomicroscopic examination for particles. A separate set of examinations was done by comparing the MGT results to those obtained by native fluorescence. The latter examinations helped with the evaluation of the MGT and also demonstrated the utility of fluorescence examinations. Additional experiments involving fluorescence are discussed in subsequent chapters. Several factors were also considered in critically assessing the MGT such as differential reactivity of particles, non-homogeneity of the transfer paper, sources of alpha-naphthol, quality control, etc.

The use of thin light colored cloth as target material for casework exemplars or for evaluating the efficiency of this method can be misleading. First, such cloth is an ideal medium for transfer because: (a) the Griess paper can make close uniform contact with the substrate, and (b) there is excellent heat transfer through the fabric. Additionally, dark particles are readily detected against the white background, while the pale straw-colored translucent particles are difficult to locate. These same particles are difficult to see on such a background even if they are residing near the surface. Of course, many particles may be hard to see because of being imbedded within the substrate from the kinetic energy prior to impact. Stereoscopic examinations can provide significantly more information than can an unaided visual inspection. This is true

not only for the direct examination of the target material, but also the transfer paper as well.

Materials

Stereomicroscope with ring light illumination (10-25X)

Combination Swivel Magnifier/Lamp, Luxo Co.

Crimescope CS-16 Tunable High Intensity Light Source

Heckler & Koch 9mm semi-automatic pistol

Smith & Wesson 357 Magnum Revolver, Model 19-2

.32 Walther PPK

.380 Colt Mustang Pocket Light

Cecil UV/VIS Spectrophotometer (Series 3000)

alpha-naphthol (99+%) Sigma or JT Baker (light crystal) for particle counts

alpha-naphthol from Aldrich, Fisher, and JT Baker (dark crystal) for comparison of alpha-naphthol reactions.

sulfanilic acid (reagent ACS) Eastman

HPLC grade or distilled water

HPLC grade methyl alcohol

white cotton/polyester blend fabric

Kodak B&W Photographic Paper Type F

Heating Iron (#6 cotton setting)

Stereomicroscopic Examination v. MGT

An assessment of the Griess method was conducted by comparing the

number of particles present on a white cotton/polyester blend target using a stereomicroscope with the number of reactions sites on Griess paper. All discharges were made from 12 to 18 inches to obviate interference from vaporous lead. All experiments were conducted using transfer paper that provided a strong reaction with the positive sodium nitrite control on each corner of the paper. Nine commonly available sources of ammunition were used for this study (Table 4). One discharge pattern was produced from each source with the exception of the PMC 357 Magnum. Two patterns were made from the latter source: a full pattern and a fourth of a pattern. Each firearm was cleaned prior to discharge each day of use. Additionally, before producing a discharge pattern, the weapon was discharged twice with each new source of ammunition.

Counting was accomplished by marking a sheet of cellulose acetate, which had been affixed to the discharge pattern or transfer paper, with an extra fine Sharpie Brand non-aqueous ink marker to note the position of a particle or reaction site. This entire process was done as gently as possible so as not to disturb the pattern. The counting was conducted by use of the swivel magnifier and stereomicroscope. The stereomicroscope was used to count visible particles, directly on the fabric, observed with the microscope illumination.

MGT v. Fluorescence

The fluorescence portion of this series of experiments was conducted by illuminating the target surface with visible light with wavelengths from 455 to 495nm, while the emission was monitored using orange barrier filter goggles.

Dark, relatively thin fabrics were used to facilitate the detection of particles via fluorescence and to more efficiently allow for the heat transfer. Dark fabrics generally produce significantly less background fluorescence compared to bright fabric. Discharge patterns were produced from a variety of ammunition by discharging various handguns onto black, dark blue, and dark grey substrates from a distance of about 12 to 18 inches. This distance was selected so that interference from the fine lead deposit would not be an additional factor in this set of experiments. Thirty-seven patterns from nine different sources of ammunition were produced and used for this experiment. Nine replications were made from the same box of Federal .38 Special ammunition, five replications from the same box of PMC 357, and a sixth from a different box with the same lot number, and five replications from the same box of Winchester .38 Special ammunition. Also, ten replications were made from Remington .38+P ammunition taken from two boxes having different lot numbers. Fewer replicate test firings or even a single test firing were used with other ammunition sources as indicated in Table 5. The firearms were cleaned and cleared before discharge as discussed above in the stereoscopic examination section. A sheet of cellulose acetate was superimposed over each GSR pattern. The transparency was marked with an extra-fine Sharpie® pen wherever a propellant particle was detected. Following the count of particles detected during native fluorescence experiments, MGT transfers were made in the usual manner using sulfanilic acid and 1-naphthol. Only Griess paper that provided

a strong reaction with the nitrite control in each corner of the paper was used.

Results and Discussion

Stereomicroscopic Examination v. MGT

Pressure, heat, and chemical reagents are simultaneously applied to particles during the Modified Griess Test. However, the test is not a perfect representation of the pattern of partially burnt particles on the target material. It is quite effective in some instances, but inadequate with certain sources of gunshot residue. With some sources of ammunition, only a fraction of partially burnt particles provide detectible reactions. One of the most striking examples of this is PMC 357 (Table 4).

The results suggest problems with the Modified Griess Test with certain ammunition. The total number of particles detected stereoscopically was 3348 v. 2151 with the Modified Griess Test. Overall, 56% more particles were detected using the stereoscopic method. The ratio of particles detected by each method was also calculated (see Table 4). The ratio calculated for each pattern demonstrates that the stereoscopic examination was superior in the detection of particles in eight of the ten patterns and equivalent in detection regarding the other two patterns. The ratio in eight of the ten patterns was in the range of 1.0 to 1.5 (stereo/mgt). The ratios calculated from the two remaining two patterns more greatly favored the stereoscopic examination. The mean ratio calculated from all ten patterns was 1.6 (stereo/MGT). It should be noted that the count process of the reaction sites on the transfer paper was done generously, that is,

a wide latitude was applied to any area suggesting a particle reaction. It is clear from the above that a variety of results are obtained depending on the ammunition source. As illustrated in Table 4, some ammunition sources provide better results with Griess than others (see Figure 33; transfers of two different ammunition sources on the same paper). Most noteworthy of the poorly reacting sources is the PMC 357. These results also indicate that there may be some problems with the detection of 357 ammunition in general. Further analysis of this as part of a future study might be of value. Since the stereoscopic experiments were conducted on white fabric, the counting of the dark particles was favored. Light colored particles are particularly difficult to detect on light backgrounds. The majority of particles in most patterns are light colored. In some instances, the particles detected stereoscopically corresponded very closely with those detected by the Modified Griess Test. In other cases, while there was a considerable overlap of the same particles detected by each method, some particles were detected by one approach but not the other. These findings suggest that the two methods may be somewhat complementary. Since this set of experiments was carried out on light backgrounds, many more particles may have been actually present that went undetected.

Fluorescence Examination v. MGT

As shown in Table 5, the total number of particles detected by fluorescence was 19,144 in contrast to 13,616 detected with the Modified Griess Test. Overall, 41% more particles were detected using the fluorescence method. The mean ratio calculated from all the patterns is 1.9 (fluorescence v. MGT). However, in 13 of the 37 patterns, the Modified Griess Test was superior to the fluorescence approach (see Table 5 for details). Thus, it is clear that there is considerable variation in the manner in which different ammunition sources will behave regarding both native fluorescence and the Modified Griess Test. An illustration of this is depicted in Figure 33. Two different sources of ammunition were discharged for this particular experiment: Remington .38+P, and CCI 357. All experimental conditions were the same except for the type of ammunition. Even the Griess paper used for the transfer was the same (an 8" x 10" sheet paper was cut in half). The reaction corresponding to the Remington ammunition is for the most part relatively intense. Conversely, the reaction corresponding to the CCI ammunition is relatively weak. By inference, these findings indicate problems for the interpretation of patterns involving the latter ammunition, since even with the strongly reacting Remington ammunition, there are some reaction sites which are barely detectible. If some sites are near the limit of detection for the Remington, what is the likelihood of detecting all the reaction sites on the paper corresponding to the CCI ammunition?

A notable example of variation involves two different sources from the

same manufacturer. The extreme of particle non-reactivity can be observed with 357 Magnum PMC ammunition. Unlike .38 PMC ammunition, the .357 PMC source always gave a weak reaction on the transfer paper. A much greater number of particles were always detected via native fluorescence with this particular ammunition (Table 5) compared to the transfer method.

The data presented in the present chapter demonstrates a variation in the number of particles that can be detected from the same source of ammunition (see Tables 4&5). A considerable amount of variation was obtained from cartridges taken from a single box of ammunition. For example, for Federal .38 Special the standard deviation of the ratio (fluorescence/MGT) from nine replicate discharges was 1.1 (mean = 2.0). Many examples of propellant variation from discharge to discharge were noted while conducting high speed photography experiments. Some of these are noted in Chapter Four.

To compare variation from lot to lot, five replicate discharges were made from two different boxes of Remington .38+P (ten patterns). The mean ratio from one box was 0.34 (s = 0.12) in contrast to 1.1 (s = 0.41) for the other. Thus, a considerable amount of variation may be found in different lots from the same source.

The clear implication of these results is that one exemplar pattern at each distance for casework is insufficient. Several discharges should be made at each incremental distance to ensure that the resulting pattern is repeatable.

Some particles may not be detected because of problems inherent in a

transfer method, or in the chemical reactions themselves. The composition of the outer surface of partially burned particles may not be the same as the interior. A number of researchers (Nesbitt & Jones; Basu, 1982) have found metals present on the surface of partially burnt particles. The surface composition is greatly dependent on the heterogenous nature of the propellant ignition, primer composition, and vaporization of materials from the projectile passing through barrel, as well as previously deposited materials from prior discharge. Obvious differences in particle appearance are often seen. Propellant particles are found that have a pale yellow exposed surface while the surface adhering to the target material is blackened, giving a charred appearance. Not only are differences among ammunition sources observed, but they also occur within the same lot, within the same box, and even within the same cartridge. In Figure 34, a portion of a Griess transfer is shown where two fairly intense reactions have taken place in opposite corners of the same paper. However, in between the two reaction sites there is a range of medium to very weak reactions that is visible. A plausible explanation for these reaction differences is that some particles are rich in surface inorganic nitrite precursors whereas others are not. In 1984, Steinberg et al., utilized eight percent ethanolic potassium hydroxide at 100^0C, for five minutes, to hydrolyze all the available nitro group constituents for a Griess type reaction. These researchers were attempting to detect GSR on the shooter's hands, and asserted that they were "increasing sensitivity" by the saponification procedure. They recognized

that some molecules, bearing nitro groups, were present on the hands of a shooter that were not in the form of inorganic nitrites, and as such would not react with Griess. It is well known that nitrate esters produce nitrite ions by alkaline hydrolysis (Yinon and Zitrin, pp. 37-38, 1981). The mechanism is believed to be:

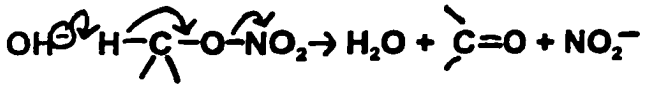

Petraco (1995) has indicated that he would often use zinc to obtain nitrites from nitrates to produce an observable reaction with Griess for the estimation of the muzzle-to-target distance. It is reported (Yinon and Zitrin, p. 38, 1981) that nitrate esters are reduced by zinc in acidic medium as indicated below:

$$RONO_2 + Zn + 2H^+ \rightarrow ROH + Zn^{++} + HNO_2$$

In addition to differential reactivities arising from the propellant charge within a single cartridge some of these observations may be due to non-homogeneity in the transfer paper itself. De Forest et al. (1995) have obtained different intensities of reaction of the same inorganic nitrite solution on the same Griess paper.

The Walker method requires the criminalist to simultaneously apply pressure and heat, under acidic conditions, while confining surface nitrites into a relatively small space. Such confinement allows the process to continue in a relatively small reaction between the substrate and the transfer paper, provided that little space exists between the paper and the particle. Without elevated temperature, under acidic conditions, the reaction will not take place between

partially burnt particles and the Griess reagent. Since the particles do not react at lower temperatures, it is apparent that no inorganic nitrite ions are available to produce the intermediate nitrous acid. Clearly, there is a difference in the nitrite ion environment of an organic source versus an inorganic source. It has been widely asserted that nitrite ions are produced during discharge and are available to react with Griess. However, all such techniques require heat to be applied as indicated above when the source is propellant particles. Since no application of elevated temperature is required for the reaction to take place when the source is an inorganic nitrite, this explanation is inadequate.

This has obvious implications for other techniques used for the detection of nitrites throughout this research, and for actual casework. If nitrites are not available for reaction, except after the application of heat, one should not expect other methods (requiring readily available inorganic nitrite ion for the positive reaction) to take place at relatively low temperatures.

If the procedure causes reaction products to be fused together on the transfer medium resulting in a relatively large reaction area, it is not clear to the examiner whether this is due to a number of particles or a single particle that has reacted very intensely. The space between reaction sites must also be relatively clear of reaction product or it will be difficult, if not impossible, to resolve reaction sites from the background and associate them with corresponding individual propellant particles. Often, ammunition from certain sources provide a very strong orange reaction area of two or three inches in

diameter around the bullet hole that obscures the small reaction sites corresponding to particles. In these cases, subsequent transfers can improve pattern features in those specific areas. However, there is no indication from the forensic science literature that repeated transfers are done in casework.

The generally accepted positive control for routine Griess test examinations, in casework, consists of the placement of inorganic nitrite (0.6% aqueous sodium nitrite w/v) at the corners of the test paper. If an orange red color develops in the four corners of the paper it is considered adequate. Since no heat is required to obtain a positive result with inorganic nitrite, we need to ask how can an examiner be sure that sufficient heat has been applied across the transfer paper to obtain an adequate reaction from an organic source? As previously noted, despite the use of relatively thin fabric for these experiments, many particles went undetected via the Modified Griess Test. In casework, a wide variety of much thicker fabrics may be encountered, which may be more difficult for the heat to permeate. The reaction volume is also increased under such conditions. It is probable that the number of undetected particles in casework is greater than in research conducted and reported here.

Since nitrous acid is a gas, for a reaction to take place on the Griess paper, there must be a relatively close contact between the two surfaces. The further the paper is from the surface containing the particle the greater the chance for the gas to diffuse resulting in little or no observable reaction. Clothing having peaks and valleys, seamed areas, and so forth, can cause

problems of this nature. Additional problems are experienced with various types of fabrics. If the propellant particles penetrate deeply enough into the interstitial spaces, dilution of the nitrous acid, caused by lateral diffusion, may result in its concentration dropping below the detection limit. Recently, Bonfanti and Gallasser (1995, p. 115) discussed problems when conducting the Modified Griess Test with targets made of polyamide/polyurethane blends. These problems were related to the melting of the target due to the elevated temperature applied for the examination. They had also encountered problems with colored woolen surfaces. They discovered that the transfer paper became a uniform orange color, and thus GSR could not be detected. They attributed this interference to the wool coloration process, since they did not experience the same problem with uncolored wool. De Forest et al. have reported that transfer efficiency is reduced by increased thickness of the fabric (1995, p. 6). This finding may be attributed to an attenuated heat transfer during the reaction process and diffusion of the formed nitrous acid. The high particle velocity, coupled with loosely woven or thin yarn, may allow these relatively small projectiles to not only penetrate deeply into the fabric but actually perforate it as well. On numerous occasions during the course of this research this was found to be true (see Chapter Four). Thus, many particles that contact the target are not available for reaction. This is not a shortcoming of the Griess reaction but must be taken into account when performing the Modified Griess Test. Fabric type must be considered, and if possible, duplicated, in estimating the muzzle-

to-target distance. Increasingly, this once-common practice has fallen out of use. Replicate test firings, using fabric as similar to the evidence substrate as possible, are advisable.

In the early stages of this research, it was noted that some transfer paper gave a weak reaction with the nitrite control. An attempt was made to determine the cause of this lack of sensitivity. It was suspected that 1-Naphthol (alpha-naphthol) might be the cause of the problem. It is known to darken when exposed to light (Merck, 1983, p. 917). The test papers that gave the weak reaction were observed to have a subtle darker cast to them, apparently corresponding to a 1-naphthol source that was dark as a powder prior to being placed in solution. Five different sources of 1-naphthol, ranging in color from very light to dark, were studied to further explore this problem. These were studied by reaction with partially burned propellant particles, spectrophotometrically, and by melting point.

The five sources of 1-naphthol were used to prepare five different Griess transfer papers. Each was made in the same manner and stored in precisely the same way until used on the following day. The only variable was the 1-naphthol source. Each paper was heat-sealed in a plastic bag and placed into the same drawer to protect it from light. Portions of each were then used to test five equal portions of the same discharge pattern. The discharge pattern was uniform. In Figure 35, five Griess transfers are shown corresponding to the five different sources of 1-naphthol. All solution concentrations and reaction

conditions were the same for each quadrant. Figure 35 illustrates the extreme color variation of the alpha-naphthol from each of the five different sources in solution. While there is a noteworthy difference in the color of each solution, and a range of melting points for crystals from each source (77°C to 94°C), it is interesting that no significant difference was obtained from the Modified Griess Test depicted in Figure 35 for each of the five 1-naphthol sources. The azo dye solutions were studied spectrophotometrically as well (Figure 36).

An aqueous solution of sodium nitrite was prepared at a concentration of 0.01M and reacted with equal volumes (500 microliters using a digital pipette) of aqueous sulfanilic acid (0.03M) and alpha-naphthol (0.02M) in methanol at room temperature. The azo dye solution was transferred to a 25ml volumetric flask and diluted to volume with water. It should be noted that once the reaction had taken place there was no visual difference in color between the five solutions. The same five sources of alpha-naphthol previously mentioned were utilized for this experiment. Each azo dye solution was scanned from 250nm to 650nm for any observable differences. None were found. The absorbance of each solution was also measured at the wavelength of maximum absorbance (with spectrophotometer held at 477nm). No significant difference was noted spectrophotometrically (Figure 36: absorbance spectrum of each solution). These results suggest that although the color of the 1-naphthol is dark it may still provide an adequate coupling reaction in this context. Additionally, the limited experimentation conducted here with the reagents in the solid state does

not suggest anything contradictory. However, the safer course in casework or research would be to use 1-naphthol that has not degraded to a dark color. More studies to clarify the situation should be conducted.

The manner in which this assessment was carried out for research, that is, by mapping the particles and azo dye reaction sites, is generally superior for analyses to the casual approach used by forensic laboratories during analysis of evidence. Casework is carried out by a relatively superficial comparison between a Griess transfer from the evidence and a visual examination of GSR patterns produced on white muslin fabric at known muzzle-to-target distances. Many details may be overlooked by such an examination.

It is concluded that the Walker transfer method, incorporating the Modified Griess Test, while providing excellent results under certain conditions, often provides less than satisfactory pattern information. As a pattern visualization and comparison tool, it is far from perfect. The low particle counts found in the previously discussed experiments illustrate the potential for interpretation problems. This research indicates that the Modified Griess Test should be used in conjunction with other approaches, and that a number of changes can improve its efficiency. In casework practice, the incorporation of a thorough stereomicroscopic and fluorescence examination appears to provide information complementary to that from the Modified Griess Test, and would make the overall process more interpretable and accurate. This subject will be considered further in the "Integrated Sequential Techniques" section.

Sodium Rhodizonate Test

It has been well established that the sodium rhodizonate test is better conducted directly on fabric instead of by transfer, since only a "fair portion" of the lead pattern will be transferred (Bashinski, 1974). In fact, the same authors stated "..if the target is a light colored fabric, it is much preferred to develop the lead pattern directly on the target." De Forest et al., (1995) have found that the method is relatively inefficient in the sense that only a fraction of the lead is transferred each time. They reported "..little pattern fidelity from transfer to transfer," and that fabric thickness influenced transfer efficiency. This does not appear to be a serious problem when the lead deposit is strong, but, when it is weak, that is, at the detection limit of the reagent, it is problematic. The latter researchers found that in the case of weak patterns, a discernible quantity of lead was still present on the target substrate, although it could not be detected on the transfer. This presents a serious problem for casework involving dark colored fabrics. The lead pattern is altered by the hot acetic acid used for the Modified Griess Test before the Sodium Rhodizonate Test. It has also been pointed out that the moisture content of the transfer paper can influence the effectiveness of the transfer (Lichtenberg, p. 55).

Bullet wipe is also adversely affected by the previous application of the Modified Griess Test. The prior treatment with acetic acid causes the diffusion of the lead around the bullet hole from one side of the fabric to the other. This quite often so seriously affects bullet wipe that it cannot be utilized to determine

the direction of travel of the projectile. A subsequent transfer attempt for Rhodizonate may further damage the bullet wipe pattern rather than make it easier to visualize. Thus, instead of transfer, a direct application of reagent would be advantageous. Better yet, the diffusion of the pattern would be virtually eliminated if bullet wipe is analyzed prior to the Griess Test being carried out for the detection of nitrites. An approach to eliminate this problem was recently introduced by De Forest et al. (1997). They used Benchkote® (a polyethylene-backed absorbent paper available from Whatman) to compare the lead transfer from each side of a bullet hole prior to conducting the MGT. The Benchkote® was cut to approximately 2.5cm^2, moistened with 5 -15% acetic acid, and applied simultaneously to both sides of the bullet hole site by finger pressure.

Another disadvantage of the rhodizonate test, direct or indirect, is that particle information towards the central area of the pattern is lacking. The particle reactions are overwhelmed or blend with the reaction resulting from the fine lead cloud residue. In the accompanying figures (37 & 38), it is in fact easier to see the particle reactions in the transfer compared to the direct application of rhodizonate, since the reaction in the latter case is uniformly strong in the central portion of the pattern. However, in casework, a transfer would not have been conducted with a white colored substrate since the direct method would be, in general, superior to the transfer technique. These figures also illustrate the lack of pattern fidelity of the transfer method in comparison to

the direct method. The lack of pattern fidelity is especially a problem in the normal casework sequence where the lead transfer follows the nitrite mapping with its integral hot acetic acid treatment. Although the pattern corresponding to the direct method does not reveal particle information, it is much more informative regarding the fine lead distribution in comparison to the transfer. Even the first transfer is not uniform and is not an adequate representation of the actual pattern.

Figure 32. Partially Burned Particle Reactivity with Griess at Room Temperature. Column A: Saponification with Potassium Hydroxide prior to Griess. Column B: no pre-treatment.

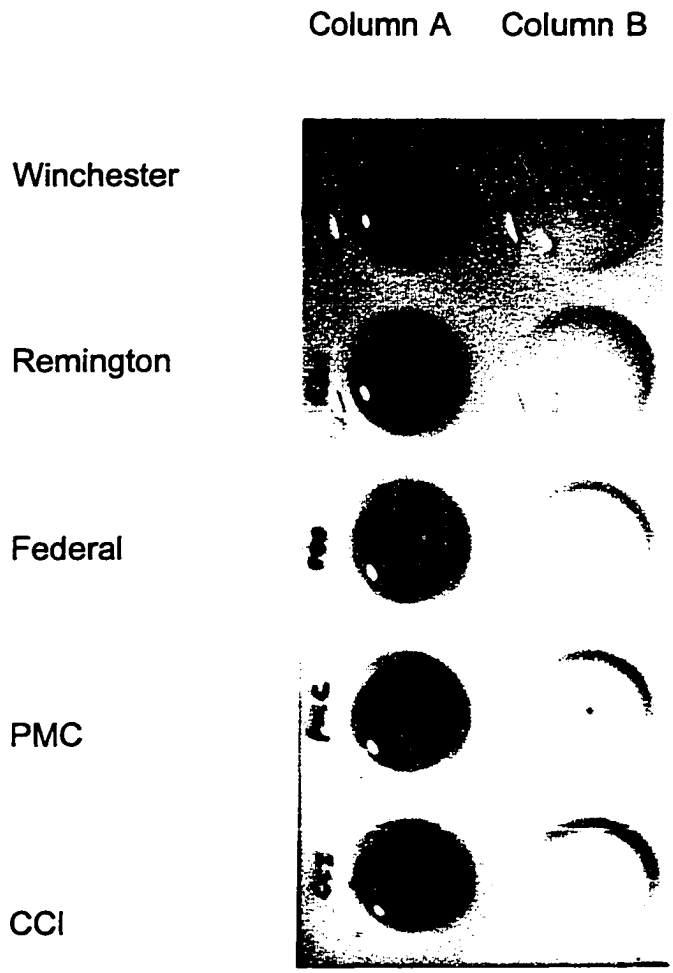

Source	Grain, head	Stereo. Exam.	MGT	Ratio Stereo/MGT
Winchester .38+P	158, SWC	80	61	1.3
Federal .38	158, SWC	34	32	1.1
Federal 357Magnum	110, JHP	573	455	1.3
Federal 9mm	115, JHP	1096	721	1.5
Remington .38+P	158, SWC	134	136	1.0
CCI 357 Magnum	158, JHP	504	401	1.3
CCI .38+P	158, TMJ	87	75	1.2
PMC .38	158, SWC	50	48	1.0
PMC 357 Magnum	125, JHP	110	47	2.3
PMC 357 Magnum	125, JHP	680	175	3.9
	total count	3348	2151	
			mean	1.6

Table 4. Comparison of Particle Counts: Stereomicroscopic Examination v. Modified Griess Test

Table 5. Particle Count: Fluorescence v. Modified Griess Test

source	Grain, Bullet	Fluorescence	(MGT)	Fluor./MGT
Fed. 38+P	125, JHP	231	162	1.43
Fed. 38 Special	158, SWC	179	146	1.23
		180	146	1.23
		327	68	4.81
		259	123	2.11
		165	66	2.50
		231	162	1.43
		86	91	0.95
		128	75	1.71
		126	67	1.88
		157	63	2.49
Remington .38+P	158, SWC	162	639	0.25
		160	721	0.22
		264	504	0.52
		213	716	0.30
		181	447	0.40
		205	506	0.41
		644	446	1.44
		525	494	1.06
		601	428	1.40
		486	434	1.12
MagTech .380		184	36	5.11
		172	43	4.00
CCI .32		121	68	1.78
CCI .380		158	87	1.82
Fed. 357 Mag.	110, JHP	306	522	0.59
PMC 357 Mag.	125, JHP	2163	500	4.33
		1231	212	5.81
		1406	266	5.29
		2031	464	4.38
		1872	460	4.07
		3035	2235	1.36
Winchester .38 Special	125, JHP	68	526	0.13
		247	400	0.62
		179	390	0.46
		280	523	0.54
		181	380	0.48
	Total	19144	13616	
			mean	1.9

Figure 33

Differential Reactivity of Two Different Sources of Discharge on the Same Griess Paper. Left side: Remington .38+P 158 grain LD SWC; Right side: CCI 357 158 grain, JHP. Both discharges were at a muzzle-to-target distance = 30cm (12inches).

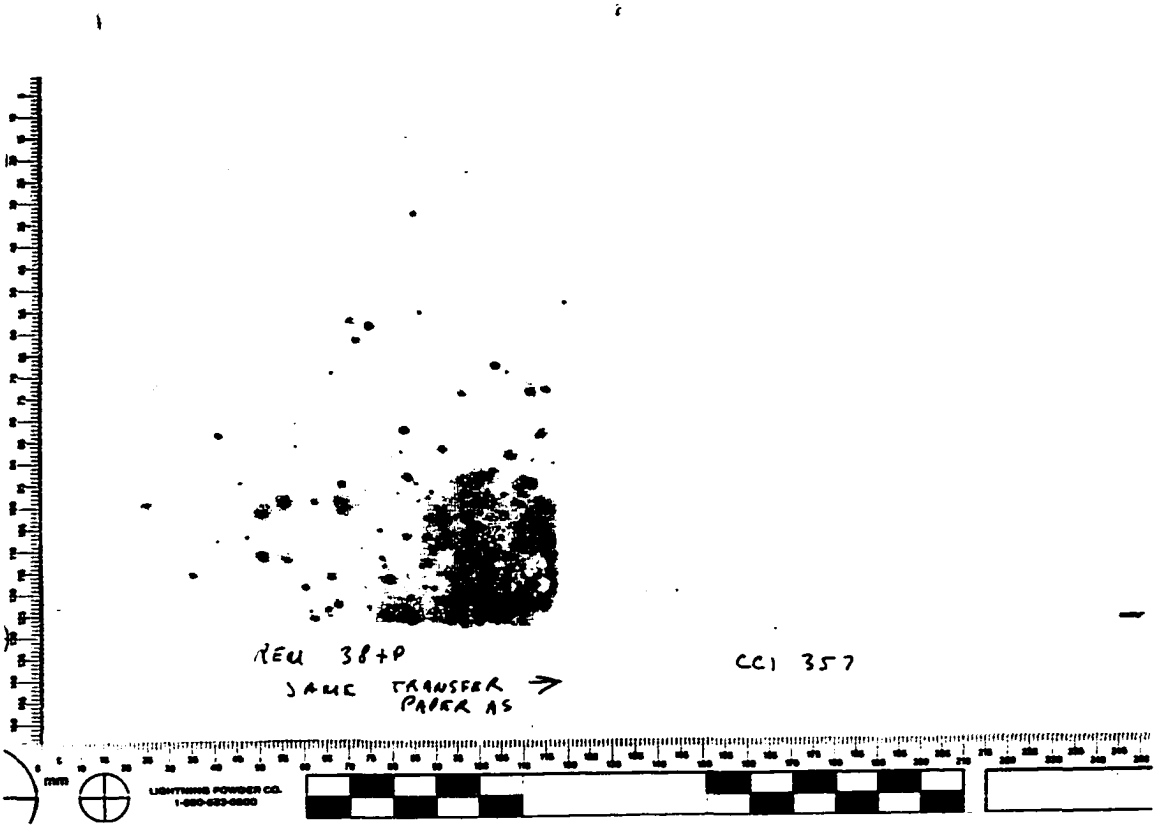

Figure 34

Continuum of Reactivities with Griess on Transfer Paper from Same Discharge. PMC 357 125gr. JHP. Muzzle Distance = 12" (30.5cm). Note Adequate Reaction Intensity at Opposite Corners.

Figure 35. Five Different Sources of 1-Naphthol (Very Dark to Clear Solutions). Upper Photo: In Solution; Lower Photo: Five Griess Transfers (using same 1-Naphthol solutions shown in upper photo.) from five sections of the same discharge pattern. Winchester .38+P, 158 gr. SWC. Muzzle D. = 18 inches.

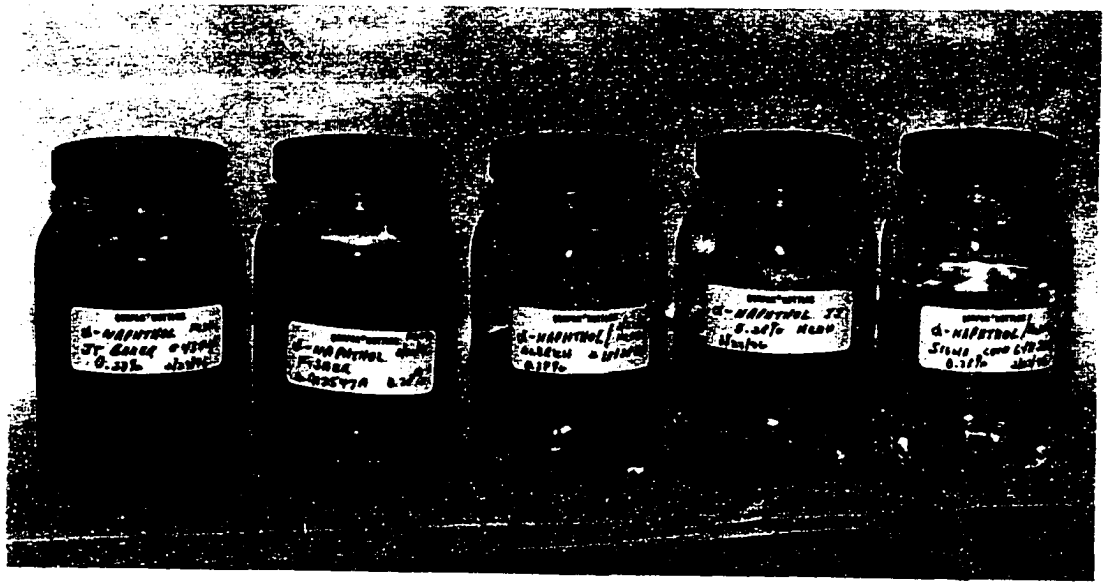

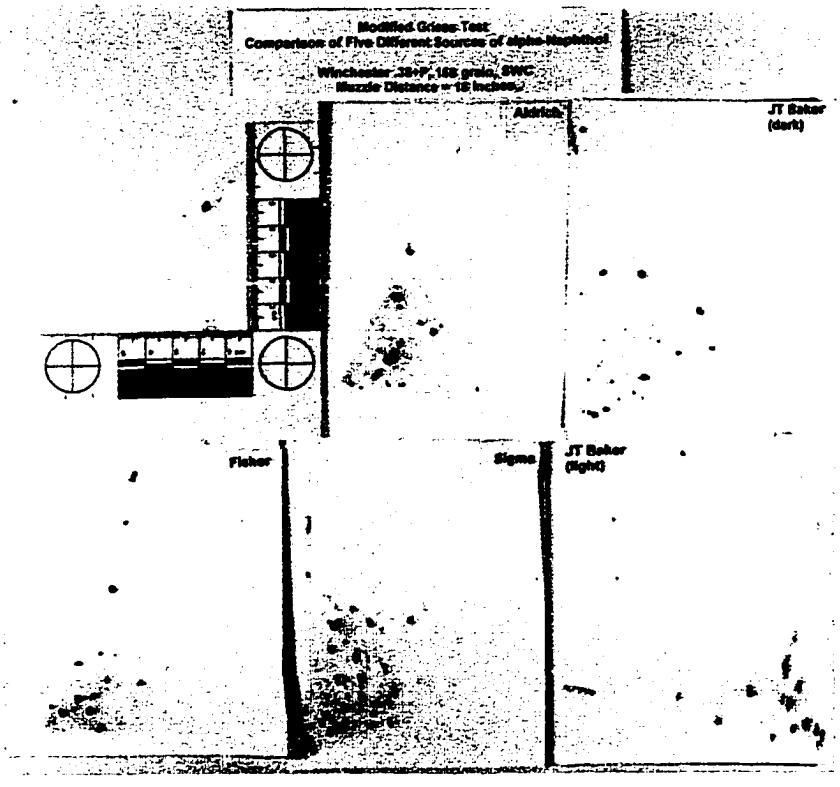

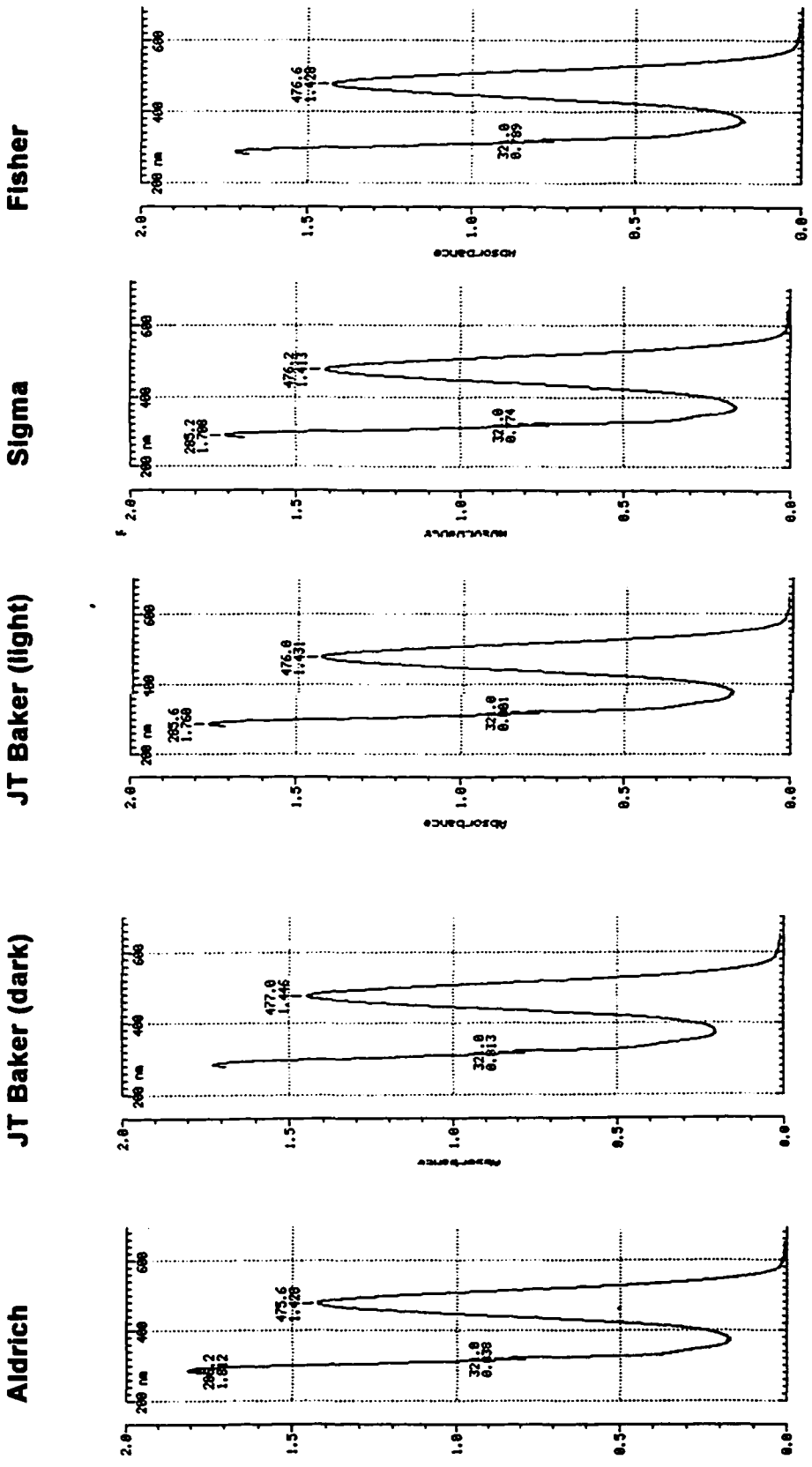

Figure 36. Absorbance Spectra of Azo Dye (Five Different Sources of 1-Naphthol)

Figure 37. Comparison of Sodium Rhodizonate Test (Bashinski Transfer v. Direct Application). First Transfer. White, Cotton/Polyester Blend. Winchester .38 Special, 158 Grain, LRN, Muzzle Distance = 10cm (4 inches).

Figure 38. Comparison of Sodium Rhodizonate Test (Bashinski Transfer v. Direct Application). Second Transfer. White, Cotton/Polyester Blend. Winchester .38 Special, 158 Grain, LRN, Muzzle Distance = 10cm (4 inches).

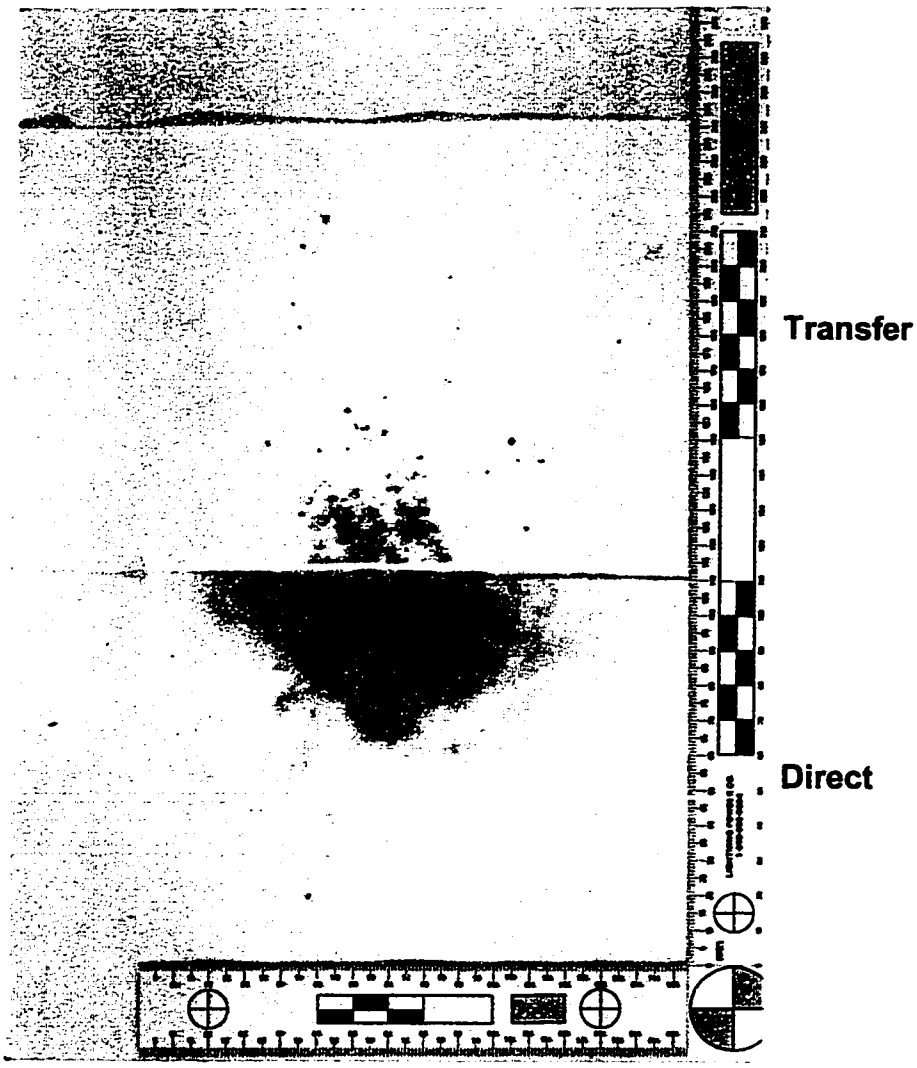

Chapter Six

Native Fluorescence

The purpose of the work described in this chapter was to further assess native fluorescence as a method for detecting gunshot residue and to evaluate this as a new method to estimate the muzzle-to-target distance. In this phase of the research, the gunshot residue patterns were not treated in any manner to induce fluorescence. No solvents were utilized. The affect of solvents and other chemical reagents on gunshot residue patterns will be considered elsewhere in this work. Likewise, low temperature enhancement experiments are discussed subsequently. This series of experiments was conducted at room temperature. The assessment detailed here was multi-faceted.

An investigation was conducted to determine the optimum excitation wavelengths for fluorescence by using shortwave ultraviolet (254nm), longwave ultraviolet (365nm), and visible light (400nm - 575nm). Various sources of propellant particles were examined to determine if they fluoresced using the above excitation wavelengths. The fluorescence of various gunshot residue patterns was compared to results obtained using the Modified Griess Test. Additionally, the two major components of most propellant particles, cellulose nitrate and nitroglycerin, as well as some common additives, were examined for fluorescence in the solid state. Other critical factors required for fluorescence observations were considered and discussed, that is, tunability of the excitation

source, and excitation intensity. Factors such as age, humidity, and the substrate were considered and discussed.

Methods and Materials

Materials:

Crimescope CS-16 Tunable Light Source

Spectroline U.V. Lamp. Model ENF-280C/12 (long and short wavelength)

Microspectrofluorometer, Farrand Optical Co. Model MSA

S&W 357 Magnum Revolver Model 19

.45 Para Ordnance

.380 Colt Mustang, Pocket Light, semi-automatic pistol

.32 Walther PPK, semi-automatic pistol

.25 Beretta Model 950 semi-automatic pistol

.22 S&W, Model 422

.22 Raven Rifle

9mm Heckler & Koch

Orange and Red Barrier Filter Goggles (see Table 31 for Transmission Data)

Orange and Red Barrier Filters (see Table 31 for Transmission Data)

Explosive Standards:

Diphenylamine, ACS Grade, JT Baker

N-nitroso-diphenylamine, Sigma

2,4-dinitrotoluene, 97%, Aldrich

2,3-dinitrotoluene, Aldrich

3,4-dinitrotoluene, Aldrich

2,6-dinitrotoluene, Aldrich

nitroguanidine, Aldrich

2,3-benzanthracene, 98%, Aldrich

dibutylphthalate, Sigma

methyl centralite, 99%, Aldrich

ethyl centralite, 99%, Aldrich

trinitroglycerin, 98%, Radian

cellulose nitrate, ATF

pyroxylin (precipitated from collodion), Fisher USP grade

carbazole, 98%, Aldrich

Silica Gel 60 (K6), (non-fluorescent plates), Whatman, 250 micron

Methods:

Thirty-nine different sources of ammunition were discharged from eight different firearms at a distance of twelve or more inches onto a dark grey or black cotton substrate for the examination of propellant particles for fluorescence. Federal .38 Special, Remington .38+P, Magtech .380, PMC 357, and Winchester .38 Special were selected for replication purposes. Refer to Table 4 for replication data regarding these sources. Additionally, an equal number of test firings were made from within six inches for experiments

conducted on the fine deposit associated with vaporized metallic species. The gunshot residue patterns that were produced were examined to determine if they exhibited a measurable fluorescence. The particles comprising these patterns, as well as the fine deposit associated with lead obtained from firearm discharges within six inches of the target, were also examined with short and long-wave ultra-violet radiation for evidence of fluorescence. Orange barrier filters (Tiffen #21, Nikon #056) were utilized as these provided the best emission observations in conjunction with visible excitation in the range of 415nm to 515nm. Red barrier filters were used for fluorescence observations where excitation wavelengths were in the range of 515nm to 575nm (Tiffen #29). The Crimescope CS-16 light source was used for the production of all photographs and illustrations in this chapter (with the exception of the microphotographs).

In addition to examining partially burned particles from actual patterns, bulk powders from twenty-four different sources (smokeless gunpowder) were studied. Several hundred particles from each source were placed into crucibles and examined, with the aid of a magnifier, using short wavelength ultraviolet, long wavelength ultraviolet, and visible (400-575nm) light. An orange barrier filter was used for observation of emissions resulting from visible light excitation from 400nm to 515nm. A red barrier filter was used for the observation of fluorescence at excitation wavelengths from 515nm to 575nm. Eleven additional sources of powders removed from actual cartridges, that were not discharged,

were also examined as indicated above. This latter group of powders was studied in an undischarged state because an appropriate firearm was not available at that particular time of examination. Thus, a total of seventy-four different sources of propellant were studied here: thirty-nine from firearm discharges, eleven from undischarged cartridges, and twenty-four from bulk powders.

Two discharged particles from each of seven popular sources of ammunition were selected for reflected light microspectrofluorometry. Only light colored particles were removed from discharge patterns and used for examination. Three different sets of excitation filters, and corresponding dichroic filters (beam splitter for the microscope & photometer), were used for the fluorescence studies. Microscopic fluorescence examinations were conveniently carried out with a 10X objective (total magnification of 100X). A 20X objective (higher numerical aperture) was used to gather a greater amount of light emission for the spectral determinations. Fluorescence observations were carried out with the following barrier filters: 420nm, 475nm, 530nm, 575nm, 610nm, and without any barrier filter. The following particles were studied: CCI 357 Magnum, Federal .38+P NYCLAD, Remington .38, Winchester .38+P Super Auto, Winchester .38+P, and PMC 357 Magnum.

Humidity has been found by several researchers (Gestring, 1994) to have a deleterious effect on the detection of nitrite with the Modified Griess Test. GSR patterns produced by Gestring in 1993 & 1994, and exposed to high

levels of humidity, were examined by this researcher for fluorescence. Portions of these same patterns produced extremely poor results with the Modified Griess Test according to Gestring (1994) and observed by this writer.

The use of native fluorescence to detect partially burned particles on relatively old GSR patterns was explored. This study was conducted by examining patterns produced by Gestring in 1993 & 1994, and by this writer in 1991.

Results and Discussion

At least some propellant particles on each pattern exhibited native fluorescence. These results are illustrated in Table 6. In essentially all instances straw or yellow colored propellant particles exhibited native fluorescence. Many particles resulting from the discharge of various sources, as delineated in Table 6, yielded excellent fluorescent patterns. The particles were easily observed and readily documented by either photography or videography. Many patterns exhibited very large numbers of fluorescent propellant particles. For example, patterns generated from discharges of Winchester (9mm), Federal .38+P (NYCLAD), Magtech 357 Magnum, and PMC 357 Magnum ammunition yielded excellent patterns of fluorescing particles. Refer to Table 4 for examples of the actual number of particles detected. See Figures 39-42 for photographs of these patterns. Griess transfers were prepared from several of these patterns and compared to the photographs of native fluorescence. Some of these results

were noteworthy. The particles resulting from a discharge of Winchester 9mm ammunition gave a barely perceptible Griess reaction on the transfer paper. This is clearly the worst Griess reaction seen with any ammunition. Conversely, an excellent reaction with the positive nitrite control was obtained in each of the four corners of the transfer paper. Magtech 357 ammunition gave a relatively weak reaction, but significantly stronger than that produced by discharge of the Winchester 9mm ammunition. An adequate Griess reaction was obtained with the Federal ammunition. The particles resulting from the discharge of PMC ammunition, as previously discussed, routinely give a poor reaction. In these four examples, the proposed approach exploiting native fluorescence provided a superior pattern to the Griess transfer.

Particles from different sources of discharged ammunition demonstrate different degrees of fluorescence. The particles comprising some discharge patterns produced little native fluorescence. Many particles appear dark grey or black with ordinary illumination. Very often, these particles were found to exhibit little or no fluorescence without additional treatment. It has been noted that some forms of physical or chemical manipulation often result in greater fluorescence. This will be discussed in detail in Chapter Nine. For example, the propellant from Winchester 30-06 ammunition produced little or no fluorescence (Table 7). It was cross-sectioned and examined for fluorescence, along its cross section, with the aid of a stereomicroscope. A moderate amount of fluorescence was noted, which was much greater than any emission seen with the coating

intact. The dark covering, which appears to be graphite, lead, carbonaceous material, or a combination apparently, behaves in varying degrees as an opaque barrier to excitation and emission radiation. It itself does not fluoresce with either an ultraviolet or visible source of excitation. The opacity of the dark outer layer varies from particle to particle within a single gunshot residue pattern. Considerable variation exists between different sources of ammunition. Some particle sources behave in extraordinary ways. For example, undischarged particles from Master .38+P, 158 grain, SWC, exhibit strong fluorescence when excited in the range from 455-515nm. However, no particles from several test firings were detected on the substrate, by any means (white light, fluorescence, or with the Modified Griess Test). These findings are consistent with the results obtained from the high speed photography. No particles were detected. Research conducted by Bynum (1995) with TLC has demonstrated that this ammunition lacks a stabilizer. Additionally, during the course of this research, visual inspection and stereoscopic examination of undischarged propellant particles have shown that no graphite or other obvious coating is present on the particles. These factors may be related to the fact that the propellant charge is apparently consumed very rapidly after ignition.

The excitation wavelength was found to be extremely important for the fluorescent examination of burnt particles. Generally, shortwave ultraviolet excitation provides no fluorescence of partially burned particles. Longwave ultraviolet light provides more fluorescence than shortwave, and in some cases

provides strong fluorescence with certain ammunition. However, it does not generally provide fluorescence approaching that from visible exciting radiation. See Figure 43 for an illustration of the general trend of decreasing particle fluorescence as the excitation wavelengths become shorter. At excitation wavelengths of 455nm to 515nm, particle fluorescence of the five sources used for that illustration was strong. However, as depicted in Figure 43, at 430nm many fewer particles were visible. At wavelengths of 415nm and shorter very few particles were observable. A similar trend of decreasing fluorescence at shorter excitation wavelengths was observed with the preponderance of the other discharged particles (Table 6), as well as with undischarged particles (Tables 7 & 8). In general, particles will also fluoresce at excitation wavelengths higher than 515nm, up to 575nm. The fluorescence at the higher range was not found to be as intense as the fluorescence in the range of 445nm to 515nm, but this range is also useful in many instances to optimize contrast with the background. In many instances when a dark coating is present on the particle, it appears to be transparent at longer excitation wavelengths permitting fluorescence observation of the interior of the particle. At the shorter wavelengths, the outer coating appears to strongly absorb the radiation rendering it opaque so that fluorescence of the underlying surface is not produced and observed. Furthermore, even when the outer coating is not present particle fluorescence is generally significantly less with ultraviolet excitation. Additionally, it was learned from solvent experiments that certain

solutions, such as dilute HCl, can help clear the outer surface of particles obscured by relatively dark, opaque material. This residue appears to be in the form of graphite, lead and other materials, resulting in part from the discharge. Many of these same particles will also fluoresce when exposed to ultraviolet radiation. However, the emission is generally much weaker. The fluorescence resulting from short wavelength excitation (254nm) is particularly weak. Many more particles are visible when exposed to long wavelength ultraviolet light (365nm) in comparison to short wavelength U.V. light. Unfortunately, many clothing fibers also fluoresce quite strongly when excited at 365nm. Fibers also fluoresce significantly at the more energetic ultraviolet radiation and this fluorescence can interfere considerably with examinations for particles. In general, the fluorescence from visible excitation is not nearly as obscured by interference from fibers (Figure 44). With visible excitation the discharged particles are prominent in comparison to extraneous fibers and little interference is noted.

Obviously, the chemical composition of the particles will also have a major influence on the observed fluorescence emission. Ignoring excitation factors for a moment, from a particle standpoint, the observation of fluorescence is strongly dependent on its surface characteristics and composition. Certainly, different mixtures of materials will be expected to fluoresce in varying intensities and at different wavelengths. Physical characteristics of the particles may also influence fluorescence. It is well

established that liquids and solids having the same chemical composition behave differently. The polymeric nature of cellulose nitrate, the most abundant ingredient in single, double, and triple base propellants, and the presence of a variety of lesser components, may produce varying degrees of fluorescence from source to source. An attempt was made to determine what is the source of fluorescence in the particles. Some compounds, reported as ingredients of smokeless powder, were also examined for fluorescence (appendix).

These observations were made in a glass spot plate. Two sources of cellulose nitrate were used for examination. These were from the ATF laboratory, and collodion (Fisher, USP grade). Cellulose nitrate was precipitated from collodion with distilled water. Upon addition of water to collodion the cellulose nitrate precipitated and was removed with a glass rod. The cellulose nitrate (pyroxylin) from collodion has a somewhat different structure, that is, the degree of nitration, in comparison to that of unburnt propellant (guncotton), (Morrison and Boyd, 1974, p. 1340). Guncotton is nearly completely nitrated (three nitrate groups for a single glucose unit), whereas pyroxylin possesses fewer nitrate groups (between two and three nitrate groups per glucose unit). The cellulose nitrate in gunshot residue is partially degraded in molecular weight and has a range that more closely resembles non-explosive cellulose nitrate (Beveridge, pp. 28, 44, 1992). Peak (1980, p. 681) reported that two spots from cellulose nitrate were found in thin layer chromatography that he performed; one at the origin corresponding to the higher molecular weight

cellulose nitrate, and the lower molecular weight near the solvent front. It was found in experiments conducted as part of this writer's research that cellulose nitrate exhibited a significant fluorescence. A fairly large piece of pyroxylin was obtained from collodion by precipitation. It exhibited a range of fluorescent colors: white, orange, and green (Figure 45). Orange appeared to be the predominant color depending on excitation wavelength. It is interesting to note that when the cellulose nitrate was initially separated from collodion it only exhibited a relatively weak fluorescence. However, over time it changed to produce a fairly strong orange fluorescence. Cellulose nitrate was also extracted via precipitation from both PMC .38 Special and 357 Magnum ammunition. Upon drying onto a glass slide both samples were examined for fluorescence. Both samples exhibited a fair amount of orange fluorescence when excited at 475nm. This corresponds to results obtained with thin layer chromatography. Toluene was used as the solvent system since this has been shown to yield excellent separation from other explosives. Silica Gel G (non-fluorescent) plates were used. Spots corresponding to the standards from ATF and from Collodion (pyroxylin) were found in the two PMC samples, at an Rf of approximately 0.74. These spots were detected with excitation at 475nm and monitoring with orange goggles. No other spots were detected with visible radiation. As visualized chromatographically, propellant exhibits far less fluorescence compared to its unaltered semi-solid state.

It is clear from the experiments conducted with the bulk powders that

excitation by visible radiation is far superior to either long or shortwave ultraviolet light. A marked trend that was observed was that excitation wavelengths became shorter, the fluorescence intensity fell. These results essentially parallel those obtained with the discharged particles and undischarged particles removed from cartridges. In a few cases, some particles behaved in a similar fashion when exposed to either long wavelength ultraviolet or visible light. However, all particles, with the exception of the "dots" appeared to quench when exposed to short wavelength ultraviolet light. In general the "dots" fluoresce very intensely with the exception of the "Green Dot" which does not fluoresce at all. The dots comprise a relatively small portion of each powder and do not appear as though they would have a meaningful impact on actual patterns (although their presence in a pattern would probably be a strong indicator of what type of powder the examiner was dealing with). It seems as though the outer coating of most ordinary particles is sparse enough to be measurably transparent in the visible region of the spectrum, somewhat so in the long UV region, and opaque in the short wavelength portion of the ultraviolet. In fact, the absorbance of short wave ultraviolet radiation is so strong, that all particles appeared black in comparison to observations with long wave ultraviolet light. Although the fluorescence of the bulk powders is much stronger in general in the visible region, it is obvious that the outer coating does obscure the fluorescence observations. In most cases, partially burned particles in which the outer surface (shiny black coating) has been removed appear to

fluoresce much more intensely than their undischarged counterparts from the same load.

The age of the pattern does not have any observable impact on the fluorescence of the particles. Figure 46 is an example of a pattern that is four years old and still exhibits excellent fluorescence. Similar results have been obtained with patterns produced more than six years age. These same results have been obtained repeatedly so long as the material bearing the pattern has been well preserved, that is, not crumpled, or otherwise mishandled.

Likewise, humidity has no measurable influence on particle fluorescence. Patterns that displayed a weak Griess reaction as part of experiments conducted with Gestring (1994, p.25) still provided readily detectable fluorescence. Continued gentle application of water (see Chapter 9 - effect of solvents) has a tendency to increase particle fluorescence by clearing the outer surface of debris.

All the reflected light microspectrofluorometric examinations of the particles confirmed the gross observations of the patterns made with the light source, that is, propellant particles will fluoresce in the visible region of the spectrum when excited with ultraviolet and shorter wavelength visible light. Microscopic examinations were readily conducted by noting the color shift to longer wavelength in comparison to the excitation wavelength or color. The spectra shown in Figure 47 were taken from a particle that appeared microscopically similar (see also Figure 48) from a fluorescent perspective to

the other particles examined in the same fashion. The particles appeared to fluoresce in a fairly broad manner from approximately 430-670 nanometers.

While elemental lead will not fluoresce at any excitation wavelength, it can often be detected via its quenching of a fluorescent background. This attribute is particularly helpful when dealing with bright fabrics which tend to provide strong fluorescent backgrounds. The spectrum from 575nm to 400nm can be quickly scanned to obtain optimum contrast. Alternatively, if this is found to be inadequate, ultraviolet excitation can often provide excellent contrast between lead and the background. A tunable light source, such as the Crimescope CS-16, can be of significant value in this regard, or when conducting examinations for particles, that is, the unit can be tuned to optimize contrast between the subject and the background.

Of greater importance than tunability in the light source, is the intensity of the excitation radiation. A comparison between the CS-16 and the Omniprint 1000 amply demonstrated the relative inadequacy the latter unit primarily due to the intensity factor. Many more particles can be detected with the more powerful unit at the same excitation wavelength for both units. The fluorescence of entire patterns can be easily photographed when illuminated by the CS-16. Its liquid light guide can be mounted on a tripod at convenient distance providing a relatively uniform lit field. This also permits easy examination of the entire pattern. To achieve similar fluorescence with the weaker unit, it must be placed very close to the pattern; long exposure times and "painting" with the

light wand is often required to completely and adequately photograph the entire pattern.

Many different fabrics have been used as substrates for firearm discharges. These include nylon, wool, cotton, cotton/polyester blends, polyester, leather, and others. The dark colored fabrics do not provide interference for examinations with native fluorescence with visible excitation. Brightly colored fabrics do often produce significant background interference. Oftentimes, this can be minimized by rapidly scanning to an optimum region and then fine-tuning. When this fails, the reverse approach can be taken, that is, find a wavelength which causes the particles to absorb, and the substrate to fluoresce, as indicated for lead examinations. These excitation wavelengths tend to be short, that is, 415, 400, 365, and 254 nanometers. Fabrics having somewhat irregular or rough textures, such as corduroy, and other features such as seams do not interfere with native fluorescence examinations. However, loose knit or similarly coarse fabrics do severely limit the utility of such an examination since the particles tend to be imbedded within the substrate.

In conclusion, the results discussed both here and in the previous chapter with regard to fluorescence observations and the "Walker" approach indicate that the two methods can provide somewhat complementary information regarding pattern distribution. In some cases, the fluorescence method may be superior to Griess, for pattern visualization purposes solely (it

does not have the identification power that the chemical test possesses), while the converse is also true. A combination of these techniques would probably be a better method in certain circumstances. This will be discussed in more detail in Chapter Eleven which is devoted to sequential integrated approaches.

Table 6. Native Fluorescence Observed as Pattern of Discharged Particles

			Excitation Wavelengths				
Brand	**Caliber**	**Grain/Bullet**	**515 - 445nm**	**430nm**	**415nm**	**365nm**	**254nm**
Winchester	.38+P	130 FMJ Super Auto	++	+	-	--	---
Winchester	.38+P	125 JHP	+++	+	-	--	---
Winchester	.38+P	158 SWC	+++	++	-	--	---
Winchester	9mm	115 FMJ Luger	++	+	-	--	---
Winchester	.45	Black Talon	++	+	-	--	---
Winchester	.22	Short, Super X	++	+	-	--	---
Winchester	9mm	115 FMJ Unleaded	+++	+	-	--	---
Winchester	357Mag.	158 LR (coated)	++	+	--	--	---
Remington	.38+P	125 JHP	+++	++	--	--	---
Remington	.38spl.	158 LR	+++	++	-	--	---
Remington	.45	145 Glaz. Safety Slug	++	+	-	--	---
Remington	.45	JHP	++	+	-	--	---
Remington	.22	Mohawk	++	+	-	--	---
Remington	.38+P	158 LR	++	-	-	--	---
Remington	357Mag.	158 SJHP	+++	++	-	--	---
Remington	357Mag.	180 SJHP	+++	++	-	--	---
Remington	9mm +P	115 JHP	+++	-	-	--	---
Federal	.38spl.	158 Nyclad	++	-	-	--	---
Federal	.38+P	125 JHP	++	-	-	--	---
Federal	9mm	115 JHP	++	-	-	--	---
Federal	357 Mag.	110 JHP	++	+	-	--	---

+++ very strong
++ strong
+ moderate
- weak
-- very weak
--- none

Table 6 Continued. Native Fluorescence Observed as Pattern of Discharged Particles

Federal	.38+P	158 Nyclad	+++	++	-	--	---
S&W	.38spl.	158 Nyclad	++	-	-	--	---
Magtech	.38spl.	158 LR	++	-	-	--	---
Magtech	9mm	124 FMC	+++	++	-	--	---
Magtech	.25	50 FMC	++	++	-	--	---
Magtech	357Mag.	158 SJSP	++	++	-	--	---
PMC	357Mag.	125 JHP	+++	++	-	--	---
PMC	.38spl.	132 FMJ	++	-	-	--	---
PMC	.38spl.	158 SWC	++	-	--	--	---
PMC	.38+P	125 Starfire	++	++	-	--	---
Speer	.38+P	158 Lawman	++	-	--	--	---
CCI	357Mag.	158 JHP	+++	++	++	--	---
CCI	.38+P	158 TMJ Lead Free	+++	++	++	--	---
CCI	9mm	124 TMJ Lead Free	++	-	-	--	---
CCI	9mm	115 TMJ	++	-	-	--	---
CCI	.45	200 JHP	++	++	+	--	---
CCI	.22	Stinger, Long Rifle	--	--	--	--	---

+++ very strong
++ strong
+ moderate
- weak
-- very weak
--- none

Table 7. Fluorescence Observed as Undischarged Particles

			Excitation Wavelengths				
Brand	**Caliber**	**Grain/Bullet**	**515 - 445nm**	**430nm**	**415nm**	**365nm**	**254nm**
CCI	10mm	200 TMJ	+	-	--	--	---
CCI	.40	180 TMJ	+	-	--	--	---
Master	.38+P	158 SWC	++	++	++	-	--
UMC	.25	50 MC	++	++	+	-	---
Remington	.32	88 LRN	++	++	+	-	---
Federal	.380	95 MC	--	---	---	---	---
Corbon	9mm +P	115 JHP	+	+	-	--	---
Winchester	.380	85 Silver Tip	++	+	-	--	---
Winchester	.270	FC	++	+	-	--	---
Winchester	30-30	RP	+	+	-	--	---
Winchester	30-06	SPRG Super	--	--	---	---	---

+++ very strong
++ strong
+ moderate
- weak
-- very weak
--- none

			Excitation Wavelengths		
			Gross Intensity of Fluorescent Particles		
Brand	**Type/#**	**Rough % w/ Vis. Ex.**	**415-555nm**	**Rough % w/365nm**	**254nm**
Accurate	#2	high %; 415-555nm	moderate	None	None
Accurate	#5	high %; 415-555nm	moderate	high % weak	None
Accurate	#7	high %; 415-555nm	moderate	high % weak	None
Accurate	#2520	high %; 415-555nm	moderate	None	None
Accurate	#4350	high %; 415-555nm	moderate	None	None
Galliant	Red Dot	high %; 430-495nm	weak	No;except dot	No;except dot
Galliant	Green Dot	high %; 415-555nm	low % mod. ; most weak	No;not even dot	No;not even dot
Hercules	Herco	high %; 415-555nm	weak	small % weak	None
Hercules	Blue Dot	high %; 415-555nm	weak to high	high % weak	None
Hercules	Unique	high %; 415-555nm	weak to moderate	high % weak	None
Hercules	Bullseye	high %; 415-555nm	weak to high	high % weak	None
Hogdon	H110	all; 415-555nm	moderate to high	high % weak	None
Hogdon	HP-38	high %; 415-555nm	weak and high	small % weak	None
IMR	PB	high %; 415-475nm	weak	high % weak	None
IMR	700-X	high %; 430-495nm	very weak	None	None
IMR	800-X	high %; 430-495nm	very weak	same as vis.ex.	None
IMR	3031	high %; 415-555nm	weak	None	None
IMR	4198	high %; 415-555nm	weak to moderate	None	None
IMR	4227	high %; 415-555nm	weak to high	None	None
Winchester	WSL1	high %; 415-555nm	weak	high % weak	None
Winchester	231	high %; 415-555nm	weak to high	high % weak	None
Winchester	296	all; 415-555nm	high	all but weak	None
Winchester	748	all; 415-555nm	moderate	all but weak	None
XMP	5744	high %; 430-495nm	weak	None	None

Table 8. Fluorescence of Undischarged Particles from Bulk Smokeless Powder

Figure 39. Winchester 9mm, 115 Grain, FMJ, Unleaded, Muzzle Distance = 46 cm (18 inches). Upper Photo: Native Fluorescence. Excited at 455nm; orange barrier filter. Lower Photo: Griess Transfer

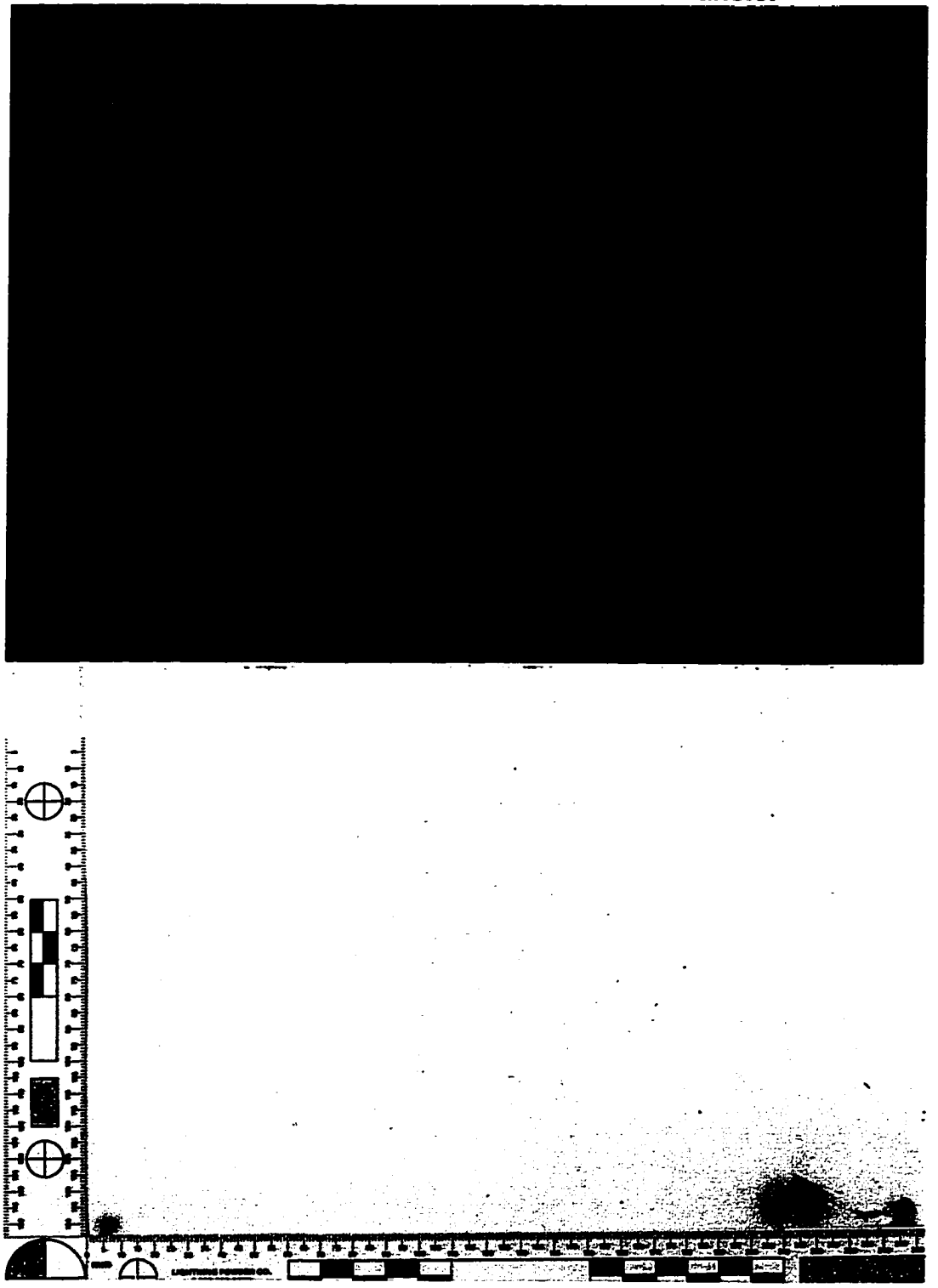

Figure 40. Comparison of Griess Transfer to Native Fluorescence. PMC 357 Magnum 125 Grain JHP. Muzzle D. = 30cm (12 inches). Upper Photo: Excited at 455nm; orange barrier filter. Lower Photo: Griess Transfer.

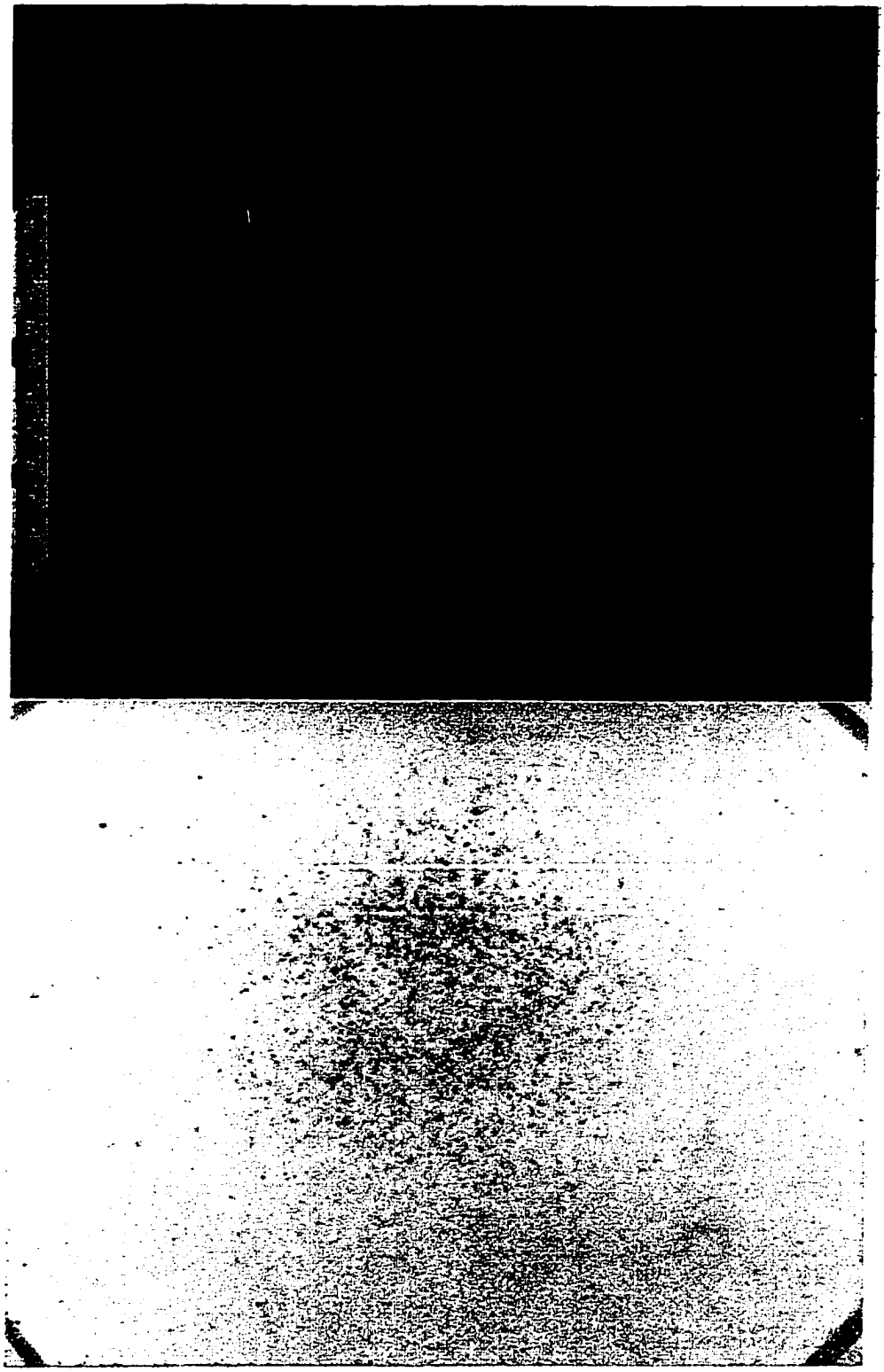

Figure 41. Federal .38+P, 158 Grain, SWC, NYCLAD. Muzzle Distance = 30cm (12 inches). Upper Photo: Native Fluorescence. Excited at 455nm; orange barrier filter. Lower Photo: Griess Transfer

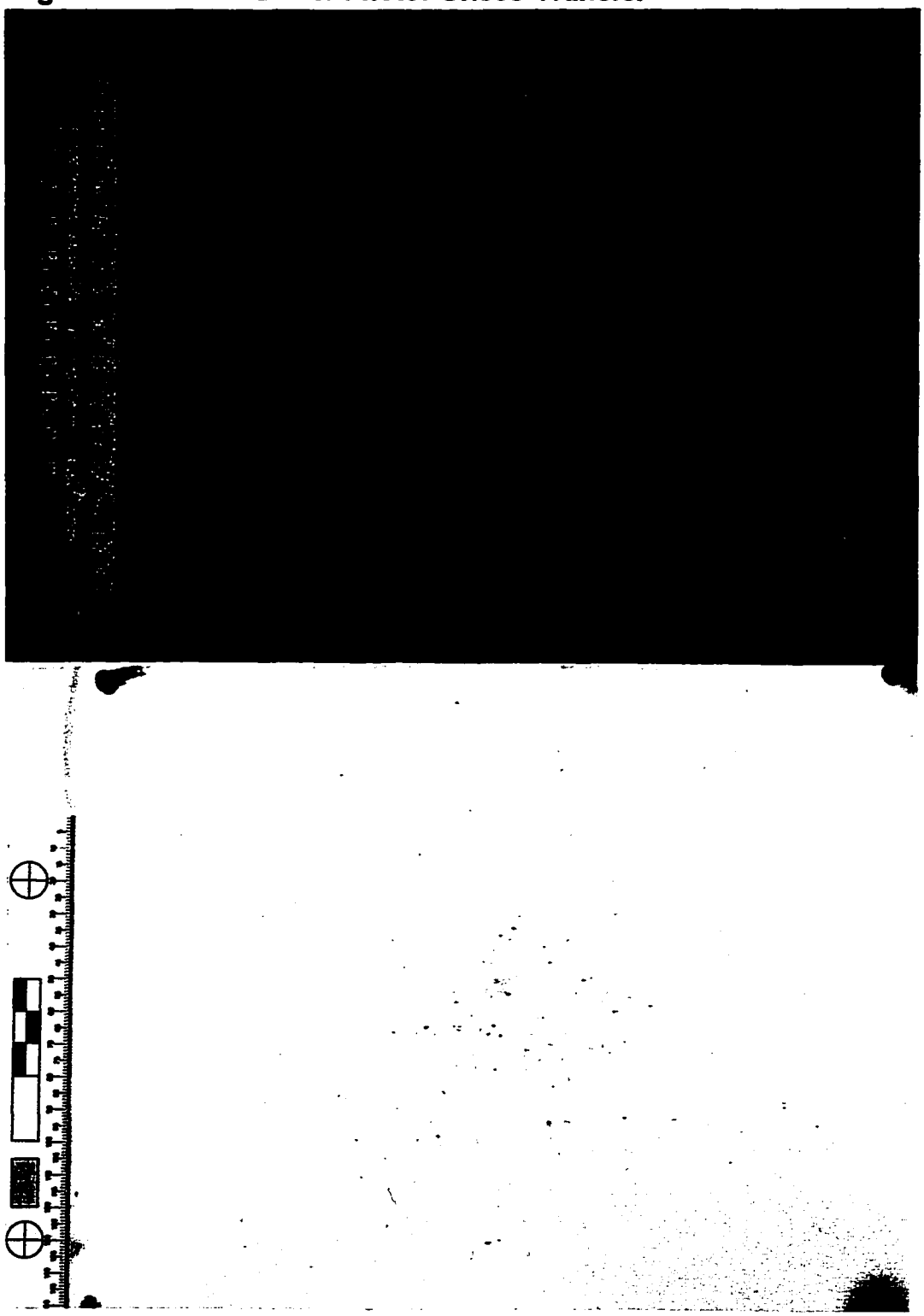

Figure 42. Magtech 357 Magnum 158 Grain, SJSP, Muzzle D. = 20cm (8 inches). Upper Photo: Native Fluorescence. Excited at 455nm; orange barrier filter. Lower Photo: Griess Transfer.

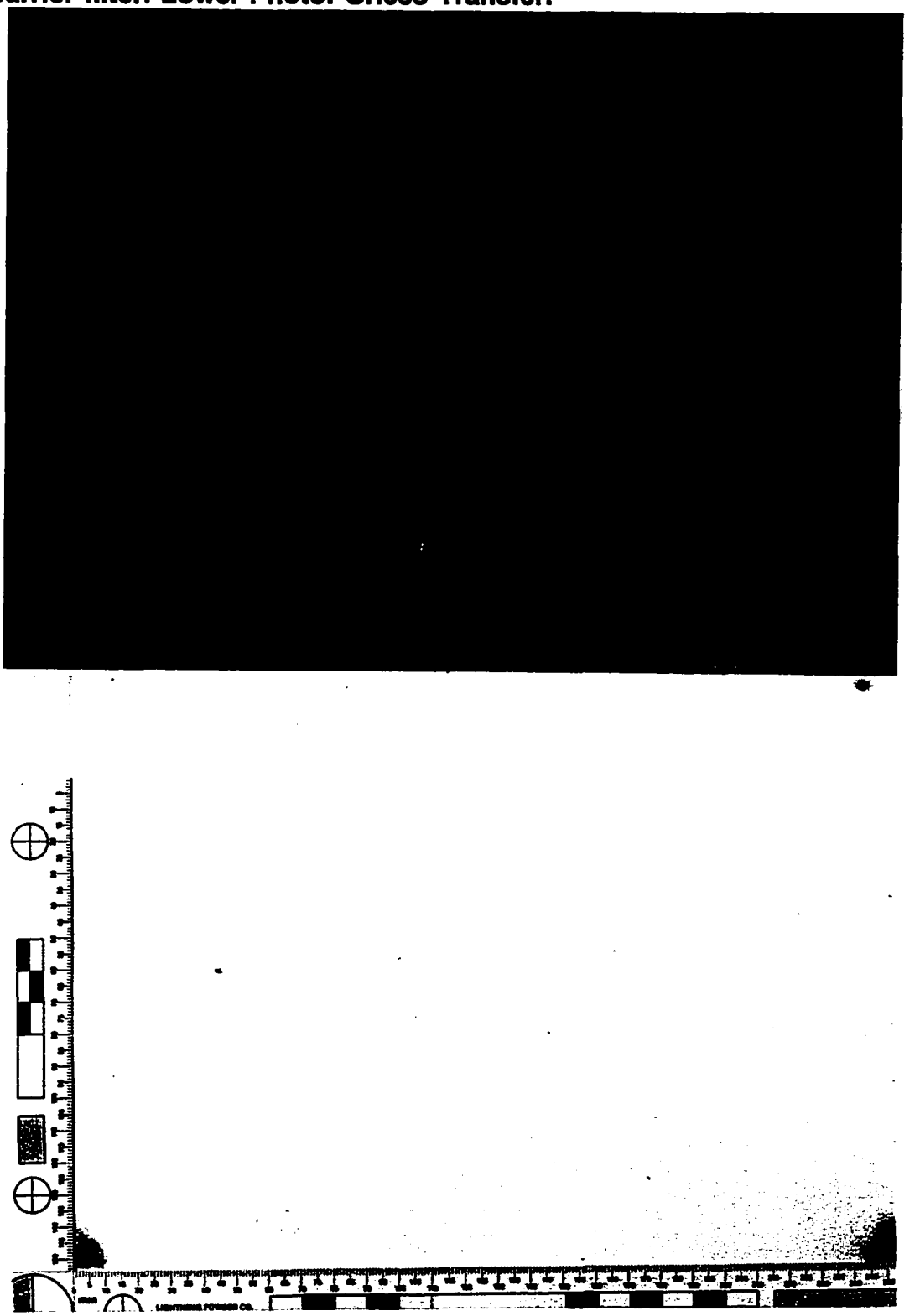

Figure 43.

Influence of Excitation Wavelength on Particle Fluorescence (Native).

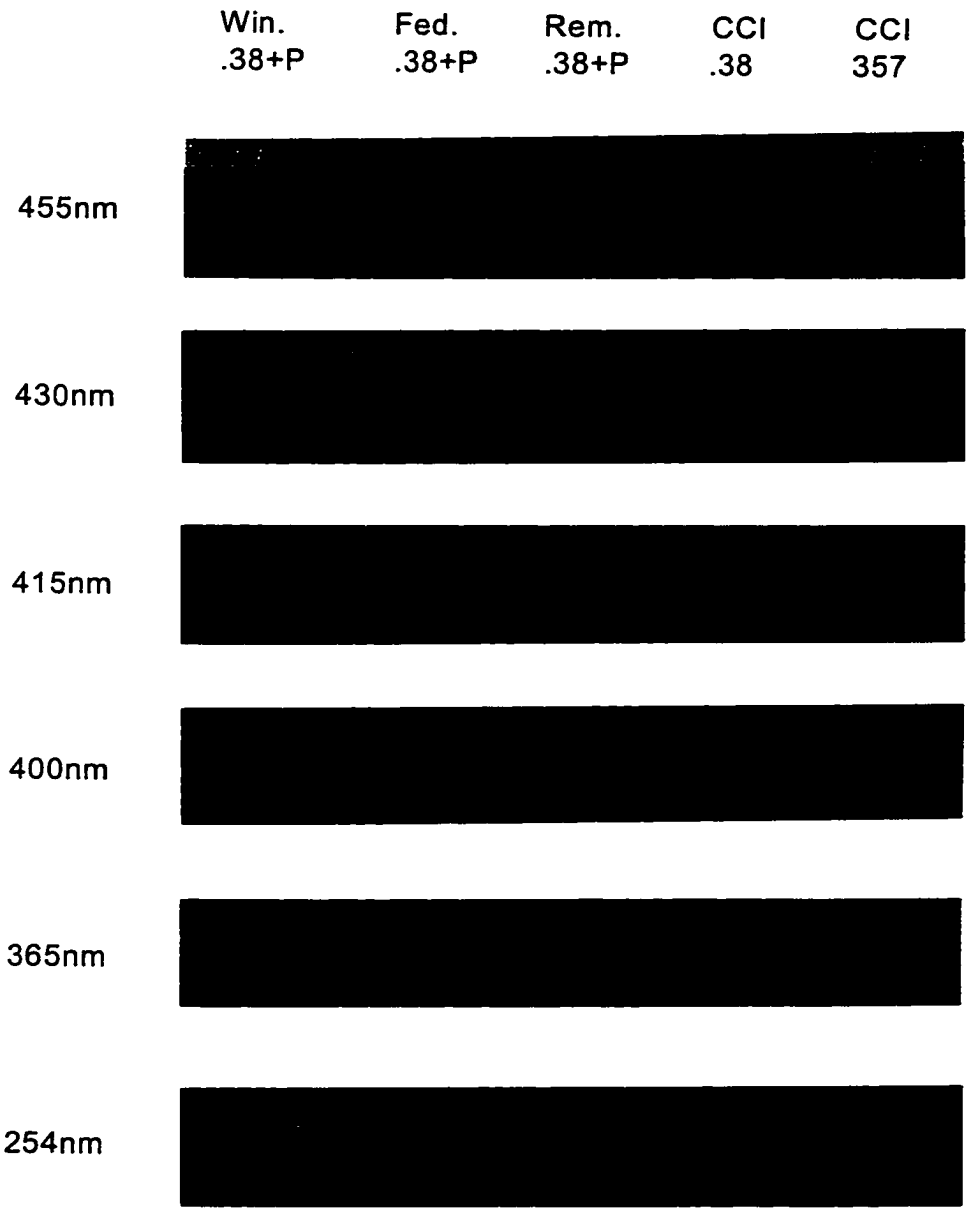

Figure 44. Comparison of Excitation Wavelengths on Particle Fluorescence and Background. Same Substrate and Pattern for both Photos. Upper Photo: 254 nm ex.; lower Photo: 455nm excitation.

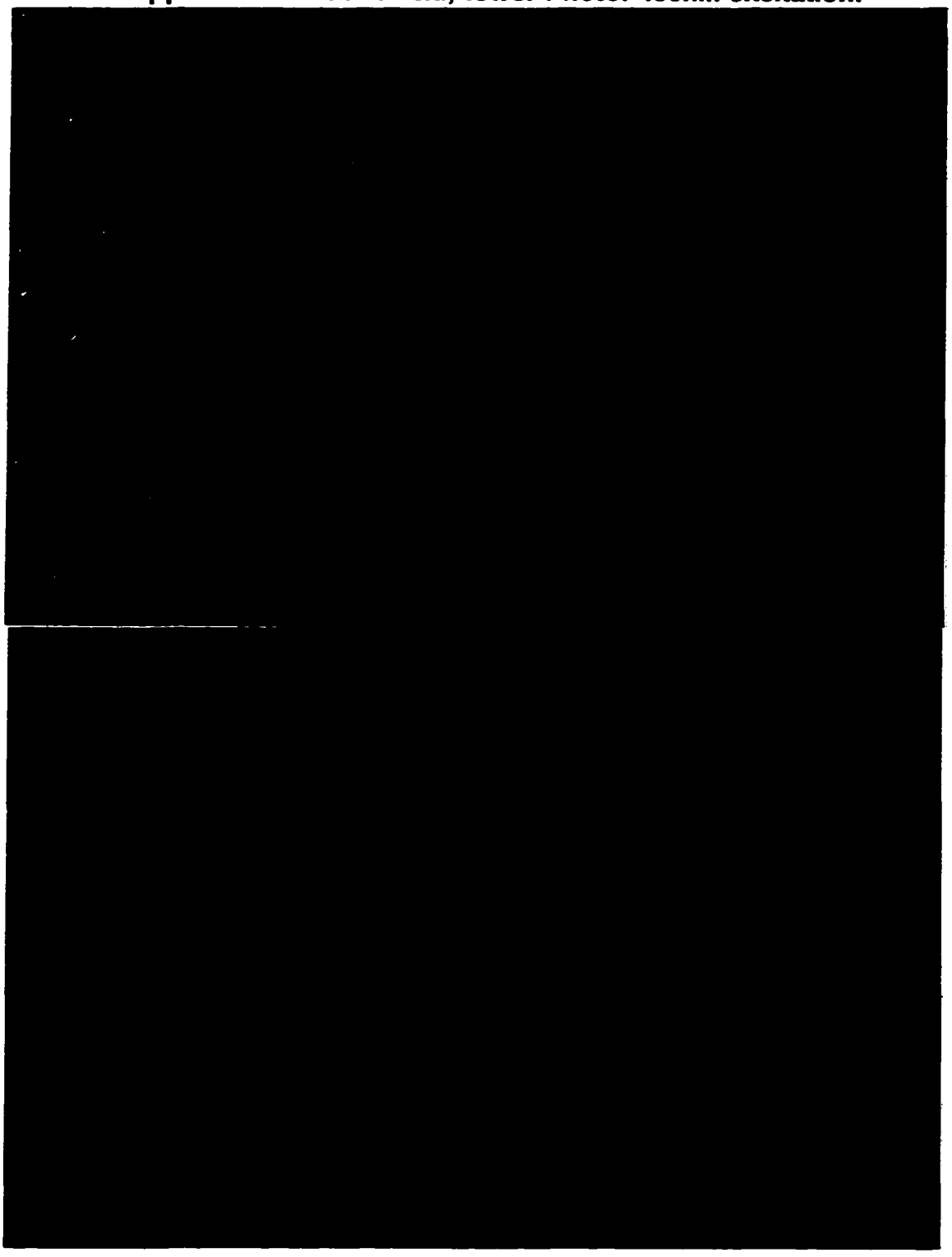

Figure 45.

Fluorescence of Cellulose Nitrate from two Different Sources. Excited at 455nm. Orange Barrier Filter.

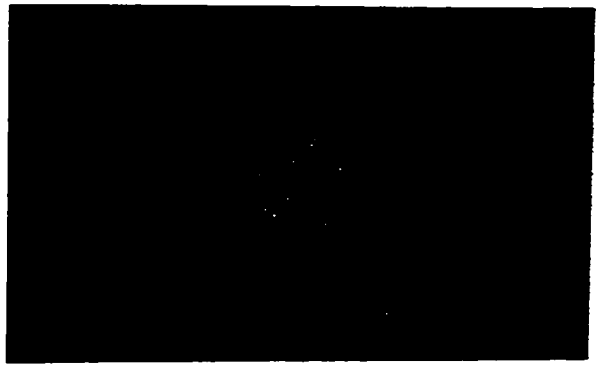

ATF Laboratory

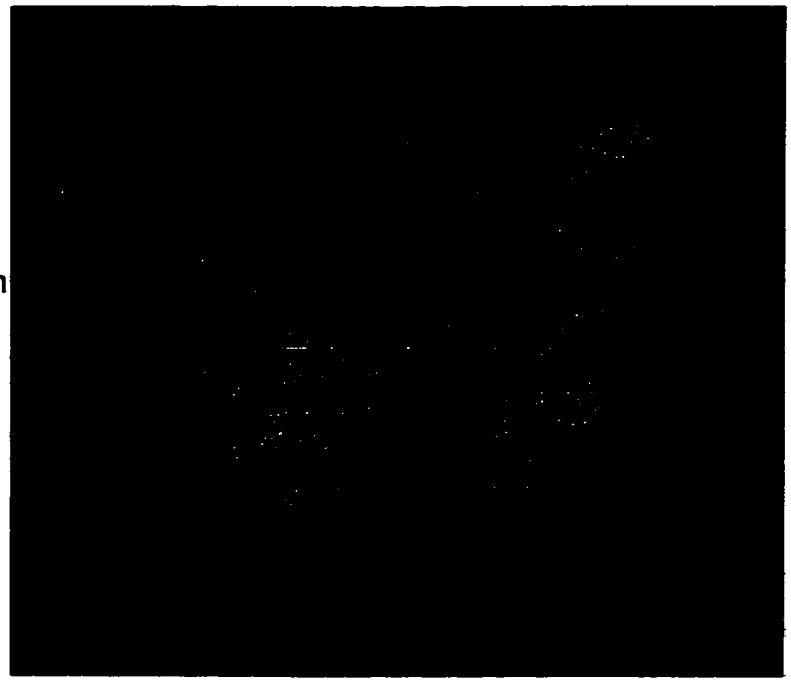

Precipitated from Collodion

Figure 46.

Four Year Old Dishcarge Pattern. Native Fluorescence. Excited at 455nm; orange barrier filter. Room Temperature. Federal .38 spl. 158 Grain, SWC, NYCLAD. Muzzle D. = 30cm (12 inches).

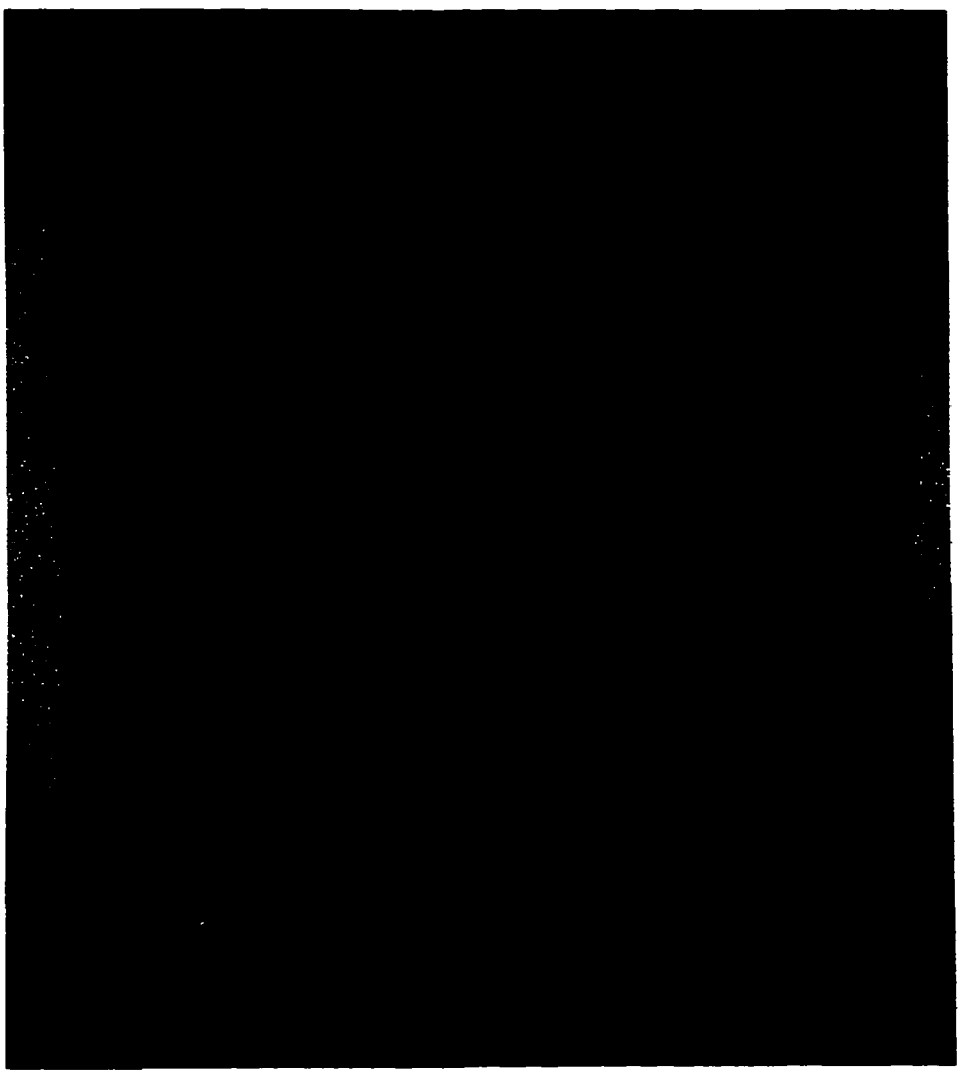

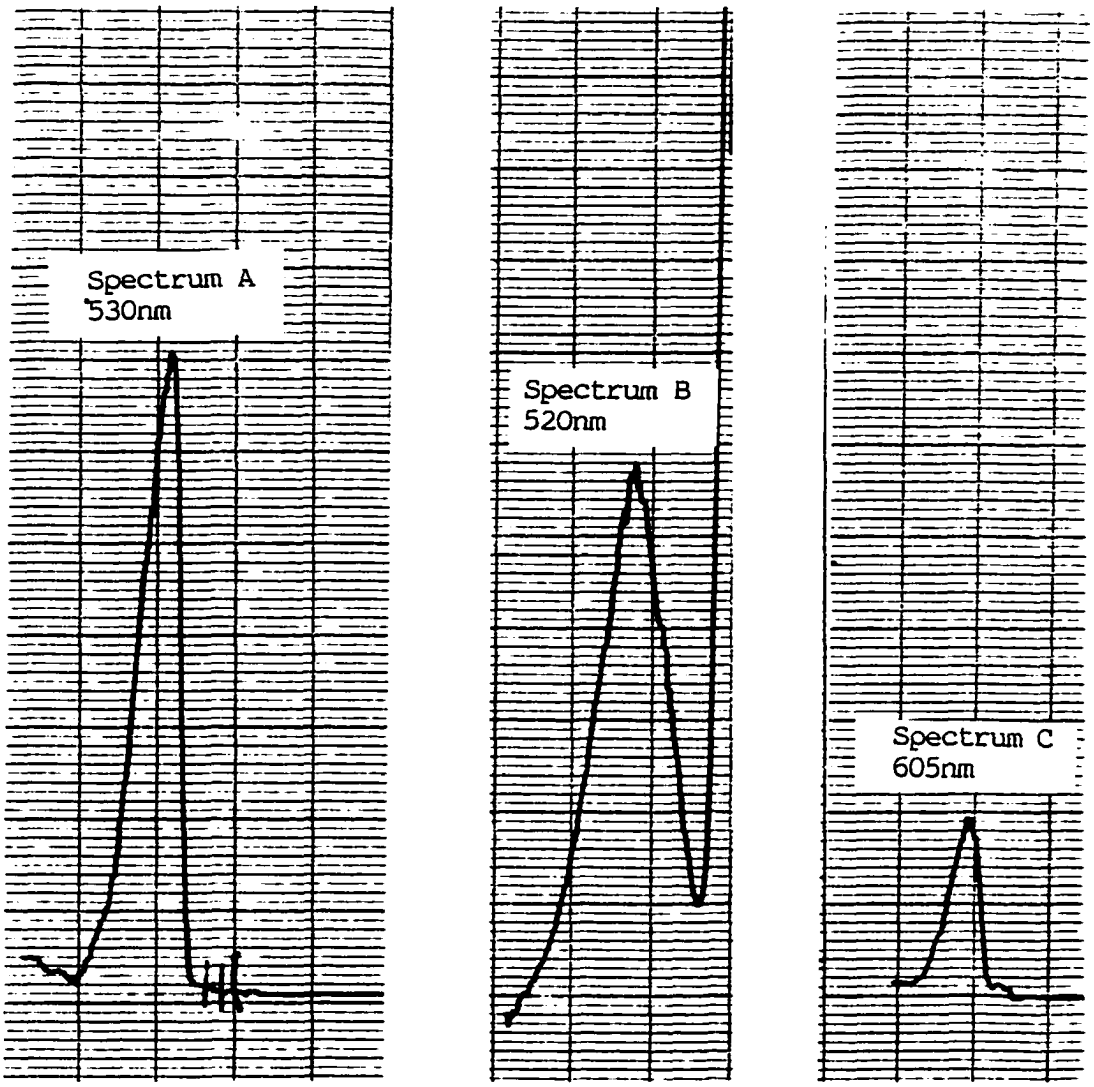

Figure 47. Fluorescence Spectra of a Single Discharged Particle (see Figure 48 for microphotograph of particle spectra were taken from). Federal .38+P, 158 Grain, NYCLAD. Spectrum A: with Blue Excitation Filter. Spectrum B: with Longwave U.V. Excitation Filter. Spectrum C: with Green Excitation Filter. All Three Spectra Obtained at Same Intensity Scale. Wavelength Scale: 100nm/division.

Figure 48. Microphotographs of Fluorescent Particles. Upper Photograph: Federal .38+P, 158 Grain, NYCLAD. Same Particle Spectra Obtained from for Figure 47. Blue Excitation, Orange Barrier Filter (570nm) Used for Both Photographs. Lower Photograph: Winchester .38+P, Super Auto, 130 Grain, FMJ. Magnification ~ 85X (both microphotographs).

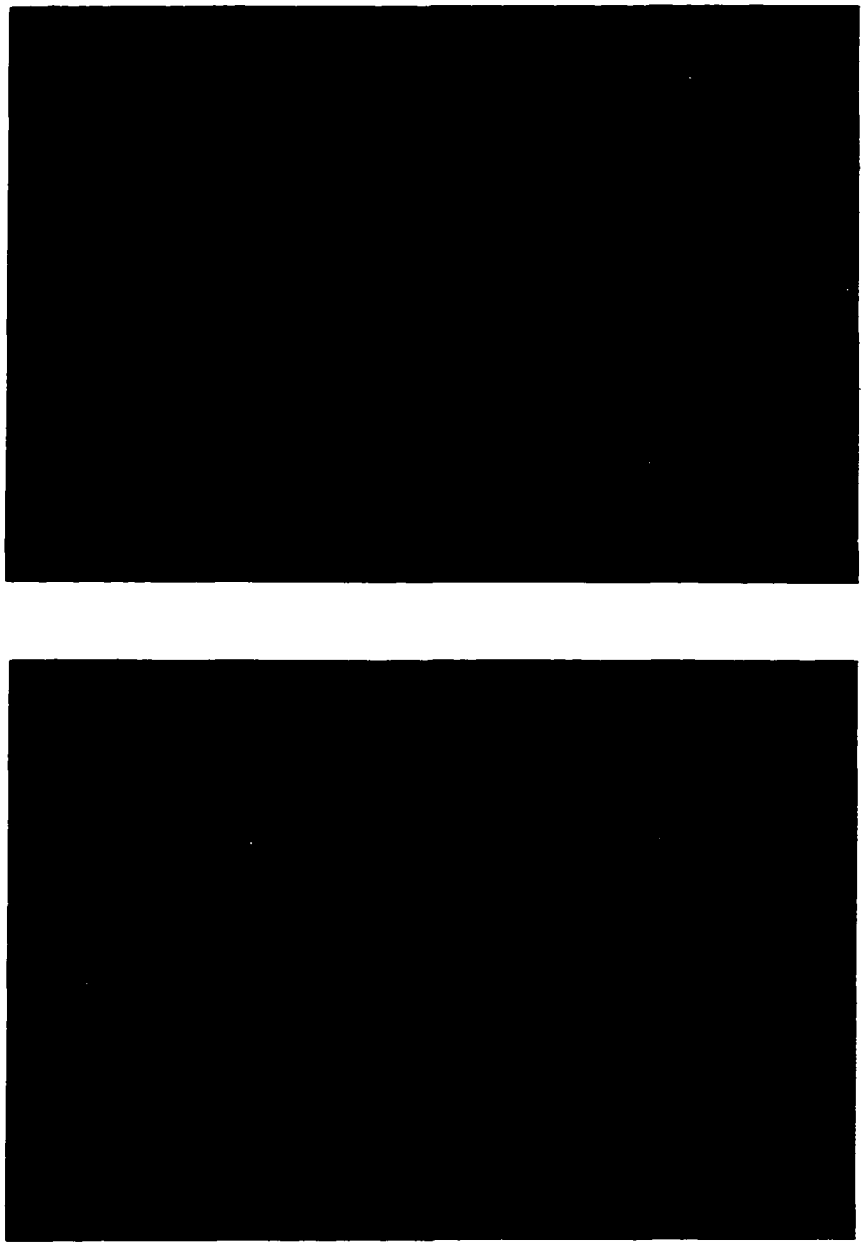

Chapter Seven

The Effect of Temperature

In the theoretical discussion, the concept that fluorescence intensity is greater in cooler materials than warm ones because of lessened intermolecular collisions was presented. These collisions can give rise to various ways for energy to be dissipated by non-fluorescent means (Hercules). The experiments discussed in this portion of the dissertation were considered only from the perspective of temperature. No chemical treatments were performed on the particles in this set of experiments. While it is well recognized that, theoretically, fluorescence will increase at colder temperatures, it has been unknown how propellant particles would actually behave at lower temperatures when excited by either ultraviolet or visible radiation. Several questions can be posed. If there was an increase in fluorescence, at the lower temperatures, what is the gain in intensity? Will particles measurably phosphoresce? What temperatures effectively enhance photoluminescent observation of particles? Does untreated lead photoluminesce at low temperatures? Because of the increased intensity, how many more particles can be detected? These were some of the questions to be answered by this series of experiments.

Methods and Materials

Equipment

Crimescope CS-16 , orange barrier filter (Tiffen #21), orange barrier goggles

35mm SLR Nikon FM2 Camera

Insulated stainless steel tray (see Chapter 3)

Liquid Nitrogen

Kodak Tech Pan Film; HC 110 developer

Kodak Resin coated paper; Dektol (1:2) developer

Cole-Parmer Thermocouple Thermometer, Digi-Sense® Model 8528-20

Hewlett Packard ScanJet 3C Scanner

SigmaScan 3 Software

Ammunition (as indicated in charts and tables)

Method

Gross Examination of 35 Patterns

To determine if the fluorescence of gunshot residue discharge patterns is enhanced significantly at low temperatures, patterns and the corresponding partially burned propellant particles from thirty-five different sources (Table 10) were examined. Test firings were conducted from distances of 12 to 18 inches to prevent interference from the fine lead deposit. Each pattern was first placed into the insulated stainless steel tray and examined for fluorescence at room temperature, followed by examination at liquid nitrogen temperatures. Excitation wavelengths in the visible region (450 - 495nm) were selected for most of these experiments based on their optimum fluorescence and contrast with the substrate. Patterns observed by excitation of the particles with ultraviolet light was also studied.

Particle Counts and Pixel Intensity Comparisons

A number of patterns were photographed both at room and low temperatures for comparison purposes. Several patterns were selected for comparison of the number of detectable particles, as well as for particle intensities. These experiments were conducted with all variables remaining exactly the same with the exception of the temperature. Photographs to be compared were taken and developed under the same conditions. The light from the CS-16 (455nm excitation) was sharply focused, using the front lens, to produce a relatively intense and uniform field of illumination immediately around the particles. The light wand was clamped into position approximately 45° from normal to the target surface. This angle was measured with a digital inclinometer. The tip of the wand was kept 28cm (11 inches) from the target surface. Each pattern was first photographed at room temperature and then at low temperature using liquid nitrogen. A Tiffen #21 barrier filter (orange) was attached to the camera lens for all photographs. The liquid nitrogen was gently introduced into a corner of the pan away from the particles to avoid the dislodging them. Enough liquid nitrogen was added to keep the target submerged. When liquid nitrogen is added to the tray, a cloud of water vapor is intermittently present above the immediate area of the target and the tray. The cloud did not appear to impede fluorescence observations. However, the photographs taken for comparison purposes were done when the cloud appeared to be at its thinnest.

Photographs to be compared were taken from the same roll of negatives. All photographs to be compared were developed under the same conditions. Prior to scanning each photograph the scanner platen was thoroughly cleaned. The scale was placed in the same position each time alongside each photograph which was also placed in the same orientation as the print it was being compared to. The intensity values of the particles at ambient and low temperature were compared by scanning photographs of the particles onto a personal computer. The images were scanned on a Hewlett Packard Scanjet 3C scanner as sharp black and white photographs using PhotoPaint (5.0) software. Preliminary cropping of the images was done using the scanning program to remove unnecessary portions of the photographs, and to reduce the file sizes to approximately 200 kilobytes. Each image was saved as a PCX file onto a network drive, and opened on a different computer having the imaging software. The images were evaluated using Sigma Scan Pro/Image measurement software. All images were scanned in a 5 x 7 inch format in the same corner of the platen. In addition, all images were scanned alongside a two-dimensional scale having white, black, and grey patches. Raw pixel intensities from particle images were obtained, stored on a spreadsheet and compared. Manual measurements were used to determine the intensity of each particle since automatic measurements produced only average pixel values for each object. The highest pixel value from each particle was determined and recorded by enlarging the image so that the change in intensity could be

interactively monitored at the bottom of the screen as the cursor was slowly moved to the brightest point on the particle. When the highest value was found the mouse was clicked to enter the value of the pixel of highest intensity into a spreadsheet. Manual measurements were compared against automatic measurements. Considerable care had to be taken when making automatic measurements for both intensity and counting purposes. Unless carefully selected threshold ranges were defined, highly exaggerated particle counts were obtained. The determination of inaccurate particle counts was based on prior visual inspection of certain photographs noting the number of particles present. Even with photographs possessing excellent contrast, automatic measurements tended to detect objects that could not be confirmed visually. Threshold values were obtained by manually obtaining an approximate range of particle and background values. The upper value was set at 255 (maximum value) and the lower set at about 75 (fifteen to twenty points higher than that obtained from the background). A preliminary automatic measurement was then made. Particles that were detected by the program were annotated in red automatically. The images were then visually compared to the actual photograph. If it appeared that spurious particles were being detected, the threshold minimum was adjusted. This had to be carefully done as well, since actual particles can be readily omitted with too high a minimum threshold value. In general, automatic measurements were judged unreliable. On the other hand, manual measurements of pixel values are dependable, but extremely

tedious. To determine the percent increase in fluorescence intensity, using the percent change in pixel intensity as a measure (manual measurements), both the ambient and low temperature images of two targets were examined side by side. The two patterns were Winchester 9mm and CCI 357 Magnum (two hundred and fifty particles). The corresponding particles on each photograph were examined and the lower values subtracted from the higher values. Background values were obtained from each corner and center of the substrate area. Additionally, values were compared from the white, black, and grey portions of each scale to verify that scanning had been carried out under the same conditions. This process would also permit a calibration to be carried out on an image's values, if necessary. In subsequent experiments involving pre- and post-reaction fluorescence, calibration was necessary to compare certain groups of particles because of varying distances from the light source and corresponding different intensities of incident light. That was not the case here since particles being compared were the same ones. Their position was kept the same for both the ambient and low temperature observations. The values of the background intensity for the data presented in this chapter were all in very good agreement (approximately 2% or less). However, the low temperatures can often change the fluorescence of the substrate as well as the particles. Additionally, while the substrate itself may not increase in fluorescence, the emission of loosely adhering fibers from other sources can significantly increase. In fact, even the fluorescence of scales will increase because of the

reduction in temperature. The use and placement of scales must be judicious since they can act as a secondary light source producing reflections or fluorescence (which is also enhanced at liquid nitrogen temperatures).

Particle counts were made directly from the photographs which were taken and developed in the same manner as that for intensity measurements. Clear plastic was superimposed over each photograph and marked with a fine Sharpie® in the positions corresponding to each particle. Four different patterns were prepared for this purpose from the following ammunition sources: Winchester .38+P, Federal .38 Special, Winchester 9mm, and CCI 357 Magnum.

Results and Discussion

Without exception all thirty-five patterns benefitted dramatically from the reduced temperatures. The increase in fluorescence was so marked (see figures 49-52) it was unnecessary to attempt to measure the change in emission intensity. However, the increase in fluorescence intensity (measured by pixel intensity) was measured as previously discussed. Winchester 9mm and CCI 357 Magnum pixel values amply illustrate the dramatic increase in particle intensity which on average is greater than 100% (see appendix). Likewise, particle counts were found to increase a similar amount (Figure 53). Similar results, as reported in Chapter Six, were obtained here with native fluorescence, using excitation in the visible region, with respect to background interference. Fewer problems were obtained at longer wavelengths (455-

495nm) as compared to 254, 365 to 430nm. Although background fluorescence may increase, particle detection may still be enhanced, even with shortwave ultraviolet radiation (Figure 52). On several occasions, it was found that background fluorescence drops sufficiently as the substrate warms, while the particle fluorescence is still substantially enhanced by the low temperatures providing adequate contrast between the particles and the substrate. Particle fluorescence appears to increase with even moderate decreases in temperature. However, the optimum range for fluorescence observations appears to be in the -140°C to -190°C range.

Lead was not expected to natively fluoresce at room temperature or at low temperatures. Predictably, numerous patterns containing lead residues did not fluoresce at even the lowest temperatures. However, if the background itself fluoresces lead can be readily visualized by its quenching action against a lighter background, as illustrated in Chapter Six (Figure 44).

The influence of temperature on fluorescence after chemical reaction is also exceptional, as demonstrated in Chapter Ten. Phosphorescence was also noted during the course of the experiments conducted and discussed here. However, phosphorescence appeared to be more intense after treatment with dilute hydrochloric acid (discussed in Chapter Ten).

Table 9. Discharged Particles that Exhibited Significant Increase In Fluorescence at Low Temperature

Brand	Caliber	Grain/Bullet
Winchester	.38+P	130 FMJ Super Auto
Winchester	.38+P	125 JHP
Winchester	.38+P	158 SWC
Winchester	9mm	115 FMJ Luger
Winchester	.22	Short, Super X
Winchester	9mm	115 FMJ Unleaded
Winchester	357Mag.	158 LR (coated)
Remington	.38+P	125 JHP
Remington	.38spl.	158 LR
Remington	.45	145 Glaz. Safety Slug
Remington	.22	Mohawk
Remington	.38+P	158 LR
Remington	357Mag.	158 SJHP
Remington	357Mag.	180 SJHP
Remington	9mm +P	115 JHP
Federal	.38spl.	158 Nyclad
Federal	.38+P	125 JHP
Federal	9mm	115 JHP
Federal	357 Mag.	110 JHP
Federal	.38+P	158 Nyclad
S&W	.38spl.	158 Nyclad
Magtech	.38spl.	158 LR
Magtech	9mm	124 FMC
Magtech	.25	50 FMC
Magtech	357Mag.	158 SJSP
PMC	357Mag.	125 JHP
PMC	.38spl.	132 FMJ
PMC	.38spl.	158 SWC
PMC	.38+P	125 Starfire
Speer	.38+P	158 Lawman
CCI	357Mag.	158 JHP
CCI	.38+P	158 TMJ Lead Free
CCI	9mm	124 TMJ Lead Free
CCI	9mm	115 TMJ
CCI	.45	200 JHP

Note: Particles Observed on Entire Discharge Pattern (One Pattern from Each Source).
(excited at 450-495nm; orange barrier filter)

Figure 49. Winchester Luger 9mm. Muzzle-to-Target Distance = 45cm (18 inches). Native Fluorescence. Excited at 485nm; Orange Barrier Filter. Upper Photo: Room Temperature. Lower Photo: in Liquid Nitrogen.

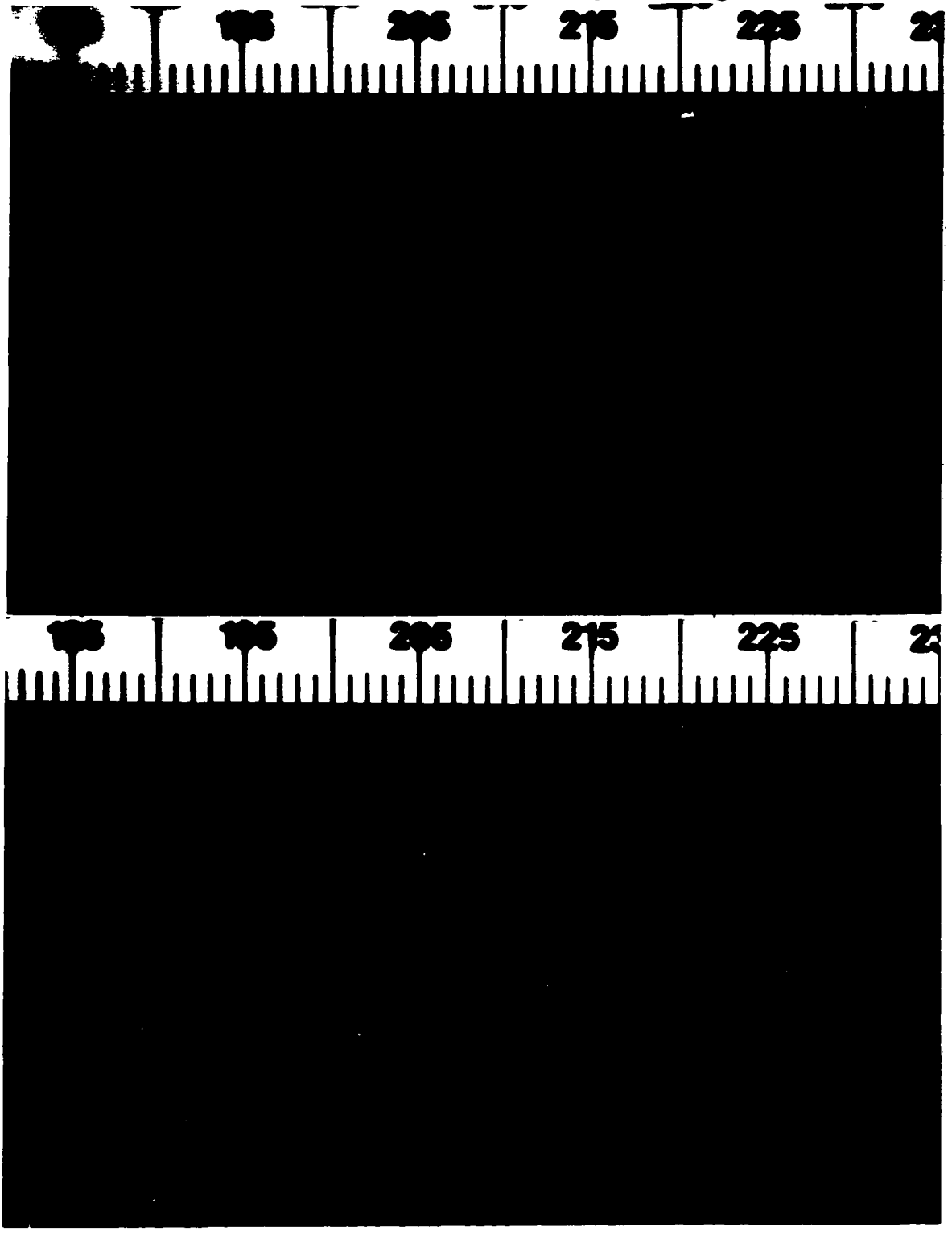

Figure 50.

Native Fluorescence at Room Temperature. 455nm excitation, orange barrier filter. CCI 357 Mag. 158gr. JHP. Muzzle-to-Target Distance = 45cm (18"). Compare to Figure 51 at Room Temperature.

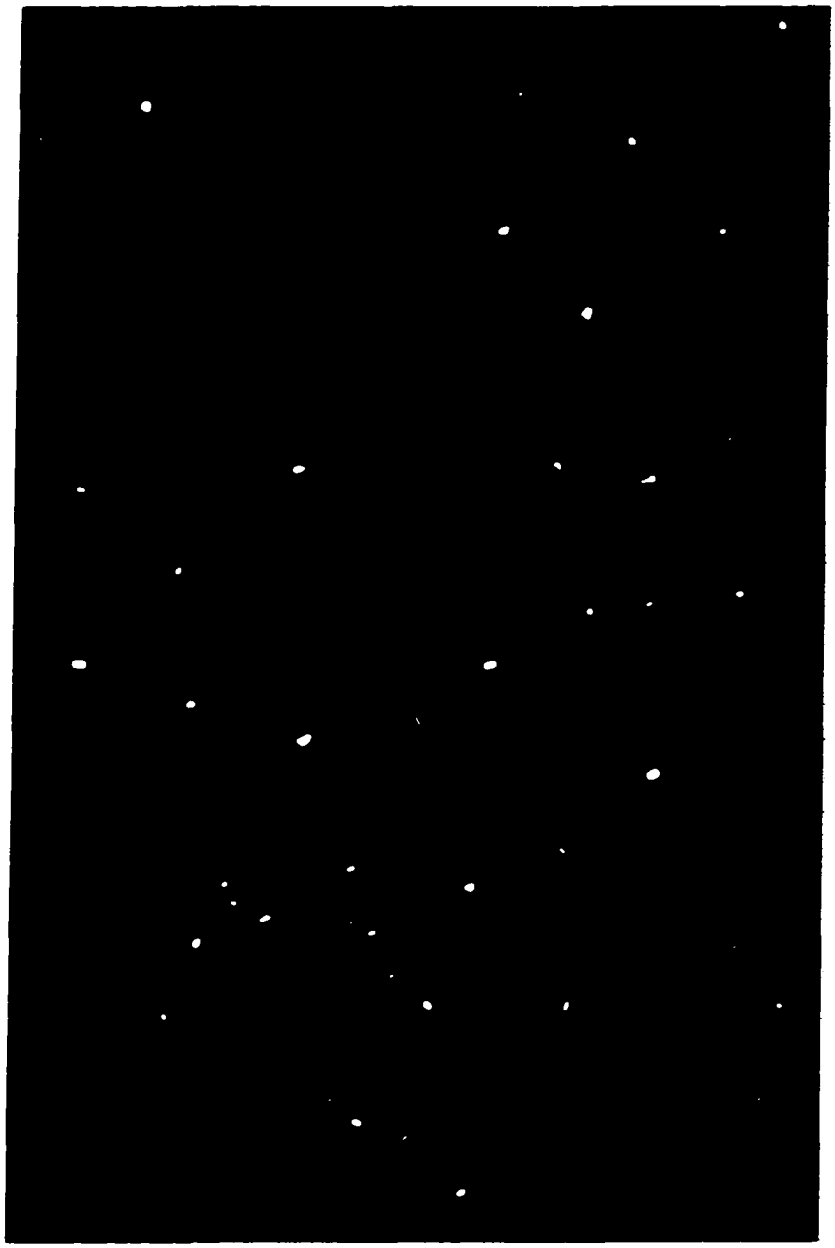

Figure 51.

Native Fluorescence at Liquid Nitrogen Temperature. 455nm excitation, orange barrier filter. CCI 357 Mag. 158gr. JHP. Muzzle-to-Target Distance = 45cm(18"). Compare to Photograph Taken from Same Pattern at Low Temperature (see Figure 50).

Figure 52.

Shortwave U.V. Native Fluorescence. Upper Photograph: Room Temperature, Lower Photograph: Liquid Nitrogen Temperature. CCI 357 Magnum, 158 grain, JHP. Muzzle-to-Target Distance = 45cm(18").

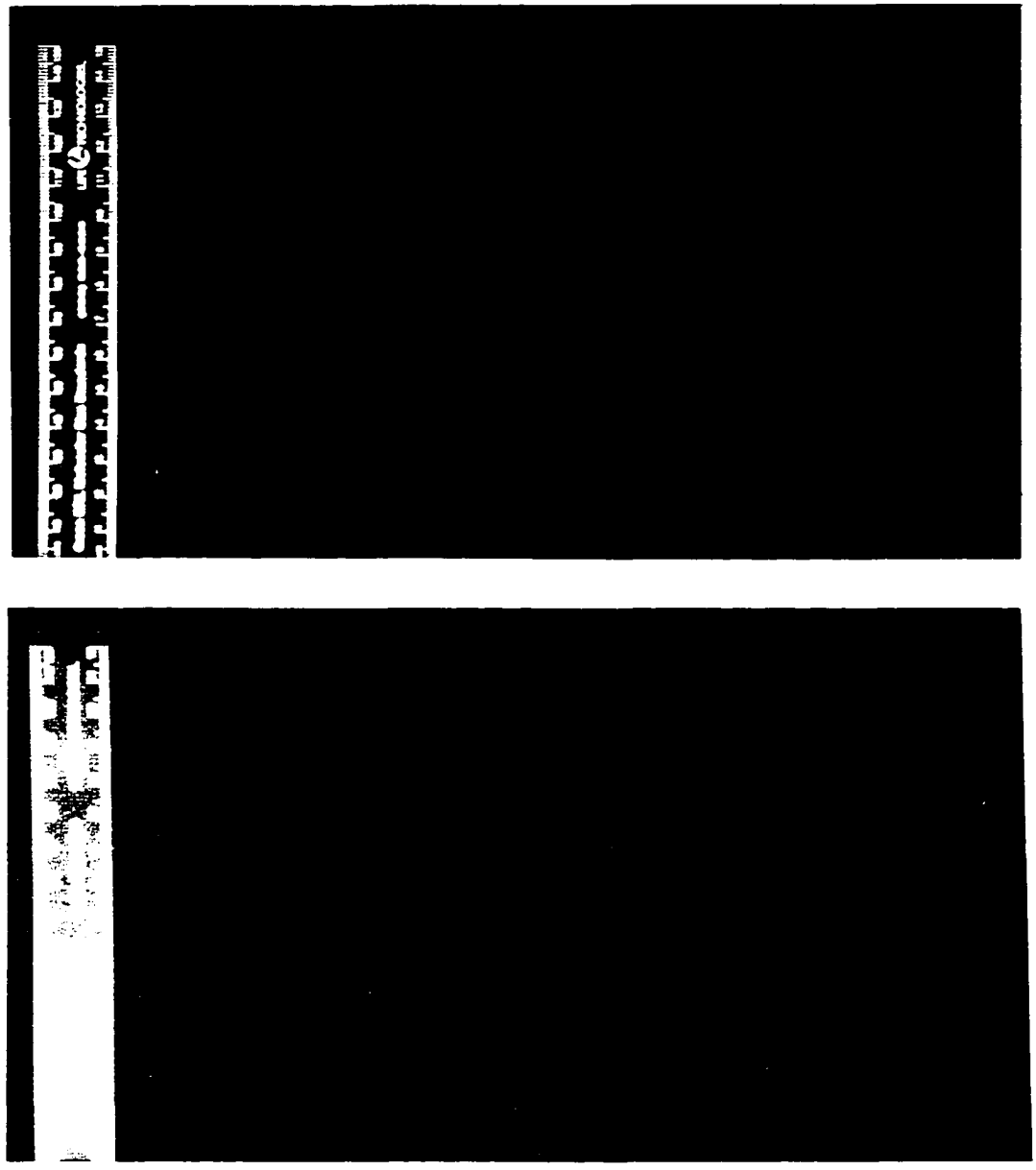

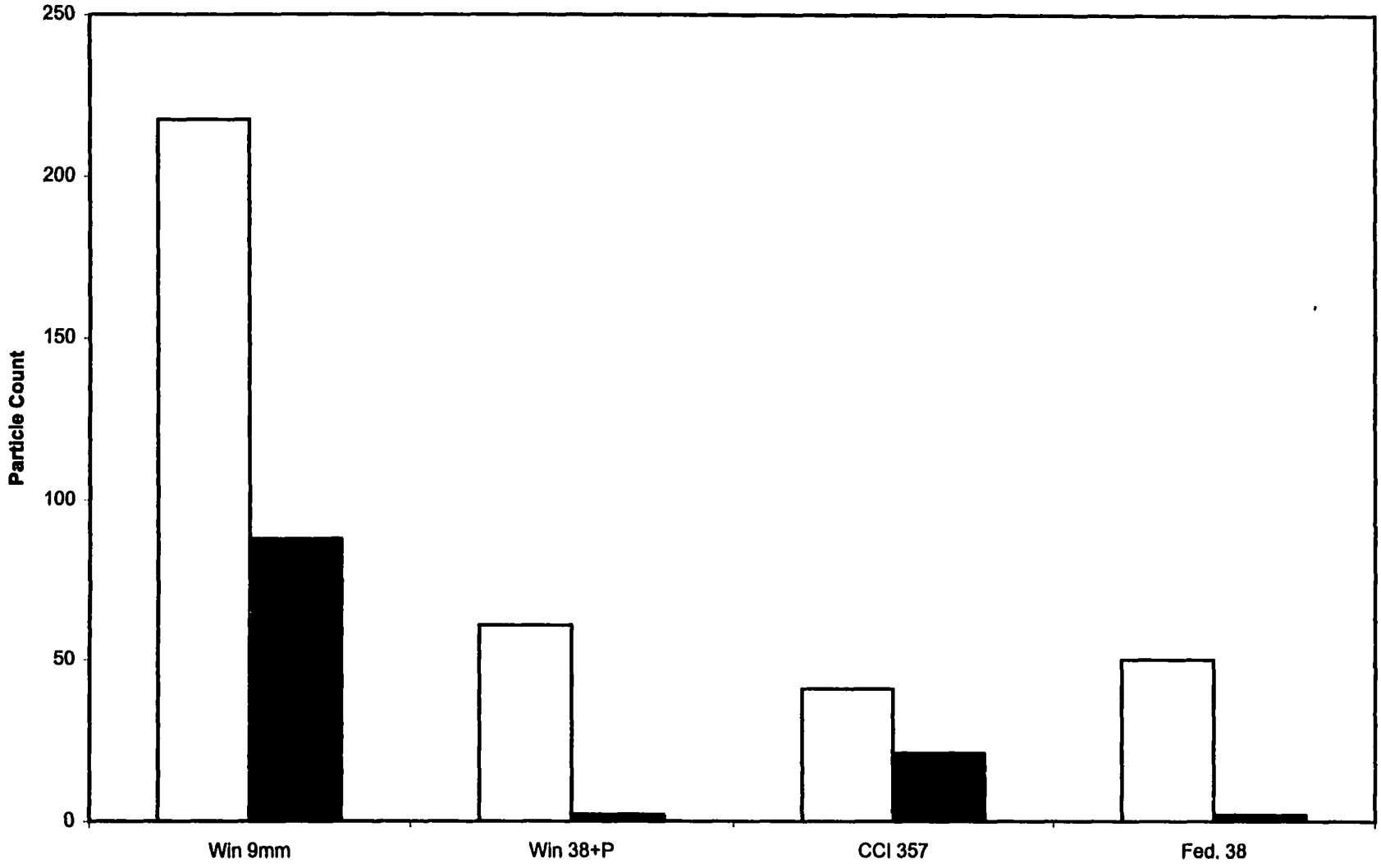

Figure 53. The Influence of Temperature on Native Fluorescence (Particle Counts)
Light Columns: Low Temperature. Dark Columns: Ambient Temperature

Chapter Eight

Griess Paper Fluorescence

During the early stages of this research, the fluorescence on a Griess transfer paper corresponding to the azo dye reaction sites was noticed serendipitously. This observation was made using visible excitation (450-495nm) while monitoring the emission with orange barrier filter goggles and with an orange barrier filter (Tiffen #21). The fluorescence was studied in more detail to determine the utility of examining the Griess transfer paper for the determination of the muzzle-to-target distance for casework.

Methods and Materials

Materials

Spex Crimescope (CS16), Tunable High Intensity Light Source

Nikon (FM2) 35mm SLR camera, Nikon lens, Kodak Ektapress 400 Color Film

Orange Barrier Filter

Spectroline U.V. Lamp, Model ENF-280C. 8 watt tubes. 470 microwatts/cm^2 of 365nm and 500 microwatts/cm^2 of 254nm at six inches.

1-naphthol, Sigma 99+%

sulfanilic acid, Eastman, Reagent ACS

glacial acetic acid, Fisher, HPLC grade

methanol, Fisher, HPLC grade

Water, Fisher, HPLC or distilled grade

Method

The data from Griess transfers produced for a variety of different examinations during the course of this research were used here (Table 10). The data listed in Table 10 were obtained using visible radiation for excitation (440-475nm). This range produced the best contrast between reaction sites and the substrate. Counts of particles were made by marking plastic overlays where reaction sites were detected.

Results and Discussion

With visible excitation, most of these sites were fluorescent. However, some sites quenched (darker than the background fluorescence from the substrate). The quenching sites always corresponded to strong colored azo dye reactions. The weak color reaction sites always provided strong fluorescence (Figures 54 & 55). Thus, in either event, it is relatively easy to detect particle reactions with visible excitation.

A comparison of the particle counts between the colored azo dye reaction sites and the fluorescent sites on the same transfer paper demonstrate the superiority of the fluorescent approach (an 87% increase in the number of particles detected overall). Of all the patterns examined, 13,217 azo dye sites

were detected on the transfer, while at least 24,667 sites, corresponding to particles, were detected by fluorescence. These data were compiled from an examination of thirty-five different discharge patterns. Of the 35 patterns that were examined, only two ammunition sources had equal or nearly equal counts with the both the fluorescence and ambient light examination (Table 10). These were the pattern obtained from the discharge of Federal 357 Magnum, 110 Grain, JHP and Magtech .380, 158 Grain, SWC. No decreases in the number of detectable reactions sites were obtained using fluorescence in comparison to the conventional MGT approach. The average increase in the number of detectable reaction sites for the Federal .38 Special ammunition (nine replications) was 189%. The lowest increase among this latter source was 40%. The remainder of the Federal ammunition displayed increases in excess of 100% (three patterns yielded approximate increases of 300%).

With certain ammunition, the reaction with Griess is so intense that the transfer pattern has poor definition due to reaction in between particle sites. In these instances, subsequent Modified Griess transfers from the same pattern, without saponification, can help produce more meaningful patterns. Sections of these patterns can be further enhanced via fluorescence using excitation indicated above.

An expensive light source is not necessary to obtain similar data in actual casework. This is an important issue since many laboratories might not be able to afford a tunable light source as used here. It was found that short

wavelength (254nm) ultraviolet light causes the azo dye sites to efficiently quench very intensely against the light fluorescent background of the transfer paper (Figure 56).

Table 10. Number of Reaction Sites Detected Conventional MGT v. Fluorescence on Transfer Paper

Source	Grain, Bullet	Conv. MGT	Fluorescence
Federal 357 JHP	110, JHP	522	522
Federal .38 Special	158, SWC	146	400
		68	95
		123	268
		66	263
		162	370
		91	265
		75	219
		67	242
		63	253
Remington .38+P	158, SWC	639	647
		721	868
		504	707
		716	763
		447	694
		506	760
		446	835
		494	903
		428	891
		343	838
Magtech .380		36	51
		43	125
CCI .32		68	110
CCI .380 Blazer		87	178
PMC 357	125, JHP	500	835
		2235	3035
		212	807
		266	1139
		464	1924
		460	1758
Winchester .38 Spl.	125, JHP	526	815
		400	673
		390	730
		523	930
		380	754
Average		378	705
Total # of Particles		13217	24667

Excitation: 440-495nm. Orange Barrier Goggles for Emission.

Figure 54.

Portion of Griess Transfer - PMC 357 Magnum 125 grain JHP - Muzzle-to-Target Distance = 30cm (12 inches). Upper Photograph: Flash, no filtration; Lower Photograph: Excited at 475nm, Orange Barrier Filter.

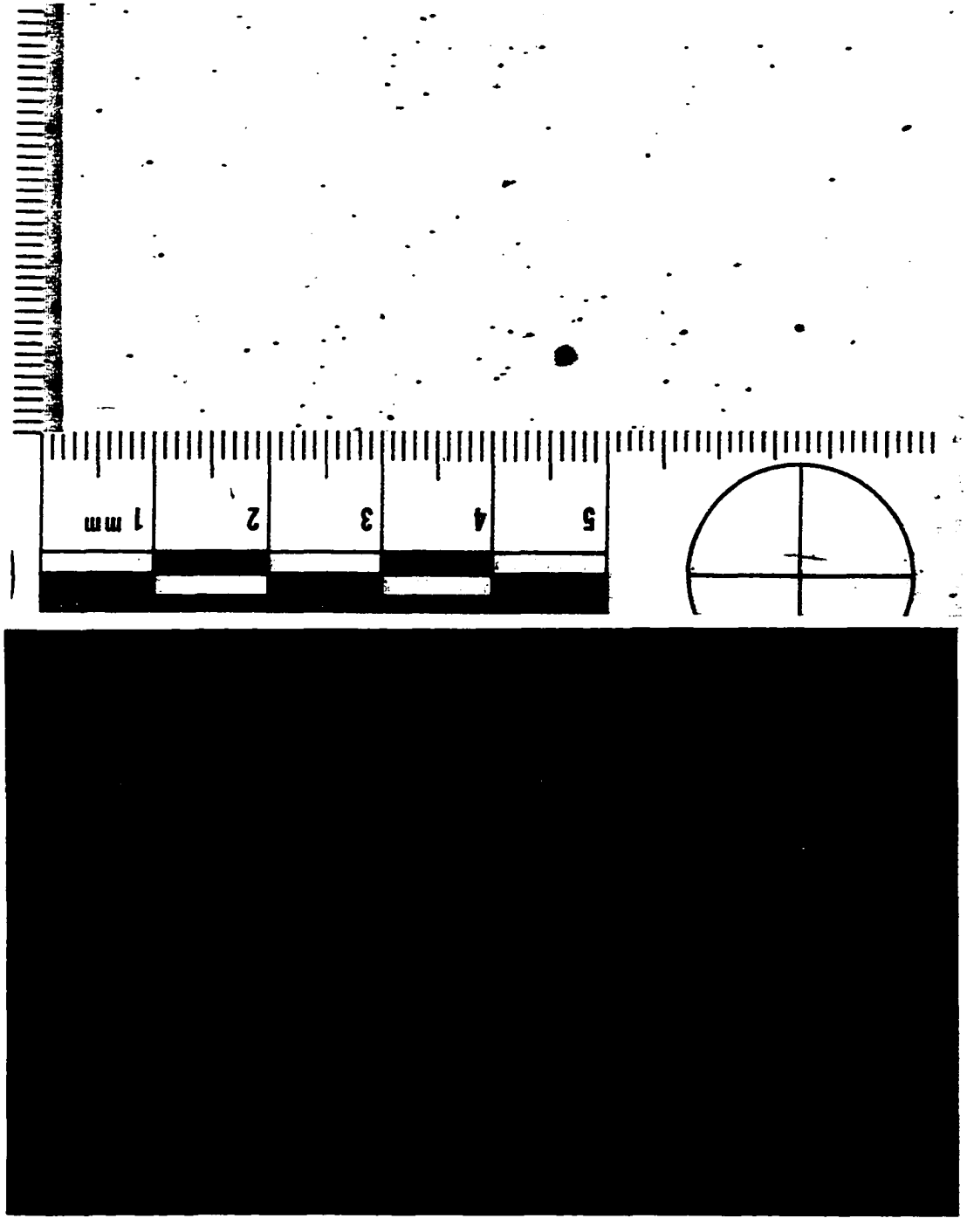

Figure 55.

Griess Transfer - PMC 357 Mag.125 grain JHP - Muzzle D. = 30cm (12 inches). Top Photo: Flash, no filtration; Lower Photograph: Excited at 475nm, Orange Barrier Filter.

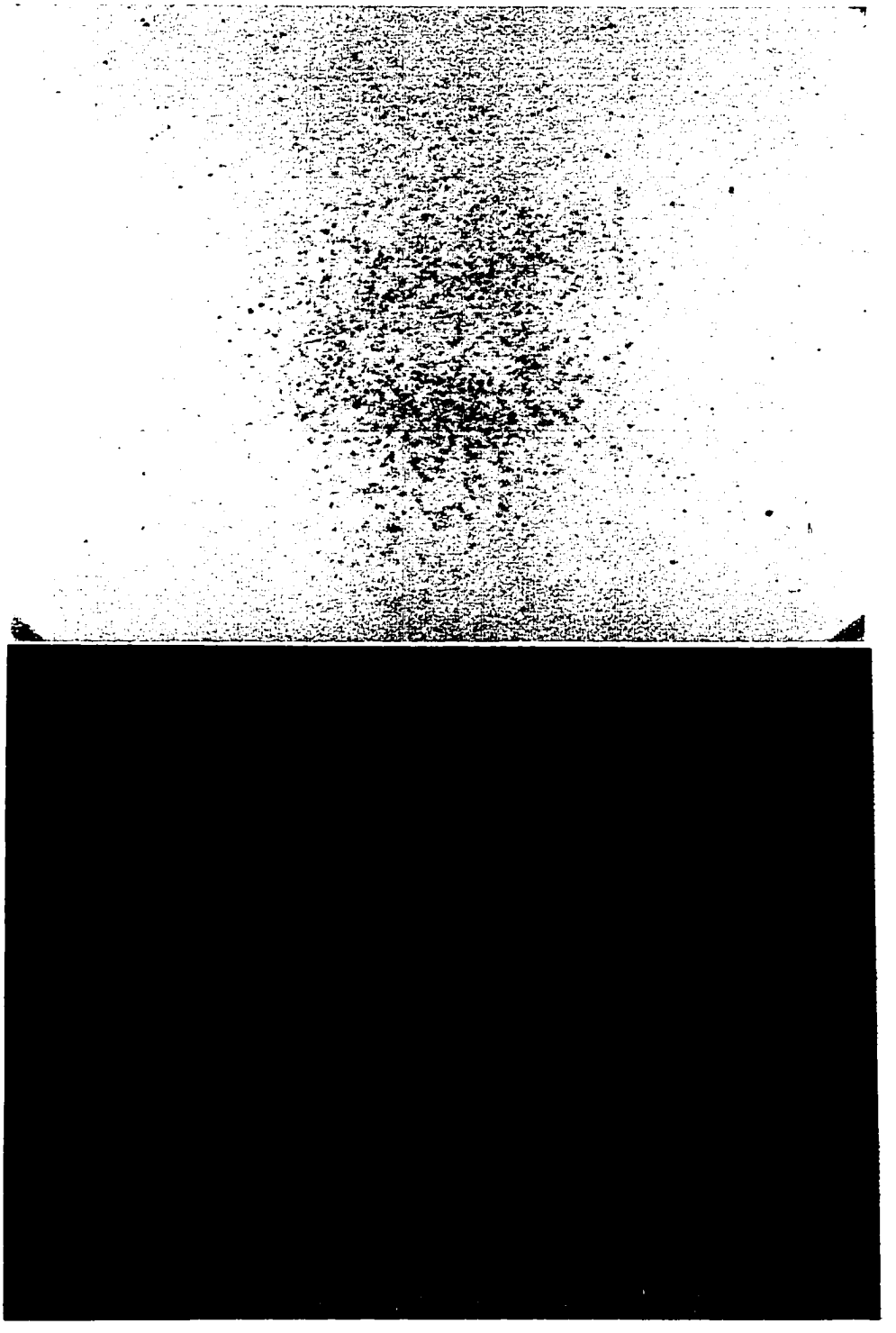

Figure 56. Upper Photo: Griess Transfer. Federal .38+P NYCLAD SWC HP (central portion of pattern treated with 1M HCl for other examination). Lower Photo: Short UV Excitation of Same Transfer

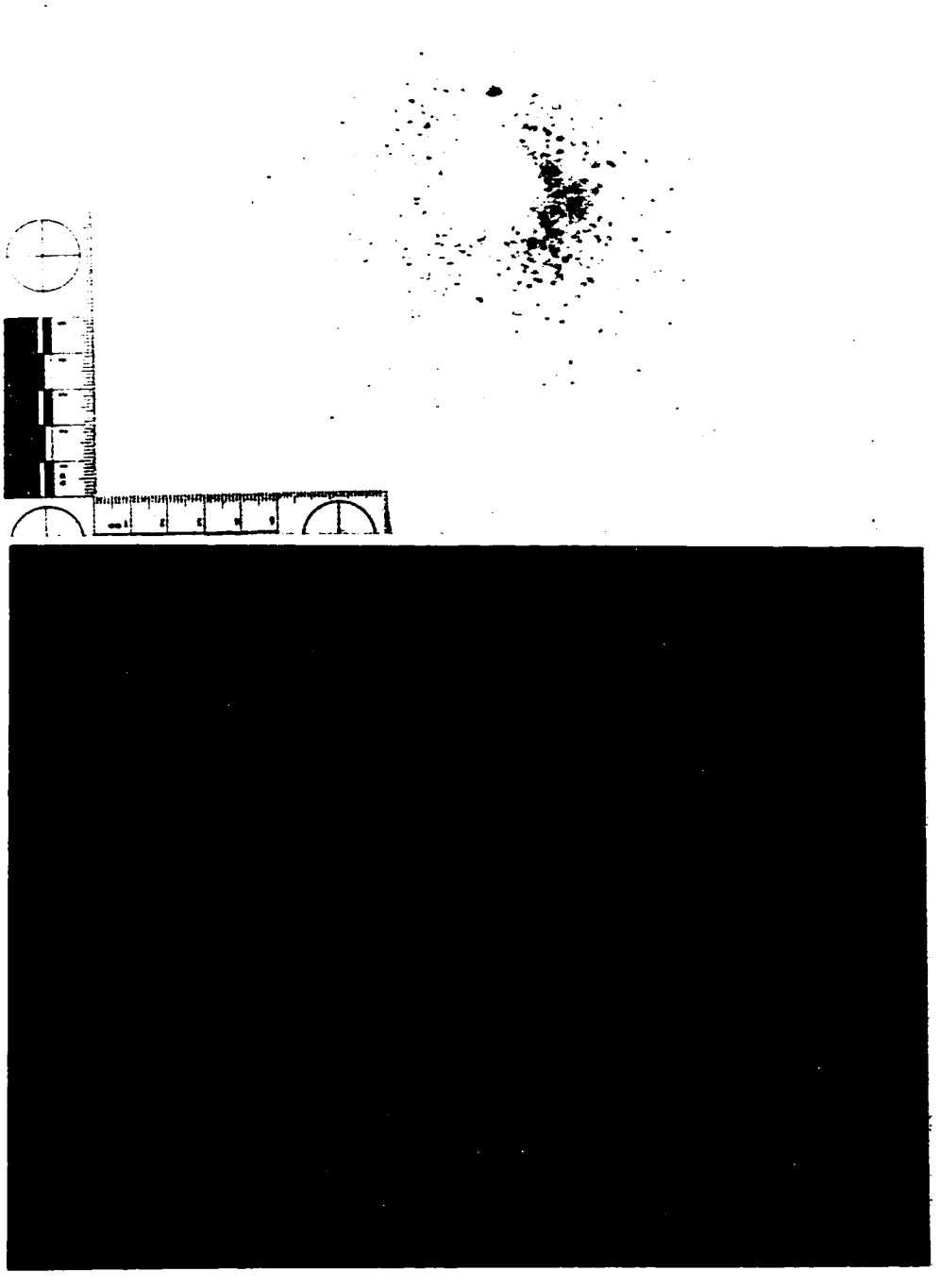

Chapter Nine

The Effect of Solvents and Steam

Preliminary experiments with various solvents and steam indicated that their application to propellant particles may induce or increase fluorescence. Discharged particles may be more or less coated with several different materials, such as: graphite, combustion products, (for example, nitrites), lead, and so forth. These materials, either individually or in combination, may effectively block the particle from being excited or emitting radiation. Water, aqueous 1M HCl, and methanol were examined at ambient and elevated temperature (approx. 50°C) to study their influence on propellant particles. Acetone was also studied for its effect on fluorescence, but only at ambient temperature.

Method & Materials

Materials

Crimescope CS-16 Light Source

acetone, Fisher, HPLC grade

methanol, Fisher, HPLC grade

acetic acid, Fisher, HPLC grade

water, Fisher, HPLC grade

aqueous 1M hydrochloric acid prepared from Fisher, Certified ACS

pressure cooker

steam iron

Solvent Experiments

Discharged particles were removed from ten different GSR patterns. Both dark and light particles were retrieved from each pattern. These experiments were conducted in white porcelain plates. Several particles from each source were placed in individual wells of the plate. This was done for both the dark and light particles as it was suspected that they might behave differently following treatment with solvent. In a separate well, another group of light and dark particles were placed to serve as controls. The control group was not exposed to solvent. Particles were treated with each solvent at both room temperature and at higher temperature (Table 11). The CS 16 was used to excite the particles in the range 475-515nm. For this experiment orange barrier goggles were used to monitor the emission.

Steam Experiment

Patterns from five different firearm discharges were divided into four equal quadrants. One quadrant was placed into a household type pressure cooker (autoclave). Each quadrant was autoclaved for up to fifteen minutes and compared to another quadrant which was untreated.

Solvent and Steam Experiment

Ten or more dark particles that exhibited little or no native fluorescence were removed from each of ten different firearm discharge patterns. These are listed in Table 13. Particles were first treated with a solution of three solvents as used in the Griess test. The solution consisted of water, methanol, and 15% aqueous acetic acid (5:5:2). The particles that exhibited measurable fluorescence were counted. Following solvent treatment, the particles were exposed to steam from an iron for approximately two minutes at a distance of about 0.5cm. The distance between the iron and the particles was controlled with ceramic tiles. Additional particles found to fluoresce after the steam treatment were counted. The results are summarized in Table 13.

Results and Discussion

Solvent Experiments

The results are summarized in Table 11. The dilute hydrochloric acid was, in general, successful at inducing the dark particles to fluoresce or fluoresce more intensely. Additionally, the intensity of the fluorescence of the light particles also increased. The hydrochloric acid may affect the surface of the particles in both a chemical and physical way. First, the acid may serve to physically "wash" the surface free of materials that provide degrees of opacity. Additionally, in the case of metallic lead coating the particle surface, some measure of lead chloride may be formed which is soluble in dilute hydrochloric acid. Acetone generally caused the particles to soften or dissolve. While in a

sense this may be helpful in the case of particles that are poorly fluorescing, because it obviates the problem of an obscuring outer surface, it permits the particle material to flow into the fabric (which is not ideal for fluorescence observations). In a spot plate, dissolving the particle did not appear to have a positive influence on fluorescence. Fluorescence seems most intense from particles left relatively intact. Intact particles seem to fluoresce more intensely than those that have dissolved. The influence of solvent on particle fluorescence is further discussed.

Steam Experiments

Results are presented in Table 12. For each of the five sources of ammunition, the autoclaving appeared to clear the surfaces of those particles of debris which originally limited or prevented fluorescence. It was clear that many more particles were now visible, and many dark particles that had not fluoresced significantly before now did so. These results are consistent with those obtained in the combination of solvent & steam experiments.

Solvent & Steam Experiments

Results here demonstrate that solvent treatment alone can have a significant impact on the fluorescence of particles. Additionally, it is clear that steam treatment following solvent treatment can significantly increase particle fluorescence in those instances where solvent treatment has not been

adequate. For example, in the case of Remington .38+P, 158 grain, SWC, of 13 dark particles that did not fluoresce appreciably prior to treatment, after solvent treatment five of these 13 produced significant fluorescence. However, after treatment with the steam iron, the remaining eight particles were found to fluoresce significantly (Table 13).

Similar results were obtained in experiments conducted to assess the direct application of the Modified Griess Test, as well as in other direct chemical application experiments (Chapter Ten).

Chemical Treatments and Observations

Solvent	Caliber	Grain, Bullet	HCl 1M	Hot HCl 1M	Water	Hot Water	Methanol	Hot Methanol	Acetone
Remington	.38+P	158, SWC	no change	increase	no change	no change	increase	increase	dissolved
Remington	9mm+P	115, JHP	increase	increase	no change	no change	no change	no change	dissolved
Federal	.38+P	158, SWC	no change	increase	no change	no change	increase	increase	dissolved
Winchester	.38+P	125, JHP	no change	increase	no change	no change	increase	increase	dissolved
CCI	.38spl.	158, SWC	increase	increase	no change	no change	no change	no change	dissolved
CCI	357Mag.	158, JHP	increase	increase	no change	no change	no change	no change	dissolved
CCI	9mm+P	115, TMJ	increase	increase	no change	no change	no change	no change	dissolved
Magtech	.38spl.	158, LRN	increase	increase	no change	no change	no change	no change	dissolved
PMC	.38spl.	158, SWC	increase	increase	no change	no change	no change	increase	dissolved
PMC	357Mag.	125, JHP	increase	increase	no change	no change	no change	increase	dissolved

Table 11. Behavior of Non-Fluorescent Particles Post Solvent Treatment (475-515nm ex.)

Brand	Caliber	Grain, Bullet	Change in Fluorescence
Winchester	.38+P	158, SWC	increase
CCI	357 Mag.	158, JHP	increase
Remington	.38+P	158, SWC	increase
Federal	.38+P	125, JHP	increase
Magtech	.38 spl.	158, LRN	increase

Table 12. Behavior of Non-Fluorescent Particles Post Steam Treatment (475-515nm ex.)

Excitation Wavelengths: 475nm-515nm (Orange Barrier Goggles for Emission)

			post solvent	post steam (after solvent)
Brand	**Caliber**	**Grain, Bullet**	**number fluorescing**	**additional number fluorescing**
Remington	.38+P	125, SJHP	1 of 12	9 of 12
Remington	.38+P	158, SWC	5 of 13	8 of 13
Remington	357mag.	180, SJHP	7 of 10	no change
Federal	.38+P	125, JHP	5 of 12	6 of 12
Federal	357mag.	110, JHP	none	5 of 10
Federal	.38+P	158, SWC HP	4 of 12	3 of 12
Winchester	.38+P	125, JHP	6 of 10	3 of 10
PMC	.38spl.	132, FMJ	5 of 10	5 of 10
PMC	.38spl.	158, SWC	none	8 of 10
PMC	357mag.	125, JHP	6 of 10	no change

Table 13. Behavior of Non-Fluorescent Particles Post Solvent and Steam Treatment

Chapter Ten

Chemical Treatments to Induce Photoluminescence

Assessment of Modified Griess Test: Direct Application to Target

The initial evaluation of this reaction to bring about or cause an increase in fluorescence of partially burned particles was carried out using the approach discussed in Chapter One. Preliminary experimentation, as well as research reported here above, indicated that the Griess Test might be of value in inducing partially burned particles to fluoresce. Certainly, reaction sites corresponding with particles were found to fluoresce on the transfer paper from Modified Griess tests. Earlier research conducted by this worker, also indicated the possible value of the reaction in this context. Preliminary experiments with filter paper gave fluorescence with inorganic nitrite. No measurable fluorescence was detected in the azo dye solution spectrofluorimetrically (emission scan 450nm - 600nm; excitation set at 450nm) at a number of different dilutions (including the ppb range). Fluorescence was found on or around burned particles on fabric substrates subsequent to transfer (Figure 59). Most of these observations involved localized fluorescence in a small area around the particles. The Modified Griess Test was further evaluated for fluorescence with particles. These results are reported here.

Methods and Materials

Materials

1-Naphthol, Sigma 99+%

sulfanilic acid, Eastman, Reagent ACS

CS-16 Crimescope, Tunable Light Source, Spex Industries

Orange Barrier Filter

Orange Filter Goggles

Digital Photometer, Model M-100A, Eseco Speedmaster

Perkin-Elmer Spectrofluorimeter, Model LS-S

Smith & Wesson 357 Magnum Revolver, Model 19-2

Wratten 80B Color Temperature Correction Filter

Kodak B&W Photographic Paper Type F

Heating Iron (#6 cotton setting)

Partially burnt particles were obtained from five different sources from firearm discharges at muzzle-to-target distances of twelve inches . These were:

Winchester 38+P	CCI 357	
Federal .38 NYCLAD	CCI .38+P	Remington .38+P

Method

One quadrant was sampled from each pattern. The particles from this quadrant were subdivided into dark and light groups. Reactions were carried out in spot plate depressions. Two sets of experiments on particles removed from GSR patterns were conducted. One set was conducted with particles treated

with 1-naphthol, sulfanilic acid, acetic acid, and heat. However, because of real concerns with actual inorganic nitrite ion availability for reaction (as demonstrated in Chapter Five), another set of experiments was conducted using 4% methanolic potassium hydroxide to hydrolyze the organic nitrate to nitrite. Heat was not applied to the latter set of particles since a positive reaction with the Griess reagents could be readily observed. It was often questionable as to whether sufficient heat was delivered to particles residing within the well of a spot plate to produce an adequate concentration of nitrite ion on the surface of a particle. Thus, the parallel experiment involving potassium hydroxide to produce nitrite via saponification was considered necessary. Heat was applied to the one set of particles with a hot iron set on #6. Five dark particles were placed into the well of a spot plate. This was also done with the lighter particles. A mixture of five dark and light particles was placed into a third well. One well of the plate was used as a negative control consisting of the reagents (no particles or nitrite). Inorganic nitrite was placed into another well as a positive control. The particles were photographed prior to introduction of the chemicals with copy stand illumination, using a Wratten 80B color temperature correction filter. Alternatively, a master and slave strobe unit was sometimes used in conjunction with daylight film. After the particles were photographed as above, the photography was repeated to document native fluorescence with 475nm excitation using an orange barrier filter. Reagents were introduced and reaction initiated. After the chemical reaction step was

completed, the particles were rephotographed.

The experiments involving the potassium hydroxide saponification were conducted in the following manner. Two drops of the methanolic potassium hydroxide were placed into the three wells corresponding to each particle source, that is, one group of light particles, a second group of dark particles, and a third group consisting of a mixture of light and dark particles. Three minutes were allowed to pass before the five drops of the diazocoupling reagent were introduced. Five drops of 15% acetic acid were then added to ensure that the solution was decidedly acidic. No heat was applied as previously mentioned. The solution gradually became a darker orange.

After five minutes had elapsed, the remaining azo dye & reagent solution was removed since it obscured fluorescence of the particles. This was accomplished with a micropipette and/or small strips of filter paper. The particles were gently washed several times with water to ensure that the observed fluorescence was coming from the particles themselves, not solution residing on the surface of the particles. This was done until the wash was relatively colorless. A 1:1 solution of methanol and water tended to remove too much azo dye product from the surfaces of the particles.

After all reactions and washings were complete, the particles were gently dried, removed from the spot plates and placed on black cardboard having a matte finish. This was done since it was extremely difficult to uniformly photograph the particles sitting in the spot plate depressions. Additionally,

reflections from the ceramic or glass surfaces exacerbated the non-uniformity of illumination. Moreover, it was not possible to bring particles close to one another to ensure equivalent illumination from the light source. This was readily accomplished by placing the particles on the non-reflective black surface. The cardboard surface was marked to locate particles in certain positions.

The light from the CS-16 was sharply focused, using the front lens, to produce a relatively intense and uniform field of illumination immediately around the particles. An ABFO L-shaped two-dimensional scale was placed adjacent to the particles. The light wand was clamped into position twenty-seven degrees from normal to the cardboard surface on which the particles resided. This angle was measured with a digital inclinometer. The tip of the wand was kept 15.5 inches from the cardboard surface. Although the illumination appeared uniform, it was not expected to be perfectly so since the light was not perpendicular to the surface. The illumination intensity corresponding to the position of each group of particles was measured with the digital photometer (Figure 60). These values were later used to calibrate the raw data obtained from measuring the fluorescence intensity of particles at significantly different locations on the cardboard.

The intensity values of the particles pre-reaction and post-reaction were compared by scanning photographs of the particles onto a personal computer. The images were scanned as sharp black and white photographs using PhotoPaint (5.0) software. Preliminary cropping of the images was done using

the scanning program to remove unnecessary portions of the photographs, and to reduce the file sizes to approximately 200 kilobytes. Each image was saved as a PCX file onto a network drive, and opened on a different computer having the imaging software. The images were evaluated using Sigma Scan Pro/Image measurement software. All images were scanned in a 5 x 7 inch format in the same corner of the platen. In addition, all images were scanned alongside a two-dimensional scale having white, black, and grey patches. The platen was cleaned immediately prior to scanning images. Raw pixel intensities from particle images pre- and post-reaction were obtained, stored on a spreadsheet and compared. Additionally, reacted particles were compared to unreacted particles. See Figure 60 for appearance of particles pre- and post- reaction.

Further evaluation of this reaction was conducted on actual patterns in situ. Five different discharge patterns were sampled, one quadrant from each pattern. One quadrant was processed with the Modified Griess Test in the conventional fashion (transfer technique). Another quadrant was sprayed with a 1:1 mixture of 1-naphthol and sulfanilic acid. A third quadrant was treated with solvent only, consisting of a 1:1 mixture of methanol and water. Both the latter quadrants were then sprayed with acetic acid (15%), and heated with the hot iron set on steam using ceramic plates as spacers (0.5cm thick). The iron was brought as close to the surface of the target as possible without directly contacting it. After three minutes the heating was terminated, as long as the particles had visibly reacted as shown by the development of color. After drying,

each pattern was exposed to 475nm excitation light and the number of the particles fluorescing in the quadrant were counted. This was accomplished by placing plastic over the target, wearing orange barrier goggles to monitor the emission, and marking the overlay in each location where a particle was detected. Figure 61 is an illustration of the above and in which a portion of the target was first treated with dilute potassium hydroxide to saponify cellulose nitrate.

Results and Discussion

Preliminary results did not show that the direct application of the reagent to the target surface was helpful (Figures 62 & 63). While particle fluorescence generally increased following reaction it was generally inferior to results obtained with solvent treatment alone (Table 15; raw data in Appendix). This was obvious visually as well as by calculation of intensity changes. On average, the increase in fluorescence after chemical reaction was 13% in contrast to the average increase of 32% after solvent treatment. The fluorescence increase after solvent treatment ranged from 8% to 64%. Despite these poor results, experiments involving the direct application of reagent to the target were carried out since preliminary experimentation conducted prior to the writing of the dissertation proposal predicted results of some value in this context. These early experiments were conducted directly on the patterns, and demonstrated fluorescence on the targets corresponding to the particle sites. This fluorescence was diffuse, but localized on the target immediately surrounding

the particles. Additionally, the fluorescence obtained on the transfer paper illustrates that fluorescent material is being produced as a result of the Griess test process. Targets treated similarly with solvent alone did not produce such fluorescence.

As was found in the preliminary experiments, diffuse fluorescence was found around particle sites that had been directly treated with the Modified Griess reagent and process (Figure 61). The results of the direct application are much poorer than that obtained with the conventional Modified Griess test (transfer process). On average, 130% more particles were detected via the conventional method (Table 16). Additionally, a similar number or greater number of particles are detected via native fluorescence.

The direct application of the Griess test may be of some value at crime scenes. However, it is quite likely that use of native fluorescence to detect particles under scene conditions would be more successful. This reaction may be of value at a crime scene as a field test for organic nitrite. The use of this reaction, as a field test for particles, is practical since nitrite can be produced readily from the saponification of cellulose nitrate with potassium hydroxide at room temperature. While there is a loss of selectivity, that is, nitrate v. nitrite, the chances of detecting a particle are significantly enhanced. In the crime scene context, a particle can be analyzed instrumentally (by GC-MS or FTIR microscopy) to confirm its identity.

Figure 57.

Localized Fluorescence Surrounding Particles Post Griess (by direct application of reagent or after transfer). Winchester .38+P, 158 grain, SWC.

Direct Application of Modified Griess Test (MGT)

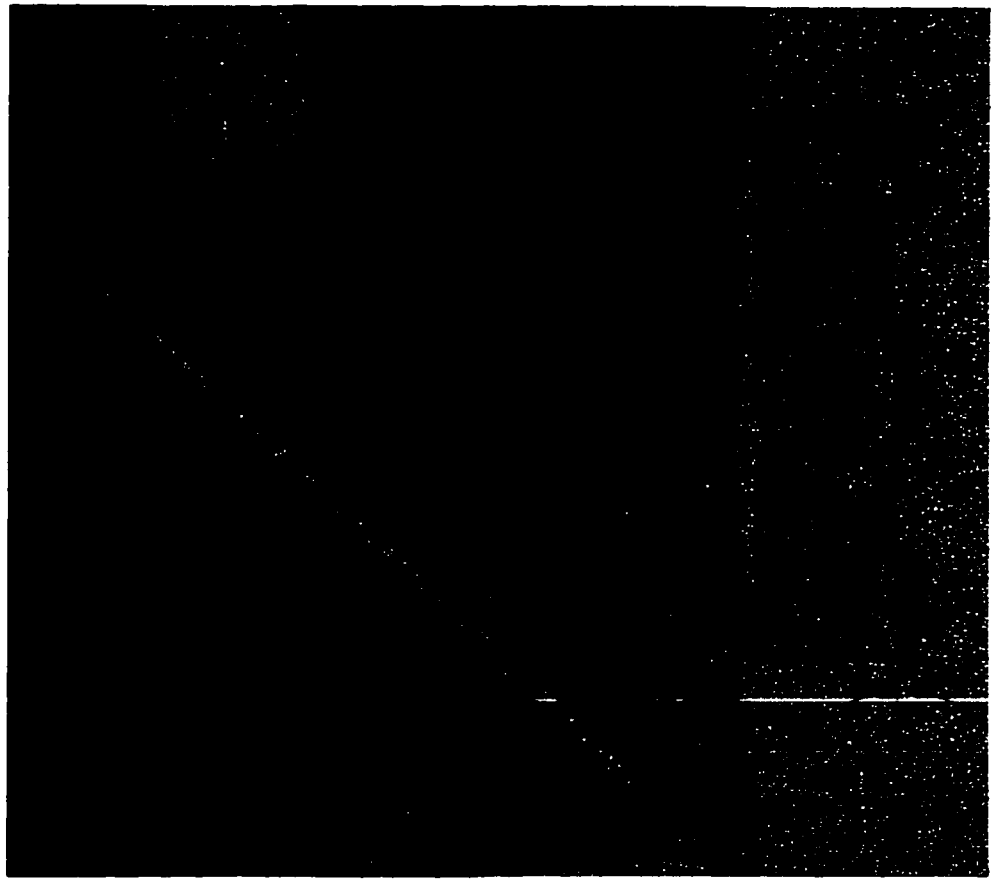

Direct Application of Solvents Used with MGT

Figure 58. Photographs of Particles Pre- and Post-Reaction (Upper Photo: pre-reaction, copy stand illumination w/80B Filter (Daylight Film); Lower Photo: Post-Reaction, strobe illumination. Column Designations: A - Remington .38+P; B - Winchester .38+P; C - Federal .38+P; D - CCI .38spl; E - CCI 357. Row Designations: 1 - Light Particles; 2 - Dark Particles; 3 - Light and Dark Particles. Same Particles as Shown in Figures 60 and 61.

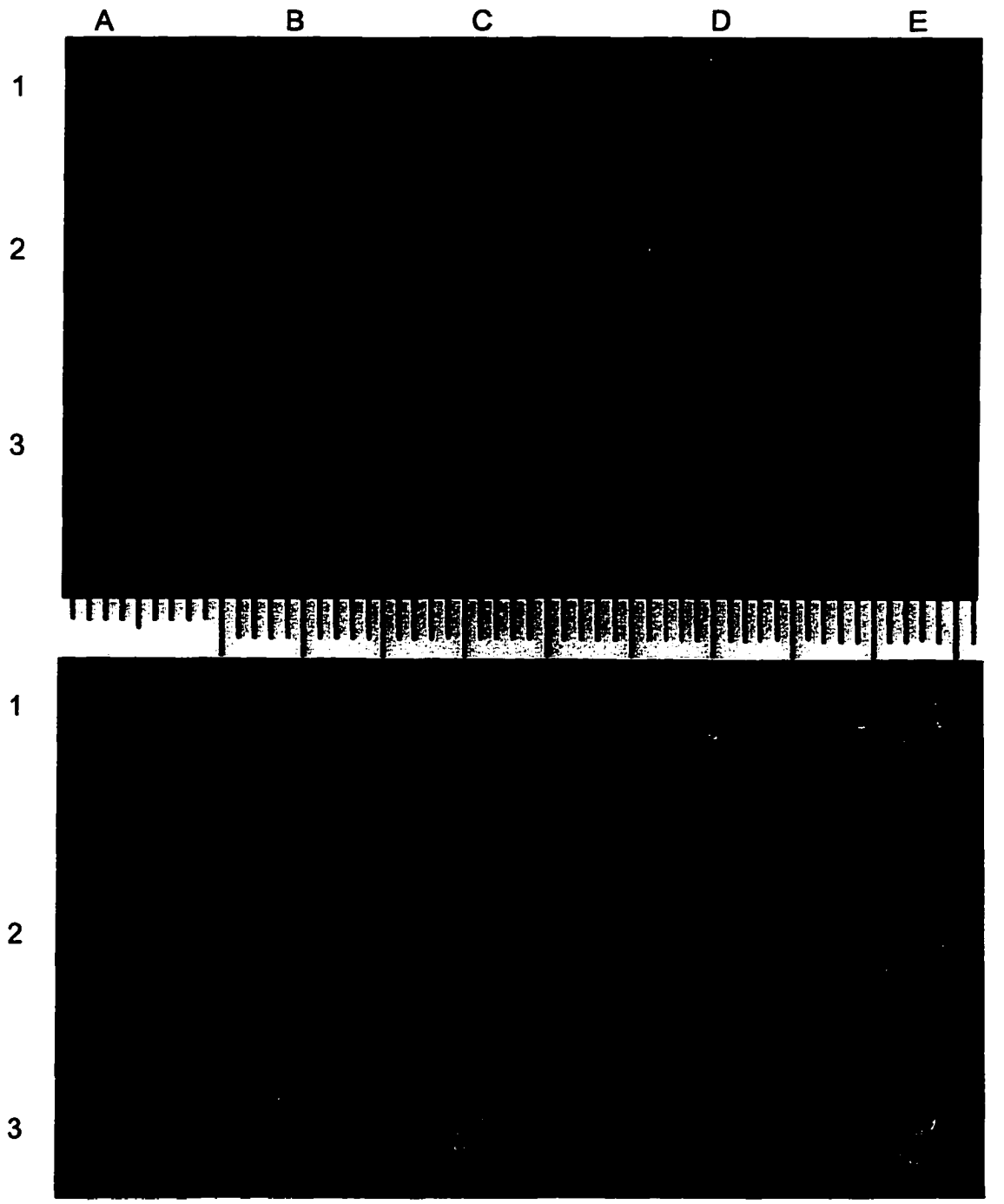

Figure 59. Entire Pattern Chemically Treated with Exception of Upper Right Fraction (neat). Upper Photo: Strobe Illumination. Lower Photo: 455nm Orange Barrier Filter. Individual Treatment of Each Portion Indicated as Labelled.

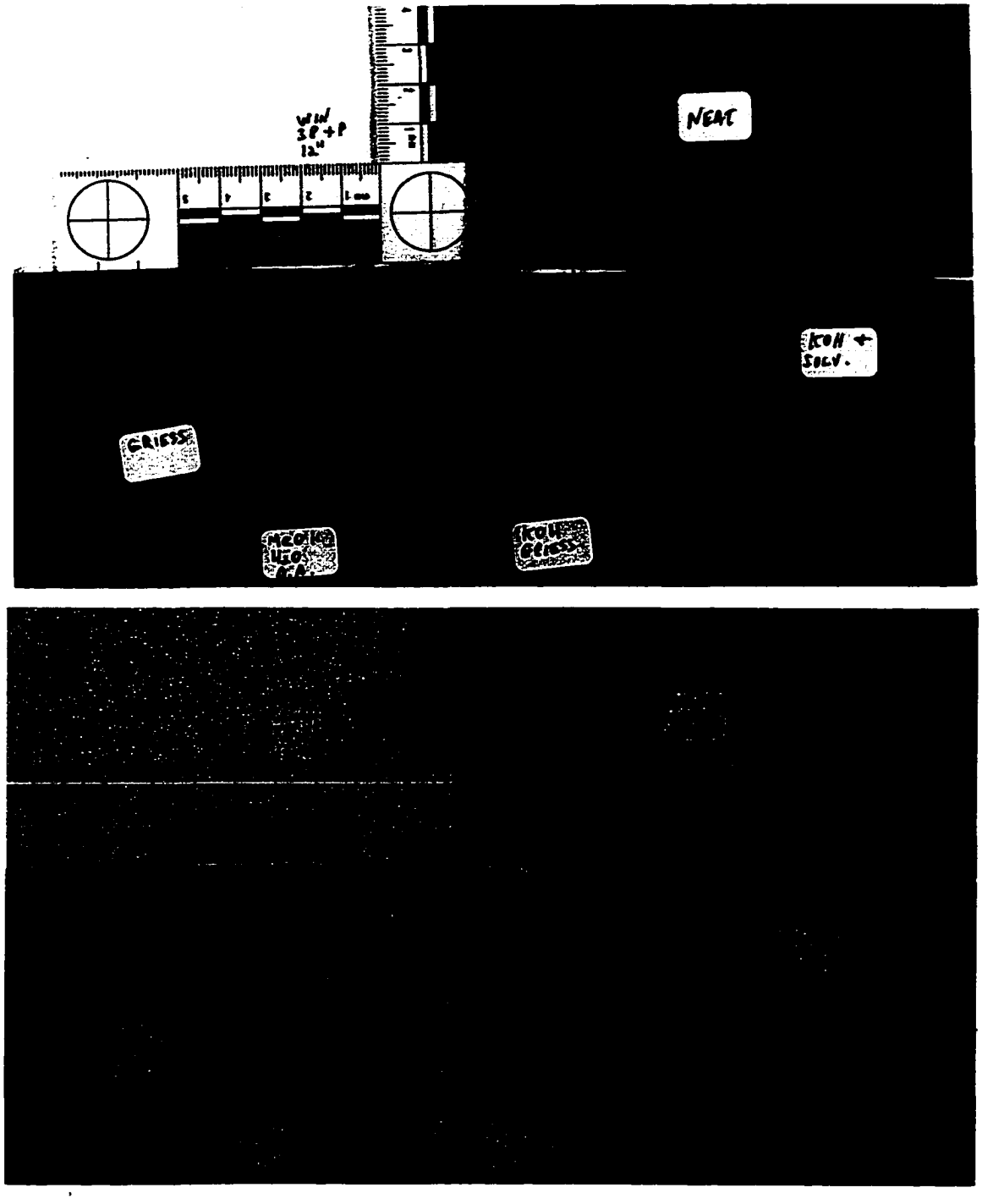

Figure 60.

Fluorescence of Particles Prior to Griess Reaction. Excitation wavelength = 475nm. Orange Barrier Filter. Column A: Light Particles; Column B: Dark Particles; Column C: Light and Dark Particles.

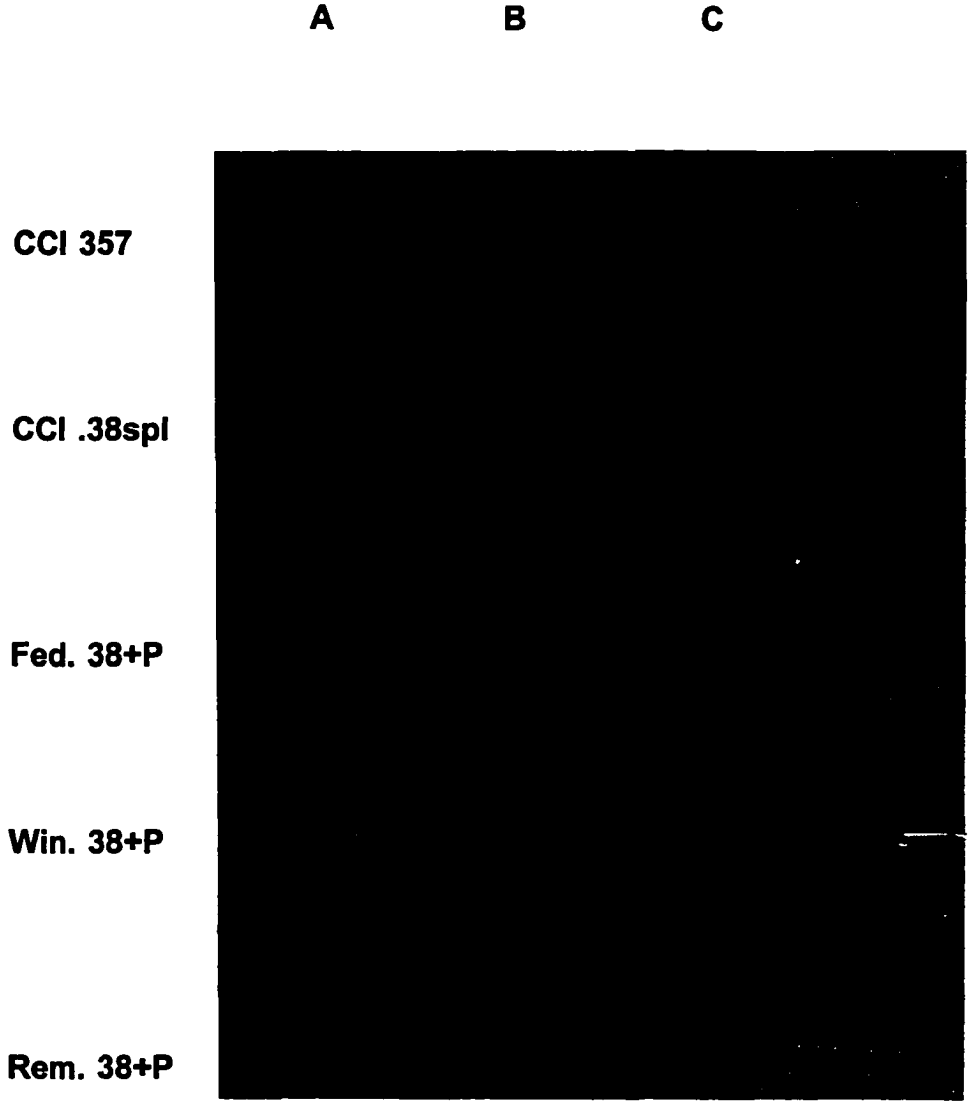

Figure 61.

Fluorescence of Particles Post Chemical Treatment. Excitation wavelength = 475nm. Orange Barrier Filter. Column A: Light Particles Post Griess Reaction; Column B: Dark Particles Post Griess Reaction; Column C: Light and Dark Particles Post Solvent.

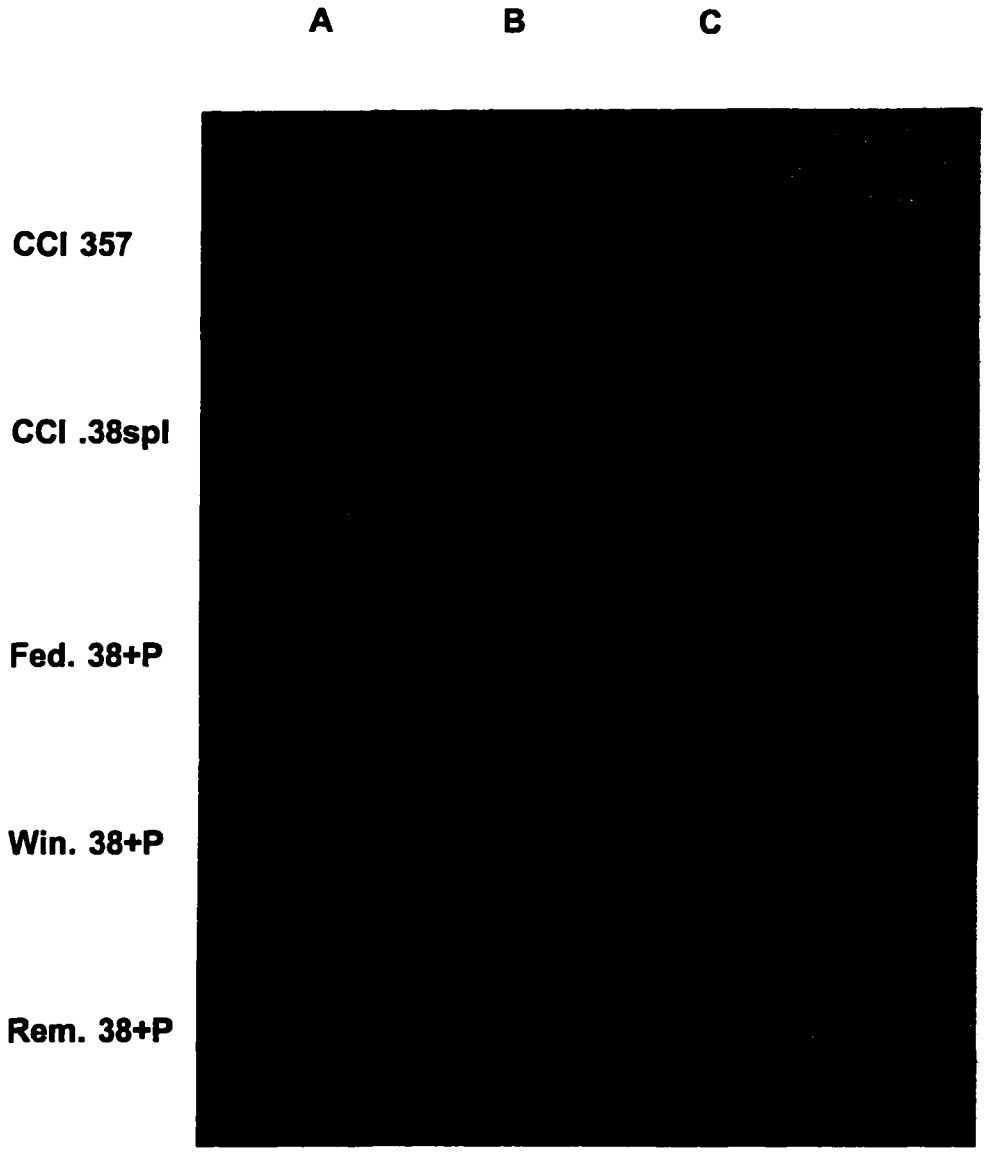

Table 14. Average Change in Fluorescence Intensity

Source	Post-Reaction	Post-Solvent
CCI 357 Magnum,158 Gr. JHP	38%	37%
CCI .38 Special, 125 Gr. JHP	9%	64%
Winchester .38+P,158 Gr. JHP	6%	11%
Remington .38+P, 125 Gr. JHP	16%	8%
Federal .38+P, 125 Gr. JHP	-3%	42%
Average	13%	32%

Table 15. Comparison of Particle Counts: MGT Direct v. MGT Transfer

Source	Direct	Transfer	Increase
CCI 357 Magnum, 158 Gr. JHP	91	151	66%
CCI .38 Special, 125 Gr. JHP	164	220	34%
Remington .38+P, 125 Gr. JHP	112	350	213%
Winchester .38+P, 158 Gr. JHP	70	152	117%
Federal 357 Mag. 110 Gr. JHP	163	522	220%
		average	130%

Assessment of Diazocoupling Reaction: p-chloroaniline & 2,6-diaminopyridine: Direct Application to Target

Dombrowski and Pratt (1972) developed a fluorimetric method for the determination of nitrite ion in a non-forensic context. Their method utilized para-chloroaniline (PCA) as a diazotization reagent, and coupling was accomplished with 2,6-diaminopyridine (DAP). The azo product was then derivatized with ammoniacal cupric sulfate producing a triazole. They found the excitation maximum to be 360nm and the emission maximum 430nm. The basic protocol is:

1. Nitrite solution is added to a test tube along with 0.1ml of 6M hydrochloric acid.
2. 0.3ml of 0.06% p-chloroaniline is added to the test tube, mixed, and placed into a ice water bath for fifteen minutes.
3. 0.3ml of 4% ammonium sulfamate is added, mixed, and after two minutes has passed 2ml of 0.025% DAP reagent is added. The solution is thoroughly mixed and placed into an ice water bath for 30 minutes.
4. The solution is then transferred to a separator and extracted with 6ml of benzene. The aqueous layer is discarded, and the benzene extract washed twice with pH 5 acetate buffer. All washings are discarded.
5. The benzene is evaporated to dryness on a steam bath with a stream of nitrogen.
6. 2ml of distilled water are added followed by 0.4ml of ammoniacal cupric

sulfate solution. The tube is stoppered and placed in a boiling water bath for 30 minutes.

7. The tube is cooled to room temperature with running water and acidified with 0.45ml of 6M hydrochloric acid.
8. The solution is brought to a 10ml volume in a flask with distilled water.
9. The solution is filtered through a fine glass frit funnel and the fluorescence is measured at 430nm using 360nm as the excitation wavelength.

Obviously, this procedure presents several problems for the detection of nitrite, as part of GSR, on clothing. Previous experiments have amply shown that surface nitrite can be easily removed from the surface of discharged particles (Gestring). This procedure incorporates considerable manipulation such as separate diazotization and coupling steps, immersion in ice water bath (2X), an extraction step, changing of pH to form a cupric triazole, immersion into boiling water, reacidification for the measuring of fluorescence, etc. Of course, the authors developed this procedure for the optimal determination of nitrite, which is not necessary in this particular criminalistics context. In order for this diazocoupling reaction to be useful in the detection of nitrite on clothing the procedure would have to be drastically changed. Additionally, although the fluorescence of the triazole is easily measured with a spectrofluorimeter it was not assumed that it could be detection by the unaided eye (which is necessary in this application) would be possible.

Initially, it was not clear if the extraction step could be eliminated. Apparently, this step was necessary for the spectrofluorimetric method since unreacted DAP exhibits strong native fluorescence. Dombrowski and Pratt (p. 2270) reported the excitation maximum to be at 345nm and the emission maximum at 408nm. The classical Griess test for nitrite also requires separate diazo and coupling steps utilizing ice baths. Nevertheless, criminalists routinely perform the Modified Griess Test as a single step. Both approaches were explored here.

Methods and Materials

Materials

p-chloroaniline, Aldrich, 98%

ammonium sulfamate, Aldrich, ACS Reagent

2,6-diaminopyridine, Aldrich, 99+%

hydrochloric acid, Fisher, ACS Reagent

sodium acetate, Fisher, ACS Reagent

Firearm Discharge Patterns from:

Winchester .38+P, 125 Grain, JHP; Remington .38+P, 125 Grain, JHP; Federal 9mm, 115 Grain, JHP; CCI 357, 158 Grain, JHP; PMC .38 Special 158 Grain, SWC.

Methods

Preliminary Experiments:

Could the fluorescence of the triazole be detected by the unaided human

eye? This, of course, is a necessary requirement. The Dombrowski - Pratt procedure was conducted in test tubes using several inorganic nitrite concentrations, i.e., 1M, 10^{-1}M, 10^{-3}M, and 10^{-6}M. The filtrate was placed into the wells of a porcelain spot plate and exposed to long wave ultraviolet light (365nm). Both distilled water and HPLC grade water were used as fluorescence blanks. Both sources of water were treated in the same exact fashion as the positive controls.

Was the extraction step essential? Experiments were conducted to answer this question. The triazole is soluble in benzene whereas diaminopyridine and p-chloroaniline are both water soluble. Clearly, an immiscible solvent extraction cannot be carried out on clothing. An experiment was conducted, in test tubes, as well as on clothing, to determine if the extraction portion of the method could be eliminated. The procedure as described by the authors was carried out with the exception of the extraction portion.

Firearm Discharge Patterns On Fabric:

The fundamental procedure, with the exception of the extraction step, was also attempted on fabric bearing firearm discharge residue. Since it was impractical and unfeasible to place fabric in boiling water, the boiling step was replaced by steaming from an iron.

Results and Discussion

In the preliminary test tube experiments, in which the original method

was followed (including the extraction step), blue fluorescence was readily detected in the filtrate at all concentrations, whereas no fluorescence was detected in either blank. In fact, the fluorescence was not visibly less intense in the weakest concentration in comparison to the highest concentration of inorganic nitrite. Thus, this method appears to work quite well on a wide range of concentrations.

A similar experiment, in test tubes, was also conducted, in which the extraction step was omitted. While the positive controls exhibited strong fluorescence, so did the negative control. Although the fluorescence of the negative control was not quite as intense as the positive control, the differences of intensity and color were too small to suggest that this approach would be a viable one for application to discharge patterns on fabric. The coupling agent, 2,6-diaminopyridine, exhibits a strong blue fluorescence, similar to that observed in the positive and negative controls. Clearly, for this method to be of value, the unreacted coupling agent must be eliminated. This does not appear to be possible without a solvent extraction, which would not be feasible in the present context. Diazotized p-chloroaniline and the azo dye do not exhibit fluorescence (Dombrowski & Pratt, p. 2270).

This set of chemical reactions is not of value in this particular context. Additional experimentation to ascertain whether the diazotization and coupling agents could be introduced simultaneously was not explored since reagent fluorescence was considered prohibitive without the extraction portion of the

technique. However, this method may still have value to criminalistics if the examiner wishes to conduct a bulk analysis for nitrite such as described by Petraco (1981) and Steinberg et al. (1984). It would have considerable merit in that particular context because of its sensitivity.

Assessment of Chelate Reaction following Diazocoupling: Direct Application to Target

In 1988, Wang et al. (pp. 212-213) introduced a fluorimetric method for the detection of nitrites in water (non-forensic context). They utilized o-aminophenol for diazotization followed by coupling with resorcinol. The resulting azo dye forms a fluorescent metal chelate with gallium chloride which fluoresces at 584nm when excited at 486nm. Their method consists of the following: 2ml of 6M HCl is added to 25ml of an aqueous solution containing nitrite, followed by 1ml of o-aminophenol solution (1.0×10^{-2}M). The solution is allowed to sit for 15 minutes. Then, 2.5 ml of resorcinol solution is added and its pH adjusted to about 12 with 6M NaOH and permitted to sit for 5 minutes. The solution is then adjusted to pH 2.8 and 1 ml of gallium trichloride is added. A sufficient quantity of 0.1M HCl/Glycine buffer (pH 2.8) is added to bring the solution to volume in a 50ml volumetric flask.

Their research demonstrated that the diazotization reaction took place as efficiently at room temperature as at cold temperatures. This aspect would make it more appealing in a forensic context. Additionally, an important benefit is that no extraction or chromatography is required for separation and detection of nitrites, unlike other chemical reactions studied during the course of the dissertation research. Diazotization was allowed to take place for fifteen minutes before the addition of the coupling reagent because fluorescence was maximized. The optimum pH for coupling was found to be 12 and the

optimum time was 5 minutes. The optimum pH for chelation was determined as 2.8.

The excitation wavelength is easily controlled via the Crimescope CS-16 and the emission monitored with an orange barrier filter or goggles. Thus, experiments were conducted to assess if this reaction could be utilized for the fluorescent detection of nitrites, associated with propellant particles, in firearm discharge patterns.

Methods and Materials

Materials

Gallium (III) Chloride, 99.99+%, Aldrich

2-aminophenol, 99%, Aldrich

resorcinol, ACS, Mallinkrodt

aqueous 0.1N hydrochloric acid/glycine buffer (pH 2.8). 0.1N HCl prepared from Hydrochloric acid Fisher, ACS Reagent. Glycine buffer prepared by adjusting 0.2M aqueous solution of glycine with 0.1N HCl.

sodium bitartrate, tartaric acid (tartrate buffer - pH 2.8). Tartrate buffer prepared by dissolving 1.9 grams of sodium bitartrate and 1.5 grams of tartaric acid in 100ml of distilled water.

1M Hydrochloric acid solution prepared from Fisher, ACS Reagent

sodium nitrite, ACS reagent, stock solution: aqueous (6mg/ml)

Crimescope CS-16 tunable high intensity light source

Experiments were carried out directly on five firearm discharge patterns. These

were: Federal .38+P 125 JHP, Winchester .38+P 158 grain LD SWC, CCI .38 125 grain JHP, PMC 357, and Magtech 9mm 124 FMC.

Method

Preliminary experiments were conducted in beakers with inorganic nitrite over a range of concentrations (0.3mg/ml to 6mg/ml). Experiments were also conducted with both glycine and tartrate buffer at the pH indicated in Wang et al. (1988, pp. 212-213). In the preliminary experiments, the more concentrated versions of NaOH and HCl used in the published protocol were replaced with diluted versions, that is, 1M concentration. It was hoped that an adequate reaction would be obtained with the lower concentrations to minimize damage to the fabric substrates and the more dilute solutions would be safer. As previously mentioned, an elevated temperature is required to make nitrites available to react with the diazotization reagent. Thus, experiments were conducted with heat to see if this would prevent the reaction from proceeding successfully. The experiments involving heat were conducted in the wells of glass spot plates using inorganic nitrite as a positive control. The application of heat from an iron did not appear to reduce the amount of fluorescence. The following protocol was attempted in beakers:

1. One ml of o-aminophenol solution, prepared in 1M HCl, was added to the nitrite control.
2. After five minutes, an equal volume of resorcinol solution was added.
3. The solution was made basic (checked with pH indicator strips) with 1M

sodium hydroxide and allowed to sit for five minutes.

4. The solution was then adjusted to pH 2.8 (checked pH indicator strips) with dilute HCl, and buffer and gallium chloride solution added.

Satisfactory results were obtained during the course of preliminary experiments with inorganic nitrite under a variety of conditions. Moderately strong fluorescence was obtained from the positive control at all concentrations examined. The negative control exhibited a very weak fluorescence under the same exact conditions as the positive control. Adequate fluorescence was obtained with 1M concentrations for both hydrochloric acid and sodium hydroxide.

Each discharge pattern was divided into four quadrants. The results of the direct application of the chelating reaction were compared visually against a Griess transfer, native fluorescence, and solvent treatment followed by fluorescence observation.

Results and Discussion

The above protocol was applied to discharge patterns on fabric substrates. Reagents were sprayed onto the patterns. With all five sources of discharge patterns, the solvent-treated quadrant exhibited at least as intense a fluorescence as the chelate reaction quadrant. Significant background fluorescence was noted in the chelate reaction in contrast to the solvent-treated quadrant which did not exhibit any noticeable background fluorescence. Interestingly, the solvent-treated quadrant had a lower background fluorescence

than the untreated cloth. The pattern in the chelate-treated quadrant was not found to be the equivalent of the patterns from the Griess transfer. The source of this background interference is not obvious. A variety of different fabrics, cotton, polyester/cotton, wool, and rayon, all exhibited significant background fluorescence. Based on these observations it does not appear that this method would be of value in this context.

Assessment of 4-Methyl-7-Aminocoumarin: Direct Application to Target

In 1993, Zhou et al. developed a precolumn derivatization method for the fluorescence determination of nitrites in water using high performance liquid chromatography (HPLC). Coumarin 120® (4-methyl-7-aminocoumarin), in sulfuric acid, reacts with nitrite ions yielding the corresponding 7-diazo compound. The strongly fluorescent 4-methyl-7-hydroxycoumarin is produced following hydrolysis. This compound emits from 340nm to 460nm (emission maxima = 380nm) following excitation at 325nm. According to the authors, the use of HPLC is essential to avoid interference from unreacted coumarin 120® and from 4-methylumbelliferone which is found in the coumarin 120® as an impurity (Zhou et al., 1993, pp. 57-60). The derivatization procedure consisted of the following:

1. Coumarin 120® (50µl) was placed into a 5ml glass-stoppered tube and mixed with 950ul of 0.5M sulfuric acid. 500ul of the nitrite solution was then added and maintained at room temperature for twenty minutes.
2. The stoppered tube was heated for 70 minutes at 100^0C and cooled to room temperature.
3. The fluorescent product was then extracted with ethyl acetate (2 x 2ml) and evaporated to a low volume with a stream of nitrogen.
4. The residue was dissolved in 400ul of ethanol, 20ul of which was injected into the chromatograph.

At the outset, it seemed apparent that success with this method would not be likely based on the presence of the interfering compounds; excess coumarin 120® and trace quantities of 4-methyl-7-hydroxycoumarin. It was anticipated that these compounds would provide significant background fluorescence that could not be removed. However, how this procedure would work on firearm discharge patterns on fabric was unknown.

Method and Materials

Materials

Crimescope CS-16, tunable high intensity light source. U.V. port (280nm to 380nm) in conjunction with 400nm longpass filter (Corion) or yellow barrier goggles.

sulfuric acid, ACS grade, Fisher

Coumarin 120®, Laser Grade, Kodak Products

heating press and steam iron

GSR patterns: Winchester .38+P, 125 grain, JHP; Federal .38+P, 158 grain, Nyclad; Remington .38+P, 125 grain, semi JHP; Federal 357magnum, 110 grain, JHP; PMC 357 magnum, 125 grain, JHP.

sodium nitrite, ACS Reagent, aqueous stock solution (6mg/ml)

Method

The derivatization procedure was applied to GSR patterns on five different patterns as indicated above, with the exception of the extraction step (an extraction step was not performed). The heating step used for the original

method was replaced with two different approaches. One involved heating the clothing in a heating press, and the other involved steaming the surface with a steam iron. One quadrant from each pattern was treated as indicated. Another quadrant was treated similarly, but with solvent only (no coumarin). A Griess transfer was conducted on a third quadrant. The fourth quadrant was left unprocessed. All four quadrants were compared after processing was completed.

Result and Discussion

As predicted, this method produced significant background fluorescence in all quadrants and patterns it was applied to. Particles were easier to visualize in the the quadrant treated only with solvent and in the untreated quadrant. It does not appear that this method would be of value in the present context.

Assessment of Hydrochloric Acid - Low Temperature Experiments: Direct Application to Target

This series of experiments was initially designed to cause the fine lead deposit from close range discharges (within twelve inches) to fluoresce. Additionally, it was hoped that the lead comprising the bullet wipe could also be induced to fluoresce. Preliminary experiments indicated that there was potential for success with the fine lead deposit and bullet wipe. Quite unexpectedly, partially burned propellant particles were also found to produce significant fluorescence. These emissions may be due, in part, to the presence of metal chloride complexes on the surface of the particles or to an increase in native fluorescence from organic compounds present in the particle matrix. The increase in native fluorescence may be attributed to increased quantum efficiency at liquid nitrogen temperatures. According to Jones and Nesbitt (1975, p. 233), Hogness and Johnson (1954, pp. 382-383, 409) showed that trivalent Sb ions complex with chloride ions in concentrated HCl:

$$Sb^{3+} + 4Cl^- \rightarrow SbCl_4^-$$

and

$$Sb^{3+} + 6Cl^- \rightarrow SbCl_6^{3-}$$

Likewise, lead ions, in concentrated HCl, form chloride complexes:

$$Pb^{2+} + 4Cl^- \rightarrow PbCl_4^{2-}$$

It is these chloride complexes that are responsible for the photoluminescence.

Fluorescence characteristics of various inorganic complexes, including the above, using hydrochloric acid at liquid nitrogen temperature, were reported by Kirkbright et al (1969). They reported that of the fifty-five ions they studied only the following fluoresced when treated with 6M hydrochloric acid and cooled to minus 196°C: Sb(III), Sb(V), Bi(III), Ce(III), Cu(I), Pb(II), Te(IV), Tl(I), Sn(IV), and U(VI). A year earlier, White & Wessler (1968, 120R), in a review paper of fluorimetric analysis, discussed observations of the fluorescence of chloride complexes of lead and antimony reported previously by Boszhevol'nov et al. (1964,1965) in HCl solution at -70° C. In 1970, White and Argauer, in a text on fluorescence analysis (p. 8) reiterated these details. Nesbitt and Jones' work (1974, p.6/60-6/71; 1975, 1977, 1978), for the bulk determination of primer-associated elements on the hands of the shooter, utilized these simple chemical reactions for a photoluminescence (spectrofluorimetric) method for the determination of lead and antimony utilizing 7M HCl in a glass state (at liquid nitrogen temperatures). They also discussed a single experiment with a bullet hole in fabric using the same acidic and temperature conditions. In this bulk analysis experiment, Nesbitt and Jones removed a section of the cloth containing the suspected GSR, soaked it in 7M HCl, and apparently conducted spectrofluorimetry to detect and measure the level of antimony and lead present. Based on this preliminary experimentation, they suggested that this approach might be feasible for the determination of the firing distance and the identification of bullet holes (1975, pg. 240, 241). It is not clear why this

chemical method was not utilized directly on clothing for inducing the GSR pattern to photoluminesce in situ. Perhaps the concentration of the HCl thought to be necessary (22%) was considered prohibitive, with respect to possible deleterious effects on other trace evidence and the substrate itself. Additionally, they may have believed that a non-spectrophotometric method (no photomultiplier for signal amplification) lacked sufficient sensitivity. For whatever reason, no literature was found regarding the development of patterns in situ on clothing with this (or any other) reagent, at any concentration, with the exception of the rhodizonate test for light-colored clothing.

At liquid nitrogen temperatures, phosphorescence might also be observed. Phosphorescence could be an ideal way of examining a variety of materials in a criminalistics context, including gunshot residue, since background fluorescence might be more readily avoided. No discussion of phosphorescence observations was found, regarding GSR, in the forensic science literature. Both fluorescence and phosphorescence experiments were conducted to determine their utility in this context.

Method and Materials

Materials:

Reagents

Hydrochloric Acid - various dilutions were made daily from concentrated HCl (ACS grade).

liquid nitrogen

Metals

lead metal was obtained from a variety of commercially available bullet heads.

antimony powder, Fisher certified grade

Equipment

Light Sources:

Spex short wave ultraviolet lamp

Spectroline short and long wavelength ultraviolet lamp (254nm/365nm)

Spex Crimescope CS-16 tunable light source - utilized for visible light for this series of experiments

Filters: Kodak 2A, barrier filter to prevent ultraviolet radiation from reaching film, Tiffen #21 orange longpass filter, variety of Corion bandpass filters; temperature correction filter (#80B) for taking color photographs with copy stand bulbs.

Film: Kodak Ektapress (color) 35mm, ASA 400; Kodak Ektachrome 35mm ASA 64

Insulated tray for target and liquid nitrogen

Cameras:

Nikon FM2, 35mm, normal and macro lens

Digital Thermocouple Thermometer - Cole Parmer Co., with fast response probe

Ammunition - see attached tables

Method:

The fundamental method used here involved hydrochloric acid being

sprayed on the target area surrounding the bullet hole (approximately a six inch radius). The treated material was given one to two minutes to react, gently dried with a heat gun, and then cooled with liquid nitrogen.

The following concentrations of hydrochloric acid were compared for their ability to cause photoluminescence with GSR: 7M, 6M, 5M, 4M, 3M, 2M, 1M, 0.1M, and 0.01M.

Shortwave ultraviolet, longwave ultraviolet, and visible light were evaluated under several different conditions to determine which provided the optimum excitation wavelength for partially burned particles and for the metals (lead and antimony) associated with primer and bullet residue. The use of other different excitation wavelengths was studied to determine if chemical selectivity, for different GSR species, could be obtained. For example, the fluorescence from lead at close range firing distances might interfere with fluorescence observations for partially burned particles. Experiments were conducted to determine if the fluorescence of lead could be observed at one wavelength, and then eliminated by switching to another wavelength at which the particles emit strongly. A number of experiments were conducted in which no change was made except for excitation wavelength. These wavelengths were: 254nm, 365nm, and 400 to 490nm.

It has been reported in the literature that chloride complexes of lead and antimony, in HCl solution, fluoresce at -70 degrees. This is, of course, a considerably warmer temperature than that of liquid nitrogen, but the higher

temperature experiments were conducted in a fluorimetric context with the luxury of a photomultiplier tube. Jones and Nesbitt conducted their spectrofluorimetric experiments with liquid nitrogen (-196^{0}C) using 7M HCl since this concentration of the acid was found to form a clear glass. Under those conditions, the lead complex possessed an emission maximum at 390nm, while the antimony complex had an emission maximum at 620nm. These wavelengths correspond to violet for lead, and a pink/orange for the antimony. Observed colors may vary somewhat due to shifts in wavelength arising from differences in concentration of hydrochloric acid, although Kirkbright et al. detected no shift for either lead or antimony over the range 6-10M (p. 70, 1969). The present experiments were carried out to determine if either lead or antimony from a firearm discharge (as gunshot residue or bullet wipe) could be visually detected, and what the optimum temperatures might be for monitoring such emissions. These experiments were conducted by using the basic method with temperature measurements using the thermocouple at different temperatures ranging from -192°C to -50°C.

The relatively dark portion of untreated gunshot residue is ordinarily visible on white or very light fabrics. Some particles are readily visible on very dark substrates; but many particles and fine residue are not. Often gunshot residue is extremely difficult to detect or examine effectively on grey substrates. Grey colored substrates were used for several different firearm discharges. A number of sources of gunshot residue were also examined with a variety of

differently colored fabrics and weaves.

Results and Discussion

It was found that satisfactory results can be obtained with any of the concentrations tested ranging from 8M to 0.1M hydrochloric acid. Preliminary experiments with 0.01M demonstrated that excessively lengthy shutter speeds were required to obtain adequate exposures with antimony metal. This concentration was omitted from additional experimentation. Satisfactory observations and photographic exposures may be obtained with dilute hydrochloric acid (1M). Bullet wipe, the fine lead cloud deposit, and partially burned propellant particles can be visualized with this concentration of reagent. Low acid concentration is less destructive to fabric and is relatively safe to work with.

Only the 1M HCl solution was utilized for the variable temperature experiments. While these observations were similar to those found previously during the native fluorescence experiments for partially burned particles, the effect of temperature for the detection of lead was striking. It was found that the fine lead deposit and bullet wipe cannot be detected at temperatures much warmer than approximately -83°C. In fact, at -75°C, no fluorescence associated with lead was observed. However, strong fluorescence was seen at temperatures ranging from -190°C to -118°C (Figure 62). Bullet wipe, the fine lead cloud, and partially burned particles are all visible simultaneously at the

low temperatures after treatment with 1M HCl solution.

Results from seven discharge patterns (an eighth of each pattern) examined with the 1M HCl method were compared to corresponding areas examined by the conventional Griess transfer method. The substrate was a dark grey cotton/polyester blend. The sources of these patterns were: (a) CCI .38+P 125 grain, JHP; (b) CCI 357 Magnum 158 Grain JHP; (c) Federal .38 Spl. NYCLAD 158 grain RN; (d) PMC .38 158 grain, SWC; (e) Remington .38 Spl. 158 grain, LRN; (f) Remington 357 Magnum 158 grain SJHP; and (g) Magtech .38 158 grain LRN. The results obtained with the MGT were all inferior to the results obtained with the HCl method, relative to particle detection, with either short or long wavelength ultraviolet excitation.

For observations of short wavelength ultraviolet fluorescence the Spectroline lamp was found to be more effective than the Spex unit. The primary reason for its superiority was its size. Since it is a longer unit, it is able to deliver uniform illumination to a much larger portion of the target than the Spex unit. This is very important for the examination of gunshot residue because uniform illumination is required for the excitation, examination, and photography of relatively large patterns distributed over a wide area on fabric substrates. Additionally, another distinct advantage of the Spectroline lamp is that it is dual wavelength, i.e., both short and long wavelength ultraviolet light is available. Observations at each wavelength, in succession, can be readily achieved by merely pressing a switch which activates a change in lamps. Thus,

errors introduced by replacing a lamp with another of a different configuration are avoided. Accordingly, the Spectroline unit was used for the bulk of these experiments. However, an advantage of the Spex unit during these experiments is that it could be brought closer to the target surface than the Spectroline unit, since the latter lamp cannot fit into the tray needed to contain the liquid nitrogen. The increased exposure of the target to the lamp, due to the lamp being closer, significantly helps with phosphorescence.

Generally, native fluorescence from shortwave ultraviolet excitation provides only minimal fluorescence of partially burned particles. However, particles treated with 1M HCl and cooled to liquid nitrogen temperatures, exhibit noteworthy fluorescence (Figures 63 & 64). This fluorescence is probably due to a number of factors. A large number of these particles probably fluoresce because of the presence of the metals lead and antimony on their surface. This is indicated by the color of the particles after treatment with dilute HCl which is in some cases blue violet and light pink/orange for others. The orange or pink fluorescence appears quite similar to that of known antimony (Figure 65). Additionally, it appears different than that obtained with native fluorescence. The blue violet color agrees closely with that due to known lead fluorescence. At close range, the fluorescence caused by excitation with shortwave ultraviolet light, is significantly obscured by the lead cloud deposit fluorescence (Figure 66). Some of the increase in fluorescence is also probably due to the surface of the particle being cleared by the HCl and

allowing native fluorescence to occur more easily. Emissions from a single particle, in some instances, may result from a combination of native fluorescence from organic compounds enhanced significantly by the lower temperatures and from the fluorescence of the metal chlorides, coating the particles, after treatment with hydrochloric acid. In general, many more particles are visible when exposed to long wavelength ultraviolet light (365nm) in comparison to short wavelength U.V. light (Figures 67 & 68). Unfortunately, many textile fibers also fluoresce quite strongly when excited at 365nm.

The propellant particles fluoresced strongly after the patterns were treated with 1M HCl, liquid nitrogen, and exposed to 365nm light. The intensity of this emission is not due to metal chloride complexes since shorter wavelengths (254nm) are required for their fluorescence, and since these are the same colors obtained natively with long wavelength ultra-violet light. Generally, the particles were found to fluoresce much more weakly when exposed to 254nm (Table 17). The reverse is true for both lead cloud deposits and bullet wipe. Since long wavelength ultraviolet or visible radiation will not cause the metal chloride complexes to fluoresce, particle fluorescence originating from the organic constituents can be observed at the relatively long wavelengths, and then the fluorescence originating from metals residing on the propellant particles, metals comprising the fine cloud deposit, as well as that of bullet wipe, can all be observed at 254nm. Thus, the fluorescence of the lead and/or antimony deposit can be observed at one wavelength, and then

eliminated by switching to another wavelength at which the particles emit strongly. With this arrangement, the strong fluorescence of the fine cloud deposit does not interfere with the observation of fluorescence of the particles at all (Figure 66).

Phosphorescence may also be observed providing the discharge patterns are kept very cold. The lead deposits, associated with the cloud and bullet wipe, will only phosphoresce extremely weakly following exposure to 254nm radiation, as expected. However, propellant particles will exhibit significant phosphorescence when excited at 365nm (see Figure 69). The phosphorescence of the propellant particles is relatively short lived, that is, less than 5-10 seconds. However, it is intense enough and of sufficient duration to permit adequate photography. Not every ammunition source, with respect to the propellant particles, exhibited the same degree of phosphorescence intensity or lifetime. Particle phosphorescence is a potentially excellent approach to visualization since the background seems less likely to produce interference as found in this series of experiments. Phosphorescence observations could be improved significantly with a gated imaging technique for photography. Because the metastable excited state is relatively long-lived, the gated imaging and signal integration on film can be done manually. It was found that the optimum excitation wavelength for the observation of phosphorescence of particles is 365nm (Table 18).

The excess hydrochloric acid can be removed by heating with a hair

dryer after the examination is complete (Bartsch et al., p.1051, 1996). This was done in most of the experiments conducted here. This step reduced frost buildup and prevented the deterioration of the fabric from the continuous exposure to acid.

The treatment of the particles with hydrochloric acid, even as dilute as the 1M concentration, prevents the direct subsequent application of the Modified Griess Test as it would be normally employed. Hydrochloric acid, as has been previously pointed out, has been utilized like acetic acid to produce nitrous acid from nitrite. Even at cold temperatures, a significant amount of nitrite will be converted to nitrous acid and lost in the form of a gas. Additionally, the solvent will effectively wash lead residues from the surface of a number of particles. Likewise, it is quite likely that liquid nitrogen mechanically removes surface materials of interest. In many instances, it may not be necessary to conduct a Griess examination since the patterns generated with the proposed method are superior. Instead, the molecular confirmation of a number of particles, by either GC-MS or FTIR microscopy, using a statistical approach for selecting the particles to be tested at random, is a more attractive method. If the examiner prefers the traditional method, this can be accomplished, as demonstrated in the next chapter, even after the dilute HCl method has been used, if an additional chemical treatment is administered.

The dilute hydrochloric acid method described here can be used for the detection of: (a) bullet wipe (Figures 70 & 71); (b) dynamic marks left by

projectiles tangentially on clothing; (c) ricochet marks on materials found at crime scenes or brought into the laboratory, and so forth. While inconvenient in a crime scene context, it certainly is not out of the question for the utilization of this method when dealing with vehicle examinations. It would not be so difficult for many forensic scientists to bring a dewar flask with them to a garage where a car was being kept. Many forensic laboratories have attached garage facilities. The spraying of the interior of vehicles with 1M HCl should not present any serious difficulties provided minor precautions are taken; any remaining unreacted HCl can be removed by evaporation with a hair dryer.

Lead chloride, once formed, is stable on fabric for an indefinite period of time. Figure 72 illustrates the fluorescence of the same pattern photographed after eight months without any additional application of hydrochloric acid. The pattern exhibits strong fluorescence, without any signs of degradation after the passage of eight months. No deterioration of the substrate was detected after the passage of eight months.

The direct visualization methods discussed here appear to be superior to currently used transfer techniques. For example, the criminalist does not have to worry abut interference from dyes migrating to the transfer medium and obscuring the resulting pattern as can be encountered during the Bashinski transfer for the rhodizonate test (Figure 73). In the case depicted in Figure 73, an excessive amount of dye was extracted by the 15% acetic acid onto the filter paper being used for the transfer. The strong violet color of the dye greatly

interfered with the gunshot residue pattern. Conversely, the direct method explored here provided an excellent representation of the lead pattern. No significant diffusion of the fine lead deposit occurs following application of the dilute hydrochloric acid directly onto any substrate. However, significant diffusion does occur during the performance of the rhodizonate test (Figure 74). This appears to be a function of the substrate as well as the enhanced solubility of lead acetate relative to lead chloride. The use of this direct method should be considered within the context of an integrated sequential approach. This concept is discussed in more detail in Chapter Eleven.

Figure 62. Influence of Temperature on Pb Fluorescence Post 1M HCl (254nm excitation/ orange barrier filter) Winchester .38+P 158gr. SWC, Muzzle Distance = 10cm (4")

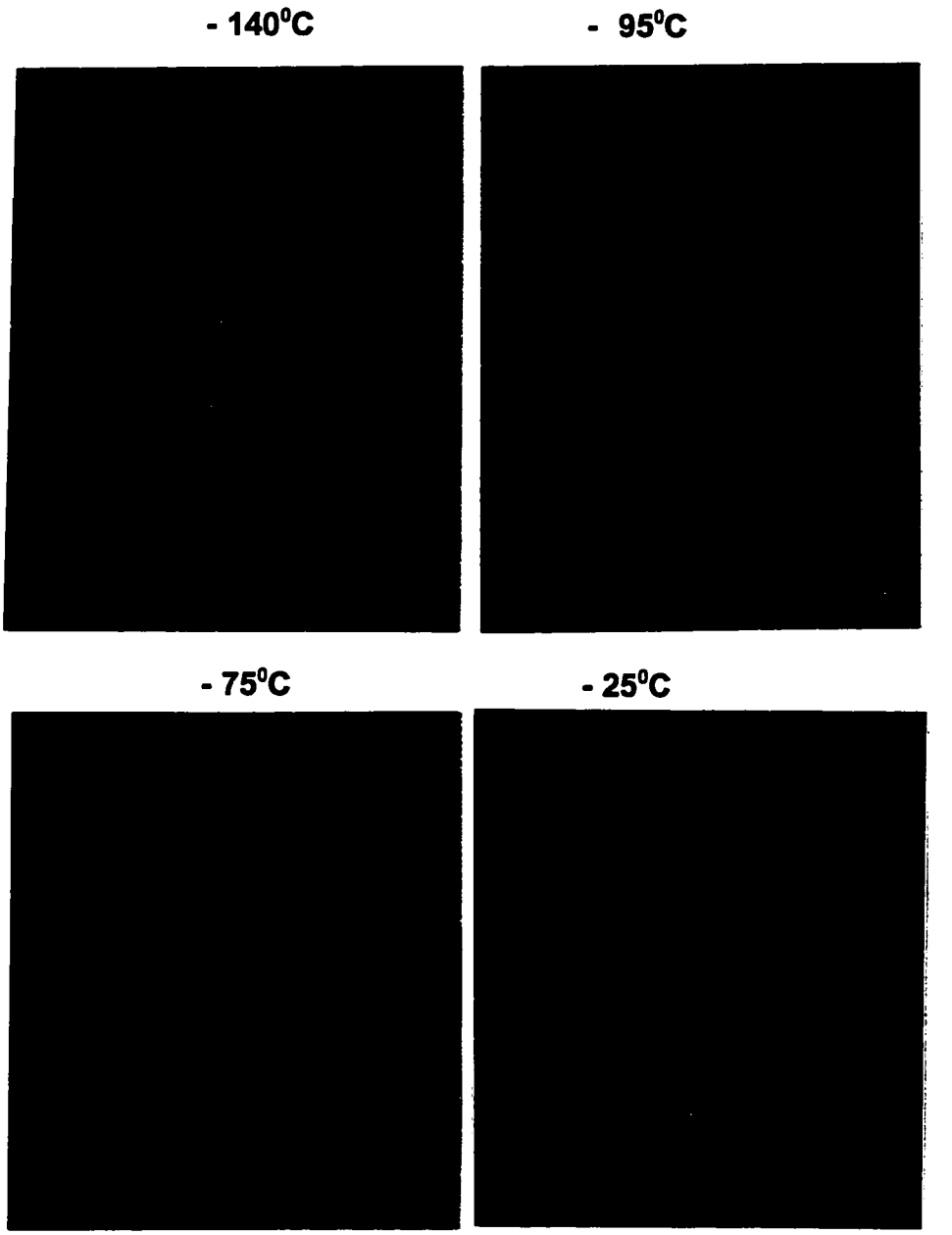

Figure 63. Strobe Photograph of Discharge Pattern on Grey, Cotton/Polyester Blend Prior to Chemical Treatment (see Figure 64) CCI .38+P, 158 Grain, TMJ. Muzzle Distance = 15cm (6 inches).

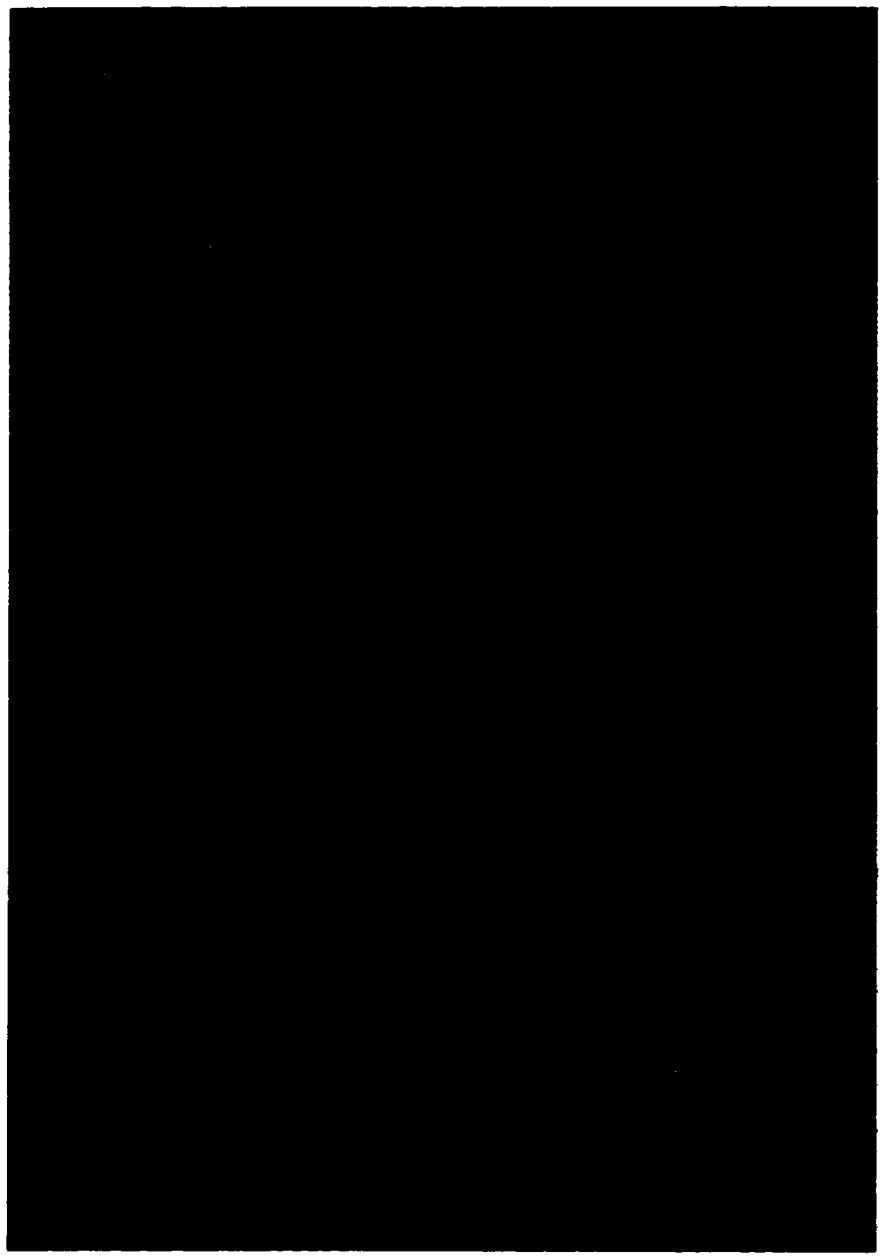

Figure 64. Comparison of Pre & Post HCl Treatment to the Same Discharge Pattern as in Figure 63. Liquid Nitrogen, 254nm excitation. Upper Photo: pre-HCl; Lower Photo: post-HCl.

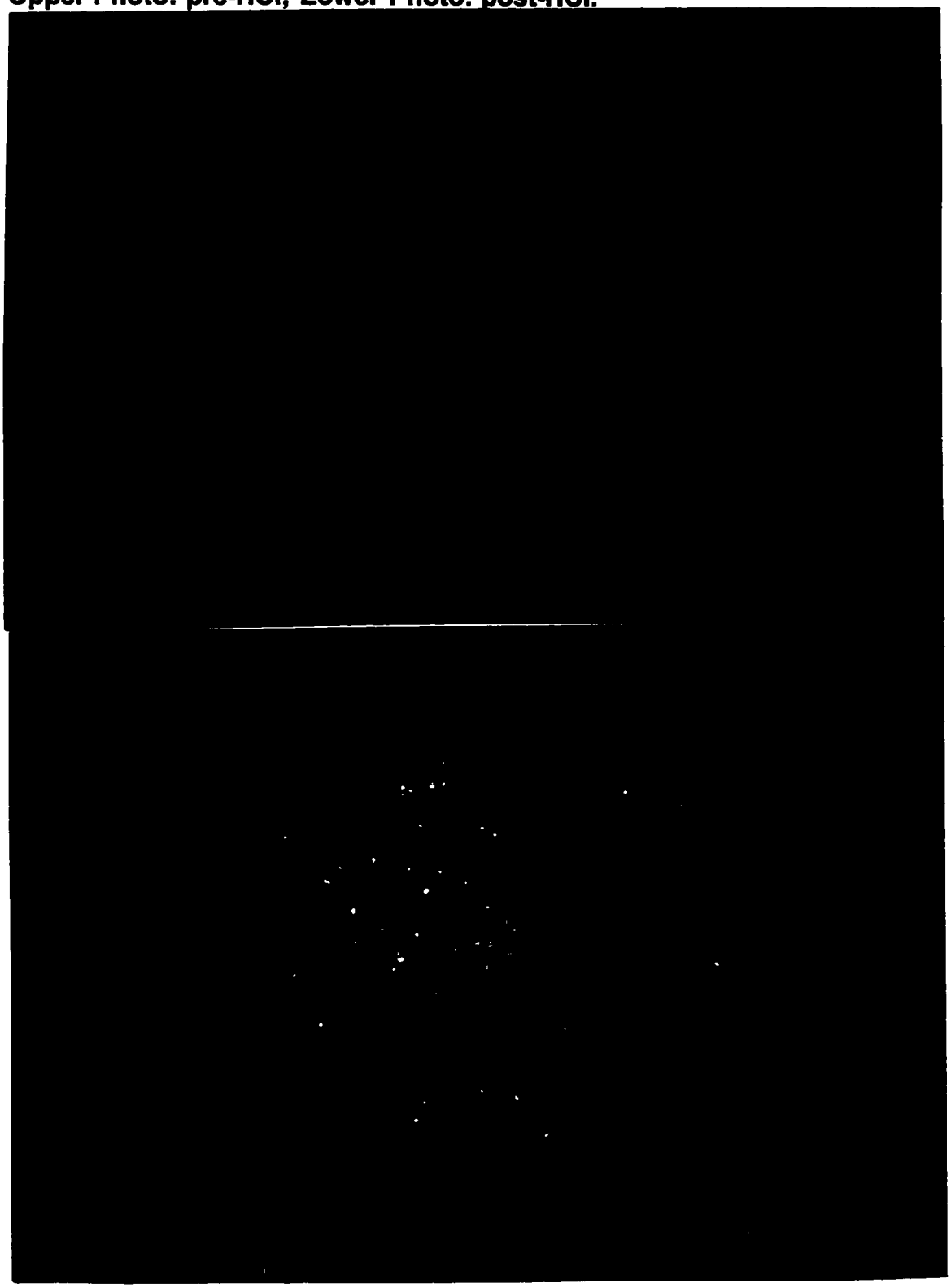

Figure 65. Lead and Antimony Fluorescence Post 1M HCl Treatment. 254nm excitation, liquid nitrogen. Sb metal control in upper left corner of photograph. Federal .38 special, LRN, 158 grain, SWC, on red Cotton fabric. Muzzle distance: within twelve inches.

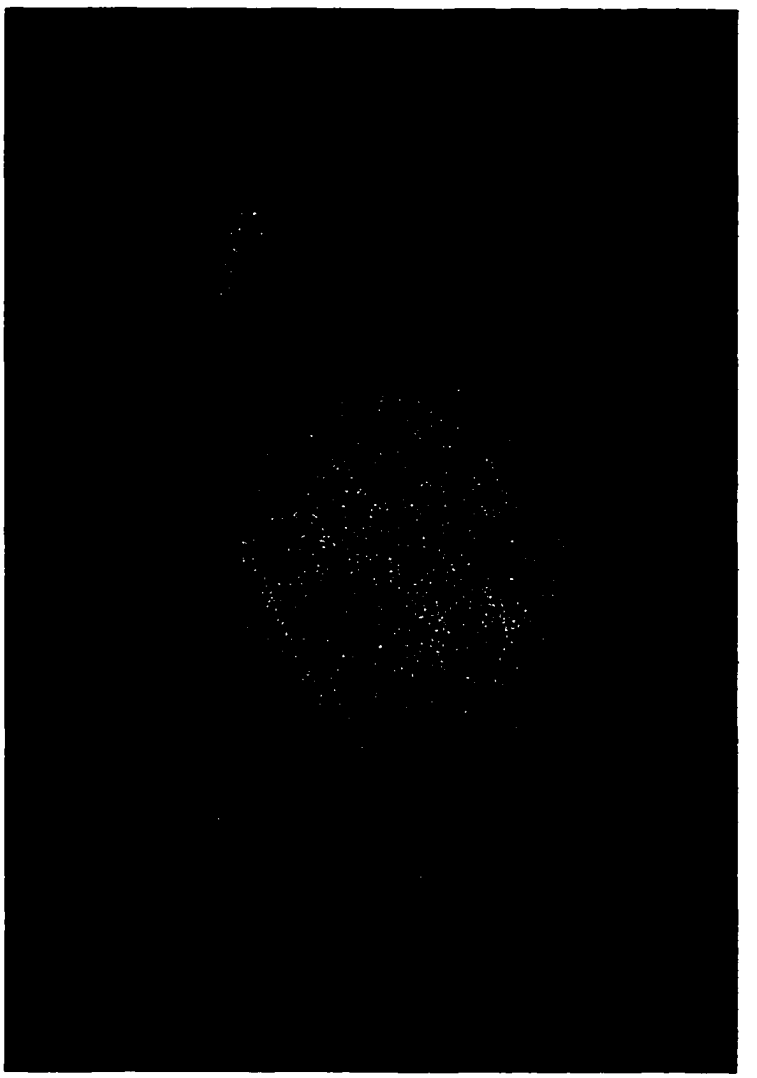

Figure 66. Short v. Long Wavelength U.V. Excitation Post 1M HCl. Liquid Nitrogen. Upper Photo: 254nm excitation; lead fluorescence obscures particle fluorescence. Lower Photo: 365nm excitation of same pattern as above; particle fluorescence - no interference from lead.

Figure 67. Particle Fluorescence. Post HCl, liquid nitrogen, 254nm excitation. Brown cotton/polyester fabric. PMC 357 Magnum, 125 Grain, JHP. Muzzle Distance = 8cm (3 inches). Compare to Figure 68.

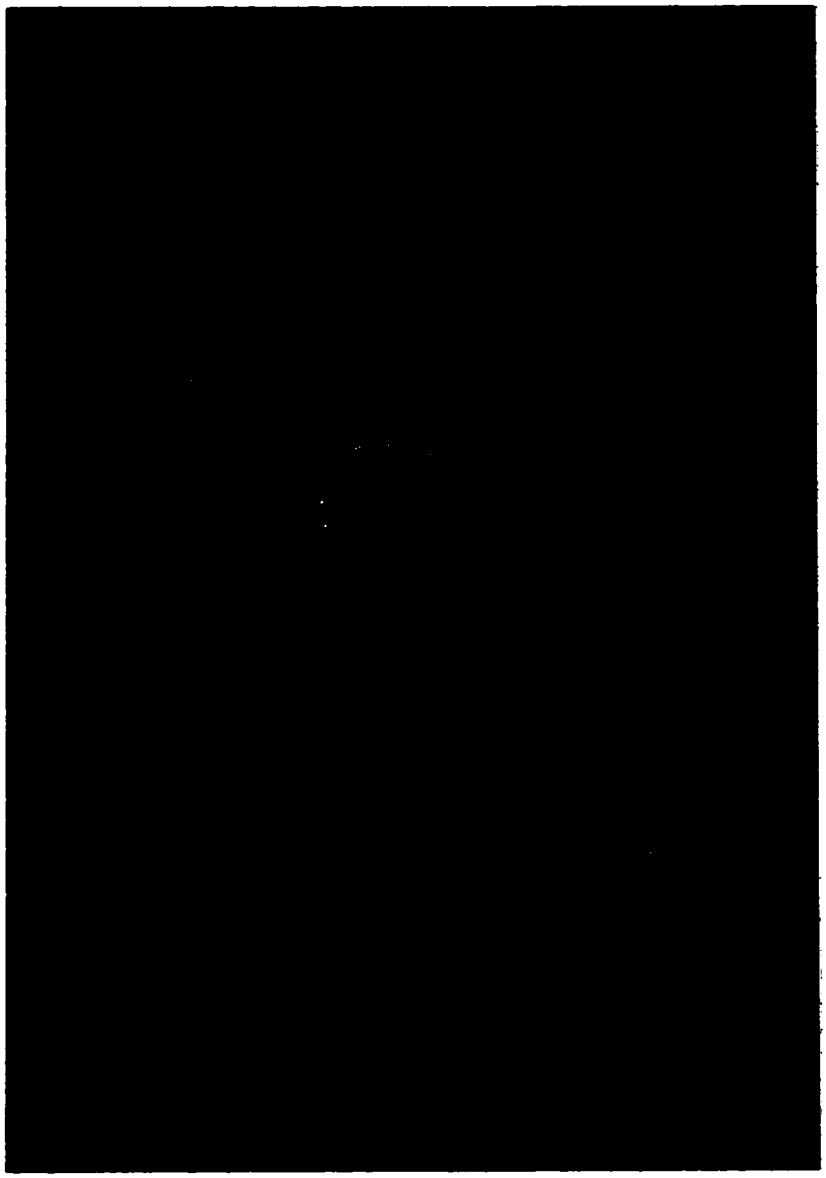

Figure 68. Particle Fluorescence. Post HCl, liquid nitrogen. Same Discharge as Figure 67. Upper Photo: 365nm excitation. Lower Photo: 455nm excitation.

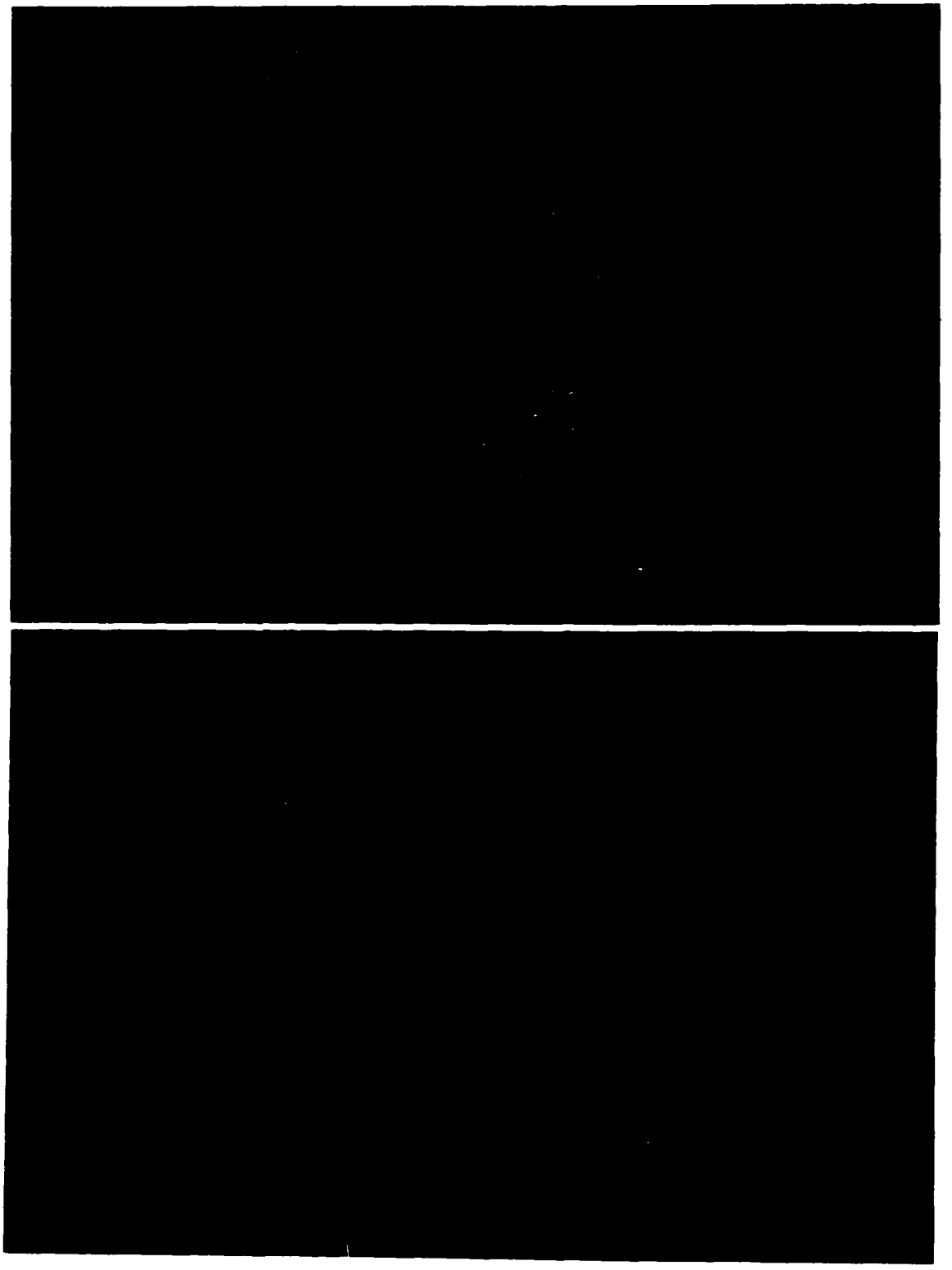

Table 16. Fluorescence of Discharged Propellant Particles Post HCl

			Room T. Short UV	Room T. Long UV	Low T. Short UV	Low T. Long UV
Winchester	.38spl.	158, LD SWC	- - -	- -	-	-
Winchester	.38+P	158, LD SWC	- - -	+	+ +	+ + +
Winchester	9mm+P	130, FMJ	- -	+ +	+	+ +
Federal	357Mag.	110, JHP	- - -	- -	- -	+ + +
Federal	.38spl.	158, LD RN	- - -	- -	-	+ + +
Federal	.38spl.	158, NYC RN	- - -	- -	+ +	+ + +
Magtech	.38spl.	158, LRN	- - -	- -	-	+ + +
Magtech	357Mag.	158, SJSP	- - -	-	-	+ + +
Remington	.38spl.	158, LRN	- - -	- -	+ +	+ + +
Remington	.38+P	158, LD SWC	- - -	- -	+ +	+ + +
Remington	357Mag.	158, SJHP	- - -	- -	+ +	+ + +
CCI	.38+P	158, TMJ	- - -	- -	+ +	+ + +
CCI	357Mag.	158, JHP	- - -	- -	+ +	+ + +
PMC	.38spl.	158, SWC	- - -	- -	- -	+ +
PMC	357Mag.	125, JHP	- - -	- -	- -	+ +

+ + + very strong
+ + strong
+ moderate
- weak
- - very weak
- - - none

Figure 69. Upper Photo: Native Fluorescence. Excited at 455nm; orange barrier filter. Liquid Nitrogen. Lower Photo: Phosphorescence Post HCl, Liquid Nitrogen, Long Wavelength Ultraviolet Excitation.

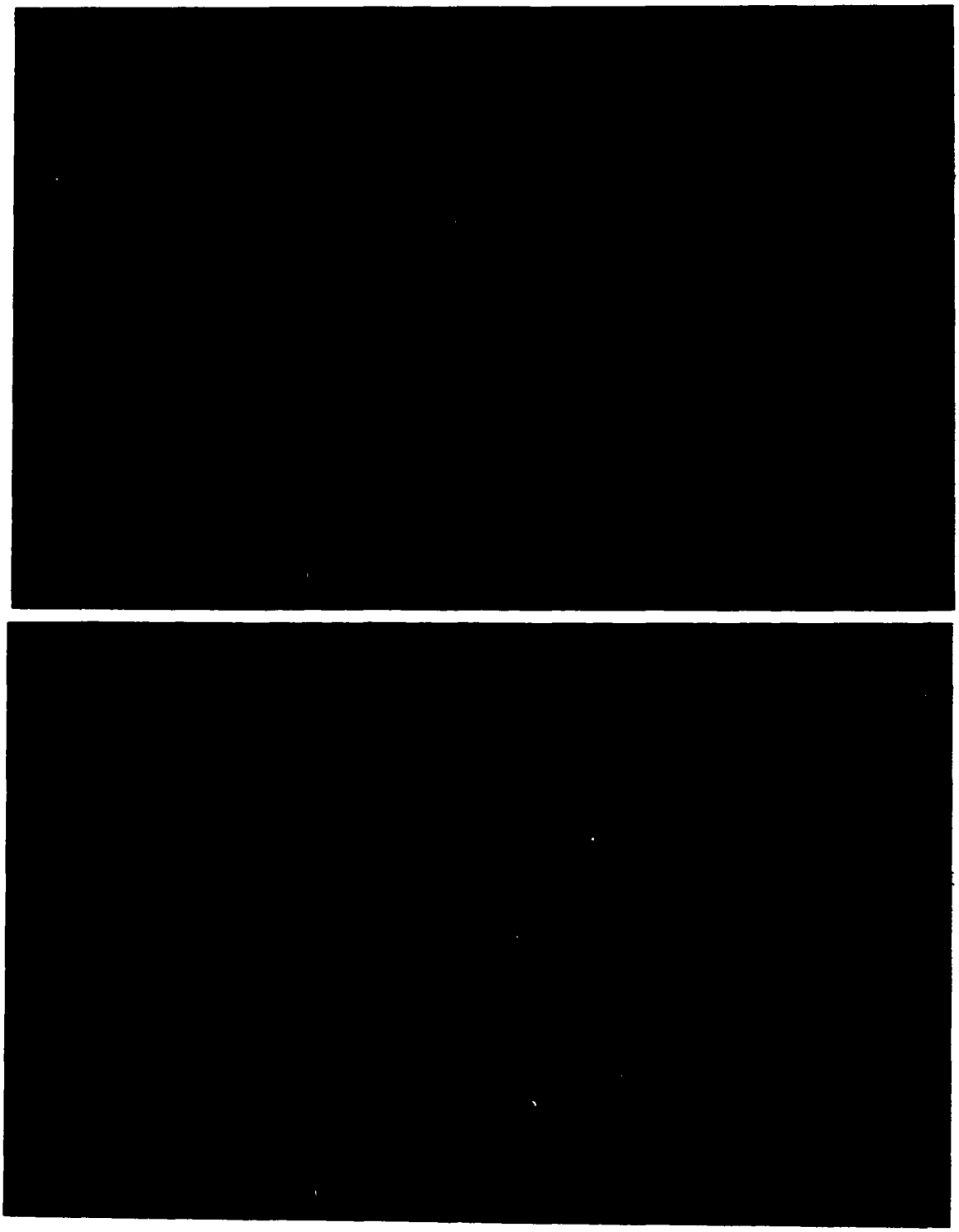

Table 17. Phosphorescence of Discharged Propellant Particles Low Temperature - UV Excitation

Brand	Caliber	Grain/Bullet	365nm ex.	254nm ex.
Winchester	.38spl.	158, LD SWC	weak	none
Winchester	.38+P	158, LD SWC	very strong	moderate
Winchester	9mm+P	130, FMJ	very strong	moderate
Federal	357Mag.	110, JHP	strong	moderate
Federal	.38spl.	158, LD RN	moderate	none
Federal	.38spl.	158, NYC RN	weak	none
Magtech	357Mag.	158, SJSP	none	none
Remington	.38+P	158, LD SWC	strong	none
CCI	.38+P	158, TMJ	strong	none
PMC	357Mag.	125, JHP	strong	none

Figure 70. Upper Photo: Ordinary Flash Photograph of Federal NYCLAD .38+P after several test firings with lead ammunition. Muzzle D. = 30". Lower Photo: Fluorescence of Bullet Wipe & Particles. Short UV Excitation, Post 1M HCl, Liquid Nitrogen.

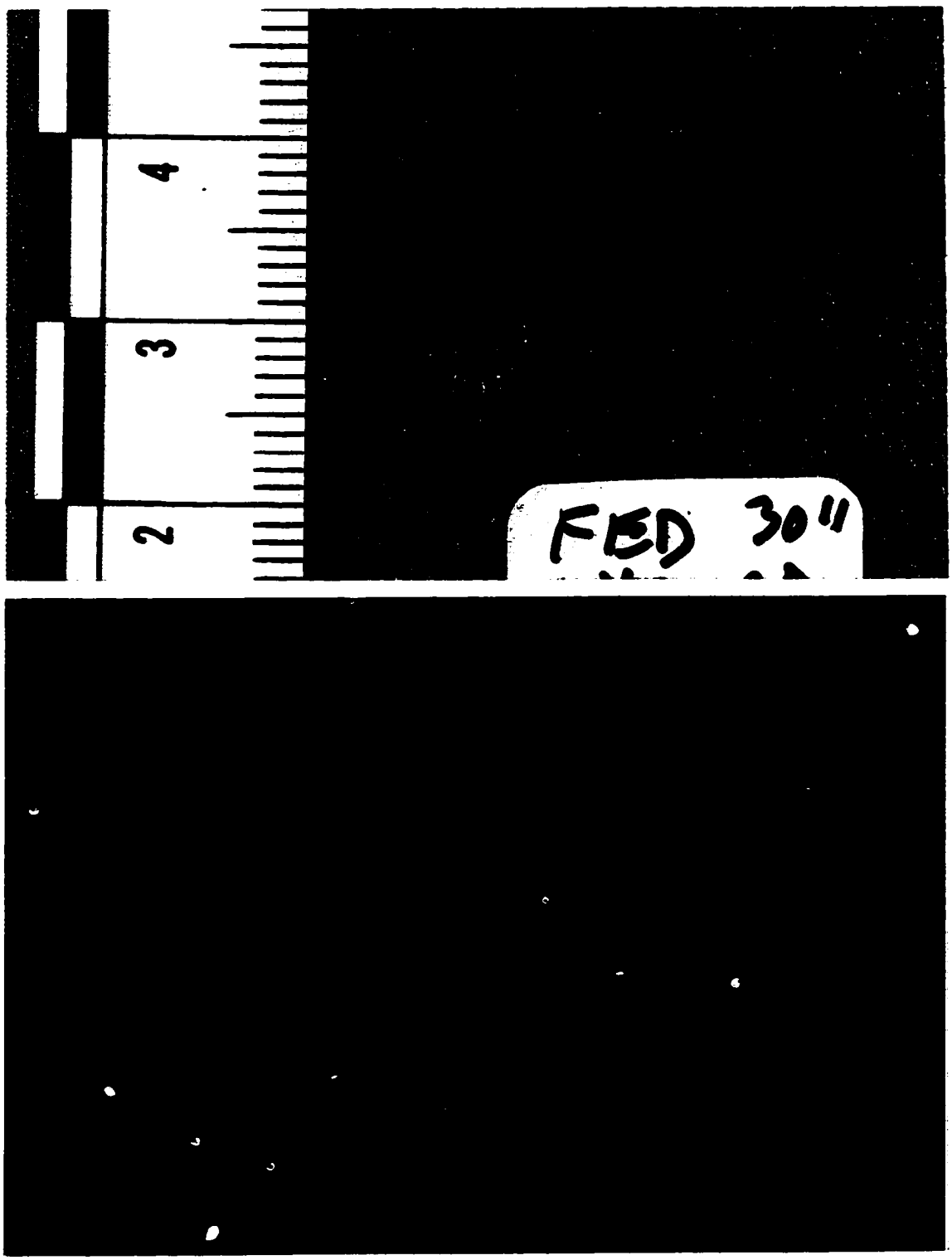

Figure 71. Bullet Wipe Fluorescence. Remington 357 Magnum, 158 Grain, SJHP. Grey cotton/polyester blend. Muzzle Distance = 142cm (56 inches). Upper Photo: Pre HCl, Flash Illumination. Lower Photo: Post HCl, liquid nitrogen, 254nm excitation.

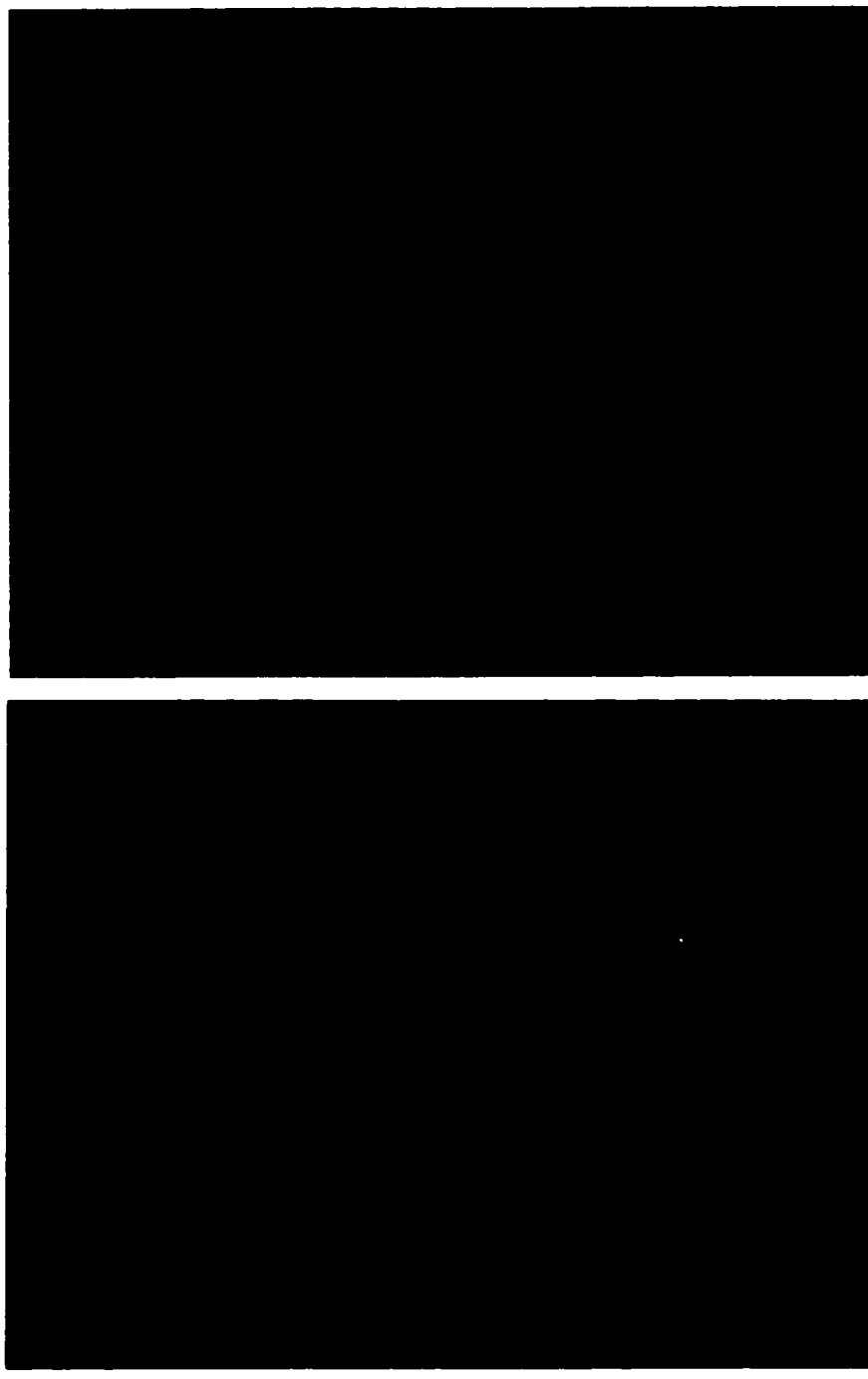

Figure 72. Stability of Lead Chloride Fluorescence. 254nm excitation, in liquid nitrogen. Upper photograph taken eight months prior to lower photograph. No HCl applied to pattern after first application. Winchester .38+P, 158 Grain, SWC. Muzzle Distance = 10cm (four inches).

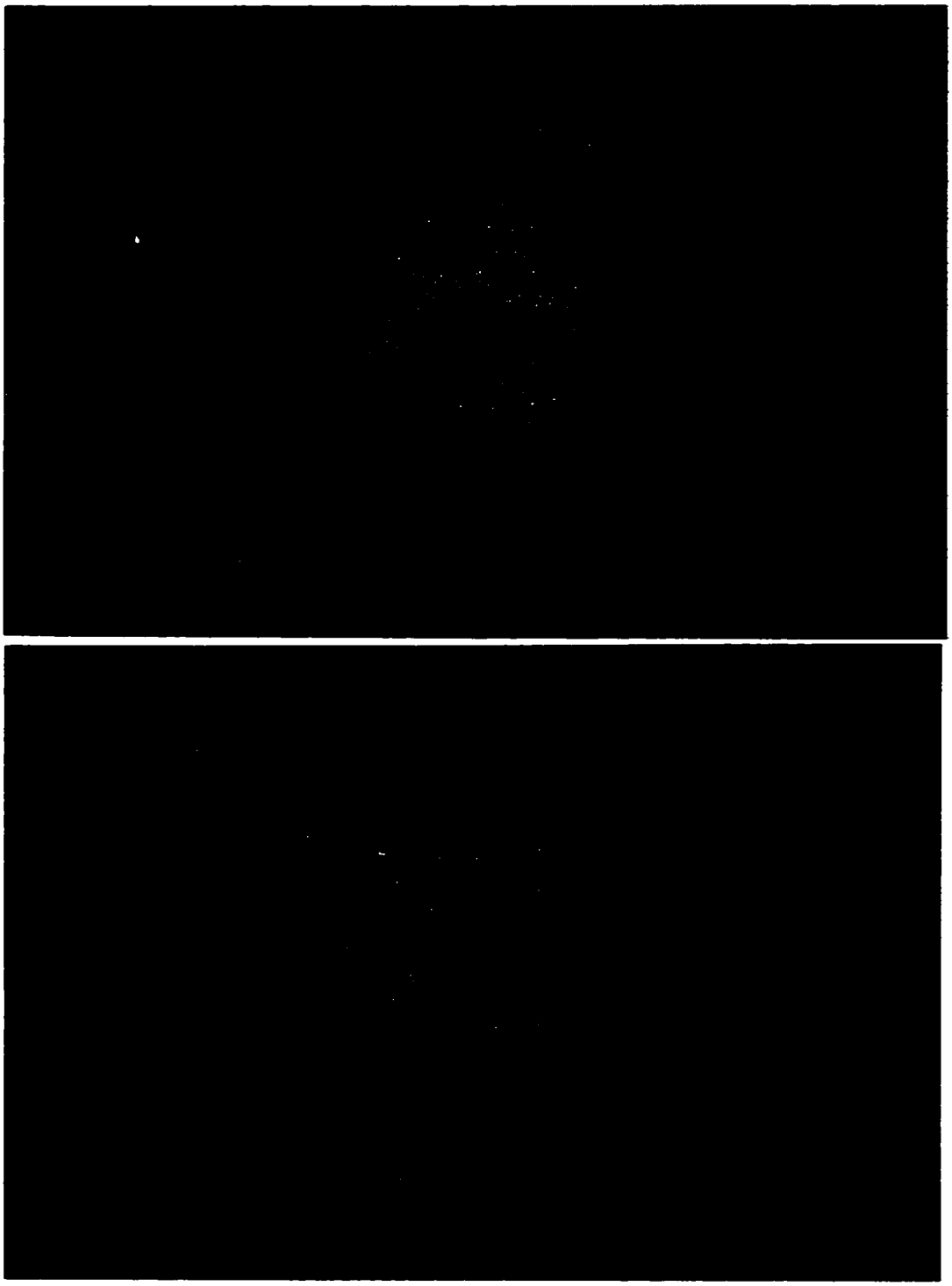

Figure 73. Extraction of Dye from Nylon Substrate to Bashinski Transfer Paper by Acetic Acid Application. All Colors on Transfer is from Dye. Strobe Photograph Taken Prior to Application of Rhodizonate Reagent.

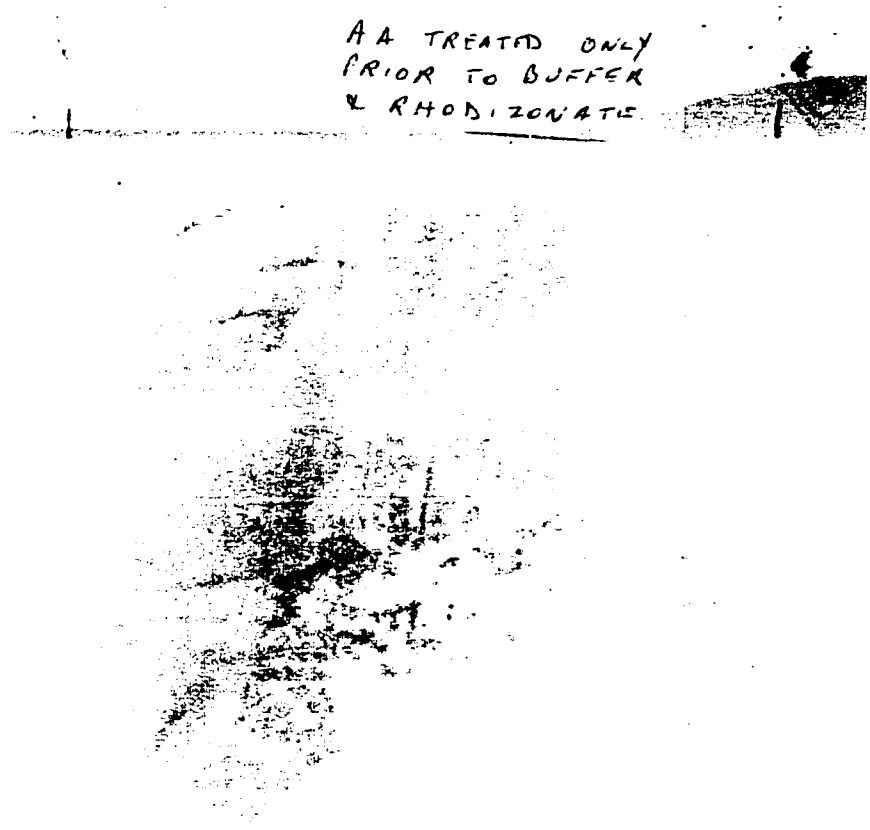

Figure 74. Rhodizonate Transfer v. Muzzle Cloud and Particle Fluorescence. Winchester .38+P, 158 Grain, SWC LD. Black Nylon. Muzzle Distance = 15cm (6 inches). Upper Photo: Post HCl, Liquid Nitrogen, 254nm excitation. Lower Photo: Rhodizonate Transfer from another discharge.

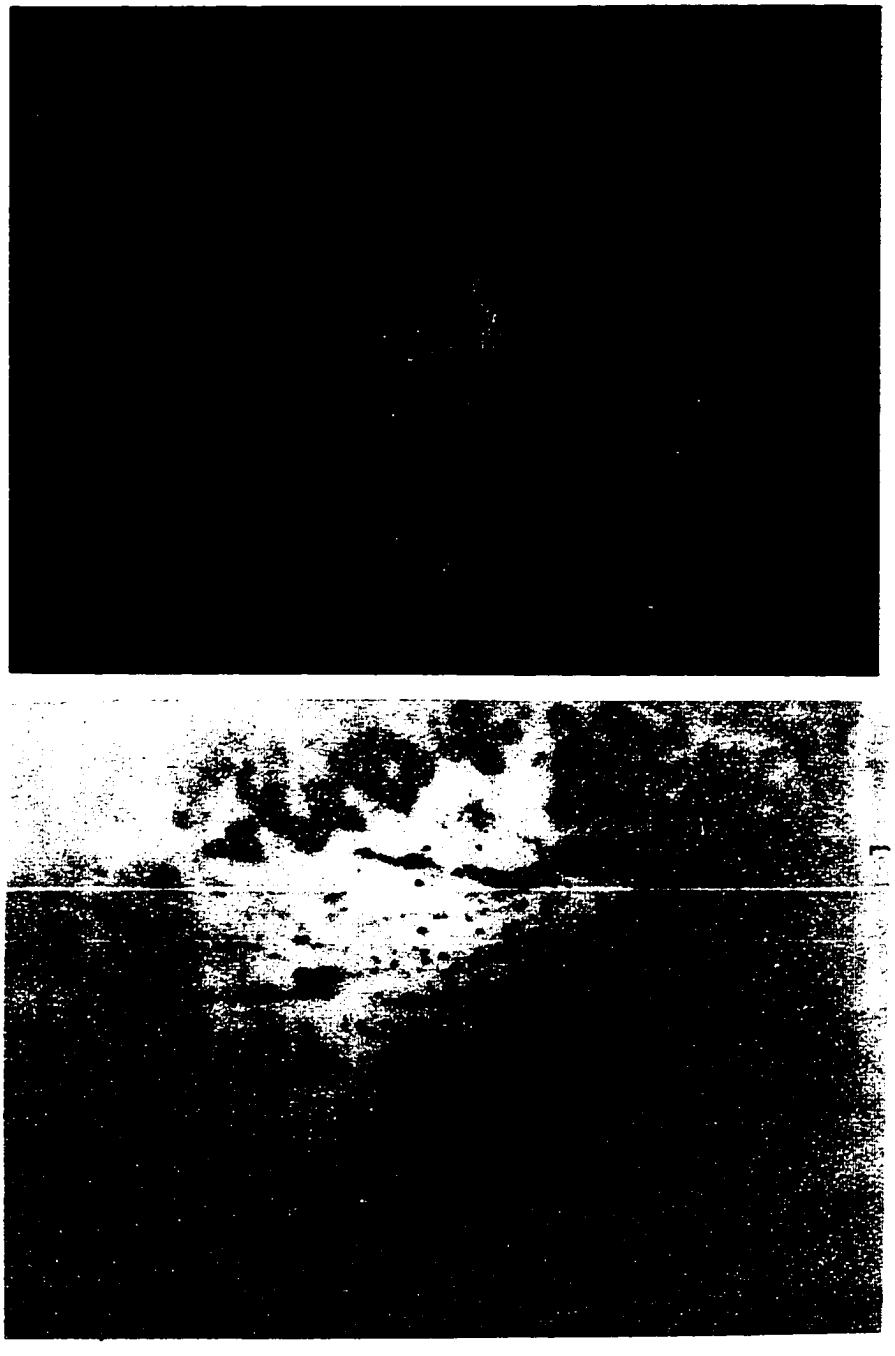

Chapter Eleven

Sequential or Integrated Approaches

The techniques in this work were considered for use sequentially or in an integrated fashion to reveal different features in gunshot residue discharge patterns on clothing. Some of these techniques might not work well in sequence with another method. For example, it was found that the application of dilute hydrochloric acid essentially prevents the subsequent use of the Modified Griess Test, without some chemical pretreatment. Still other applications clearly improve the state-of-the-art without the need for any additional experimentation beyond that presented here. Sequential approaches that do not require additional experimentation will now be discussed. Additional experimentation regarding sequential applications was conducted and also discussed in this chapter. Each proposed sequence is presented and discussed separately. Each approach assumes that a thorough stereoscopic examination has already been conducted in the conventional fashion as recommended by Dillon prior to any chemical examination.

Method One: Native Fluorescence - MGT - Rhodizonate Test

This sequence is considered the least intrusive of the various sequential methods compared to currently used methods. It assumes that the examiner possesses certain basic equipment such as a tuneable high intensity light

source. This simple approach consists of the following steps:

1. Scan the pattern with visible light from 400nm to 555nm to obtain the maximum contrast between particles and the substrate. Use orange barrier filter from 400nm to about 515nm. Switch to a red barrier filter from 515nm to 555nm. Fine tune the light source for optimum contrast. The fluorescence portion of this sequence is conducted at room temperature.
2. Photograph the subject using the appropriate barrier filter. Use a relatively high speed film, with reasonably fine grain, such as Kodak Ektapress 400. This can be developed with the normal C41 process. Push processing is also possible, but not normally necessary. Use a fluorescent scale. The scale should not be placed too close to the pattern since its fluorescence can obscure particle fluorescence.
3. Examine the pattern utilizing its fluorescence for pattern distribution information, such as diameter, and so forth. Using a stereoscope, examine some of the particles to confirm the morphological appearance of the particles. Fibers do not provide much interference in the visible region, although some do fluoresce strongly. However, their general appearance is easily distinguished from that of gunpowder particles even at low magnification. A swivel-arm lamp/magnifier (approx. magnification = 2x), commonly available in stationery supply houses, can facilitate a low power observation.

4. In addition to photography, mapping the position of particles on a clear overlay is valuable (This should not be done until it has been confirmed that the photography of step 2 has been successful).The overlay mapping can be rapidly done by affixing a piece of transparency film onto the surface by stapling or with a piece of cellophane tape. This should be done gently so as to minimize any damage to the pattern. If the laboratory atmosphere is very dry, it is advisable to humidify the room to about 55% relative humidity to prevent the adhesion of the particles to the plastic. Using the office magnifier and the appropriate barrier filter (normally the orange bandpass goggles; 455-495nm), mark the overlay corresponding to the position of each particle with an extra fine point Sharpie® or similar permanent marker. Also mark the position of the bullet hole. Note the position of other pertinent features. Lead deposits will not fluoresce in this region. However, with certain substrates, the lead may be seen as dark spots or areas (that is, a quench) against a brighter, fluorescent background.
5. Place a few marks on both the pattern and plastic overlay to index and document the orientation of the map prior to removal. Gently remove the plastic ensuring that the cloth is not disturbed. Note the presence of any adhering particles and preserve these for additional examination if considered necessary.
6. Conduct the MGT in the usual fashion.

7. Examine the Griess transfer paper for fluorescence. Map out the position of particles in the same way as was done previously (step 4) directly on the pattern ensuring that you have marked the position of the bullet hole and several other reference points. The optimum wavelength for examining the transfer may not be exactly the same as that for examining the pattern directly. The transfer should also be scanned and fine tuned to obtain the best wavelength for differential contrast (440nm - 495nm).
8. Conduct the Rhodizonate test in the usual fashion. Use the recently reported technique of Bartsch et al. (1996). Remove excess HCl as suggested.

Discussion

This sequence often eliminates many of the Griess transfer-related problems such as: (a) sufficient heat transfer; (b) colored wool substrates (Bonfanti et al., 1995); (c) inconsistent sensitivities of the transfer medium; (d) weak ammunition reaction; (e) poor resolution (especially in the central portion of the patterns), and so forth. This sequential approach provides supplementary information and a convenient way of examining the entire pattern via the mapping approach. Interference with the classical approach is avoided. Weakly reacting colored azo dye sites on the transfer almost always provide strong fluorescence. The strong reaction sites, unfortunately, quench on the paper.

However, this is not considered a problem since those sites are not difficult to detect on the transfer paper in any case.

The mapping also provides another dimension to the test than has been previously considered. The classical approach is more of a casual superficial approach of pattern recognition. The more detailed mapping technique forces the examiner to obtain a more profound knowledge of the number, position, and distribution of the particles on the pattern itself or on the transfer paper.

Method Two: Native Fluorescence at Liquid Nitrogen Temperature/Molecular Confirmation of Select Particles - Rhodizonate Test

Some patterns consistently provide excellent fluorescence. The patterns from these specific sources could be adequately examined for native fluorescence. Excellent patterns can be obtained by reducing the temperature with liquid nitrogen. A number of particles can be randomly selected from several positions in the pattern and analyzed by GC/MS or FTIR. Subsequently, lead can be detected in the usual fashion by Rhodizonate Test.

Method Three: Native Fluorescence at Liquid Nitrogen Temperature/Molecular Confirmation of Select Particles/ SUV (254nm Excitation) - HCl - Liquid Nitrogen (LN2)

Method Two would be utilized with the exception of the last step. It would

be replaced with the dilute HCl fluorescence technique.

Method Four: HCl - LN2 - Visible (VIS)/SUV/LUV (365nm excitation)/methanolic potassium hydroxide/MGT

This is the most comprehensive of all the methods. Tests were run to determine if the Modified Griess Test could be applied after the application of dilute hydrochloric acid. Additional experimentation was conducted to determine if dilute potassium hydroxide could be applied to patterns as a saponification agent to provide a Griess reaction after the application of hydrochloric acid. In many cases, it is not considered necessary to perform a Modified Griess Test. This approach can provide a means to conduct the Modified Griess Test after the other steps have been performed.

Methods and Materials

Griess Reactivity Post-HCl

Portions (an eighth of each pattern) of seven different discharge patterns were sprayed with 1M HCl and allowed to react for one minute. The substrate was a dark grey cotton/polyester blend. A Griess transfer was then applied to each treated portion as well as an untreated one. These sources of these patterns were: (a) CCI .38+P 125 grain, JHP; (b) CCI 357 Magnum 158 Grain JHP; (c) Federal .38 Spl. NYCLAD 158 grain RN; (d) PMC .38 158 grain, SWC; (e) Remington .38 Spl. 158 grain, LRN; (f) Remington 357 Magnum 158 grain

SJHP; and (g) Magtech .38 158 grain LRN. Six other different types of fabric were also examined with discharge patterns from only CCI .38+P ammunition. The fabrics used were 100% cotton (one dark blue and one white); black rayon; 100% wool (one black and one multi-colored); light grey cotton/polyester blend.

Griess Reactivity Post-HCl & potassium hydroxide (KOH)

Fresh portions of the above seven patterns were treated with aqueous 1M hydrochloric acid, followed by 2% methanolic potassium hydroxide. A Griess transfer was then attempted and compared to the reactions obtained with the post-HCl and previously untreated transfers. This procedure was also repeated on the additional six substrates listed above.

Results and Discussion

The application of the Modified Griess Test after hydrochloric acid treatment was essentially unsuccessful. The hydrochloric acid, by either chemical or physical reaction, strips the particle surface of available nitrite to react with the diazotization and coupling agent. Hydrochloric acid, reacts with nitrite to produce nitrous acid (Chapter Two). Nitrous acid, which is volatile, is no longer available for reaction with the transfer paper. All that is obtained is an exceedingly weak reaction.

However, the portions of patterns treated with dilute potassium hydroxide and transferred in the conventional fashion produced at least as strong, and in most patterns stronger, reactions than the untreated sections (Figure 75). The

potassium hydroxide-treated rayon substrate appeared to have deteriorated. The remaining substrates are still in good condition after the passage of twenty-two months.

The following is an explanation of how this sequence would be actually carried out:

1. Spray the surface with 1M hydrochloric acid, allowing one minute for the reaction to take place.
2. Submerge in liquid nitrogen.
3. Expose to short wavelength (254nm) ultraviolet light. This must be a relatively strong UV source. Use an orange bandpass filter for observation to remove shorter wavelengths, if necessary, with the film being used. Lead and antimony will fluoresce intensely under these conditions. The fine lead deposit, bullet wipe, and particles containing metals will fluoresce at this stage. Phosphorescence observations may also be conducted at this point. The aperture should be at its most open setting (f/1.8) and the shutter held open for several seconds. The lamp must be held very close to the pattern prior to snapping the photograph. After the pattern has been radiated closeup for several seconds, rapidly remove the lamp and open the shutter. If a significant amount of lead is present from the cloud deposit, it will essentially overwhelm bullet wipe and particle fluorescence at this excitation wavelength.
4. Switch to long wavelength (365nm) ultraviolet light. The temperature

should be checked before the start of each step with a thermocouple thermometer to ensure that it is still very cold (-140^{0}C or colder). This step will eliminate the interference from the lead cloud deposit. Particles will fluoresce much more intensely at this wavelength compared to 254nm. Lead will not fluoresce at all. Photographs of phosphorescence should also be taken during this step.

5. Expose to visible radiation, using an orange bandpass filter. Scan from 400nm to 515nm. Switch to a red bandpass filter at 515nm and continue to scan to 555nm. Lead does not interfere appreciably at these wavelengths, and less interference is seen from fibers compared to ultraviolet excitation.
6. If desired, select particles at random for molecular confirmation.
7. In many cases, only steps 1-6 are necessary. If the Modified Griess Test is desired, or considered necessary, prior saponification of the particles may be necessary to obtain an adequate Griess Transfer. The transfer, without pretreatment, can be attempted in the usual fashion but will likely provide a very weak reaction. The reaction on the transfer paper can be enhanced by fluorescence techniques (short ultraviolet excitation or visible excitation). If a strong reaction is desired, apply 2% - 4% (0.4-0.7M) methanolic potassium hydroxide to the pattern, and allow it a few minutes to react. Conduct the Modified Griess Test in the usual fashion.
8. Respray with hydrochloric acid to neutralize the potassium hydroxide.

Heat the pattern with a hair dryer to remove excess hydrochloric acid.

Method Five: Native Fluorescence at Liquid Nitrogen Temperature - MGT - Rhodizonate Test

There is a dramatic increase in the intensity of fluorescence and an increase in the number of detectable particles when the temperature is decreased. Also, not all particles are detected by fluorescence. It would be advantageous if the Modified Griess Test could be conducted after the fluorescence examination. It was not clear if the liquid nitrogen application might interfere with the subsequent chemical reaction.

Methods and Materials

Five different patterns were submerged in liquid nitrogen in a stainless steel tray for approximately ten minutes. They were removed from the tray and brought to room temperature. Each pattern was subjected to the Modified Griess Test in the usual fashion.

Results and Discussion

Excellent Griess test patterns were obtained from each discharge pattern. When applying the liquid nitrogen, propellant particles can be dislodged if it is done in too vigorous a fashion directly to the area bearing the GSR deposit. If the liquid nitrogen is applied gently in a section of the pattern that

does not possess any particles, little loss or displacement has been found.

Method Six: Bullet Wipe via Pb Fluorescence. Post-HCl - LN2 - Native Fluorescence - MGT

The application of the Modified Griess Test causes the diffusion of the lead deposit at the bullet hole site to the extent that examination for the direction of travel is not possible. A desirable first step would be the examination for bullet wipe using fluorescence. It was seen that the application of hydrochloric acid to produce lead fluorescence at liquid nitrogen temperatures essentially prevents the subsequent utilization of the Modified Griess Test without a saponification pre-treatment step. Experiments were conducted to assess whether or not it would be practical to apply dilute hydrochloric acid to the immediate area surrounding the bullet hole and then submerge the target in liquid nitrogen for a limited examination of that section of the target, followed by a traditional Griess Test.

Methods and Materials

Several discharge patterns were treated with 1M hydrochloric acid in a one inch (2.5cm) diameter area around the bullet hole, and were then submerged in liquid nitrogen. Both sides of each pattern were examined for fluorescence with short wave (254nm) U.V. radiation. The patterns were then removed and allowed to reach room temperature. The Modified Griess Test

was conducted in the usual fashion.

Results and Discussion

Bullet wipe was clearly visible on the entrance side of each target. Some fluorescence was noted on the exit side, but much less than the entrance side. Normal Griess transfer patterns were obtained from each discharge pattern with one consistent difference. The area of HCl application provided little or no azo dye product on the transfer paper. This area of the pattern was about 2.5cm (one inch) in diameter (Figure 76). However, the remaining area of each pattern produced a normal Griess transfer.

Method Seven: Short Wavelength UV Excitation of Transfer Paper for Azo Dye Quench

Not all laboratories possess a tunable high intensity light source. Despite this, excellent results can be obtained with merely a dual-use (short and long wavelength) ultraviolet lamp. It was seen (Chapter Eight), that azo dye sites strongly quench when exposed to short wavelength ultraviolet radiation, while unreacted sites of the transfer paper fluoresce. Hence, very intense contrast is obtained. In any of the methods with a step in which the paper was excited for fluorescence purposes, the visibility of the azo dye sites may be increased, by causing them to quench, by exciting the transfer paper with shortwave ultraviolet light.

Method Eight: Fractional Approach

Any of these methods can be employed on a portion, such as one or two quadrants, of a pattern, and the other fractions examined by traditional transfer methods.

Conclusion

Before an evidentiary pattern is treated by any chemical method, an exemplar should be examined using the proposed technique, with the same ammunition, firearm, and type of substrate is used (as in the evidence) to ensure that the technique is suitable under those specific conditions.

All the photoluminescent methods explored in this work may benefit from image intensification techniques in conjunction with thorough photographic documentation.

Figure 75. Upper Photo: CCI 357 Mag. 158gr. JHP Blazer. Muzzle D. = 12". Post HCl, liquid nitrogen, long wave U.V. excitation. Lower Photo: same pattern treated with 4% methanolic potassium hydroxide prior to Griess Transfer.

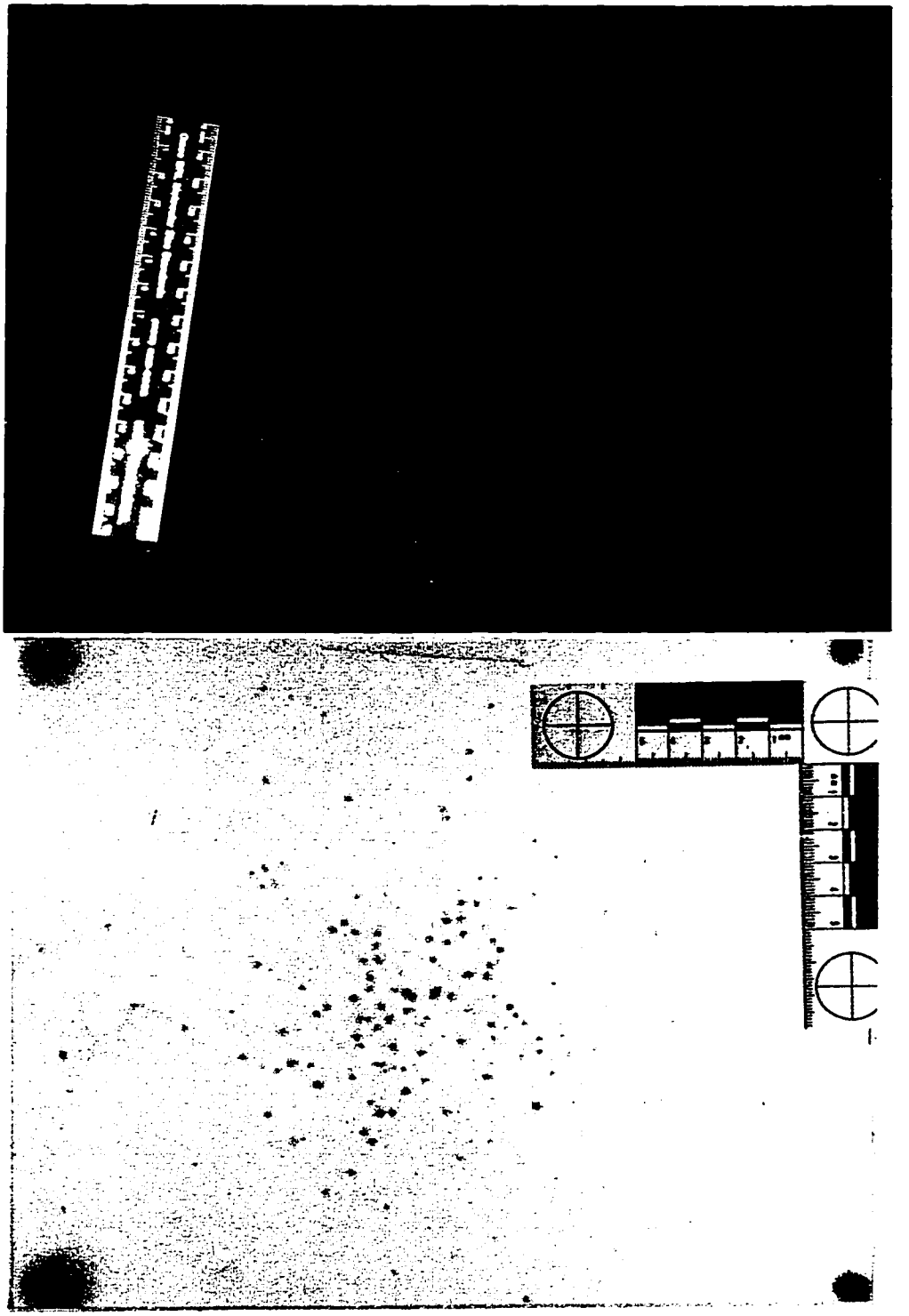

Figure 76. Upper Photo: Transfer of Pattern Treated w/1M HCl at Area Immediately Surrounding Bullet Hole. Lower Photo: Short UV Excitation of Same Transfer.

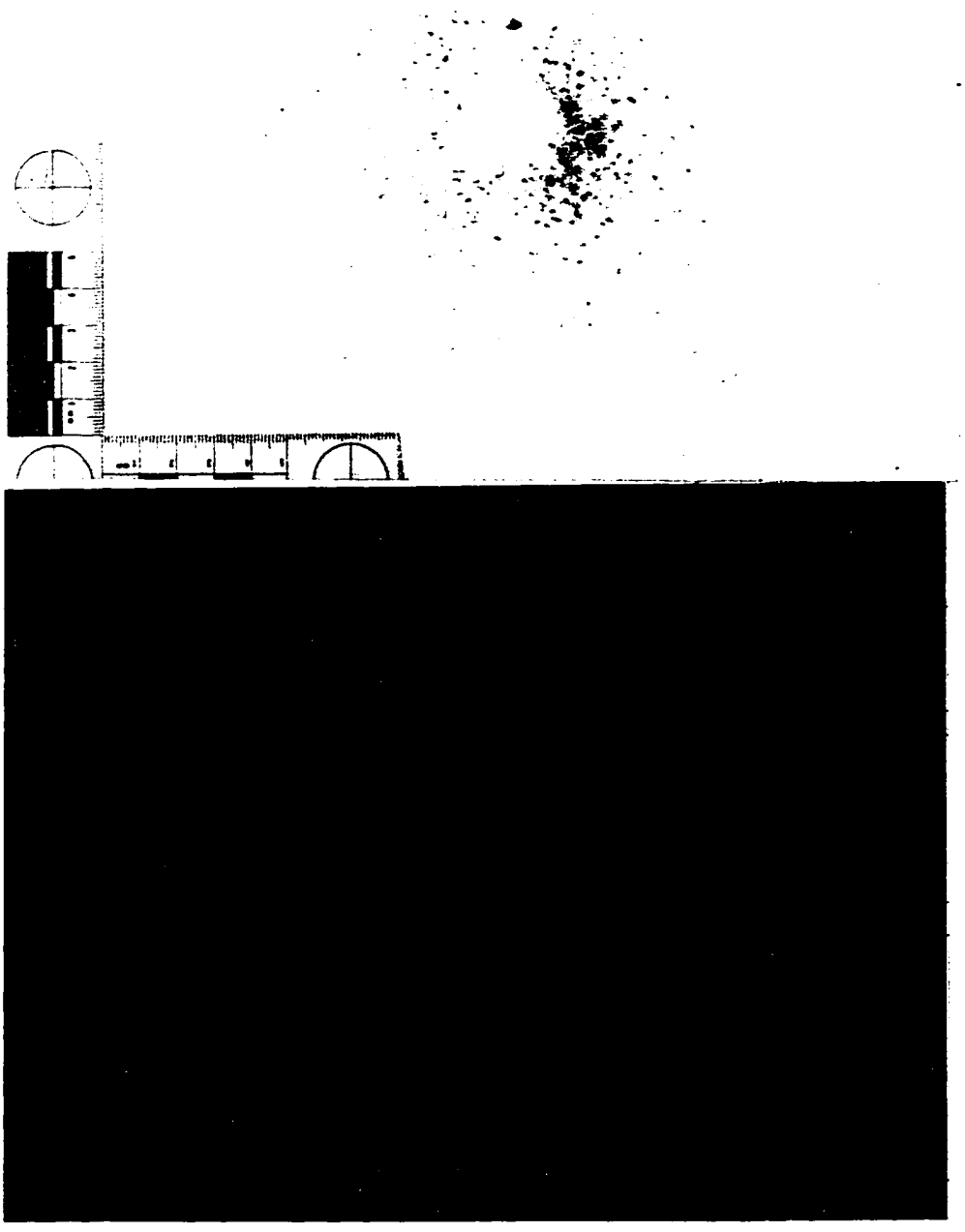

Chapter Twelve

Conclusion

High Speed Studies - GSR Dynamics - Particles

The research conducted here regarding gunshot residue dynamics has demonstrated that propellant particles attain surprisingly high velocities. This enables them to penetrate or even perforate clothing and other kinds of fabric directly ahead or somewhat to the side of the shooter. This information is exceedingly important in criminalistics and crime scene reconstruction as it shows that currently practiced superficial examinations of an individual's clothing for propellant particles is woefully inadequate. Examiners must consider the possibility that propellant particles may have become imbedded within the outer layer of clothing or could have even passed through this layer wind up on inner layers of clothing. Casework examinations of clothing and furnishings require more vigorous examination for gunshot residue than is currently practiced. Photoluminescent techniques developed and discussed in this dissertation clearly improve the state-of-the-art regarding the detection of such particles.

High Speed Study - GSR Dynamics - Cloud Movements

In a closely related area, experiments conducted here demonstrated that at least a portion of a fine gunshot residue cloud moves slowly toward the

shooter shortly after discharge, in addition to the portion which make up a rapidly forward-moving cloud. It was learned that the slowly moving cloud is subject to influence from wind velocity or rapid movements of the shooter and/or other person in close proximity to the weapon at the moment of discharge. These factors can affect the amount of gunshot residue deposited on the person's hands. Some forensic scientists have testified in criminal proceedings that the presence of a few gunshot residue particles on an individual's hands show that they held a weapon when it was fired. High speed photography conducted and reported here provides evidence that some particles can possess unpredictable trajectories. These particles can move laterally to a considerable degree with respect to the shooter and can be deposited on nearby persons who did not hold the weapon. The research reported here suggests that unanswered questions still remain regarding these issues and points to the need for further research beyond the scope of this work. These findings should also help non-scientists, such as attorneys and judges, comprehend some of the complexities and anomalies involved.

Muzzle-to-Target Distance

This research also focused on another major area of criminalistics and crime scene reconstruction: the estimation of the distance from which a firearm was discharged. This is often referred to as the muzzle-to-target distance. The estimate of the muzzle-to-target distance is crucial to crime scene

reconstruction since it can either help corroborate or refute suspects' or witnesses' statements. Methods currently used in criminalistics laboratories for the estimate of the muzzle-to-target distance have changed little over the past fifty years. These methods employ transfer techniques, rather than a direct approach, since color reactions do not provide an adequate contrast with dark fabrics. Unfortunately, a critical assessment of these transfer methods had not been reported in the forensic science literature. This research shows that these transfer methods suffer from several problems which can adversely influence their interpretation. Alternative approaches for direct pattern development and visualization involving photoluminescence were studied and developed. Several techniques for the detection of propellant particles and metal deposits have been developed and presented in this work. These include approaches for use individually by criminalists or in conjunction with classical transfer methods. The new methods developed include: (a) use of native fluorescence for the detection of partially burned particles; (b) low temperature enhancement of photoluminescent methods for particles and the fine metal deposits; (c) a phosphorescent method for the detection of partially burned particles; (d) chemical treatment to induce fluorescence of particles and metal deposits; and (e) a fluorescence method for vastly improving the detection of reaction sites on the transfer medium for particles.

Sequential Integrated Methods

Several sequentially integrated approaches, incorporating the above improvements for the detection and enhancement of discharge patterns, have been developed and described. Each of these provides an improvement in the state-of-the-art. Most of these newly developed techniques can be integrated with the long accepted classical methods, improving them significantly.

Table A1. Muzzle and Retrograde Cloud Data

Federal .38 Spl.158 Gr. LRN	Muzzle Cloud			
dist. from muzzle (inches)	inches - interval	cm	microsec.	fps
5.13 - 6.50	1.37	3.48	200	571
6.50 - 7.38	0.88	2.24	200	367
7.38 - 9.50	2.12	5.38	400	443
9.50 - 10.8	1.30	3.30	200	541
10.8 - 11.8	1.00	2.54	200	417
11.8 - 12.8	1.00	2.54	200	417
12.8 - 13.0	0.30	0.76	200	125
13.0 - 14.0	1.00	2.54	200	417
14.0 - 14.5	0.50	1.27	200	209
14.5 - 15.5	1.00	2.54	200	417
15.5 - 17.0	1.50	3.81	200	626
			mean	414
Winchester .38+P, 158 Gr. SWC	Muzzle Cloud			
dist. from muzzle (inches)	inches - interval	cm	microsec.	fps
6.50 - 8.50	2.00	5.08	200	833
8.50 - 9.25	0.75	1.91	200	313
9.25 - 9.75	0.50	1.27	200	208
9.75 - 11.5	1.75	4.45	200	731
11.5 - 12.6	1.10	2.79	200	459
12.6 - 14.0	1.40	3.56	200	584
14.0 - 15.0	1.00	2.54	400	208
			mean	477
Remington 357 Mag.180 Gr. SJHP	Muzzle Cloud			
dist. from muzzle (inches)	inches - interval	cm	microsec.	fps
7.88 - 8.75	0.87	2.21	200	363
8.75 - 9.00	0.25	0.64	200	105
9.00 - 10.5	1.50	3.81	200	627
10.5 - 12.5	2.00	5.08	400	417
12.5 - 14.6	2.10	5.33	400	436
14.6 - 15.5	0.90	2.29	200	376
			mean	387
Winchester .38 Spl.158 Gr.SWC LRN				
	Retrograde Cloud			
	inches - interval	cm	millisec.	fps
	1.00	2.54	20ms	4.17
	1.50	3.81	25ms	4.99
	3.00	7.62	125ms	2.00
	3.00	7.62	50ms	4.99
			mean	4.04

Table A1 Continued. Muzzle Cloud Data

Remington 9mm +P 115 Gr. JHP	Muzzle Cloud			
distance from muzzle	inches - interval	cm	microsec.	fps
7.00-12.0	5.00	12.70	600	712
12.0 -13.0	1.00	2.54	100	833
13.0 -15.8	2.80	7.11	500	459
15.8 -17.5	1.70	4.32	300	469
17.5 - 20.0	2.50	6.35	600	347
			mean	564
		Muzzle Cloud		
Federal 9mm 115 Gr. JHP				
13.0 - 15.50	2.50	6.35	400	522
15.50 - 16.50	1.00	2.54	200	417
16.50 - 18.30	1.80	4.57	200	751
18.30 - 19.88	1.58	4.01	400	129
19.88 - 20.50	0.62	1.57	200	102
20.50 - 21.00	0.50	1.27	200	82
			mean	334
five sources of ammunition	**mean (total)**	**429 fps**		
(35 discharges)				

Table A2. Retrograde Cloud Experiments - Velocity Estimate

Source	Caliber	Grain, Bullet	in 1st Frame (by Hand)	Velocity (Above Hand)	Velocity (by hand)
	S&W 357 Magnum				**1st - 2nd frame**
Remington	.38 Spl.	158, LN	yes	2 fps	2fps
Remington	.38 Spl.	158, LN	yes	8 fps	7fps
Remington	.38 Spl.	158, LN	yes	6 fps	7fps
Remington	.38 Spl.	158, LN	yes	3 fps	3fps
Remington	.38 Spl.	158, LN	yes	3 fps	3fps
Remington	.38 Spl.	158, LN	yes	3 fps	2fps
Remington	.38 Spl.	158, LN	yes	3 fps	3fps
Remington	.38 Spl.	158, LN	yes	3 fps	3fps
Remington	.38 Spl.	158, LN	yes	3 fps	2fps
Remington	.38 Spl.	158, LN	yes	none	none
Remington	.38 Spl.	158, LN	yes	3 fps	3fps
Remington	.38 Spl.	158, LN	yes	3 fps	3fps
Winchester	.38+P	158, SWC	yes	3 fps	3fps
Winchester	.38+P	158, SWC	yes	3 fps	3fps
Winchester	.38+P	158, SWC	yes	3 fps	3fps
Winchester	.38+P	158, SWC	yes	3 fps	3fps
Winchester	.38+P	158, SWC	yes	3 fps	3fps
Winchester	.38+P	158, SWC	yes	3 fps	2fps
Winchester	.38+P	158, SWC	yes	3 fps	3fps
Winchester	357 Mag.	158, SWC	yes	3 fps	2fps
Winchester	357 Mag.	158, SWC	yes	3 fps	3fps
CCI Blazer	.38 Spl.	158, SWC	yes	3 fps	3fps
CCI Blazer	.38 Spl.	158, SWC	yes	3 fps	3fps
CCI Blazer	357 Mag.	158, JHP	yes	none	none
CCI Blazer	357 Mag.	158, JHP	yes	none	none
CCI Blazer	357 Mag.	158, JHP	yes	none	none
Federal	.38 Spl.	158, LRN	yes	3fps	3fps
Federal	.38 Spl.	158, LRN	yes	3fps	3fps
Federal	.38 Spl.	158, LRN	yes	3fps	3fps
Federal	.38 Spl.	158, LRN	yes	3fps	2fps
			mean	**3fps**	**3fps**
	S&W .38 Model 36				
Remington	.38 Spl.	158, LN	yes	5fps	3fps
Remington	.38 Spl.	158, LN	yes	1fps	1fps
Remington	.38 Spl.	158, LN	yes	5fps	1fps
Remington	.38 Spl.	158, LN	yes	3fps	3fps
Remington	.38 Spl.	158, LN	yes	3fps	3fps
Remington	.38 Spl.	158, LN	yes	3fps	3fps
Remington	.38 Spl.	158, LN	yes	3fps	3fps
Federal	.38 Spl.	158, LRN	yes	1fps	1fps
Federal	.38 Spl.	158, LRN	yes	1fps	1fps
Federal	.38 Spl.	158, LRN	yes	1fps	1fps

Table A2. Retrograde Cloud Experiments - Velocity Estimate

Federal	.38 Spl.	158, LRN	yes	1fps	1fps
Federal	.38 Spl.	158, LRN	yes	1fps	1fps
Federal	.38 Spl.	158, LRN	yes	1fps	1fps
			mean	**2fps**	**2fps**
	H&K 9mm	**Model VP70Z**			
Remington	9mm+P	115, JHP	five discharges	none	none
Federal	9mm	115, JHP	five discharges	none	none

Table A3. Self-Luminous Particles

Source	Caliber	Grain, bullet	no. of frames w/o self-luminous particles	no. of self-luminous particles	no. of particles odd trajectories
Winchester	.38spl.	158, SWC	40	4	0
Winchester	.38spl.	158, SWC	30	0	0
Winchester	.38spl.	158, SWC	7	2	0
Winchester	.38spl.	158, SWC	27	5	1
Winchester	.38spl.	158, SWC	20	13	4
Winchester	.38spl.	158, SWC	2	1	0
Federal	.38+P	125, JHP	33	3	2
Federal	.38+P	125, JHP	16	2	0
Federal	.38+P	125, JHP	3	0	0
CCI	.38spl.	158, LRN	9	3	0
CCI	.38+P	158, TMJ	6	10	1
CCI	.38+P	158, TMJ	4	0	0
Speer	.38+P	158, TMJ	4	2	0
Speer	.38+P	158, TMJ	7	0	0
Master	.38+P	158, SWC	0	10	1
Master	.38+P	158, SWC	3	0	0
Federal	357 Mag	110, JHP	4	5	0
Remington	.38spl.	158, SWC	6	1	0
Remington	357 Mag	180, SJHP	2	1	0
Winchester	.38spl.	158, SWC	26	2	0
CCI	.38+P	125 JHP	10	0	0
CCI	.38+P	158, TMJ	7	0	0
Federal	.38+P	125, JHP	6	0	3
Master	.38+P	158, SWC	8	0	0
Remington	.38spl.	158, SWC	9	0	0
Remington	357 Mag	180, SJHP	3	0	0
CCI	357 Mag	158, JHP	10	0	0
Federal	357 Mag	110, SJHP	6	0	0
Winchester	357 Mag	158, LD	2	2	0
Federal	357 Mag	158, RN	13	10	5
Speer	9 mm	147,TMJ	35	0	0
CCI	9 mm	124, TMJ	20	64	11
Union Metallic	9 mm	115, FMJ	19	88	3
	total frames w/o self-luminous particles: 397				
	total number of self-luminous particles in 72 frames: 228				
	total number of self-luminous particles having odd trajectories: 31				

Note Regarding Table A3.

Discharges from fourteen different sources of ammunition were studied for self-luminous particles. This involved the examination of 469 frames from negatives (469 separate discharges). As indicated by the totals, self-luminous particles were not found in 397 discharges. Of course, not the entire relevant field was observed. Most of these negatives displayed an area of about 10-15 inches in length. The total number of self-luminous particles detected in 72 discharges was 228. Nearly 87% of these particles exhibited straight trajectories. Only 31 (about 13% of the total self-luminous particles) displayed strange or odd trajectories. If it is assumed that each discharge yields at least 300 propellant particles (a conservative estimate), 472 discharges would produce approximately 142,000 particles. Thus, the total number of self-luminous particles (228) represents only about 0.2% of the total number of particles. Further, the total number of self-luminous particles having unusual trajectories would be about seven times smaller than 0.2%. However, some sources of ammunition displayed much more than the remaining ammunition (Union Metallic, 9mm). It does not appear that these particles have a significant effect on the interpretation of discharge patterns. It should be noted that since these particles provide their own illumination, the occurrence of them is independent of the flash and associated time delay.

Table A4. Native Fluorescence: Ingredients of Smokeless Propellant

Compound	visible ex.	365nm ex.	254nm ex.
Diphenylamine	quench	white	white
N-nitroso-diphenylamine	very weak	quench	quench
2,3-dinitrotoluene	strong orange	orange	quench
3,4-dinitrotoluene	quench	quench	quench
2,6-dinitrotoluene	quench	quench	quench
2,4-dinitrotoluene	quench	quench	quench
nitroguanidine	weak white	quench	quench
2,3-benzanthracene	strong orange	yellow	quench
dibutylphthalate	weak white	weak white	quench
methyl centralite	weak white	weak white	quench
ethyl centralite	weak white	quench	quench
nitroglycerine	weak white	white	pale blue
carbazole	orange	strong	strong
cellulose nitrate	white/orange& green	quench	quench

Table A5. Remington 9mm+P 115 Grain, JHP.
(Data for Figure 10 and Table Two)

Muzzle Distance (in.)	Vertical Distance (in.) from Muzzle	Distance Between Particle Images	V(cm/s)	V (ft/s)
17.8	-0.8	22.4	3.E+04	889
16.6	-0.9	21.6	3.E+04	857
26.4	1.8	15.7	2.E+04	623
26.5	1.6	24.6	3.E+04	977
24.8	2.3	24.9	3.E+04	988
25.4	-2.5	12.3	1.E+04	488
22.4	2.1	8.2	1.E+04	326
21.5	-0.8	4.3	5.E+03	171
24.0	-3.3	5.0	6.E+03	200
25.6	-3.6	10.5	1.E+04	420
27.3	-3.1	6.8	8.E+03	272
23.8	-2.6	9.7	1.E+04	388
26.2	-1.1	14.6	2.E+04	584
23.1	-0.4	7.9	1.E+04	316
21.8	-0.3	11.7	1.E+04	468
22.4	-0.6	8.5	1.E+04	340
23.9	0.4	7.4	9.E+03	296
23.6	0.5	8.7	1.E+04	348
24.4	0.3	6.4	8.E+03	256
24.8	1.8	11.6	1.E+04	464
24.8	1.9	10.9	1.E+04	436
27.4	1.6	10.1	1.E+04	404
26.8	1.6	9.4	1.E+04	376
21.6	0.9	8.0	1.E+04	320
24.9	3.3	11.4	1.E+04	456
25.9	3.4	20.0	2.E+04	801
23.9	3.4	8.2	1.E+04	328
31.3	0.2	11.3	1.E+04	471
31.0	0.5	11.5	1.E+04	479
33.4	3.4	13.9	2.E+04	579
28.3	3.4	16.7	2.E+04	696
33.6	1.1	9.6	1.E+04	400
34.6	2.7	15.3	2.E+04	638
33.0	-3.1	11.5	1.E+04	479
32.8	-3.4	31.1	4.E+04	1296
33.0	-3.3	12.2	2.E+04	508
32.1	-3.6	21.1	3.E+04	879
29.5	-2.9	8.8	1.E+04	367
28.4	-1.1	12.1	2.E+04	504
31.8	1.1	18.3	2.E+04	763
32.8	0.8	15.8	2.E+04	658

The Distance Between Particle Images Corresponds to 100 microsec.
The (-) or (+) symbols indicate position above and below the muzzle.

Table A5. Remington 9mm+P 115 Grain, JHP.
(Data for Figure 10 and Table Two)

34.9	3.4	10.3	1.E+04	429
34.5	3.3	13.1	2.E+04	546
34.3	1.3	19.2	2.E+04	800
33.8	-1.1	19.2	2.E+04	800
32.0	-1.4	15.8	2.E+04	658
28.9	-0.5	8.7	1.E+04	363
40.0	-2.4	13.6	2.E+04	567
41.1	0.2	11.7	1.E+04	488
37.2	1.9	21.6	3.E+04	900
36.4	2.0	18.4	2.E+04	767
34.5	2.9	11.1	1.E+04	463
40.5	-2.1	10.9	1.E+04	454
37.5	-1.3	19.5	2.E+04	813
37.3	-2.6	13.1	2.E+04	546
39.8	1.7	11.8	1.E+04	492
41.1	0.6	12.3	2.E+04	513
37.8	0.1	18.7	2.E+04	779
37.8	-0.4	9.9	1.E+04	413
36.8	-2.1	9.4	1.E+04	392
48.0	-0.6	15.4	2.E+04	642
48.5	-0.8	11.4	1.E+04	475
45.0	-3.0	10.5	1.E+04	438
41.8	-3.3	8.8	1.E+04	367
44.0	1.4	12.8	2.E+04	533
53.0	-0.8	10.9	1.E+04	447
48.0	3.3	12.3	2.E+04	504
49.3	2.0	9.1	1.E+04	373
51.0	-1.6	15.3	2.E+04	627
			mean	538

The Distance Between Particle Images Corresponds to 100 microsec.
The (-) or (+) symbols indicate position above and below the muzzle.

Table A6. CCI 9mm 115 Gr. TMJ (Data for Fig. 11, Tables 2 and 3)

Muzzle Distance (in.)	Vertical Dist.(in.) from muzzle	Distance Between 1st Set of Particle Images	V(cm/s)	V (ft/s)	Distance Between 2nd Set of Particle Images	V (ft/s)	loss in v. (fps)
19.9	0.1	11.2	1.E+04	366			
19.1	-2.1	14.8	1.E+04	487			
17.8	-1.7	8.1	8.E+03	264			
17.8	-0.6	1.3	1.E+03	41			
17.1	0.8	1.7	2.E+03	57			
16.5	2.0	4.1	4.E+03	134			
17.3	-2.8	11.5	1.E+04	379			
17.7	-2.5	11.6	1.E+04	382			
18.5	3.3	17.1	2.E+04	560			
19.3	3.4	16.7	2.E+04	547			
18.5	3.9	27.6	3.E+04	907			
20.6	1.5	15.5	2.E+04	509			
20.6	2.4	21.3	2.E+04	700			
25.2	2.7	8.2	8.E+03	268			
22.0	-0.8	7.6	8.E+03	249			
23.5	-0.7	14.5	1.E+04	476			
20.8	-3.0	4.9	5.E+03	162			
20.1	-2.3	8.3	8.E+03	271			
21.0	-2.3	3.5	4.E+03	115			
20.9	0.8	4.3	4.E+03	140			
21.6	1.0	4.8	5.E+03	159			
23.8	0.8	14.3	1.E+04	470			

The Distance Between Particle Images Corresponds to 100 microsec.
The (-) or (+) symbols indicate position above and below the muzzle.

Table A6. CCI 9mm 115 Gr. TMJ (Data for Fig. 11, Tables 2 and 3)

23.6	1.6	7.8	8.E+03	255	
24.3	-2.8	18.1	2.E+04	595	
23.4	-2.8	9.7	1.E+04	318	
29.8	-0.6	7.9	8.E+03	260	
29.1	-0.9	11.9	1.E+04	389	
28.8	-3.6	13.0	1.E+04	426	
27.4	0.7	3.9	4.E+03	129	
25.4	2.2	3.6	4.E+03	120	
29.6	0.3	2.2	2.E+03	74	
26.9	0.7	10.9	1.E+04	359	
25.6	0.4	6.4	6.E+03	208	
26.8	-0.9	14.3	1.E+04	469	
28.0	-2.1	21.9	2.E+04	717	
29.1	1.6	15.1	2.E+04	496	
28.8	2.1	14.2	1.E+04	465	
28.1	3.1	18.3	2.E+04	600	
29.8	-2.1	16.0	2.E+04	526	
27.1	-2.1	12.1	1.E+04	398	
26.4	0.1	14.1	1.E+04	462	
26.8	-0.4	11.4	1.E+04	373	
35.9	-0.7	24.8	2.E+04	814	
34.6	-1.1	18.5	2.E+04	608	
34.1	-1.8	19.8	2.E+04	649	
34.1	-2.6	22.8	2.E+04	747	
31.8	0.8	9.1	9.E+03	297	
31.1	1.2	11.2	1.E+04	368	

The Distance Between Particle Images Corresponds to 100 microsec.
The (-) or (+) symbols indicate position above and below the muzzle.

Table A6. CCI 9mm 115 Gr. TMJ (Data for Fig. 11, Tables 2 and 3)

33.4	1.3	7.4	7.E+03	243			
31.5	-0.1	13.5	1.E+04	443			
31.6	-0.4	13.8	1.E+04	453			
32.4	-0.8	25.8	3.E+04	845			
35.2	-3.4	16.9	2.E+04	554			
30.9	1.8	21.6	2.E+04	710			
33.9	-1.9	22.5	2.E+04	737			
32.9	-1.6	19.1	2.E+04	625			
32.6	-2.1	13.4	1.E+04	439			
31.3	-2.3	16.6	2.E+04	544			
30.0	-2.1	15.2	2.E+04	500			
29.8	-2.6	11.4	1.E+04	375			
33.2	1.1	14.3	1.E+04	470			
30.6	1.9	15.5	2.E+04	507			
30.6	1.6	20.4	2.E+04	669			
31.6	3.3	22.7	2.E+04	743			
32.4	2.7	14.5	1.E+04	476			
35.5	-0.1	19.3	2.E+04	632			
32.5	-1.3	12.3	1.E+04	402	11.6	382	20
32.6	-2.0	20.4	2.E+04	669	19.8	649	20
35.3	-2.3	16.0	2.E+04	524	15.6	510	14
36.0	-2.3	16.6	2.E+04	544	16.2	531	14
35.5	-1.4	12.7	1.E+04	416	12.5	409	7
34.4	1.3	14.5	1.E+04	476	13.6	446	30
34.1	-0.3	14.8	1.E+04	487	13.9	456	30
39.0	1.5	22.6	2.E+04	740	21.9	720	20

The Distance Between Particle Images Corresponds to 100 microsec.
The (-) or (+) symbols indicate position above and below the muzzle.

Table A6. CCI 9mm 115 Gr. TMJ (Data for Fig. 11, Tables 2 and 3)

40.3	0.7	14.3	1.E+04	470	13.7	449	20
37.6	1.6	13.5	1.E+04	443	13.0	426	17
37.1	1.6	13.3	1.E+04	436			
36.8	-3.6	10.7	1.E+04	351			
36.6	-3.9	10.2	1.E+04	335			
37.2	-1.4	16.3	2.E+04	534			
35.6	-0.2	14.4	1.E+04	473			
45.1	-1.3	21.9	2.E+04	720			
46.0	1.1	15.8	2.E+04	518			
45.3	2.2	24.4	2.E+04	800			
43.3	3.6	20.0	2.E+04	657			
40.7	-1.9	13.9	1.E+04	456			
50.0	-0.6	12.9	1.E+04	425			
47.0	3.1	15.4	2.E+04	506			
46.1	0.4	15.0	1.E+04	491			
47.4	-2.3	17.4	2.E+04	572			
46.1	-1.5	12.9	1.E+04	425			
47.3	0.2	13.4	1.E+04	439			
47.3	1.3	16.5	2.E+04	541			
46.3	3.5	19.0	2.E+04	625			
50.1	0.9	16.8	2.E+04	551			
50.5	2.6	9.6	1.E+04	316			
48.4	4.5	15.7	2.E+04	516			
48.5	3.9	11.9	1.E+04	390			
46.9	2.3	20.5	2.E+04	674			
47.5	2.2	16.6	2.E+04	544			

The Distance Between Particle Images Corresponds to 100 microsec.
The (-) or (+) symbols indicate position above and below the muzzle.

Table A6. CCI 9mm 115 Gr. TMJ (Data for Fig. 11, Tables 2 and 3)

46.5	-0.5	16.9	2.E+04	555			
51.4	-0.6	16.3	2.E+04	534			
51.9	-1.1	21.4	2.E+04	702			
51.0	-2.6	18.9	2.E+04	621			
46.5	-0.6	12.6	1.E+04	414	12.3	404	11
48.6	-0.7	21.3	2.E+04	699			
51.7	1.0	20.2	2.E+04	663			
			mean	471		mean	18

The Distance Between Particle Images Corresponds to 100 microsec.
The (-) or (+) symbols indicate position above and below the muzzle.

Table A7. Win. .38+P 158 Grain HP, LN (Data for Fig. 12 and Table 2).

	C	D	E	J	K
1	**Muzzle**	**Vertical Dist. (in.)**	**Distance**	**V(cm/s)**	**V (ft/s)**
2	**Distance (in.)**	**from muzzle**	**Between**		
3			**Particle Images**		
4					
5	37.8	1.9	9.6	1.E+04	431
6	37.9	-2.3	12.0	2.E+04	539
7	43.4	-0.1	12.2	2.E+04	552
8	33.5	0.0	9.4	1.E+04	426
9	36.0	3.2	10.2	1.E+04	462
10	33.8	0.8	8.4	1.E+04	380
11	34.5	-2.7	8.7	1.E+04	394
12	32.1	-1.4	10.7	1.E+04	484
13	37.3	-0.4	11.7	2.E+04	534
14	36.3	2.8	16.4	2.E+04	748
15	33.1	2.4	11.8	2.E+04	538
16	30.1	-2.8	9.3	1.E+04	433
17	29.3	2.2	8.6	1.E+04	401
18	30.5	1.7	7.4	1.E+04	345
19	29.8	1.7	7.4	1.E+04	345
20	28.2	-1.7	18.7	3.E+04	871
21	30.0	0.2	10.5	1.E+04	489
22	27.4	0.0	5.6	8.E+03	261
23	31.0	1.8	13.3	2.E+04	615
24	29.9	1.9	14.7	2.E+04	680
25	29.5	0.6	16.9	2.E+04	782
26	29.4	0.9	13.0	2.E+04	601
27	29.3	2.5	8.8	1.E+04	407
28	29.4	1.7	11.1	2.E+04	513
29	29.1	-2.5	22.3	3.E+04	1032
30	30.0	4.0	8.9	1.E+04	412
31	28.1	3.0	14.9	2.E+04	689
32	31.1	-1.7	13.6	2.E+04	643
33	27.1	-1.0	9.8	1.E+04	463
34	30.0	-0.1	15.2	2.E+04	718
35	27.8	2.7	13.1	2.E+04	619
36	28.5	-0.1	15.1	2.E+04	713
37	30.3	1.2	8.0	1.E+04	378
38	29.0	-2.1	6.7	1.E+04	317
39	28.9	-2.3	6.0	9.E+03	283
40	28.8	-2.3	8.4	1.E+04	397
41	32.1	1.9	1.1	2.E+03	52
42	26.5	1.5	14.8	2.E+04	675

The Distance Between Particle Images Corresponds to 100 microsec.
The (-) or (+) symbols indicated position above and below the muzzle.

Table A7. Win. .38+P 158 Grain HP, LN (Data for Fig. 12 and Table 2).

	C	D	E	J	K
43	25.2	1.6	8.9	1.E+04	406
44	24.4	-2.4	8.8	1.E+04	401
45	25.9	-3.0	9.8	1.E+04	447
46	23.1	-1.8	10.1	1.E+04	461
47	22.8	-0.2	10.9	2.E+04	497
48	24.6	2.3	15.6	2.E+04	711
49	25.8	-1.7	7.3	1.E+04	333
50	26.2	-0.4	6.5	9.E+03	296
51	22.7	0.4	10.8	2.E+04	493
52	23.6	0.4	5.2	7.E+03	237
53	24.0	1.4	11.1	2.E+04	506
54	25.3	3.7	19.0	3.E+04	866
55	26.5	2.8	15.6	2.E+04	711
56	23.5	0.1	0.6	8.E+02	27
57	23.5	0.4	1.6	2.E+03	73
58	25.1	0.9	12.1	2.E+04	552
59	26.4	-2.0	17.6	2.E+04	751
60	24.4	-1.6	9.4	1.E+04	401
61	23.0	-1.8	6.4	8.E+03	273
62	27.1	2.8	15.0	2.E+04	640
63	24.9	0.3	14.2	2.E+04	606
64	25.1	-0.9	13.1	2.E+04	559
65	23.4	1.3	0.6	8.E+02	26
66	22.8	2.9	7.3	9.E+03	311
67	26.6	1.3	13.7	2.E+04	584
68	24.2	0.1	11.9	2.E+04	508
69	24.7	0.1	11.6	2.E+04	495
70	23.9	-0.1	15.2	2.E+04	648
71	22.8	1.3	22.1	3.E+04	943
72	26.9	-1.1	13.3	2.E+04	567
73	26.5	0.0	17.5	2.E+04	746
74	23.5	2.1	8.1	1.E+04	345
75	25.6	-1.3	11.7	2.E+04	499
76	22.5	-2.3	11.5	1.E+04	490
77	23.6	-0.6	7.7	1.E+04	328
78	22.9	1.8	13.6	2.E+04	580
79	23.1	1.8	14.9	2.E+04	635
80	25.1	1.5	16.5	2.E+04	704
81	24.3	1.5	11.5	1.E+04	490
82	23.6	1.4	17.3	2.E+04	738
83	25.9	-0.7	18.4	2.E+04	785
84	25.1	-3.9	16.8	2.E+04	717

The Distance Between Particle Images Corresponds to 100 microsec.
The (-) or (+) symbols indicated position above and below the muzzle.

Table A7. Win. .38+P 158 Grain HP, LN (Data for Fig. 12 and Table 2).

	C	D	E	J	K
85	26.6	1.8	11.3	1.E+04	482
86	26.6	3.1	14.7	2.E+04	627
87	25.4	-2.6	14.3	2.E+04	610
88	26.6	-1.9	13.1	2.E+04	559
89	23.6	1.9	17.8	2.E+04	759
90	23.2	1.0	17.2	2.E+04	734
91	19.8	-3.0	27.9	4.E+04	1190
92	19.6	0.4	3.6	5.E+03	154
93	18.3	-2.6	10.8	1.E+04	461
94	20.8	0.7	13.1	2.E+04	559
95	18.3	-0.7	2.5	3.E+03	107
96	18.7	-0.1	5.9	8.E+03	252
97	16.8	-0.1	4.8	6.E+03	205
98	17.8	0.1	14.9	2.E+04	635
99	18.9	0.3	10.8	1.E+04	461
100	18.9	1.1	6.1	8.E+03	260
101	19.0	2.0	4.0	5.E+03	171
102	20.3	2.4	14.0	2.E+04	597
103	20.3	2.1	11.9	2.E+04	508
104	20.4	2.0	10.1	1.E+04	431
105	19.1	2.9	9.8	1.E+04	418
106	21.3	2.6	9.9	1.E+04	422
107	20.5	1.6	8.7	1.E+04	371
108	21.3	1.6	13.2	2.E+04	563
109	19.0	-0.4	9.0	1.E+04	390
110	17.8	0.5	12.3	2.E+04	533
111	19.3	3.1	11.4	2.E+04	494
112	19.6	2.6	14.9	2.E+04	645
113	21.0	1.9	9.0	1.E+04	390
114	20.2	1.8	8.7	1.E+04	377
115	19.9	1.9	7.1	9.E+03	307
116	21.3	-2.3	4.5	6.E+03	195
117	20.9	-2.1	5.8	8.E+03	251
118	21.4	-2.9	17.4	2.E+04	754
119	19.5	-1.2	15.4	2.E+04	667
120	20.8	-1.2	11.9	2.E+04	515
121	20.5	-0.9	7.4	1.E+04	320
122	20.4	0.3	8.5	1.E+04	368
123	18.3	-0.6	9.0	1.E+04	390
124	16.9	-1.1	6.1	8.E+03	264
125	17.2	2.1	6.1	8.E+03	264
126	18.7	0.3	1.5	2.E+03	65

The Distance Between Particle Images Corresponds to 100 microsec.
The (-) or (+) symbols indicated position above and below the muzzle.

Table A7. Win. .38+P 158 Grain HP, LN (Data for Fig. 12 and Table 2).

	C	D	E	J	K
127	19.5	0.3	4.9	6.E+03	212
128	21.0	2.2	17.8	2.E+04	759
129	20.9	2.7	17.7	2.E+04	755
130	20.6	2.8	13.1	2.E+04	559
131	21.0	3.5	20.8	3.E+04	887
132	19.7	3.3	15.1	2.E+04	644
133	19.5	2.4	11.0	1.E+04	469
134	20.3	-1.9	18.7	2.E+04	798
135	17.0	-1.0	13.2	2.E+04	563
136	16.9	-1.5	13.5	2.E+04	576
137	17.6	-1.8	14.7	2.E+04	627
138	16.1	-2.3	5.4	7.E+03	230
139	18.9	-0.8	9.0	1.E+04	384
140	19.3	-1.0	1.2	2.E+03	51
141	14.4	-1.4	9.6	1.E+04	416
142	14.6	-0.9	10.5	1.E+04	455
143	14.9	-1.1	6.2	8.E+03	269
144	15.3	-1.1	2.9	4.E+03	126
145	16.1	-1.3	8.2	1.E+04	355
146	16.0	-1.6	5.3	7.E+03	230
147	16.0	-1.8	12.5	2.E+04	541
148	15.1	-1.6	7.2	1.E+04	312
149	15.2	2.6	9.7	1.E+04	420
150	14.6	2.8	7.3	1.E+04	316
151	15.7	2.1	17.1	2.E+04	741
152	15.8	1.1	8.5	1.E+04	368
153	14.9	1.1	13.9	2.E+04	602
154	14.5	1.3	7.2	1.E+04	312
155	14.6	1.2	6.3	8.E+03	273
156	13.6	0.3	9.7	1.E+04	420
157	16.1	1.8	5.9	8.E+03	256
158	15.6	0.0	6.7	9.E+03	290
159	14.9	0.1	14.8	2.E+04	641
160	10.3	-3.0	19.7	3.E+04	866
161	10.4	-2.7	19.1	3.E+04	840
162	9.8	1.7	10.7	1.E+04	470
163	11.3	2.3	13.1	2.E+04	576
164	11.3	2.9	1.7	2.E+03	75
165	10.1	-1.7	14.5	2.E+04	637
166	8.8	-1.3	3.6	5.E+03	158
167	7.8	2.6	14.2	2.E+04	624
168	8.3	2.4	15.7	2.E+04	690

The Distance Between Particle Images Corresponds to 100 microsec.
The (-) or (+) symbols indicated position above and below the muzzle.

Table A7. Win. .38+P 158 Grain HP, LN (Data for Fig. 12 and Table 2).

	C	D	E	J	K
169	9.3	2.3	15.7	5.E+03	158
170	9.1	1.0	3.6	4.E+03	132
171	9.3	0.5	3.0	2.E+04	550
172	10.3	0.4	12.5	5.E+03	167
173	7.7	-1.0	3.8	1.E+04	413
174	11.2	-1.4	9.4	1.E+04	312
175	11.0	-0.9	7.1	2.E+04	818
176	11.6	-0.4	18.6	2.E+04	519
177	5.9	0.3	11.8	2.E+04	507
178	6.3	-0.5	7.5	1.E+04	322
179	6.1	1.0	11.6	2.E+04	499
180	5.4	0.9	7.3	1.E+04	314
181	6.5	-0.5	4.9	6.E+03	211
182	6.1	-0.5	6.1	8.E+03	262
183	6.6	2.2	17.1	2.E+04	735
184	6.6	1.7	6.9	9.E+03	297
185					
186				mean	476

The Distance Between Particle Images Corresponds to 100 microsec.
The (-) or (+) symbols indicated position above and below the muzzle.

Table A8. Magtech 9mm 124 Gr, FMC (Data for Fig. 13 and Table 2)

	C	D	E	J	K
1	Muzzle	Vertical Dist. (in.)	Distance	V(cm/s)	V (ft/s)
2	Distance (in.)	from Muzzle	Between		
3			Particle Images		
4	27.5	-1.3	5.5	6.E+03	209
5	27.5	-2.3	9.1	1.E+04	346
6	27.7	-2.4	15.3	2.E+04	582
7	27.0	-0.9	5.3	6.E+03	202
8	27.0	-0.7	4.5	5.E+03	171
9	25.2	-2.9	9.1	1.E+04	346
10	24.4	-2.8	9.3	1.E+04	354
11	24.8	2.7	9.5	1.E+04	362
12	24.3	3.2	9.2	1.E+04	350
13	23.1	4.4	9.1	1.E+04	346
14	24.1	3.2	6.7	8.E+03	255
15	25.6	3.1	10.3	1.E+04	392
16	25.4	3.7	10.3	1.E+04	392
17	33.6	2.3	17.4	2.E+04	674
18	34.0	2.1	10.4	1.E+04	403
19	33.1	2.2	9.0	1.E+04	348
20	30.6	2.3	9.2	1.E+04	356
21	31.0	3.8	10.1	1.E+04	391
22	30.7	1.4	10.9	1.E+04	422
23	32.1	-0.1	11.8	1.E+04	457
24	31.9	0.8	8.1	1.E+04	314
25	33.1	-2.3	14.9	2.E+04	577
26	32.3	-0.8	15.9	2.E+04	616
27	30.3	-0.3	9.2	1.E+04	356
28	28.3	-2.8	13.1	2.E+04	507
29	32.7	-1.4	9.6	1.E+04	372
30	32.6	0.9	9.2	1.E+04	491
31	31.8	2.5	12.9	1.E+04	441
32	32.6	2.6	9.2	1.E+04	349
33	34.2	1.9	12.8	1.E+04	422
34	33.1	0.6	11.5	9.E+03	288
35	30.8	0.8	9.1	1.E+04	434
36	31.0	2.8	11.0	1.E+04	464
37	30.7	4.4	7.5	1.E+04	403
38	30.4	2.3	11.3	1.E+04	326
39	31.9	-0.3	12.1	1.E+04	349
40	32.6	-0.3	10.5	2.E+04	568
41	33.3	-0.4	8.5	1.E+04	361
42	33.6	-0.1	9.1	1.E+04	449

The Distance Between Particle Images Corresponds to 100 microsec.
The (-) or (+) symbols indicate position above and below the muzzle.

Table A8. Magtech 9mm 124 Gr, FMC (Data for Fig. 13 and Table 2)

	C	D	E	J	K
43	33.9	0.9	14.8	2.E+04	507
44	31.3	-1.4	9.4	3.E+04	1048
45	32.8	-2.5	11.7	1.E+04	449
46	34.6	1.3	13.2	2.E+04	502
47	34.6	-0.7	27.3	3.E+04	1039
48	34.6	-1.0	25.7	3.E+04	978
49	35.0	-0.3	9.7	1.E+04	369
50	34.8	0.7	8.6	1.E+04	327
51	39.5	3.9	15.9	2.E+04	605
52	36.6	0.8	14.1	2.E+04	527
53	36.7	-0.3	13.2	2.E+04	494
54	39.3	-2.6	12.6	1.E+04	471
55	35.9	-2.4	14.6	2.E+04	546
56	34.8	-1.2	15.4	2.E+04	576
57	34.8	1.9	7.8	9.E+03	292
58	34.9	1.8	18.1	2.E+04	677
59	39.1	3.3	13.3	2.E+04	497
60	39.1	2.9	12.4	1.E+04	464
61	39.5	-1.6	8.0	9.E+03	299
62	36.8	-0.9	9.3	1.E+04	348
63	35.1	-0.3	9.4	1.E+04	352
64	35.0	0.2	12.1	1.E+04	453
65	34.6	0.5	7.7	9.E+03	288
66	37.1	3.3	16.8	2.E+04	628
67	36.4	2.1	7.1	8.E+03	266
68	35.1	-2.1	17.8	2.E+04	666
69	36.3	-1.3	5.5	6.E+03	206
70	37.0	-0.5	7.1	8.E+03	266
71	35.8	-1.3	7.0	8.E+03	262
72	37.4	3.3	3.6	4.E+03	135
73	40.0	-2.9	12.2	1.E+04	464
74	39.9	-1.7	12.7	1.E+04	483
75	37.4	-1.8	14.4	2.E+04	548
76	37.1	-1.3	9.1	1.E+04	346
77	35.9	0.6	8.1	9.E+03	308
78	36.1	0.3	10.0	1.E+04	381
79	37.9	1.9	10.5	1.E+04	400
80	37.1	2.9	9.0	1.E+04	343
81	37.3	4.0	23.6	3.E+04	898
82	37.3	-0.8	7.1	8.E+03	270
83	36.5	-0.8	9.3	1.E+04	354
84	34.0	0.6	7.7	9.E+03	293

The Distance Between Particle Images Corresponds to 100 microsec.
The (-) or (+) symbols indicate position above and below the muzzle.

Table A8. Magtech 9mm 124 Gr, FMC (Data for Fig. 13 and Table 2)

	C	D	E	J	K
85	34.6	0.3	9.1	1.E+04	346
86	35.1	-1.6	12.4	1.E+04	472
87	38.4	0.9	9.6	1.E+04	365
88	43.3	3.6	12.7	1.E+04	479
89	44.0	3.2	10.2	1.E+04	385
90	40.6	-1.9	10.9	1.E+04	411
91	41.4	-3.5	14.3	2.E+04	540
92	46.8	-0.6	15.3	2.E+04	577
93	40.4	1.3	8.5	1.E+04	321
94	44.3	0.8	7.8	9.E+03	294
95	43.6	0.6	8.6	1.E+04	324
96	43.5	1.8	7.5	9.E+03	283
97	44.7	-1.5	7.5	9.E+03	283
98	44.8	-1.1	3.8	4.E+03	143
99	44.8	-0.6	3.9	4.E+03	147
100	41.9	-1.5	10.1	1.E+04	381
101					
102				mean	421

The Distance Between Particle Images Corresponds to 100 microsec.
The (-) or (+) symbols indicate position above and below the muzzle.

Table A9. CCI .38+P 125 Gr. (Data for Fig. 14, Tables 2 and 3)

	C	D	H	K	L	M	P	Q
1	Muzzle	Vertical Dist. (in.)	Distance	V(cm/s)	V (ft/s)	Distance	V (ft/s)	loss in V (fps)
2	Distance (in.)	from Muzzle	Between			Between		
3			1st Set of			2nd Set of		
4			Particle Images			Particle Images		
5	46.5	-2.8	18.4	1.8E+04	605	17.4	572	33
6	45.3	-1.3	16.0	1.6E+04	524	15.4	506	19
7	45.3	-3.5	13.8	1.4E+04	454			
8	41.4	-2.9	16.8	1.7E+04	553			
9	40.8	-1.8	17.6	1.8E+04	576			
10	39.5	-1.4	12.2	1.2E+04	402			
11	39.5	-1.4	16.3	1.6E+04	534			
12	38.9	-0.6	8.2	8.2E+03	269			
13	40.0	0.0	12.5	1.3E+04	411			
14	40.8	0.0	17.1	1.7E+04	562			
15	41.0	2.0	17.1	1.7E+04	562			
16	39.5	0.9	14.0	1.4E+04	458			
17	40.3	0.8	15.6	1.6E+04	510			
18	37.6	-0.6	22.0	2.2E+04	723	21.3	698	25
19	35.8	-3.3	18.8	1.9E+04	617			
20	37.0	-2.5	15.5	1.5E+04	507			
21	34.8	0.1	15.5	1.5E+04	507			
22	35.0	-4.3	16.5	1.7E+04	542			
23	35.5	1.6	13.9	1.4E+04	457	13.5	442	15
24	38.7	2.0	13.5	1.3E+04	442			
25	40.6	2.0	21.7	2.2E+04	713			
26	34.0	0.8	25.6	2.6E+04	838			
27	35.0	1.1	24.9	2.5E+04	818			

The Distance Between Particle Images Corresponds to 100 microsec.
The (-) or (+) symbols indicate position above and below the muzzle.

Table A9. CCI .38+P 125 Gr. (Data for Fig. 14, Tables 2 and 3)

	C	D	H	K	L	M	P	Q
28	34.0	-1.6	17.3	1.7E+04	567			
29	38.9	1.8	19.1	1.9E+04	627			
30	35.5	1.6	21.1	2.1E+04	693			
31	35.6	2.5	10.6	1.1E+04	346			
32	38.3	-0.8	18.7	1.9E+04	612			
33	43.1	-0.6	17.4	1.7E+04	570	17.1	559	10
34	42.5	0.5	20.9	2.1E+04	687	20.5	671	15
35	42.8	1.2	18.8	1.9E+04	615	18.3	600	15
36	47.0	-3.0	17.1	1.7E+04	559	16.3	534	25
37	38.9	-2.1	17.1	1.7E+04	559	16.4	539	20
38	40.1	0.9	24.6	2.5E+04	809	24.0	788	20
39	43.1	-0.6	14.5	1.5E+04	476	13.8	454	22
40	42.5	0.5	11.7	1.2E+04	385			
41	42.8	1.2	16.7	1.7E+04	547			
42	47.0	-3.0	20.7	2.1E+04	680	19.7	647	33
43	38.9	-2.1	11.0	1.1E+04	362			
44	40.1	0.9	18.4	1.8E+04	604	18.0	590	14
45	46.9	-3.5	17.7	1.8E+04	580			
46	10.9	1.9	4.4	4.4E+03	145			
47	11.3	1.9	21.2	2.1E+04	694			
48	9.4	1.9	25.7	2.6E+04	844			
49	13.4	-0.4	19.3	1.9E+04	633			
50	14.1	-0.3	14.0	1.4E+04	460			
51	12.5	-0.3	10.4	1.0E+04	342			
52	13.1	-0.5	7.3	7.3E+03	239			
53	8.7	-0.4	9.0	9.0E+03	296			
54	9.8	-0.8	10.4	1.0E+04	342			

The Distance Between Particle Images Corresponds to 100 microsec.
The (-) or (+) symbols indicate position above and below the muzzle.

Table A9. CCI .38+P 125 Gr. (Data for Fig. 14, Tables 2 and 3)

	C	D	H	K	L	M	P	Q
55	9.8	-0.8	8.2	8.2E+03	267			
56	10.1	0.3	7.0	7.0E+03	230			
57	13.5	0.3	3.7	3.7E+03	122			
58	10.0	2.8	10.2	1.0E+04	333			
59	10.0	2.6	13.4	1.3E+04	441			
60	32.8	-3.5	18.1	1.8E+04	593			
61	33.5	1.6	18.1	1.8E+04	593			
62	33.8	2.1	20.2	2.0E+04	664			
63	31.5	2.9	9.9	9.9E+03	324			
64	29.8	2.9	14.3	1.4E+04	469			
65	30.0	2.8	13.8	1.4E+04	453			
66	31.4	1.6	15.7	1.6E+04	515			
67	30.9	1.1	11.3	1.1E+04	371			
68	30.0	0.9	17.3	1.7E+04	566			
69	29.3	1.0	20.6	2.1E+04	675			
70	27.8	2.1	11.5	1.2E+04	379			
71	30.3	-0.9	21.8	2.2E+04	714			
72	29.6	-1.6	14.5	1.5E+04	476			
73	28.3	-3.0	13.0	1.3E+04	426			
74	27.8	-1.9	9.4	9.4E+03	308			
75	33.4	-0.7	20.6	2.1E+04	675			
76	33.9	-0.4	13.1	1.3E+04	429			
77	32.8	-1.0	15.9	1.6E+04	523			
78	29.6	-4.3	8.3	8.3E+03	273			
79	29.3	-3.7	14.6	1.5E+04	480			
80	28.6	-0.8	8.8	8.8E+03	289			
81	30.0	-0.5	20.8	2.1E+04	683			

The Distance Between Particle Images Corresponds to 100 microsec.
The (-) or (+) symbols indicate position above and below the muzzle.

Table A9. CCI .38+P 125 Gr. (Data for Fig. 14, Tables 2 and 3)

	C	D	H	K	L	M	P	Q
82	30.6	-0.4	13.7	1.4E+04	449			
83	30.3	0.9	10.0	1.0E+04	328			
84	29.1	1.1	22.4	2.2E+04	734			
85	29.1	1.4	13.7	1.4E+04	449			
86	29.4	1.6	19.6	2.0E+04	644			
87	31.6	2.1	30.3	3.0E+04	996			
88	28.8	3.2	11.9	1.2E+04	390			
89	28.1	2.5	10.7	1.1E+04	351			
90	29.8	5.1	20.5	2.0E+04	672			
91	31.7	-0.2	14.3	1.4E+04	469	13.6	445	24
92	32.1	-1.7	23.8	2.4E+04	780	23.0	756	24
93	33.6	-0.6	17.8	1.8E+04	583			
94	33.7	-0.9	18.2	1.8E+04	598			
95	34.0	-1.9	18.0	1.8E+04	591			
96	31.8	-2.3	18.0	1.8E+04	591			
97	30.9	-1.9	22.0	2.2E+04	720			
98	30.0	-2.7	14.0	1.4E+04	461			
99	32.2	4.0	20.6	2.1E+04	677			
100	33.2	-2.9	26.9	2.7E+04	882			
101	31.4	4.8	16.7	1.7E+04	547			
102	31.4	4.1	19.1	1.9E+04	626			
103	32.8	2.8	15.4	1.5E+04	504			
104	31.3	1.3	22.6	2.3E+04	740			
105	29.9	1.1	22.1	2.2E+04	724			
106	29.4	0.4	4.0	4.0E+03	130			
107	27.1	-2.3	1.3	1.3E+03	43			
108	29.4	-3.1	16.6	1.7E+04	543			

The Distance Between Particle Images Corresponds to 100 microsec.
The (-) or (+) symbols indicate position above and below the muzzle.

Table A9. CCI .38+P 125 Gr. (Data for Fig. 14, Tables 2 and 3)

	C	D	H	K	L	M	P	Q
109	30.8	-3.1	21.5	2.1E+04	705			
110	28.4	1.8	2.0	2.0E+03	67			
111	24.6	4.0	12.6	1.3E+04	413			
112	23.6	-2.3	7.7	7.7E+03	252			
113	27.8	-1.3	18.7	1.9E+04	614			
114	27.9	-0.9	19.6	2.0E+04	642			
115	27.6	-1.4	7.2	7.2E+03	236			
116	28.7	-1.8	15.8	1.6E+04	520			
117	28.0	-2.6	22.6	2.3E+04	740			
118	28.4	1.9	13.1	1.3E+04	429			
119	26.2	1.1	16.0	1.6E+04	524			
120	26.8	0.1	24.6	2.5E+04	807			
121	26.6	-0.2	23.4	2.3E+04	768			
122	24.5	1.1	17.0	1.7E+04	559			
123	25.0	2.7	10.2	1.0E+04	335			
124	25.3	1.9	19.3	1.9E+04	634			
125	25.3	-3.6	13.9	1.4E+04	457			
126	26.3	0.3	26.3	2.6E+04	862			
127	26.9	0.3	15.7	1.6E+04	516			
128	28.0	-2.0	13.2	1.3E+04	433			
129	25.9	-3.8	10.8	1.1E+04	354			
130	27.9	4.3	24.7	2.5E+04	811			
131	28.6	4.8	16.4	1.6E+04	539			
132	24.9	-3.4	16.8	1.7E+04	551			
133	23.4	-0.7	8.6	8.6E+03	283			
134	22.8	1.0	14.5	1.5E+04	476			
135	23.8	0.3	9.2	9.2E+03	303			

The Distance Between Particle Images Corresponds to 100 microsec.
The (-) or (+) symbols indicate position above and below the muzzle.

Table A9. CCI .38+P 125 Gr. (Data for Fig. 14, Tables 2 and 3)

	C	D	H	K	L	M	P	Q
136	23.9	0.5	13.1	1.3E+04	429			
137	26.8	1.9	17.8	1.8E+04	583			
138	26.8	2.4	20.8	2.1E+04	681			
139	26.9	-0.5	17.3	1.7E+04	567			
140	27.6	-1.8	15.7	1.6E+04	516			
141	27.8	-1.0	22.2	2.2E+04	728			
142	23.2	3.9	24.1	2.4E+04	791			
143	23.5	-0.1	10.1	1.0E+04	331			
144	28.5	-0.6	13.7	1.4E+04	449			
145	26.2	-2.3	10.3	1.0E+04	339			
146	27.9	3.4	15.6	1.6E+04	512			
147	23.5	2.6	19.1	1.9E+04	626			
148	27.4	2.9	13.6	1.4E+04	445			
149	26.9	1.7	17.3	1.7E+04	567			
150	21.8	2.8	18.2	1.8E+04	596			
151	23.1	-2.7	10.1	1.0E+04	332			
152	22.5	-2.6	16.5	1.6E+04	540			
153	22.8	0.1	20.7	2.1E+04	680			
154	20.2	-1.0	9.6	9.6E+03	316			
155	21.1	-1.3	14.5	1.5E+04	476			
156	22.0	2.8	25.0	2.5E+04	821			
157	20.3	3.1	9.8	9.8E+03	320			
158	20.6	3.2	23.4	2.3E+04	769			
159	23.5	3.1	12.0	1.2E+04	392			
160	22.4	-3.9	23.4	2.3E+04	769			
161	20.1	-4.4	23.7	2.4E+04	777			
162	20.3	-1.8	8.3	8.3E+03	272			

The Distance Between Particle Images Corresponds to 100 microsec.
The (-) or (+) symbols indicate position above and below the muzzle.

Table A9. CCI .38+P 125 Gr. (Data for Fig. 14, Tables 2 and 3)

	C	D	H	K	L	M	P	Q
163	18.3	-2.0	2.9	2.9E+03	96			
164	18.8	2.3	3.1	3.1E+03	100			
165	21.5	0.2	10.1	1.0E+04	332			
166	20.5	0.1	12.9	1.3E+04	424			
167	20.5	2.1	10.6	1.1E+04	348			
168	21.9	1.8	19.4	1.9E+04	636			
169	18.5	1.0	15.7	1.6E+04	516			
170	18.4	0.6	12.2	1.2E+04	400			
171	18.6	1.4	14.2	1.4E+04	464			
172	15.9	3.2	11.1	1.1E+04	363			
173	15.1	3.3	7.1	7.1E+03	234			
174	16.8	3.4	9.8	9.8E+03	323			
175	16.9	1.8	14.1	1.4E+04	464			
176	18.1	-0.7	6.6	6.6E+03	218			
177	13.9	-0.9	8.7	8.7E+03	287			
178	17.5	-0.8	13.2	1.3E+04	432			
179	17.8	-2.5	11.6	1.2E+04	379			
180	18.8	-3.5	12.1	1.2E+04	395			
181	17.5	-4.0	16.7	1.7E+04	549			
182	16.8	-3.5	13.7	1.4E+04	448			
183								
184				mean	507			
185							loss in V.	21

The Distance Between Particle Images Corresponds to 100 microsec.
The (-) or (+) symbols indicate position above and below the muzzle.

Table A10. Federal .38+P, 125 Gr., JHP (Data for Fig. 15 and Table 2)

	C	D	E	J	K
1	**Muzzle**	**Vertical Dist. (in.)**	**Distance**	**V(cm/s)**	**V (ft/s)**
2	**Distance (in.)**	**from Muzzle**	**Between**		
3			**Particle Images**		
4	28.1	-2.9	18.2	2.E+04	717
5	29.9	2.6	22.0	3.E+04	866
6	30.5	2.5	18.8	2.E+04	740
7	28.3	1.8	7.1	9.E+03	280
8	30.3	-2.0	20.2	2.E+04	795
9	33.5	2.1	25.5	3.E+04	1004
10	33.4	1.3	22.1	3.E+04	870
11	30.9	3.3	15.3	2.E+04	602
12	32.3	0.4	12.1	1.E+04	476
13	31.0	-1.5	18.4	2.E+04	724
14	32.6	4.4	25.5	3.E+04	1004
15	31.9	3.3	22.6	3.E+04	890
16	29.3	-0.4	7.7	9.E+03	303
17	30.3	0.1	19.7	2.E+04	776
18	33.3	2.0	16.0	2.E+04	630
19	30.8	1.6	12.4	1.E+04	488
20	30.3	2.4	10.9	1.E+04	429
21	31.0	3.1	12.4	1.E+04	488
22	31.9	-0.1	15.1	2.E+04	594
23	31.2	-0.3	17.1	2.E+04	673
24	32.9	-1.1	14.7	2.E+04	579
25	31.9	-1.4	10.3	1.E+04	406
26	31.8	-1.8	13.2	2.E+04	520
27	34.3	2.5	14.8	2.E+04	583
28	31.5	-1.4	13.5	2.E+04	527
29	30.6	-2.2	13.9	2.E+04	543
30	28.4	0.9	17.0	2.E+04	664
31	27.8	-1.9	11.5	1.E+04	449
32	32.1	1.3	13.8	2.E+04	539
33	31.8	2.9	13.9	2.E+04	543
34	28.9	0.2	10.6	1.E+04	414
35	30.8	-0.3	17.2	2.E+04	672
36	30.5	-0.6	15.7	2.E+04	613
37	34.0	1.6	22.5	3.E+04	878
38	31.0	-3.7	4.8	6.E+03	187
39	29.6	3.4	18.5	2.E+04	722
40	31.5	0.2	20.7	2.E+04	808
41	30.8	2.4	11.8	1.E+04	461
42	29.5	-2.9	15.2	2.E+04	593

The Distance Between Particle Images Corresponds to 100 microsec.
The (-) or (+) symbols indicate position above and below the muzzle

Table A10. Federal .38+P, 125 Gr., JHP (Data for Fig. 15 and Table 2)

	C	D	E	J	K
43	29.9	-3.6	18.1	2.E+04	707
44	29.8	-0.6	14.1	2.E+04	550
45	28.7	1.3	12.1	1.E+04	472
46	28.6	0.9	11.5	1.E+04	449
47	28.1	2.8	13.5	2.E+04	527
48	28.4	2.4	16.9	2.E+04	660
49	29.9	2.3	14.1	2.E+04	550
50	32.1	-1.5	18.2	2.E+04	711
51	30.3	-4.3	18.3	2.E+04	714
52	34.0	2.6	15.6	2.E+04	609
53	28.6	1.4	12.9	2.E+04	504
54	27.3	1.5	8.4	1.E+04	328
55	29.1	0.9	10.9	1.E+04	426
56	28.5	3.8	1.7	2.E+03	66
57	27.5	3.9	6.1	7.E+03	238
58	29.2	-0.1	7.3	9.E+03	285
59	33.7	0.6	16.5	2.E+04	644
60	31.8	2.3	10.1	1.E+04	394
61	32.3	-1.0	18.3	2.E+04	714
62	32.1	-0.8	13.6	2.E+04	531
63	33.9	-2.4	13.4	2.E+04	523
64	33.5	-1.6	16.6	2.E+04	648
65	29.9	-4.2	8.1	1.E+04	316
66	29.5	-3.4	11.0	1.E+04	429
67	31.1	2.6	13.2	2.E+04	515
68	31.8	1.3	15.2	2.E+04	593
69	34.1	1.6	14.3	2.E+04	558
70	28.1	0.8	5.1	6.E+03	199
71	27.3	1.2	1.3	2.E+03	51
72	27.4	0.3	11.7	1.E+04	457
73	25.8	1.6	16.7	3.E+04	833
74	25.0	1.9	15.4	2.E+04	768
75	27.1	1.5	5.7	9.E+03	284
76	27.2	1.3	10.5	2.E+04	524
77	27.0	0.8	14.0	2.E+04	698
78	25.8	-1.1	8.2	1.E+04	409
79	25.5	-0.1	18.2	3.E+04	908
80	24.1	-2.6	12.5	2.E+04	623
81	24.8	-2.2	16.5	3.E+04	823
82	23.1	-0.4	11.8	2.E+04	588
83	22.8	0.0	7.1	1.E+04	354
84	21.3	-1.6	8.1	1.E+04	404

The Distance Between Particle Images Corresponds to 100 microsec.
The (-) or (+) symbols indicate position above and below the muzzle

Table A10. Federal .38+P, 125 Gr., JHP (Data for Fig. 15 and Table 2)

	C	D	E	J	K
85	23.9	1.3	11.5	2.E+04	573
86	21.2	0.3	7.3	1.E+04	364
87	24.1	2.1	15.5	2.E+04	773
88	23.3	2.6	16.3	2.E+04	813
89	20.1	-0.8	10.3	2.E+04	514
90	20.1	0.2	11.6	2.E+04	578
91	20.6	2.0	12.3	2.E+04	613
92	21.1	-1.3	5.6	9.E+03	279
93	21.2	-1.6	9.5	1.E+04	474
94	21.3	2.8	5.6	9.E+03	279
95	19.4	-1.9	4.2	6.E+03	209
96	19.5	-2.0	4.7	7.E+03	234
97	20.6	-2.1	7.8	1.E+04	389
98	22.9	-2.9	7.1	1.E+04	354
99	23.3	-1.6	6.5	1.E+04	324
100	39.8	0.1	13.1	2.E+04	653
101	38.5	-0.5	10.6	2.E+04	529
102	41.1	-2.4	8.2	1.E+04	409
103	38.0	-2.1	14.1	2.E+04	703
104	37.5	-1.5	9.4	1.E+04	469
105	37.2	-1.6	9.6	1.E+04	479
106	40.4	3.3	9.4	1.E+04	469
107	38.9	0.4	13.5	2.E+04	673
108	37.8	2.6	12.4	2.E+04	618
109	35.1	2.8	10.6	2.E+04	529
110	34.9	0.4	7.8	1.E+04	389
111	36.0	1.9	9.1	1.E+04	454
112	42.1	-0.3	10.2	2.E+04	509
113	41.9	-0.8	9.9	2.E+04	494
114	38.3	-1.8	8.3	1.E+04	414
115	39.0	-0.9	11.2	2.E+04	559
116	39.1	0.1	9.7	1.E+04	484
117	39.9	0.9	6.7	1.E+04	334
118	41.0	3.1	9.8	1.E+04	489
119	34.8	1.4	13.3	2.E+04	663
120	36.4	1.1	11.0	2.E+04	549
121	36.3	2.2	7.7	1.E+04	384
122	36.0	0.9	10.8	2.E+04	539
123					
124				mean	539

The Distance Between Particle Images Corresponds to 100 microsec.
The (-) or (+) symbols indicate position above and below the muzzle

Table A11. Federal 357 Mag., 110 Gr. JHP (Data for Tables 2 and 3)

Distance (mm) Between 1st Set of Particle Images	V(cm/s)	V (fps)	Distance (mm) Between 2nd Set of Particle Images	v (fps)	loss in V (fps)
18.9	1.9E+04	621	18.2	596	25
18.2	1.8E+04	596	16.9	556	40
21.6	2.2E+04	707			
11.9	1.2E+04	389	11.1	364	25
25.6	2.6E+04	839			
14.0	1.4E+04	460	12.9	424	35
18.3	1.8E+04	601	17.2	566	35
29.1	2.9E+04	955	27.3	894	61
17.4	1.7E+04	571			
17.6	1.8E+04	576			
18.0	1.8E+04	591			
16.8	1.7E+04	551			
23.1	2.3E+04	758	21.1	692	66
14.8	1.5E+04	485			
17.9	1.8E+04	586			
18.2	1.8E+04	596			
28.0	2.8E+04	920			
25.3	2.5E+04	829			
19.4	1.9E+04	637			
18.5	1.8E+04	606	17.1	561	45
19.1	1.9E+04	627			
18.8	1.9E+04	616			
24.3	2.4E+04	798	23.6	773	25
14.2	1.4E+04	465	13.1	429	35
19.7	2.0E+04	647			
14.3	1.4E+04	470			
9.4	9.4E+03	308			
14.2	1.4E+04	465	12.9	424	40
12.2	1.2E+04	399	11.4	374	25
15.6	1.6E+04	510	14.3	470	40
11.7	1.2E+04	384			
18.6	1.9E+04	611	17.6	576	35
25.6	2.6E+04	839			
19.4	1.9E+04	637			
20.3	2.0E+04	667	19.1	627	40
20.3	2.0E+04	667	19.4	637	30
13.6	1.4E+04	445			
27.3	2.7E+04	894			
21.3	2.1E+04	697			

The Distance Between Particle Images Corresponds to 100 microsec.

Table A11. Federal 357 Mag., 110 Gr. JHP (Data for Tables 2 and 3)

12.8	1.3E+04	419	11.9	389	30
18.2	1.8E+04	596			
22.3	2.2E+04	733			
25.1	2.5E+04	824			
25.9	2.6E+04	849			
12.3	1.2E+04	404			
10.3	1.0E+04	339			
10.3	1.0E+04	339			
12.6	1.3E+04	414			
14.0	1.4E+04	460			
22.2	2.2E+04	728			
19.4	1.9E+04	637			
	mean	603		mean	35

The Distance Between Particle Images Corresponds to 100 microsec.

Table A12. CCI 357 Mag., 158 Gr. JHP (Data for Table 2 and 3).

Distance (mm) Between 1st Set of Particle Images	V(cm/s)	V (ft/s)	Distance (mm) Between 2nd Set of Particle Images	v (ft/s)	loss in V. fps
20.2	2.E+04	663			
16.1	2.E+04	527			
18.1	2.E+04	592			
15.3	2.E+04	502			
19.6	2.E+04	643	18.5	607	35
17.3	2.E+04	567			
17.7	2.E+04	582			
16.7	2.E+04	547			
19.6	2.E+04	643			
16.8	2.E+04	552			
19.0	2.E+04	622			
20.7	2.E+04	678	20.2	663	15
21.0	2.E+04	688			
15.5	2.E+04	507			
18.7	2.E+04	612	18.2	597	15
15.6	2.E+04	512			
17.4	2.E+04	572	17.0	557	15
17.9	2.E+04	587	17.3	567	20
14.8	1.E+04	487			
19.4	2.E+04	638	18.8	617	20
19.7	2.E+04	648			
19.6	2.E+04	643			
18.5	2.E+04	607			
15.9	2.E+04	522			
18.2	2.E+04	597	17.4	572	25
17.0	2.E+04	557	16.2	532	25
17.4	2.E+04	572			
19.1	2.E+04	627			
15.1	2.E+04	497			
19.3	2.E+04	632	18.5	607	25
18.1	2.E+04	592			
18.2	2.E+04	597	17.3	567	30
19.7	2.E+04	648	19.1	627	20
18.7	2.E+04	612	17.7	582	30
18.1	2.E+04	592	17.3	567	25
18.8	2.E+04	617	18.1	592	25
17.7	2.E+04	582	17.0	557	25
18.1	2.E+04	592	17.0	557	35
18.5	2.E+04	607			

The Distance Between Particle Images Corresponds to 100 microsec.

Table A12. CCI 357 Mag., 158 Gr. JHP (Data for Table 2 and 3).

15.5	2.E+04	507			
9.8	1.E+04	321			
	mean	583			
				mean	24

The Distance Between Particle Images Corresponds to 100 microsec.

Table A13. Native Fluorescence. Ambient v. Low Temperature. CCI 357 Magnum

Ambient Temp.	Low Temp.	Difference	% Increase
220	255	35	15.9
57	255	198	347.4
46	255	209	454.3
60	163	103	171.7
75	165	90	120.0
124	255	131	105.6
127	255	128	100.8
135	255	120	88.9
254	255	1	0.4
77	255	178	231.2
145	255	110	75.9
218	255	37	17.0
210	255	45	21.4
208	255	47	22.6
251	255	4	1.6
134	167	33	24.6
228	252	24	10.5
118	254	136	115.3
84	251	167	198.8
197	255	58	29.4
99	175	76	76.8
199	255	56	28.1
210	255	45	21.4
172	248	76	44.2
164	255	91	55.5
146	255	109	74.7
165	255	90	54.5
186	255	69	37.1
64	238	174	271.9
239	251	12	5.0
58	180	122	210.3
63	91	28	44.4
49	80	31	63.3
90	196	106	117.8
117	255	138	117.9
138	255	117	84.8
68	131	63	92.6
73	227	154	211.0
48	218	170	354.2
85	255	170	200.0
62	232	170	274.2
93	255	162	174.2
176	229	53	30.1
111	255	144	129.7
128	255	127	99.2

Table A13. Native Fluorescence. Ambient v. Low Temperature. CCI 357 Magnum

109	218	109	100.0	
193	255	62	32.1	
117	235	118	100.9	
171	255	84	49.1	
52	118	66	126.9	
61	127	66	108.2	
50	209	159	318.0	
			mean	113%

Table A14. Native Fluorescence: Ambient T. v. Low T. Winchester 9mm Luger

	A	B	C	E
1	**Low Temp.**	**Ambient T.**	**difference**	**% increase**
2	136	63	73	116
3	192	93	99	106
4	165	69	96	139
5	196	128	68	53
6	185	122	63	52
7	114	68	46	68
8	128	86	42	49
9	146	76	70	92
10	180	118	62	53
11	140	60	80	133
12	215	105	110	105
13	66	48	18	38
14	238	104	134	129
15	105	60	45	75
16	87	58	29	50
17	181	90	91	101
18	139	73	66	90
19	213	130	83	64
20	157	73	84	115
21	127	64	63	98
22	97	55	42	76
23	197	77	120	156
24	187	99	88	89
25	180	139	41	29
26	70	56	14	25
27	161	80	81	101
28	169	67	102	152
29	154	88	66	75
30	237	141	96	68
31	210	119	91	76
32	164	111	53	48
33	159	57	102	179
34	160	80	80	100
35	155	90	65	72
36	218	80	138	173
37	136	69	67	97
38	230	90	140	156
39	164	61	103	169
40	247	111	136	123
41	117	64	53	83
42	123	68	55	81
43	169	84	85	101
44	131	57	74	130

Table A14. Native Fluorescence: Ambient T. v. Low T.
Winchester 9mm Luger

	A	B	C	E
45	151	108	43	40
46	182	92	90	98
47	81	48	33	69
48	162	108	54	50
49	236	161	75	47
50	208	34	174	512
51	208	73	135	185
52	114	62	52	84
53	178	85	93	109
54	102	60	42	70
55	235	83	152	183
56	249	95	154	162
57	103	51	52	102
58	86	57	29	51
59	75	40	35	88
60	115	43	72	167
61	125	46	79	172
62	141	39	102	262
63	158	65	93	143
64	137	70	67	96
65	108	49	59	120
66	174	72	102	142
67	106	43	63	147
68	113	44	69	157
69	86	69	17	25
70	188	72	116	161
71	93	38	55	145
72	99	42	57	136
73	242	77	165	214
74	90	36	54	150
75	126	66	60	91
76	80	56	24	43
77	93	55	38	69
78	87	53	34	64
79	105	52	53	102
80	119	74	45	61
81	74	55	19	35
82	136	66	70	106
83	123	47	76	162
84	255	64	191	298
85	107	56	51	91
86	113	50	63	126
87	255	120	135	113
88	195	53	142	268

Table A14. Native Fluorescence: Ambient T. v. Low T.
Winchester 9mm Luger

	A	B	C	E
89	123	69	54	78
90	226	118	108	92
91	183	79	104	132
92	164	70	94	134
93	90	35	55	157
94	224	75	149	199
95	255	165	90	55
96	198	70	128	183
97	225	127	98	77
98	150	100	50	50
99	124	76	48	63
100	166	55	111	202
101	201	100	101	101
102	99	72	27	38
103	140	70	70	100
104	160	67	93	139
105	138	51	87	171
106	223	115	108	94
107	178	47	131	279
108	83	52	31	60
109	99	61	38	62
110	152	65	87	134
111	178	72	106	147
112	122	73	49	67
113	255	159	96	60
114	120	33	87	264
115	113	34	79	232
116	151	38	113	297
117	255	99	156	158
118	251	173	78	45
119	227	203	24	12
120	140	61	79	130
121	186	120	66	55
122	147	47	100	213
123	138	35	103	294
124	210	57	153	268
125	171	65	106	163
126	134	35	99	283
127	186	60	126	210
128	202	77	125	162
129	255	77	178	231
130	174	84	90	107
131	84	34	50	147
132	171	33	138	418

Table A14. Native Fluorescence: Ambient T. v. Low T.
Winchester 9mm Luger

	A	B	C	E
133	67	35	32	91
134	70	35	35	100
135	71	35	36	103
136	170	70	100	143
137	109	36	73	203
138	255	75	180	240
139	190	61	129	211
140	92	46	46	100
141	93	43	50	116
142	221	64	157	245
143	207	42	165	393
144	97	33	64	194
145	189	74	115	155
146	220	58	162	279
147	217	70	147	210
148	182	50	132	264
149	218	70	148	211
150	165	49	116	237
151	135	48	87	181
152	102	35	67	191
153	78	33	45	136
154	87	34	53	156
155	134	30	104	347
156	125	36	89	247
157	232	137	95	69
158	233	76	157	207
159	106	105	1	1
160	121	49	72	147
161	117	33	84	255
162	130	32	98	306
163	255	180	75	42
164	228	173	55	32
165	137	53	84	158
166	81	34	47	138
167	116	88	28	32
168	205	81	124	153
169	101	58	43	74
170	195	169	26	15
171	237	84	153	182
172	105	35	70	200
173	130	35	95	271
174	159	62	97	156
175	146	31	115	371
176	136	84	52	62

Table A14. Native Fluorescence: Ambient T. v. Low T.
Winchester 9mm Luger

	A	B	C	E
177	239	202	37	18
178	202	98	104	106
179	215	52	163	313
180	103	34	69	203
181	223	73	150	205
182	86	35	51	146
183	74	35	39	111
184	86	35	51	146
185	105	35	70	200
186	180	58	122	210
187	114	33	81	245
188	142	34	108	318
189	94	35	59	169
190	97	32	65	203
191	83	31	52	168
192	125	41	84	205
193	125	73	52	71
194	121	40	81	203
195	208	81	127	157
196	169	142	27	19
197	138	67	71	106
198	154	91	63	69
199	164	161	3	2
200	161	109	52	48
201	175	111	64	58
202	86	57	29	51
203	83	35	48	137
204	117	42	75	179
205	192	76	116	153
206	140	102	38	37
207			std. dev.	84
208			mean	139

Table A15. Pre- v. Post-MGT Particle Fluorescence (Pixel Value Data for Table 14)

CCI 357 Pre-Reaction		CCI 357 Post-Reaction		CCI 357 Pre Solvent		CCI Post Solvent	
142		150		166	cal +14%	197	cal +14%
139		158		174	cal +14%	198	cal +14%
125		167		139	cal +14%	186	cal +14%
129		165		124	cal +14%	185	cal +14%
115		165		87	cal +14%	180	cal +14%
136	cal +6%	160	cal +6%				
144	cal +6%	155	cal +6%				
98	cal +6%	162	cal +6%				
77	cal +6%	156	cal +6%				
57	cal +6%	159	cal +6%				
116		160		138		189	
	% increase: 38					% increase: 37	
CCI .38 Pre-Reaction		CCI .38 Post Reaction		CCI .38 Pre-Solvent		CCI .38 Post-Solvent	
125		162		144	cal +14%	198	cal +14%
127		160		148	cal +14%	219	cal +14%
129		161		144	cal +14%	198	cal +14%
71		158		63	cal +14%		
157	cal +6%	135	cal +6%				
192	cal +6%	102	cal +6%				
134		146		125		205	
	% increase: 9					% increase: 64	

Table A15. Pre- v. Post-MGT Particle Fluorescence (Pixel Value Data for Table 14)

Fed. NYC .38+P, 158 Gr.			Fed. NYC .38+P, 158 Gr.			Fed. NYC .38+P, 158 Gr.			Fed. NYC .38+P, 158 Gr.	
Pre Reaction			Post Reaction			Pre-Solvent			Post-Solvent	
169			132			160	cal +14%		197	cal +14%
101			132			138	cal +14%		174	cal +14%
120			145			139	cal +14%		193	cal +14%
128			144			157	cal +14%		214	cal +14%
113			151	cal +6%		91	cal +14%		197	cal +14%
191	cal +6%		138	cal +6%						
186	cal +6%		143	cal +6%						
127	cal +6%		140	cal +6%						
183	cal +6%		148	cal +6%						
146			141			137			195	
	3% decrease							42% increase		
Win. .38+P, 158 Gr.			Win. .38+P, 158 Gr.			Win. .38+P, 158 Gr.			Win. .38+P, 158 Gr.	
Pre Reaction			Post Reaction			Pre-Solvent			Post-Solvent	
172			145			148	cal +14%		214	cal +14%
164			155			181	cal +14%		193	cal +14%
165			151			204	cal +14%		203	cal +14%
166			159						206	cal +14%
137			152						169	cal +14%
155	cal +6%		141							
128	cal +6%		153							
85	cal +6%		148							
81	cal +6%		159							
			153							
			117							
	mean: 139			mean: 148		mean: 178			mean: 197	
	6% increase					11% increase				

Table A15. Pre- v. Post-MGT Particle Fluorescence (Pixel Value Data for Table 14)

Rem..38+P, 158 Gr. Pre-Reaction		Rem..38+P, 158 Gr. Post-Reaction		Rem..38+P, 158 Gr. Pre-Solvent		Rem..38+P, 158 Gr. Post-Solvent	
148		149		190	cal +14%	194	cal +14%
117		151		204	cal +14%	214	cal +14%
142		146		159	cal +14%	218	cal +14%
128		149		168	cal +14%	184	cal +14%
105		149				165	cal +14%
177	cal +6%	178	cal +6%				
163	cal +6%	144	cal +6%				
176	cal +6%	158	cal +6%				
85	cal +6%	147	cal +6%				
56	cal +6%	140	cal +6%				
130		151		180		195	
	16% increase				8% increase		

%T at Select Wavelengths (nanometers)

	300	350	400	450	500	550	600	650	700
Filters/Goggles									
Nikon #056 Orange	0	0	0	0	0	20	95	97	97
Tiffen #21 Orange	0	0	0	0	0	24	83	87	86
Orange Goggles	0	0	0	0	0	15	82	82	83
Tiffen #23A Orange	0	0	0	0	0	0	77	83	83
Tiffen #15 Orange	0	0	0	0	0	80	90	91	91
Tiffen #29 Red	0	0	0	0	0	0	7	84	87
Red Goggles	0	0	0	0	0	0	30	86	90
Long Pass 350nm	0	25	82	84	85	85	85		
Long Pass 370nm	0	0	78	83	85	85	85		
Long Pass 400nm	0	0	50	82	87	87	87		
Long Pass 475nm	0	0	0	0	80	92	92		
Long Pass 505nm	0	0	0	0	27	88	90		

Filters for Reflected Light Fluorescence Microscopy & Spectrofluorimetry
Appproximate Values Based on Spectra

	Ex.Filters	Central Wavelength	Cut-off (0%T)	Barrier Filters (Longpass)
U.V.	UG-1	365nm	400nm	420nm
Blue	BG12	400nm	500nm	530nm
Green	IF-545	550nm	575nm	590nm
	BG-36	500 and 550nm	575nm	

Interference Filters of Crimescope CS-16 Tunable High Intensity Light Source
Wheel One Filters Used for Excitation: 40nm Bandwith. Central Wavelength as Indicated in Chapter Three (Equipment). Fine tuning achieved by tilting selected filter.

Table A16. Spectal Data for Filters and Goggles

Table A17. Data from Federal Spl. 158 Grain, SWC (all cartridges taken from same box)

Griess Paper Reaction Sites (Fluorescence v. Ambient Illumination)				
Data Excerpted from Table 10.				
Conventional MGT	fluorescence	difference	% increase	
146	400	254	174	
68	95	27	40	
123	268	145	118	
66	263	197	298	
162	370	208	128	
91	265	174	191	
75	219	144	192	
67	242	175	261	
63	253	190	302	
		mean	189	
		Std. Dev.	87	
Particle Counts - Data Excerpted from Table 5				
Same Discharges as above				
	Fluorescence/MGT			
	ratio			
	1.23			
	1.23			
	4.81			
	2.11			
	2.50			
	1.43			
	0.95			
	1.71			
	1.88			
	2.49			
mean	2.03			
std dev	1.11			

Table A18. Table of Abbreviations

FMC	full metal case
FMJ	full metal jacket
Gr.	grain
GSR	gunshot residue
H&K	Heckler and Koch
HP	hollow point
LD	lead (in context of bullet description)
LUV	long wavelength ultraviolet light
LRN	lead round nose
LN	lead nose
LN2	liquid nitrogen
Mag.	Magnum
MGT	Modified Griess Test
nm	nanometers
Pb	lead
Photo.	photograph
RN	round nose
Spl.	special
S&W	Smith and Wesson
SUV	short wavelength ultraviolet light
SWC	semi-wad cutter

SJHP	semi-jacketed hollow point
T.	temperature
THILS	Tunable High Intensity Light Source
TMJ	Total Metal Jacket

Figure A19. Diagram of Measurement of Particle Inter-Image Distances

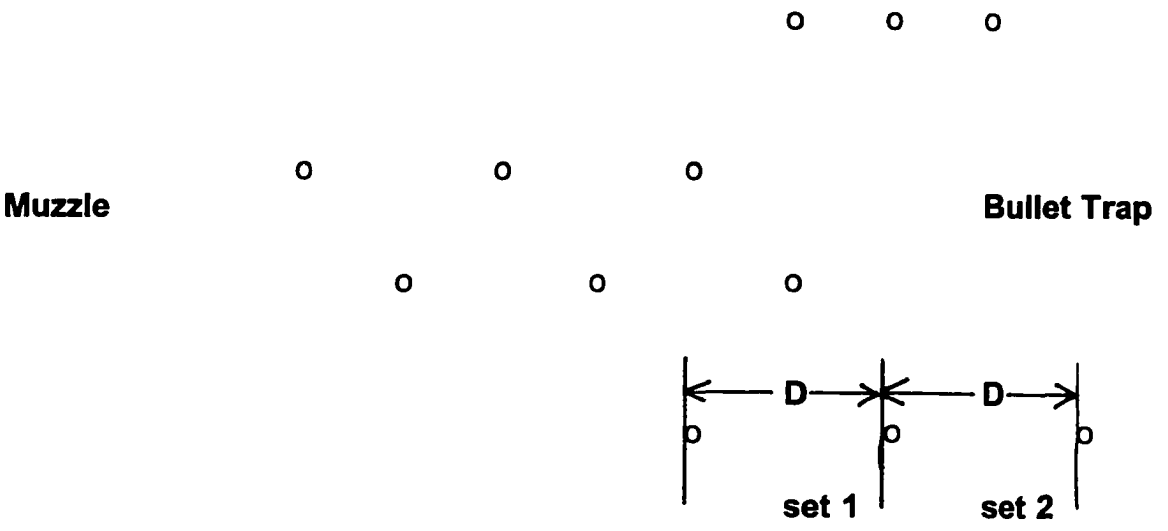

For velocity measurements, the distance between either set 1 or set 2 was measured. Unless otherwise indicated, this interval corresponded to 100 microseconds. If deceleration data was required both sets of distances were measured. The set closest the muzzle, as indicated above, was designated as set 1. Since the illumination for set 2 occurred later than set 1, it was always somewhat shorter in length than that of set 1. The same edge (all left or all right) of each image, associated with a particular particle, was measured to determine distances between images. Only those images belonging to the same particle were measured. This was determined in part by an obvious straight trajectory, similar colors, size, and overall general appearance. Thus, it was impossible to measure the velocity of many particles.

Figure A20. Chemical Reactions and Structures

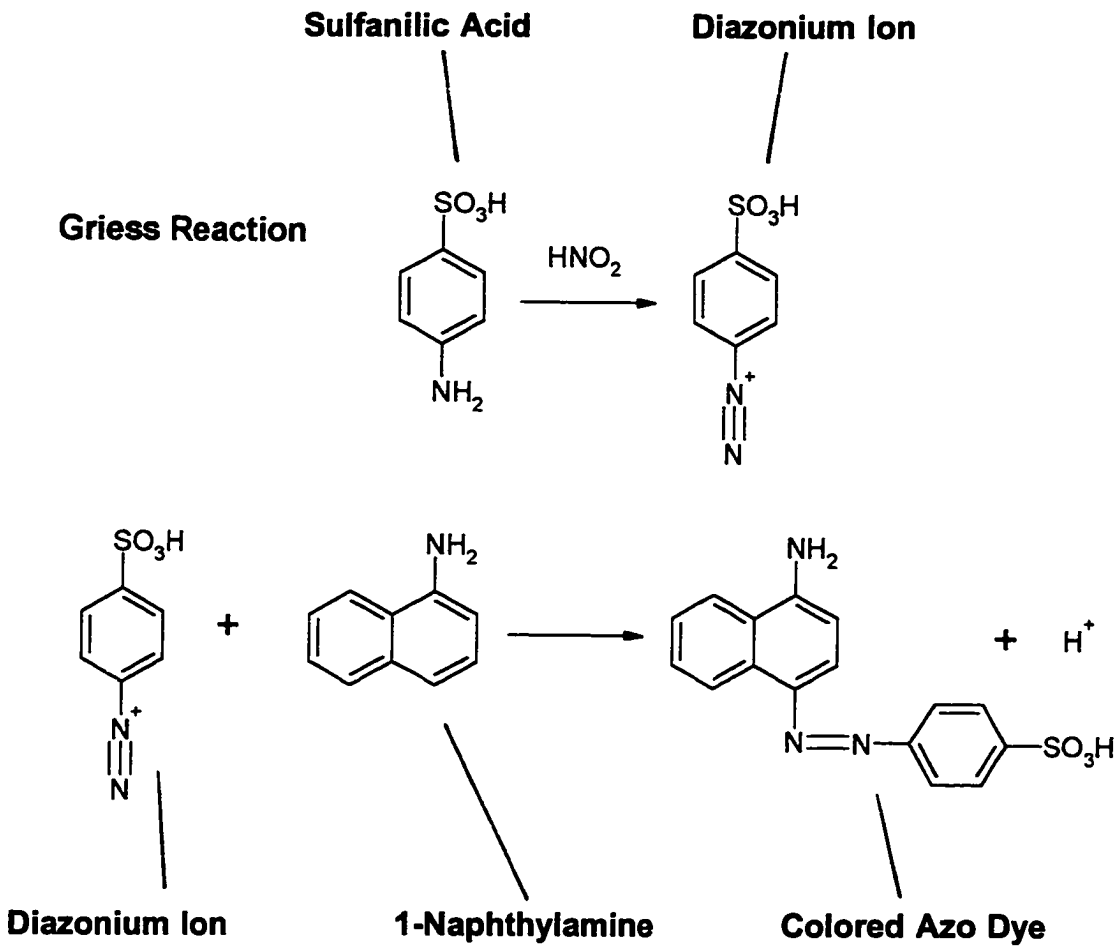

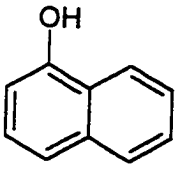

1-naphthol

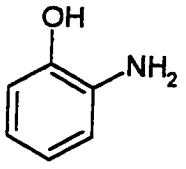

2-aminophenol

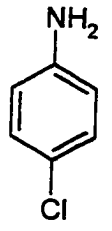

p-chloroaniline

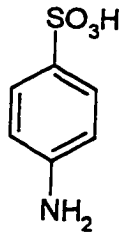

sulfanilic acid

dinitrotoluene isomers

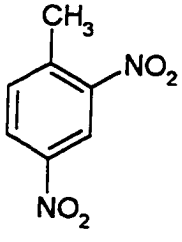

2,4

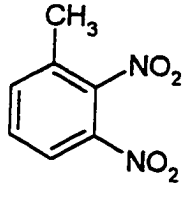

2,3

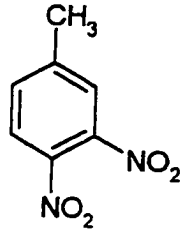

3,4

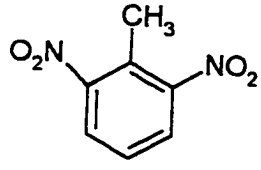

2,6

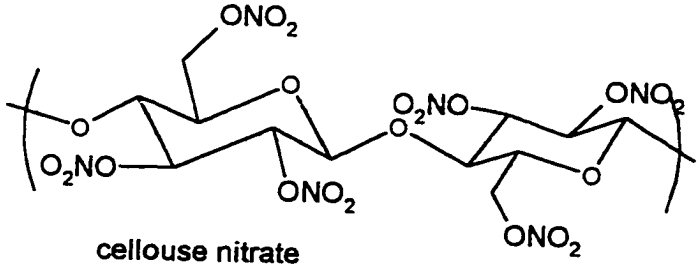

cellouse nitrate

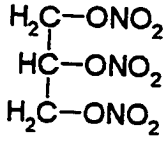

trinitroglycerine

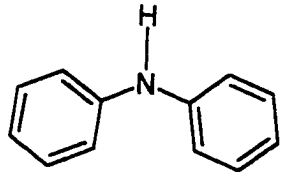

diphenylamine

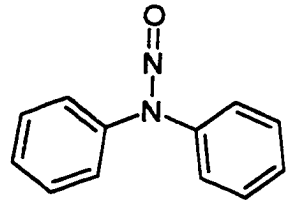

N-nitroso-diphenylamine

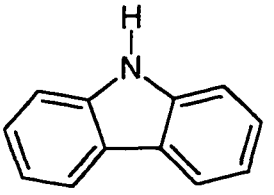

Carbazole

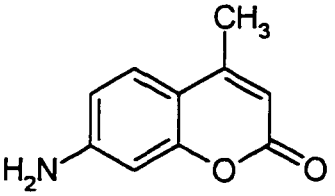

Coumarin 120
(4-methyl-7-aminocoumarin)

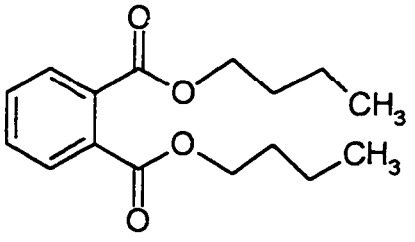

dibutyl phthalate

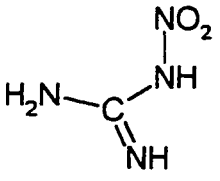

Nitroguanidine

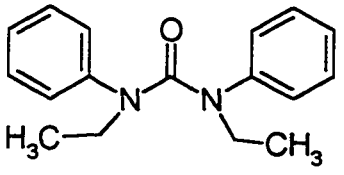

Ethyl Centralite
(N,N'-Diethyl-N,N'-diphenylurea)

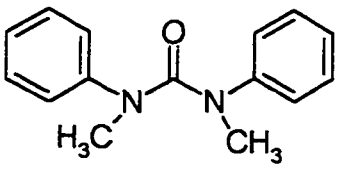

Methyl Centralite
(N,N'-Dimethyl-N,N'-diphenylurea)

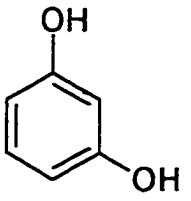

Resorcinol
(1,3-Benzenediol)

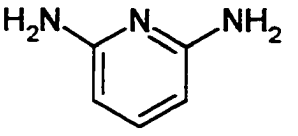

2,6 Diaminopyridine

Bibliography

Bartsch, M.R., Kobus, H.J., Wainwright, K.P. (1996). An update on the use of the sodium rhodizonate test for the detection of lead originating from firearm discharges, Journal of Forensic Sciences, 41 (6), 1046-1051.

Bashinski, J.S., Davis, J.E., and Young, C. (1974). Detection of lead in gunshot residues on targets using the sodium rhodizonate test, AFTE Journal, 6, (4), 5-6.

Basu, S. (1982). Formation of gunshot residues. Journal of Forensic Sciences, 27 (1), 72-91.

Basu, S., Boone, C., Denio, D., & Miazga, R. (1997). Fundamental studies of gunshot residue deposition by glue-lift. Journal of Forensic Sciences, 42 (4), 571-581.

Beckett, J., Nelson, D. (1981). Trace metal determinations by liquid chromatography and fluorescence detection, Analytical Chemistry, 53, 909-911.

Beijer, R. (1994) Experience with zincon, A useful reagent for the determination of firing range with respect to leadfree ammunition, Journal of Forensic Sciences, 39, (4), 981-987.

Beveridge, A.D. (1992). Development in the detection and identification of explosives residues, Forensic Science Review, 4 (1), 18-49.

Boltz, D. F., and Howell, J. A. (Eds.). (1978). Colorimetric determination of nonmetals. (pp. 216-217). New York, Chichester, Brisbane, Toronto. A Wiley-Interscience Publication, John Wiley & Sons.

Bonfanti, M., and Gallasser, A. (1995, April) Problems encountered in the detection of gunshot residues, AFTE Journal, Vol. 27, No. 2, p. 115.

Brazeau, J., and Wong, R. (1997) Analysis of gunshot residues on human tissues and clothing by x-ray microfluorescence, Journal of Forensic Sciences, 42 (3), 424-428.

Bynum, K., De Forest, P.R., Martir, K., Pizzola, P.A. (1995). Thin Layer Chromatographic Separation of Components of Propellant Particles Utilizing Fluorescent and Chemical Visualization Techniques. Paper presented at the annual meeting of the Northeastern Association of Forensic Scientists, Mystic, CT.

Ceccaldi, P.F. (1962). The examination of firearms and ammunition. In F. Lindquist, (Ed.), Methods of Forensic Science, Vol.1. (pp. 593-637). New York/London: Interscience Publishers a division of John Wiley & Sons.

Cornelius, R., & Timperman, J. (1974). Gunfiring detection method based on Sb, Ba, Pb, and Hg deposits on hands. Evaluation of the credibility of the test. Medicine, Science and the Law, 14 (2), 98-116.

De Forest, P.R., Gaensslen, R.E., Lee, H.C. (1983). Forensic science: An introduction to criminalistics. New York: McGraw-Hill Book Co.

De Forest, P.R., Nelson, D., and Roberts, K. (1995, March), Preliminary findings: an investigation of the efficiency of the transfer method pertaining to techniques used in the detection of gunshot residue (GSR), Report update of GSR project to Forty-Five Foundation, p. 6.

De Forest, P.R., Pizzola, P.A.. (1997, February). A Recommended Protocol for Carrying out Gunshot Discharge Residue Testing on Garments. Paper presented at the annual meeting of the American Academy of Forensic Sciences, New York City, NY.

Dillon, J.H. (1990a). The Modified Griess Test: A chemically specific chromophoric test for nitrite compounds in gunshot residue. AFTE Journal, 22 (3), 243-250.

Dillon, J.H. (1990b). A protocol for gunshot residue examinations in muzzle-to-target distance determinations. AFTE Journal 22 (3), 257-268.

Dillon, J.H. (1990c). The sodium rhodizonate test: A chemically specific chromophoric test for lead in gunshot residues. AFTE Journal, 22 (3), 251-256.

Dombrowski, L.J., Pratt, E.J. (1972). Fluorometric method for determining nanogram quantities of nitrite ion, Analytical Chemistry, 44 (14), 2268-2272.

Federal Bureau of Investigation. (1996). Uniform crime reports for the United States 1995. Washington, DC: U.S. Government Printing Office.

Feigl, F. & Anger, V. (1975). Spot tests in organic analysis (Rev. ed.). (R. E. Oesper, Trans.). Amsterdam, Oxford, New York: Elsevier Scientific Publishing Co. (Original work published in 1937).

Fox, J.B. (1979). Kinetics and mechanisms of the Griess reaction. Analytical Chemistry, 51, (9), p. 1493-1502.

Gansau, H., and Becker, U. (1982) Semi-automatic detection of gunshot residue (GSR) by scanning electron microscopy and energy dispersive x-ray analysis (SEM/EDX), Scanning Electron Microscopy, I, 107-114.

Gestring, B., (1194). The impact of the stability and retention of nitrites in gunshot residue pattern interpretation, Master's Thesis, John Jay College of Criminal Justice.

Guilbault, G.G. (1973). Practical fluorescence. New York: Marcel Dekker, Inc.

Hagel, R., Redecker, K. (1986) Sintox-a new, non-toxic primer composition by Dynamit Nobel AG, Propellants, Explosives, Pyrotechnics, 11, 184-187.

Harris, A. (1995) Analysis of primer residue from CCI Blazer® lead free ammunition by scanning electron microscopy/energy dispersive x-ray, Journal of Forensic Sciences, 40 (1), 27-30.

Harrison, H.C. and Gilroy, R. (1959) Firearms discharge residues, Journal of Forensic Science, 4, 184.

Hercules, D. (Ed), (1966). Fluorescence and phosphorescence analysis: Principles and applications, Interscience Publishers, New York.

Jingou, X., Xiangqun, G. (1990) Study on the photochemical-fluorimetric method: The determination of trace nitrite in natural water, Fenxi Huaxe (Anal. Chem.), 18 (7), 664-667.

Jones, Jr., E.L. Gunpowder atlas, Ventura SO, CAC News, California Association of Criminalists, 1995.

Jones, P.F., and Nesbitt, R.S. (1975). A photoluminescence technique for detection of gunshot residue, Journal of Forensic Sciences, 20 (2), 231-242.

Kirk, P., (1953). Crime investigation: Physical evidence and the police laboratory, Interscience Publishers, Inc., New York.

Kirkbright, G.F., Saw, C.G., and West, T.S. (1969). Fluorescence characteristics of inorganic complexes in hydrochloric acid medium at liquid-nitrogen temperature, Talanta, 16, 65-73.

Krishnan, S.S. (1968). Advances in forensic activation analysis in the examination of firearm discharge residues. S.I. Cohn (Ed.), Law Enforcement Science and Technology II. Proceedings of the Second National Symposium on Law Enforcement Science and Technology, 2, 313-356.

Law Enforcement Assistance Administration, U.S. Department of Justice, National Institute of Law Enforcement and Criminal Justice. (1970). Trace metal detection technique in law enforcement, (PR 71-1). Washington, DC: U.S. Government Printing Office.

Lichtenberg, W. (1990). Methods for the determination of shooting distance, Forensic Science Review, 2 (1), 38-62.

Maehly, A., & Stromberg, L. (1981). Chemical criminalistics. Springer-Verlag, New York, pp. 183-199.

Maloney, R.S., and Thornton, J.I. (1982) Color tests for diphenylamine stabilizer and related compounds in smokeless gunpowder, Journal of Forensic Science, 27 (2), 318-329.

Midkiff, Jr., C.R. (1975). Detection of gunshot residues: Modern solutions for an old problem. Journal of Police Science and Administration, 3 (1), 77-83.

Morrison, R.T. & Boyd, R.N. (1974). Organic chemistry. (3rd ed.). Boston: Allyn and Bacon, Inc.

Nennstiel, R. (1983) High speed and spark flash photography, Journal of the American Firearms and Toolmark Examiners, 15 (1),11-29.

Nesbitt, R.S., Wessel, J.E., and Jones, P.F. (1974). Conclusive detection of gunshot residue by the use of particle analysis, Law Enforcement Development Group, Prepared for National Institute of Law Enforcement and Criminal Justice, Law Enforcement Assistance Administration, U.S. Department of Justice, pp. 1-56.

Nesbitt, R.S., Wessel, J.E., Wolten, G.M., and Jones, P.F. (1977). Evaluation of a photoluminescence technique for the detection of gunshot residue, Journal of Forensic Sciences, 22 (2), 288-303.

Northrop, D.M., Martire, D.E., MacCrehan, W.A. (1991). Separation and identification of organic gunshot and explosive constituents by micellar electrokinetic capillary electrophoresis, Analytical Chemistry, 63, 1038-1042.

Northrop, D.N., & Mac Crehan, W.A. (1992) Sample collection, preparation, and quantitation in the micellar electrokinetic capillary electrophoresis of gunshot residues, Journal of Liquid Chromatography, 15 (6) 1041-1063.

O'Hara, C., Osterburg, J. (1949). An introduction to criminalistics: The application of the physical sciences to the detection of crime. Bloomington:

Indiana University Press.

O'Hara, J. (1976). Fundamentals of criminal investigation, 4th ed. Springfield, Illinois: Thomas.

Palflash 500 Owner's Manual, The Cooke Corporation.

Peak, S.A. (1980). A thin-layer chromatographic procedure for confirming the presence and identity of smokeless powder flakes. Journal of Forensic Sciences, 25 (3), 679-681.

Petraco, N., Yander, M., and Sardone, J. (1981) A method for the quantitative determination of nitrites in gunshot residue cases. Forensic Science International, 18, 85-92.

Rider, B.F., and Mellon, M.G. (1946). Colorimetric determination of nitrites, Industrial and Engineering Chemistry, 18 (2), 96-99.

Sawicki, C.R., Scaringelli, F.P. (1971). Colorimetric determination of nitrate after hydrazine reduction to nitrite. Microchemical Journal, 16, 657-672.

Sawicki, E., Stanley, T.W., Pfaff, J., D'Amico, A. (1963). Comparison of fifty-two spectrophotometric methods for the determination of nitrite. Talanta, 10, 641-655.

Steinberg, M., Leist, Y., Goldschmidt, P., Tassa, M. (1984). Spectrophotometric determination of nitrites in gunpowder residue on shooter's hands, Journal of Forensic Sciences, 29 (2), 464-470.

Unenfriend, S. (1962). Fluorescence Assay in Biology and Medicine (Vol. 1). New York: Academic Press.

Voskertchian, G.P., Pavilova, G.V. (1993) Spectrophotometric determination of time since discharge of firearms, Crime Laboratory Digest, 22 (1), 5-10.

Wang, Y., Huang, Y. (1988). Fluorimetric - absorptiometric determination of nanogram amounts of nitrite in natural and polluted water. Lihua Jianyan, Huaxue Fence, 24, (4), 212-213.

Walker, J.T. (1940). Bullet holes and chemical residues in shooting cases, Journal of the American Institute of Criminal Law and Criminology, 31, 497-519.

Wallace, J. (1990). Chemical aspects of firearms ammunition, AFTE Journal, 22 (4), 364-387.

Wessel, J.E., Jones, P.F., Kwan, Q.Y., Nesbitt, R.S., and Rattin, E.J. (1974). Equipment systems improvement program: Gunshot residue detection: Survey & assessment & identification of alternative concepts. ATR-75(7915)-1, The Aerospace Corporation, El Segundo, California. Prepared for the National Institute of Law Enforcement and Criminal Justice, Law Enforcement Assistance Administration, U.S. Dept. of Justice, September.

White, C., Argauer, R. (1970). Fluorescence analysis, New York: Marcel Dekker, Inc.

White, C., Wessler, A. (1968). Fluorometric analysis. Analytical Chemistry, 40 (5), 116R-135R.

Windholz, M. (Ed.). (1983). The Merck index: An encyclopedia of chemicals and drugs (10th ed.). (pp. 917-918). Rahway: Merck & Co., Inc.

Yinon, J., Zitrin, S. (1981). The analysis of explosives, Pergamon Series in Analytical Chemistry (Vol. 3). Oxford: Pergamon Press.

Zhou, J., Prognon, P., Dauphin, C., Hamon, M. (1993). HPLC fluorescence determination of nitrites in water using precolumn derivatization with 4-methyl-7-aminocoumarin, Chromatographia, 36, 57-60.

IMAGE EVALUATION TEST TARGET (QA-3)

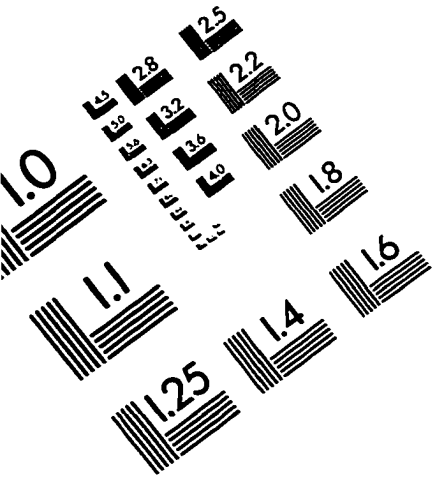

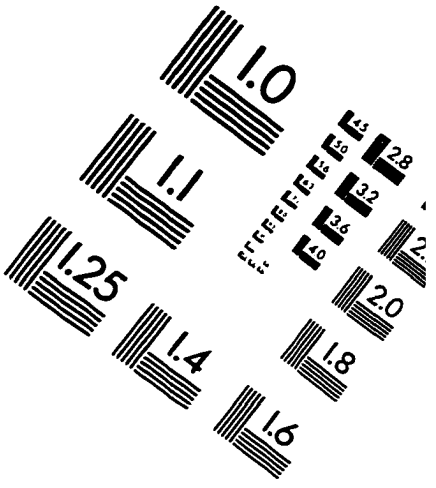

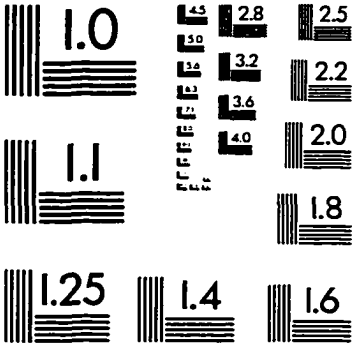

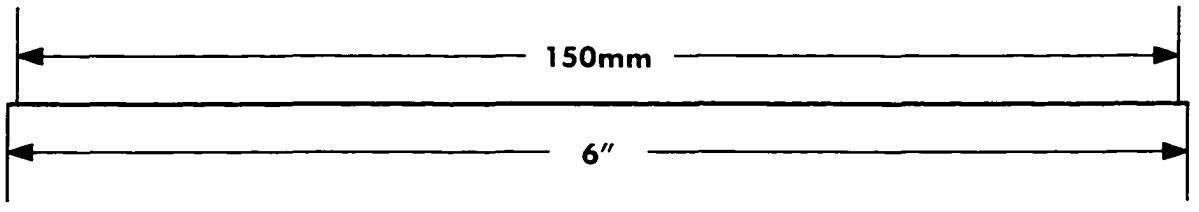

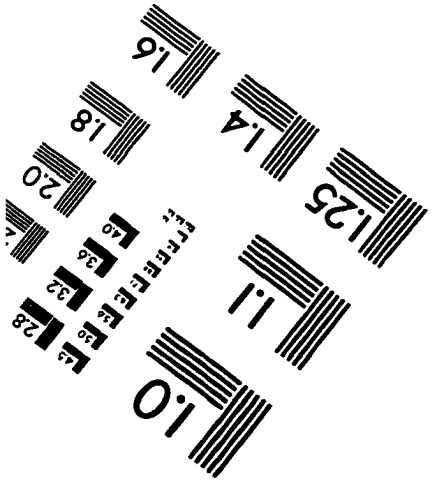

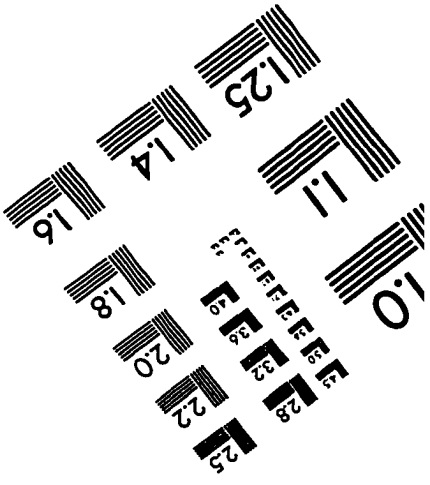

APPLIED IMAGE, Inc
1653 East Main Street
Rochester, NY 14609 USA
Phone: 716/482-0300
Fax: 716/288-5989